

Mapping the Glycan Shields of Enveloped Viruses

by

Yasunori Watanabe
渡辺恭永

Glycobiology Institute, Department of Biochemistry
St Peter's College, University of Oxford

A thesis submitted for the degree of *Doctor of Philosophy*
Hilary term, 2020

Supervised by
Prof. Max Crispin, Prof. Thomas Bowden and Dr Mark Wormald

Declaration

The work presented in this thesis was undertaken in Prof. Max Crispin's laboratory at the Oxford Glycobiology Institute, Department of Biochemistry, University of Oxford/ the School of Biological Sciences, Faculty of Environmental and Life Sciences, University of Southampton, and Prof. Thomas Bowden's laboratory at the Division of Structural Biology, Wellcome Centre for Human Genetics, University of Oxford between 2016 and 2020.

I, Yasunori Watanabe, declare that all the work presented here is my own, with the following exceptions. A number of recombinant proteins were provided by collaborators, as detailed in Table 2.1. The evolutionary analyses of Lassa virus and coronavirus glycoproteins were performed by Dr Jayna Raghwani (University of Oxford). The imaging of the Lassa virus VLPs was performed by Dr Sai Li (University of Oxford). The comparative cryo-EM analysis of the glycan shields of SARS-CoV-1 and HIV-1 was performed by Dr Zachary Berndsen in Prof. Andrew Ward's lab (The Scripps Research Institute). Neutralization assays of H3N2 influenza viruses with 2G12 were carried out by Dr David Lee in Prof. Ian Wilson's lab (The Scripps Research Institute).

The introduction of this thesis is based on my first-author review in *Biochimica et Biophysica Acta - General Subjects* titled "Exploitation of glycosylation in enveloped virus pathobiology". Chapter 3 is based on my paper in *Proceedings of the National Academy of Sciences*, titled "Structure of the Lassa virus glycan shield provides a model for immunological resistance". Chapter 4 is based on my papers in *Science* and *Nature Communications*, titled "Site-specific glycan analysis of the SARS-CoV-2 spike" and "Vulnerabilities in coronavirus glycan shields despite extensive glycosylation", respectively. Chapter 5 is based on my joint first-author paper which has been submitted to

Host Cell & Microbe titled “Anti-HIV-glycan antibody 2G12 broadly neutralizes human H3N2 influenza viruses during natural evolution of the hemagglutinin glycan shield”.

A full list of publications to which I have contributed throughout my DPhil is provided in Appendix C. This work has not been submitted for another degree at this, or any other university.

Word count (excluding references): 36,000

Table of Contents

Acknowledgements **6**

Abstract **7**

1. Introduction – Glycosylation in enveloped virus pathobiology **8**

1.1 Glycoprotein folding and trafficking 17

1.2 Glycosylation in viral release 19

1.3 Immune evasion using secreted and shed viral glycoproteins 20

1.4 Immune evasion by molecular mimicry and glycan shielding 23

1.4.1 HIV-1 envelope glycoprotein 24

1.4.2 Influenza hemagglutinin 25

1.4.3 Coronavirus spike protein 26

1.4.4 Lassa virus glycoprotein complex 27

1.4.5 Ebolavirus glycoprotein 28

1.4.6 Nipah virus fusion protein 29

1.5 Glycans as attachment factors and enhanced uptake by immune cells 31

1.6 Host glycans as attachment factors 35

1.7 Soluble lectins of the innate immune system and complement activation 38

1.8 Glycans as antibody epitopes 40

1.8.1 HIV-1 envelope glycoprotein 40

1.8.2 Dengue virus envelope protein 41

1.9 Concluding remarks 42

1.10 Mapping the glycan shields of enveloped viruses 43

2. Materials and Methods **44**

2.1 DNA plasmids constructs 44

2.2 Recombinant protein expression and purification 44

2.2.1 Recombinant protein expression in HEK cells 45

2.2.2 Expression and purification of LASV VLPs 45

2.2.3 Ni^{2+} affinity purification 46

2.2.4 Size-exclusion chromatography 46

2.3 Analysis of total glycan profiles and compositions 46

2.3.1 In-gel release of N-linked glycans 46

2.3.2 Fluorescent labelling of N-linked glycans 47

2.3.3 HILIC-UPLC analysis 47

2.3.4 Glycosidase digestions of labelled glycans 47
2.3.5 Ion-mobility mass spectrometry analysis of released N-linked glycans 48
2.4 Site-specific glycan analysis 48
2.4.1 Reduction, alkylation and proteolytic digestion 48
2.4.2 Liquid chromatography-mass spectrometry of glycopeptides 49
2.5 Immunoassays 52
2.5.1 Enzyme-linked immunosorbent assay (ELISA) 52
2.5.2 Western blot 52
2.6 Model building 52
2.7 Clustering analysis of viral glycan shields 53
3. The structure of the Lassa virus glycan shield provides a model for immunological resistance 54
3.1. Glycan processing of trimeric LASV GPC 56
3.2. Structural clustering of under-processed glycans on the GPC 61
3.3. Amino acid sequence diversification occurs at antibody-accessible sites on the GPC 66
3.4. Glycosylation of Lassa virus immunogens 70
3.5 Discussion 73
4. Vulnerabilities in coronavirus glycan shields despite extensive glycosylation 76
4.1 Glycan Processing of Trimeric SARS and MERS Spike proteins 79
4.2 Structural Clustering of Underprocessed Glycans on MERS S. 81
4.3 Sequence Diversification Occurs at Antibody-accessible Regions of CoV spikes 86
4.4 Visualising the HIV-1 and SARS glycan shields by cryo-EM 89
4.5 Comparison of Viral Glycosylation Reveals Disparate Shielding Efficacies 91
4.6 Site-specific glycan analysis of the SARS-CoV-2 Spike 94
5. Anti-HIV-glycan antibody 2G12 broadly neutralizes human H3N2 influenza viruses during natural evolution of the hemagglutinin glycan shield 107
5.1 N-linked glycosylation sites accumulate on human H3N2 HA during evolution 108
5.2 2G12 broadly neutralizes human H3N2 viruses from the past thirty years 109
5.3 Oligomannose-type glycans are enriched on the HA head in more recent H3N2 viruses 111
5.4 The glycoform at N165 depends on the presence of N246 115
5.5 Structural analysis of the 2G12 neutralization mechanism 117
5.6 Discussion 120
6. Concluding remarks 125

List of Abbreviations **127**

Appendix A: Signature of antibody domain exchange by native mass spectrometry and collision-induced unfolding **130**

Appendix B: Glycan analysis of class II viral fusion proteins **147**

B.1. Glycan variation of eastern equine encephalitis virus expressed in insect vs mammalian cell lines 147

B.2. Mapping the site-specific glycosylation of recombinant Dengue and Zika antigens used in serological monitoring 149

Appendix C: List of publications **162**

References **164**

Acknowledgements

I am deeply grateful to all those who have helped and supported me throughout my DPhil. Firstly, I would like to thank Prof. Max Crispin for welcoming me into his lab and for his invaluable guidance over the years. If only he were as good at chess as he is at supervision.

I would also like to thank Prof. Thomas Bowden for co-supervising me and hosting me in my second year in his lab. I enjoyed my time there and learned a great deal from him.

I am grateful to everyone at the Oxford Glycobiology Institute for making it such a welcoming and friendly place to work at the start of my DPhil, particularly Prof. Raymond Dwek, Prof. Nicole Zitzmann and Dr. Mark Wormald. I would also like to specifically thank Prof. David Harvey for sharing his endless expertise regarding mass spectrometry and for his patient teaching. I must also thank Snezana for her guidance and patience with me.

A huge thank you to everyone in the Crispin Group, past and present: Lan, Anna, Weston, Kirstin, John, Charlie, Hannah, Lydia, Al, Abi, Himanshi, and Maddy. Also, thanks to Rhys, Alice, Rob, Vicky, Liz, Serban, Ilona, Max, Helen, and Weng in STRUBI who made it such an inviting place to work.

A particular mention must go to Joel and Gemma; you've made these 4 years incredible.

両親え感謝の気持ちを伝えるのはたぶん無理だけど、今までサポートされて本当にありがとうございました。つらい時もあったけど、何と無くよく行きましたね。マー君もありがとうな。

Abstract

Glycosylation is a ubiquitous post-translational modification responsible for a multitude of crucial biological roles. As obligate parasites, viruses exploit host-cell machinery to glycosylate their own proteins during replication. Viral envelope proteins form a myriad of human pathogens including HIV-1, influenza virus, Lassa virus, coronaviruses, Zika virus, dengue virus, and Ebola virus have evolved to be glycosylated to varying degrees. These host cell derived glycans facilitate diverse structural and functional roles during the viral life-cycle ranging from aiding glycoprotein folding to enhancement of immune cell infection. As the primary focus of the humoral immune response, vaccine development efforts often concentrate on the viral glycoproteins that protrude from the virion envelope.

This thesis primarily focuses on immune evasion of viruses by molecular mimicry and glycan shielding. The work presented here reveals how viral glycan shields from evolutionarily distinct pathogens share conserved features, namely clusters of underprocessed oligomannose-type glycans. Furthermore, this thesis explores how an anti-HIV-1 antibody, 2G12, that targets oligomannose-type glycans cross-reacts and neutralises more recent influenza strains, as they have evolved to accrete *N*-linked glycosylation sites on their respective hemagglutinins, which result in the formation of oligomannose clusters. These findings provide a potential avenue for the development of a broad class of antivirals, that can target conserved features of viral glycosylation.

Comparisons of several viral glycan shields are also carried out which probes the rules governing glycan processing and the disparate efficacies of them. Given the prominence of *N*-linked glycosylation on viral glycoprotein surfaces, it is suggested that the compositional and structural data presented here can aid vaccine development and therapeutic efforts to combat these diseases.

1. Introduction – Glycosylation in enveloped virus pathobiology

The increasing emergence of infectious diseases, particularly those caused by viral infections, constitutes a significant threat to global health (*1*). Numerous enveloped viral pathogens, have evolved to take advantage of host-cell processes, including glycosylation pathways, to decorate the surface of their proteins with "self" glycan moieties. The analysis of viral glycosylation across different families has revealed significant variation in the structure, density and conservation of glycans. Understanding the endogenous functionality and the immunological basis driving viral diversity has the promise of guiding the development of the next generation of vaccines and anti-virals. In the introduction, I discuss the varying roles that glycosylation plays in the viral lifecycle and host immune responses to infection.

Viral glycosylation has been investigated in the context of a number of envelope glycoproteins, including the envelope glycoprotein (Env) of human immunodeficiency virus-1 (HIV-1) (*2–4*), hemagglutinin glycoprotein (HA) of influenza virus (*5–7*), coronavirus glycoprotein spike (S) (*8–10*), glycoprotein (GP) of Ebola virus (*11*, *12*), glycoprotein complex (GPC) of Lassa virus (LASV) (*13*), envelope (E) glycoprotein of dengue, Zika, and other flaviviruses (*14*, *15*). However, glycosylation on viruses is not limited to envelope glycoproteins. Many secreted viral proteins present glycans which are necessary for their respective functions, such as the non-structural protein-1 (NS1) of flaviviruses (*16*), the secreted GP of Ebola (*17*), and the secreted glycoprotein G (sgG) of herpes simplex virus (HSV) (*18*).

Protein-displayed glycosylation is fundamental to a wide range of molecular and cellular processes, which can be divided according to intrinsic and extrinsic functions (*19*, *20*). Intrinsic functions are based upon the intramolecular properties of glycoproteins, while

extrinsic functions result from modulation of intermolecular interactions of glycoproteins with glycan-binding partners, such as lectins and antibodies. While several forms of glycosylation occur in nature (*21*, *22*), here, I focus on the intrinsic and extrinsic functions of N-linked and mucin-type O-linked glycosylation, which are the most relevant in viral pathogenesis (**Figure 1.1**). N-linked glycosylation occurs on asparagine residues of Asn-X-Ser/Thr sequons, where X is any amino acid except proline. Viral proteins are glycosylated by the host-cell as viruses are able to hijack cellular glycosylation. In addition, as the presence of glycans are genetically encoded, glycosylation and can be under significant selective pressure from factors such as immune evasion, and functioning in glycoprotein folding and assembly (*23*). The initial step of N-linked glycan biosynthesis involves the covalent *en bloc* attachment of the N-linked glycan precursor onto an asparagine residue of a nascent polypeptide chain by oligosaccharyltransferase (OST) early in the endoplasmic reticulum. From this point, other glycan processing enzymes trim down and subsequently build up the glycans, resulting in a potentially vast assortment of different classes of glycans such as: oligomannose, hybrid, and complex-type N-glycan structures (**Figure 1.1.B**). It is important to note that in the context of viruses, glycosylation pathways may not be strictly linear and it is evident that some viral particles bud off early/translocate in the glycosylation pathway, which may account for the presence of unusual glycans on some viral glycoproteins (*24*, *25*). Furthermore, it is known that many viral glycoproteins do not follow the classical secretion pathway but can, for example, traffic directly from the ER to the plasma membrane bypassing glycan maturation in the Golgi apparatus. This particular route is exhibited by HCV and yields viral populations that are dominated by oligomannose-type glycans (*26*).

The existence of non-classical secretion routes also has important experimental implications. For example, the Env glycoprotein from HIV-1 pseudoviruses exhibit unusually elevated levels of oligomannose-type glycans compared to those of infectious virus produced in peripheral blood mononuclear cells (*27*). This is likely due to deviations away from a native-like virus budding pathway in the pseudoviral system (*3*, *28*, *29*). The cellular basis of these effects are not entirely clear; however, it is known that virus budding can compromise native membrane integrity (*30*). If variations in budding routes are apparent in experimental systems, it is likely that virus biology, and its associated glycosylation, is heterogeneous in the setting of a native infection.

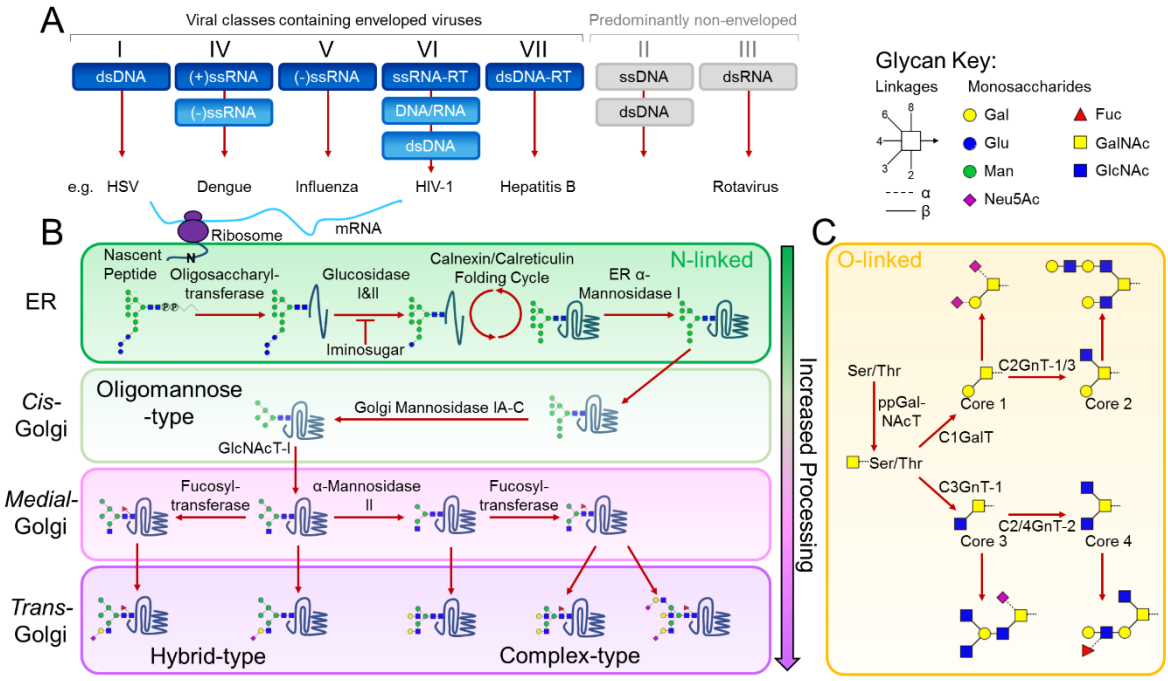


Figure 1.1: Glycosylation of a viral glycoprotein in the classical mammalian N-linked and mucin-type O-linked pathways. (A) Viral classes containing predominantly enveloped and non-enveloped viruses are coloured in blue and grey, respectively. Although not enveloped, viruses such as rotaviruses can also exploit the host-glycosylation pathways to modify their proteins. **(B)** Following mRNA synthesis, the mature tri-glucosylated N-linked glycan precursor, dolichol-P-P-glycan, is co-translationally transferred en bloc by oligosaccharyltransferase to the asparagine residue of an Asn-X-Ser/Thr sequon on a nascent polypeptide chain. Following transfer of the precursor glycan to the protein, glucosidases in the ER remove the three glucose residues while the protein folds in the Calnexin/Calreticulin cycle. A series of ER and Golgi mannosidases subsequently cleave mannose residues down to the Man5GlcNAc2 glycan. The action of GlcNAc transferase-I (GlcNAcT-I) initiates the first branch of the N-glycan. Once α-Mannosidase II removes the two remaining outer mannose residues, other glycan processing enzymes such as galactosyl-, fucosyl- and sialyl-transferases, can act to construct a huge assortment of complex-type glycans. **(C)** Mucin-type O-linked glycosylation pathways is initiated by a family of ppGalNAc transferases that covalently link a N-acetylgalactosamine (GalNAc) monosaccharide to any serine, threonine and tyrosine residue. Following this conjugation, a series of glycosyltransferases can act upon the primary GalNAc residue to generate the four common O-linked glycan cores. Each of these cores can be extended and processed further to generate numerous mucin-type O-linked glycans. Glycans are presented using Consortium for Functional Glycomics symbolic nomenclature and Oxford system linkages (*31*), as per the key.

In mucin-type O-linked glycosylation, serine, threonine and tyrosine (*32*) residues are covalently linked to a GalNAc residue by polypeptide-N-acetylgalactosaminetransferases (ppGalNAcT) to form the so called ‘Tn antigen’. There is

a total of 8 mucin-type O-glycan cores, with 4 common core structures (cores 1-4), each of which can be processed further as proteins pass through the Golgi apparatus (**Figure 1.1.C**). Unlike N-linked glycosylation, which is identifiable by a specific amino acid sequon, no such simplicity has been identified for O-linked glycosylation, most likely due to differential peptide substrate preferences of multiple ppGalNAcTs. However, O-linked glycosylation in mucin-like domains can be detected by their high levels of serine, threonine and proline residues (*33*, *34*), and more recent developments have improved prediction of individual O-linked glycosylation sites in non-mucin-like domains (*33*, *35–37*). As such, the heterogeneous occupancy and composition of O-linked glycosylation constitutes a major challenge in studies of glycan structure and function. A number of viral proteins, notably Ebola GP and sGP (*38*), Herpes simplex virus gC protein (*39*), and respiratory syncytial virus G protein (*40*) contain mucin-like domains with high populations of serine and threonine residues, that are heavily modified by mucin-type O-linked glycans.

Whilst most known viruses typically utilise the N- and O-linked host-cell glycosylation pathways to adorn their glycoproteins with carbohydrate modifications, it is important to mention known exceptions. There are a few notable examples of viruses that encode some, if not all, of the enzymes involved in the glycosylation of their proteins and other macromolecules such as, chloroviruses and mimiviruses (*41–44*).

The characterization of N- and O-linked glycans has presented a particular analytical challenge due to the extraordinary heterogeneity and complexity arising from the number of glycan processing enzymes residing in the ER and Golgi apparatus. However, coincident with the advent of potent mass spectrometric and chromatographic techniques and the commercial availability of recombinant glycosidases, investigation of these post-translational modifications has become more feasible (*45*). These advances have enabled

experimental approaches including matrix assisted laser desorption ionisation (MALDI) and electrospray ionisation (ESI) mass spectrometry, allowing characterization of viral glycome (i.e. the carbohydrate repertoire of a specific viral protein in isolation or as presented by the pathogen). More recently, with the augmentation of biophysical techniques, namely in-line liquid chromatography mass spectrometry (LC-MS) (*46*), it has been possible to define the exact glycan structure presented at individual glycosylation sites (*47*). Additionally, investigation of carbohydrate-protein interactions has been aided by the development of glycan microarrays capable of screening the carbohydrate specificity of glycan-binding proteins to immobilized and pre-defined glycan structures (*48*, *49*). Furthermore, advances in computational biology and sequencing technologies have also provided crucial understanding of the evolution of viral glycosylation (*50*, *51*). These bioinformatics approaches can allow greater prediction and understanding of how viruses evolve to utilise glycosylation.

Given that any particular cell exhibits a specific portfolio of glycan processing enzymes, the cellular origin of viral replication has a potential to significantly influence viral glycosylation (*52*). Similarly, any multicellular target host will display a range of tissue-specific glycosylation that will potentially influence viral tropism (*53*). At one extreme, glycosylation can be qualitatively different across different species and this is an important feature of zoonosis of envelope viruses when considering the potential impact of host immunity on transmission. Many human pathogens are zoonotic viruses with animal reservoirs and although the mammalian N-linked glycan pathway is largely well-conserved (*54*), several key differences can impact the antigenicity of the virus (*55*). For example, humans lack the galactose-α-1,3-galactose epitope that are a common structure at the terminals of mammalian glycans (*56*) and antibody-based immunity against these epitopes

can limit cross-species viral infectivity (*57*). Similarly, O-linked glycans and glycolipids can exhibit pronounced compositional differences across species. At the other extreme, these immunological effects of host-specific protein and lipid glycosylation can also influence the spread of viruses within a species. Such glycan differences are evident within the human population as the ABO blood group system, with people of blood group A and blood group B expressing a fucosylglycoprotein α-N-acetylgalactosaminyltransferase and fucosylglycoprotein galactosyltransferase, respectively (*58*). The presence of antibodies against the glycan structures of foreign blood groups, for example anti-A present in a blood group B individual, can limit viral transmission from a blood group B to blood group A individual. These effects have been documented in the infectivity of HIV-1 (*59*) and other viruses (*60*), and the distribution of blood groups may be a selective pressure shaping the presence and distribution of viral spread (*60*). Similarly, the targeting of specific blood groups as attachment factors in both viral and bacterial entry may also influence prevalence of particular viral strains based on the frequency of blood groups within a population (*61*).

Tissue-specific glycosylation is also a key determinant of interspecies viral transmission potential and can lead to targeting of vulnerable tissues within a host (*61*). For example, the capacity of the avian influenza HA to interact with both α2,3- and α2,6-linked sialic acid has been shown to facilitate spill-over of the virus from birds to humans (*53*, *62*, *63*). In addition, differential expression of these sialic acid structures between the upper and lower respiratory tracts in humans can shape the distribution of influenza infection within an individual (*64*, *65*).

The presence and distribution of glycan specific cell surface lectins together with the host-specific viral glycosylation also influence transmission. For example, in the zoonosis of insect-borne virus to mammals, the founder virus will display features specific to

invertebrate glycosylation whilst subsequent virions manufactured in the new host will contain mammalian glycosylation. Thus, viral glycosylation undergoes a switch at zoonosis that will influence the interaction with immunological receptors and responses which will also influence viral tropism. Invertebrates display chiefly paucimannosidic structures (*66*), thus for insect-borne diseases such as Dengue and Zika, these structures may affect lectin-utilisation, infectivity, and tropism depending on the origin of viral replication.

Overall, it can be extremely important to consider the cellular biosynthetic origins of viruses, both naturally and in experimental systems. In this introduction, I survey the wide-ranging factors shaping the presence and processing of viral glycosylation and the role glycosylation plays in viral pathogenesis (**Figure 1.2**).

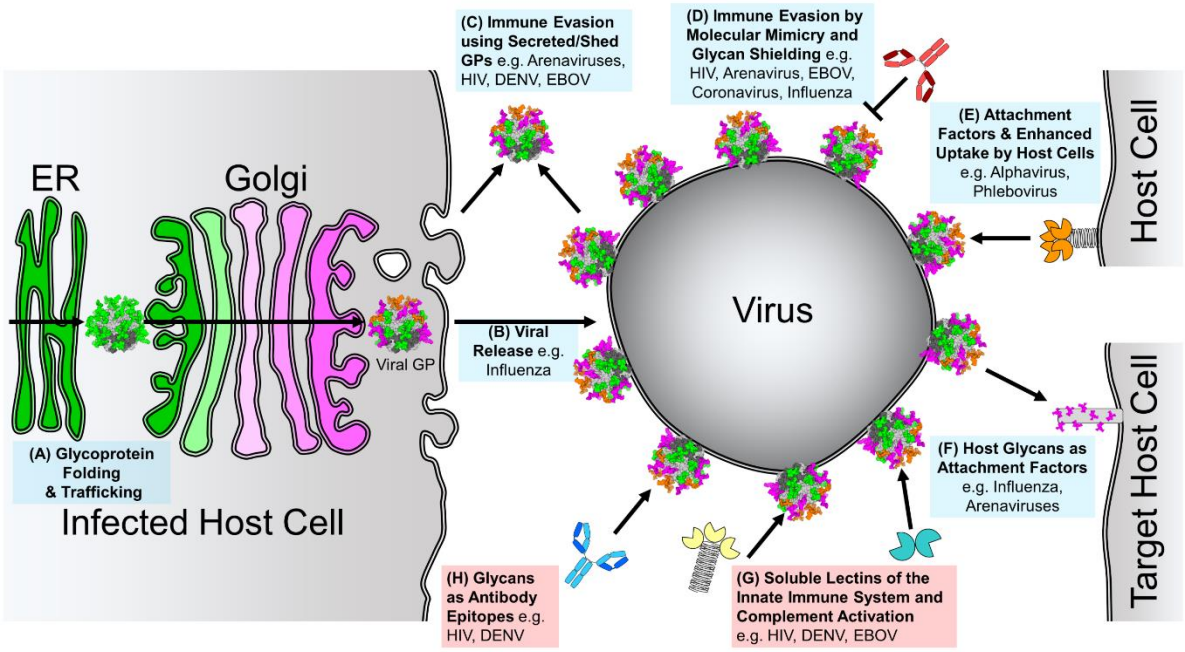


Figure 1.2. Roles of Glycosylation in Viral Pathogenesis. The roles contributing to viral pathogenesis and host-cell strategies used to respond to viral infection are coloured blue and red, respectively. Green and pink indicate oligomannose and complex-type N-linked glycan processing states, respectively. **(A)** Glycoprotein Folding and Trafficking. As with all glycoproteins, glycans on viral glycoproteins aid in folding and trafficking through the host secretory pathway. **(B)** Glycosylation in Viral Release. Glycosylation of infected host cell proteins can influence viral spread. **(C)** Immune Evasion Using Secreted/Shed Glycoproteins. Viruses can shed or secrete glycoproteins to act as immune decoys. **(D)** Immune Evasion by Molecular Mimicry and Glycan Shielding. Extensively glycosylated viral proteins shield themselves from the host immune response by occluding the immunogenic proteinous surface with a dense coat of host-derived glycans. **(E)** Glycans as Attachment Factors and Enhanced Uptake by Immune Cells. Some virus envelope-displayed glycoproteins contain under-processed oligomannose-type glycans that function as host-cell attachment factors to augment or facilitate infection of immune cells. **(F)** Host Glycans as Attachment Factors. Viruses can recognise glycans presented on host cell-surface proteins to facilitate host cell attachment. **(G)** Soluble Lectins of the Innate Immune System and Complement Activation. As under-processed glycans are rarely presented on mature host cell glycoproteins (*67*, *68*), the innate immune system is able to recognise these glycans as pathogen-associated molecular patterns (PAMPs) using soluble lectins. **(H)** Glycans as Antibody Epitopes. Where glycan shielding is conserved on viral glycoproteins, it is possible for the humoral immune response, in rare cases, to elicit neutralising antibodies that target sugars as part of their epitopes.

1.1 Glycoprotein folding and trafficking

One of the most crucial roles of protein glycosylation is its effect on glycoprotein folding, structure, sorting, trafficking, and stability (*69*). Glycans can be structurally integrated into the protein fold and exhibit significant glycan-protein interactions to stabilise the protein, for example by increasing the solubility of proteins and interacting with surface hydrophobic residues. In addition, glycans can also assist glycoprotein folding by mediating chaperone interaction during biosynthesis (*70*).

Glycoprotein maturation in the ER requires the stepwise removal of the two terminal glucose residues of the N-linked glycan precursor, by ER α-glucosidases I and II, to leave the monoglucosylated precursor. ER chaperones, calnexin and calreticulin, bind to this substrate glycan to sequester the glycoprotein in the ER such that the protein is able to properly fold. Once correctly folded, the chaperones are released and alpha-glucosidase II cleaves off the final glucose residue; if the glycoprotein at this stage is properly folded, it is processed further and exported to the Golgi apparatus for further modification. Conversely, if the glycoprotein is incorrectly assembled, it is re-glucosylated by UDP-glucose:glycoprotein glucosyltransferase (UGGT), resulting in the glycoprotein being chaperoned once more. This feedback loop acts as a quality control mechanism ensuring that solely correctly folded glycoproteins exit the ER.

Due to this dual effect on protein folding, it can be difficult to determine the contribution of any single glycan to glycoprotein folding and assembly. However, comprehensive mutagenesis studies of individual N-linked glycosylation site knockouts of several viral glycoproteins, and direct biophysical analysis of glycan-protein interactions, have demonstrated their reliance on the host's translational machinery for correct protein folding, and thereby pathogenesis (*14*, *16*, *71–78*). For example, the importance of N-linked

glycosylation on HIV-1 Env protein folding and stabilization has also been investigated thoroughly, including a study that systematically dissected the role of each N-linked glycan site, which highlighted integral glycans necessary for correct gp160 incorporation into virions (*79*, *80*). This effect seemingly arises due to misfolding of trimeric Env, preventing efficient secretion and display on the viral surface, highlighting crucial roles for specific N-linked glycans (*79–82*).

Due to the importance of protein folding for viral protein function, certain sugar mimetics, namely iminosugars, have been investigated for their antiviral activity. Iminosugars, such as NB-DNJ, inhibit ER α-glucosidase activity, resulting in the generation of unfolded, non-functional viral glycoproteins (**Figure 1.1.B**). The antiviral activity of iminosugars has been tested on a diverse spectrum of viruses including HIV (*83–85*), influenza viruses (*86*, *87*), Ebola virus (*88*), arenaviruses (*89*), and flaviviruses (*90–92*). A variety of iminosugar compounds have been shown to potently inhibit the release of infectious virion particles and the number of infected cells (*93*). The inhibition of Dengue pathogeny by these compounds demonstrates the importance of glycosylation in Dengue glycoprotein folding and virulence. Despite these promising antiviral properties, iminosugars have yet to be clinically approved for antiviral indications. One barrier to their clinical application at the concentrations required to treat viral infections, such as HIV, appears to be the off-target effects of the drug which impede host gut glucosidases leading to diarrhoea and abdominal pains (*85*). However, further derivatives are being investigated that may increase anti-viral specificity (*94*).

As per N-linked glycosylation, O-linked glycosylation has also been shown to be crucial for efficient viral particle formation and infectivity. In the case of HSV-1, which possess eight structural glycoproteins featuring O-linked glycosylation, viral expression in

a cell line that only displays truncated Tn and sialylated Tn antigens resulted in severely reduced viral titres (*35*). Whilst the exact mechanisms are yet to be elucidated, it is conceivable that correct processing and elongation of O-linked glycosylation is integral for either viral glycoprotein trafficking, stability and viral particle formation, or infectivity (*35*). N-linked glycosylation of HSV-1 glycoproteins have also been shown to play a significant impact in intracellular trafficking and folding (*78*). I direct readers to the review by Bagdonaite et al. which covers glycosylation of herpesviruses thoroughly (*95*).

1.2 Glycosylation in viral release

Viral replication and infectivity do not always solely rely upon glycosylation of viral proteins, but also that of host-cell proteins. Some viruses utilise host glycans as receptors and attachment factors (**Figure 1.2.F**), however these same interactions can impede viral budding from the infected cell. Consequently, such viruses have evolved carbohydrate-cleaving enzymes to facilitate efficient viral budding and release. The most notable example is the ability of neuraminidases of influenza viruses to cleave sialic acid residues on the host cell surface to negate the ability of hemagglutinins (HA) to bind the host-cell receptor sugars (*96, 97*). During virus budding at the cell membrane, HA spikes continue to bind virion particles to sialic acid residues on the cell surface until the sialidase activity of NA removes the terminal sugar residue. Additionally, NA cleaves sialic acid residues from the glycoproteins on the virus envelope itself and enhances infectivity by preventing aggregation of virus particles (*98*). Furthermore, NA is thought to act upon sialic acid residues on mucins to gain access to epithelial cells, potentially playing a secondary role in aiding virus entry to host cells (*99*). Interestingly, a variety of paramyxoviruses, including mumps (*100*), parainfluenza (*101*), and Newcastle disease (*102*) viruses possess hemagglutinin-neuraminidase (HN) glycoproteins as attachment proteins that possess the

capability to both bind and cleave sialic acid residues. These viral glycoproteins that play an integral role in determining host and cellular tropism can often be useful in classifying new and emerging paramyxoviruses based on their structural conservation (*103*).

A variety of therapeutics have been developed to mimic sugars to bind to the relatively deep sugar binding site of NA (compared to HA) to combat influenza virus infection. These NA-inhibitors are most commonly N-Acetylneuraminic acid (Neu5Ac) derivatives, which competitively inhibit NA activity (*104*). Additionally, structure-based development of competitive inhibitors against the glycan binding sites of HN glycoproteins have been explored (*102*, *105*).

Beyond the role of NA in viral release, this viral glycoprotein has emerged as a focus in vaccine development. Current influenza vaccines poorly display NA epitopes that do not produce anti-NA antibodies (*106*), whilst during infection many NA-reactive B cells and antibodies are produced. The development of recombinant influenza vaccines, which improve or remove the display of influenza NA, may provide a novel method of vaccine optimisation to improve targeting of NA for broader protection against divergent influenza strains circulating in human populations (*106–108*).

1.3 Immune evasion using secreted and shed viral glycoproteins

Shedding or secretion of viral glycoproteins constitutes an important stratagem employed by some viruses to misdirect the humoral immune response. This can either occur by absorbing neutralising antibodies or by modulating the immune response to target non-neutralising epitopes. The GP gene of Ebola virus contains a poly-U stutter region that drives transcriptional frame-shifting that generates three glycoproteins: a dimeric secreted GP (sGP) that accounts for approximately 75% of transcripts, the full-length membrane-bound fusion protein (GP) accounting for ~25% of transcripts, and trace levels of a small soluble

GP (ssGP) (*17*, *109*). Whilst the function of ssGP is yet unknown, sGP that is secreted by infected cells has been associated with viral immune evasion by acting as an antibody decoy (*17*). Ebola sGP has been found to "antigenically subvert" the immune system, wherein sGP redirects the humoral immune response to target epitopes shared with the full-length GP. The study by Mohan et al. also demonstrated that sGP also subverts the host immune response of mice previously immunised against Ebola GP (*17*). As the major antigenic transcript, most antibodies isolated from Ebola survivors and macaques are directed towards sGP rather than GP (*110*, *111*); importantly these antibodies are likely to be non-neutralising and the neutralising antibodies elicited against GP may cross-react and be absorbed by the more abundant sGP (*112*). The extent to which mimicry of the glycan component of GP by sGP contributes to the overall antigenic mimicry in immune decoy functions is unknown. However, given both that glycans have been shown to contribute to epitope formation on sGP/GP (*113*), and that there is congruence in their glycan processing (*11*), glycans are likely to be an important component of these functions.

Shedding of attachment glycoprotein subunit (GP1) of LASV has also been observed during acute Lassa fever in humans (*114*, *115*). Whilst the exact function of shed GP1 is yet to be elucidated, it has been proposed that it may act as an immunological decoy in a manner akin to Ebola sGP. In the case of LASV, the soluble GP1 structure (*116*) undergoes a major conformational change compared to the trimeric spike (*117*), further highlighting its potential function as an immune decoy, since shed GP1 will likely present immuno-dominant epitopes from a non-functional conformation eliciting non-neutralising antibodies against LASV. The conservation of such substantial structural rearrangements of isolated GP1 subunits from other Old World arenaviruses, such as Loei River (*118*) and Morogoro

virus (*119*) may highlight a conserved mechanism of immune evasion across these pathogens.

Dengue virus non-structural protein-1 (NS1) is an intriguing glycoprotein that is secreted from infected cells. NS1 exhibits two N-linked glycosylation sites that have been shown, via mutagenesis studies, to be essential for a number of crucial roles, including hexamer formation, facilitating secretion and modulating protein stability (*120*). NS1 binds to heparin sulphate and chondroitin sulphate glycosaminoglycans on the surface of various cells (*121*). NS1 has been shown to play a role in both viral replication (*122*) and immune evasion (*123, 124*), and it has been hypothesised that immune recognition of NS1 on endothelial cell surfaces may facilitate vascular leakage during severe Dengue infection (*125*). The use of secreted/shed GPs in order to subvert the immune system and/or enhance infectivity appears to be a common phenomenon utilised by viruses. Other examples include the secreted form of respiratory syncytial virus G glycoprotein, which distracts the antibody-immune response by acting as a decoy (*126*), and secreted BARF1 and soluble gp42 glycoproteins of Epstein-Barr virus, which interfere with macrophage differentiation and activation, and MHC class II-mediated antigen presentation respectively (*127, 128*).

Untethered monomeric gp120 subunits from HIV-1 Env can also arise due to improper processing of the spike or by gp120 shedding (*129*). These viral envelope fragments can divert the humoral immune response by exposing immunodominant protein epitopes not presented on functional Env proteins, thereby eliciting undesirable non-neutralising antibodies during HIV-1 infection (*129–131*). The role of non-neutralising epitopes in subverting the host immune response, away from neutralising epitopes, is an important consideration in vaccine development, and has stimulated the development of immunogens that closely mimic the native states of the HIV viral spike (*131, 132*).

1.4 Immune evasion by molecular mimicry and glycan shielding

Many viruses, including HIV-1, influenza, LASV, coronaviruses, and Ebola have evolved to shield their respective envelope glycoproteins with host-derived glycans to prevent antibody recognition of the underlying protein surface. The importance of N-linked glycosylation of envelope proteins, with respect to immune evasion, has been observed across many viruses including: Hepatitis C (*133*, *134*), Hepatitis B (*135*), Hendra (*136*), Newcastle Disease (*137*) and Herpes Simplex virus (*138*, *139*). Some class I fusion proteins exhibit particularly high densities of glycans, consistent with their role in shielding. In this thesis, I focus on the glycan shields of the trimeric class I fusion proteins from Influenza, Coronaviruses, and LASV (**Figure 1.3**).

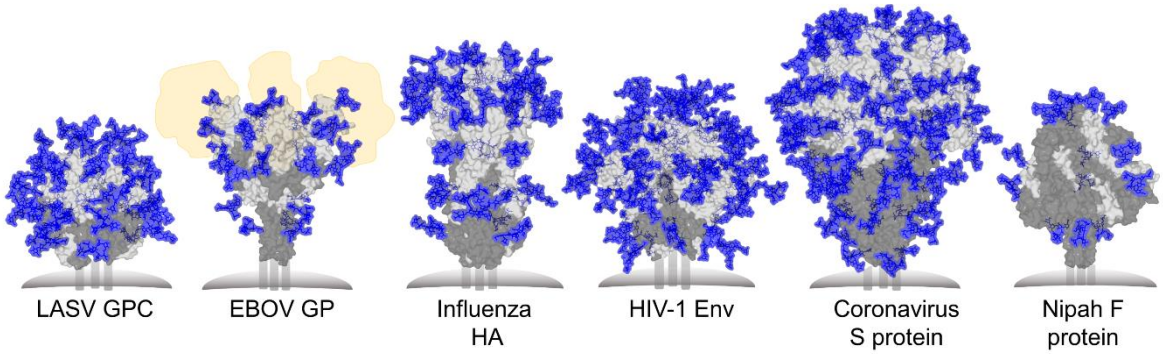


Figure 1.3. Glycan Shielding of Viral Class I Fusion Proteins. Left to right: Glycan shield models of LASV GPC (PDB ID: 5VK2) (*117*, *140*), Ebola GP (PDB ID: 5JQ3) (*141*), A/H3N2/361/Victoria/2011 H3N2 Influenza virus hemagglutinin (PDB ID: 4O5N) (*7*, *142*), BG505 SOSIP.664 HIV-1 Env (PDB ID: 4ZMJ) (*3*, *143*), human coronavirus-NL63 (HCoV-NL63) S protein (PDB ID: 5SZS) (*8*), Nipah F protein (PDB ID: 5EVM) (*144*). Glycans and proteins are shown in blue and grey, respectively. The fusion protein subunit is shown in dark grey. The positions of mucin-like domains of Ebola GP are shown in yellow. Most predominant sugar compositions were modelled onto each N-linked glycan site, using pre-existing GlcNAc residues if possible, with $Man_5GlcNAc_2$ modelled on if compositional information was lacking.

1.4.1 HIV-1 envelope glycoprotein

One of the best characterised glycan shields is that of HIV-1 Env, which is the sole viral glycoprotein found on the virus surface (*145*). Mature Env exists as a trimer of non-covalently associated gp120-gp41 heterodimers that are generated by furin cleavage of a gp160 polypeptide precursor (*146*). The gp120 receptor binding subunit facilitates host cell tropism and attachment to CD4 receptor and CXCR4/CCR5 co-receptors, while gp41 facilitates viral and host cell membrane fusion upon receptor binding by gp120, and the extensive conformational changes of Env that follow. HIV-1 Env presents between 18-33 glycans per gp120 monomer, with a median of 25 glycan sites on gp120 and 4 glycans on the gp41 subunit (*23*). The extent of these post-translational modifications, combined with the intrinsic flexibility of the trimeric Env (*147*, *148*) and constant evolution of the glycan shield, renders HIV-1 Env an immunologically challenging target (*149*, *150*). The result of the dense glycosylation on the viral protein surface leads to the formation of the so-called intrinsic and trimer associated mannose-patches (IMP and TAMP, respectively) (*151–155*), which arises due to the steric blocking of glycan-processing enzyme in the ER and Golgi apparatus by neighbouring glycans (*156*). These often under-processed glycans are weakly immunogenic, since they are produced by the host-processing pathway, thereby limiting the response to deviating glycosylation (*157*). Astoundingly, in the case of HIV, the conservation of these under-processed glycans can elicit broadly neutralising antibodies (bnAbs) that actually target these immunoquiescent host-derived glycans as part of their epitope (*158–163*). As more bnAbs have been discovered, it has become clear that they can not only recognise the viral mannose patches, but some have also evolved to recognise complex and hybrid-type glycans (*164*). However, since bnAbs only develop in a subset of patients, and only after several years, underscores the fact that the glycan shield of HIV-1 has evolved under sustained immunological pressure, and represents an extreme challenge

for the immune system and an important consideration in vaccination strategies (*145*, *158*, *165–168*).

1.4.2 Influenza hemagglutinin

Considerable antigenic evolution enables the persistence and spread of influenza virus in human populations (*169*). The surface glycoprotein HA exists as a trimer of hetero-dimers that is synthesised as a single polypeptide (HA0) that is subsequently cleaved into the receptor binding HA1 domain and the membrane-fusion mediating HA2 subunit by host cell proteases. Similarly to HIV-1 Env, HA is a class I viral fusion protein (**Figure 1.3**) and plays a vital role for viral entry by binding to host receptors via the receptor binding site (RBS) located on HA1. As the main focus of the immune response, HA evolves at the highest rate compared to other influenza viral proteins (*170*), and the presence and acquisition of N-linked glycosylation sites on HA plays a crucial role in immune evasion (*171*). The constantly evolving glycan shield of HA constitutes an important strategy to escape from natural immunity and mask neutralising epitopes (*172*). In 1968, H3N2 HAs possessed 6 N-linked glycosylation sites per protomer. Since then, H3N2 HAs have acquired and retained over twice as many sites, with current strains exhibiting approximately 13 PNGs per HA1-HA2 protomer (*7*, *171*). Similarly, from the Spanish flu in 1918 to its temporary departure from human circulation in 1957, H1N1 strains have incorporated between 1 to 3 N-linked glycan sites per HA1-HA2 protomer (*50*, *173*). Interestingly, the seasonal accumulation of glycans on HAs are most-commonly incorporated at the globular head domain (HA1), in regions of variability where the majority of antigenic sites lie (*174–181*), seemingly due to the preference of neutralising antibodies to target the RBS-proximal regions (*171*).

The accretion of N-linked glycans that occlude antigenic sites on HA can, however, affect HA binding to its receptor, particularly when they neighbour the RBS (*182*). This

functional constraint renders HAs not able to be completely shielded by glycans. Indeed, there appears to be a maximum number of N-linked glycosylation sites allowed on HAs at any one time, resulting in the replacement of non-conserved glycosylation sites with an alternative N-linked glycan sequon (*171*). In other words, the plateauing of the number of glycosylation sites on HAs appears to derive from a balance between functionality and immune evasion.

Despite the potential fitness cost of increased glycosylation sites, their presence has been shown to compensate for the fitness costs associated with other antibody escape mutations (*183*). Compositionally, although the total number of glycans present on HAs is significantly less than on HIV-1 Env, glycosylation analyses has revealed the abundance of oligomannose-type glycans at specific sites (*142*, *184*, *185*), indicating a restriction in glycan processing in potential areas of higher glycan density and shielding.

Glycan shielding of hemagglutinins from H3N2 influenza strains will be further discussed in Chapter 5.

1.4.3 Coronavirus spike protein

Epitope masking by glycosylation has also been observed on coronavirus spike (S) proteins (*8*, *186*). As with HIV-1 Env and influenza HAs, which use N-linked glycosylation to shield conserved CD4 (*187*) and sialic acid binding sites (*188*, *189*), respectively, coronaviruses appear to also occlude receptor binding domains by utilising N-linked glycans (*8*). The S proteins of coronaviruses are large glycoproteins with between 23-38 potential N-linked glycan sites per protomer. Glycan analysis performed by Ritchie et al. of severe acute respiratory syndrome (SARS) S protein revealed a significant population of oligomannose-type glycans (30%) (*10*). Furthermore, compositional analysis of the glycan shield of alpha- and delta-coronaviruses, expressed in Drosophila S2 cells, also displayed a wide variety of

oligomannose-type glycans in addition to fly-type paucimannosidic glycans (*8*, *9*). Whilst it is extremely likely that N-linked glycan sites on coronavirus spikes have been incorporated to occlude certain epitopes, it remains unclear how effective the glycan shield is at facilitating immune evasion, since antibodies that target S proteins are readily elicited (*190–192*). The sparsity of the glycan shield may be reflected in the overall oligomannose-type glycan proportions which is low (30%) (*10*) compared to the other "evasion strong" (*165*, *193*) viruses such as HIV-1, Influenza, and LASV (>50%) (*3*, *140*, *142*) indicating less dense glycosylation across the surface, permitting the processing of glycans by enzymes in the ER and Golgi apparatus, and allowing antibodies to target the protein surface. As with other viral glycoproteins, it appears that glycans surrounding the receptor binding sites can negatively impact functionality (*194*), suggesting that the slightly limited glycan shield of coronaviruses may result from the necessity to ensure efficient receptor binding.

Glycan shielding of coronavirus spikes will be further discussed in Chapter 4.

1.4.4 Lassa virus glycoprotein complex

LASV is a highly pathogenic arenavirus that causes severe haemorrhagic fever in humans. Arenaviruses are generally categorised as Old and New World pathogens, based on geographical, genetic, and antigenic properties (*195*). Both Old and New World Arenavirus GPCs are extensively glycosylated with a remarkable conservation of the glycosylation sequons (*13*, *140*, *196–198*). Arenaviral GPCs are expressed as a single polyprotein precursor that is proteolytically processed by subtilase SK-1/S1P and displayed as a trimer of tripartite protomers, with each protomer consisting of a receptor-binding GP1 domain, a class I membrane fusion GP2 domain, and a retained myristoylated stable signal peptide. The oft-inadequate antibody immune response elicited against arenaviruses has been, in part, attributed to the shielding of would-be antigenic epitopes by conserved N-linked glycans

(*13*). I have previously reported the composition and model of the LASV glycan shield, which comprises approximately 25% of the glycoprotein mass, revealing the extent of shielding across GPC, which consisted of a dense cluster of oligomannose-type glycans on the side of trimer (*140*). These N-linked glycans protect the vulnerable regions of the GPC, including the putative primary receptor, α-dystroglycan, binding site located at the trimer apex (*199*), the secondary receptor, LAMP-1, binding site (*116*, *119*, *200*), and regions across the GP2 glycoprotein including the fusion loop on the GP2 subunit (*117*). Further evolutionary analysis of LASV GPC revealed that residues with elevated nonsynonymous to synonymous substitutions (dN/dS) ratios co-localise to regions on LASV GPC with lower levels of glycan density. This provided a rationale for how the LASV glycan shield protects the proteinous surface from the humoral antibody response of the host (*140*). Additionally, it has been hypothesized that the Old World Loei River arenavirus GPC, which encodes two additional N-linked glycans on the GP1 subunit that are not observed on most other Old world arenaviruses may contribute to a more expanded oligomannose-type glycan cluster than that on LASV GPC (*118*). Nevertheless, with the conservation of N-linked glycosylation sites on arenaviral GPCs it seems extremely likely that the glycan shielding of the protein surface is conserved across the family to facilitate immune evasion.

Glycan shielding of Lassa virus GPC will be further discussed in Chapter 3.

1.4.5 Ebolavirus glycoprotein

Ebola virus is a highly virulent pathogen capable of causing severe haemorrhagic fever, in humans. The Ebola virus envelope surface glycoprotein (GP) also exhibits dense glycosylation, suggesting a role in immune evasion within its natural bat reservoir. Ebola GP is initially expressed as pre-GP that is cleaved by furin into two subunits, GP1 and GP2, which are associated by a disulphide bridge. This heterodimer assembles into a trimer,

mediated by extensive interactions between GP1-GP2 and GP2-GP2 subunits, on the surface of nascent virions to form mature Ebola GP that is solely responsible for receptor attachment, fusion and entry into target cells (*201*). Ebola GP is extensively glycosylated by approximately 17 N-linked glycosylation sequons per protomer, but also by an extensive mucin-like domain (**Figure 1.3**). Both the dense N-linked glycosylation (*112*, *202*, *203*) of Ebola GP and the extensive O-linked glycosylation of the mucin-like domain (*38*) has been shown to negatively impact immunogenicity by hiding immunogenic protein epitopes (*112*). Interestingly, antibodies elicited against the so called "glycan cap" and the mucin-like domain of Ebola GP have been characterised, although compared to antibodies that bind other epitope classes, such as the GP base, GP2-resident fusion-loop, and the GP1-head domain, neutralisation was compromised (*113*). It has been hypothesised that variation in neutralising potential within "glycan cap" and mucin antibodies may be due to heterogeneity in both N-and O-linked glycosylation processing states (*113*).

1.4.6 Nipah virus fusion protein

Glycan shielding of paramyxoviruses, such as Nipah virus, is influenced by the different protein architecture of this family (**Figure 1.3**), although a similar theme in immune evasion has been reported. Nipah virus is a deadly emerging paramyxovirus that infects host cells using two envelope glycoproteins; the attachment (G) protein that binds to cell receptors (*204*), and the fusion (F) glycoprotein that subsequently implements membrane fusion. Paramyxovirus F proteins, unlike the other class I fusion proteins, described above, do not participate in receptor binding and exhibit significantly varied protein architectures compared to other class I fusion proteins (*205*). However, they all share similarities in the utilisation of N-linked glycans in order to protect against the humoral immune response. Nipah virus F protein possesses 5 PNGs per protomer, which does not indicate the presence

of an extensive shield that occludes much of the protein surface, as exemplified in **Figure 1.3**. The lack of a dense glycan shield is likely related to the fact that the N-linked glycans on Nipah F protein reduces the efficiency of membrane fusion and viral entry (*206*), and that it is not necessary to maintain infection in natural bat reservoirs. Nevertheless, these carbohydrate moieties have been shown to protect virions from neutralisation by antibodies, suggesting a trade-off between the evolutionary advantage of increased protection against the immune system and the effects on protein functionality. As a surface-displayed protein, Nipah virus G protein is also under immunological pressure and N-linked glycans on the G protein have been shown to play a role in shielding virions against antibody neutralization (*207*).

Overall, immune evasion by glycan shielding and molecular mimicry by exploiting the host glycosylation pathway is a common feature observed on viral class I fusion proteins. One important consideration is understanding the potentially varied roles of glycan shields between the long-term residency within its natural reservoir versus its role in an outbreak following zoonosis. Regardless of these potential influences, the widespread use glycosylation as a tactic to thwart the response of the humoral immune system underscores the strong immune pressure to occlude immunogenic protein epitopes. Some of these viruses such as HIV-1, Influenza, and LASV appear to be "evasion strong" pathogens (*165*) that utilise varied mechanisms to change how immunogenic epitopes are presented on their respective envelope proteins, of which glycan shielding plays a critical role. However, shielding of the protein surface of the viral glycoprotein with glycans is not fool-proof, and can lead to evolution of anti-glycan antibodies and recognition by the host immune response; both innate and humoral.

1.5 Glycans as attachment factors and enhanced uptake by immune cells

Oligomannose-type glycans can both impede and facilitate viral propagation. On one hand, these glycans can trigger a sterilising innate immune response, for example by the activation of the complement cascade. On the other hand, viruses can exploit innate immune receptors such as dendritic cell-specific ICAM-3-grabbing nonintegrin (DC-SIGN) (*208–214*) to facilitate and/or augment infection. DC-SIGN possesses a C-type carbohydrate recognition domain (CRD) that co-ordinates a calcium ion in the primary subsite to facilitate the binding of oligomannose-type glycans found on viruses (**Figure 1.4.C**). DC-SIGN binds to the Manα1-3(Manα1-6)Manα tri-mannose structure found on oligomannose type glycans (*215*, *216*). Importantly, not all glycoforms can be bound by DC-SIGN; selectivity to oligomannose-type glycans is conferred by the presence of a phenylalanine side chain in the CRD that acts as a steric block obstructing the GlcNAc residues of N-linked glycan core, when a core mannose residue of a complex-type glycan attempts to bind (*216*). This selectivity to oligomannose-type glycans ensures that DC-SIGN interactions are predominantly with foreign pathogens, due to the rarity of oligomannose-type glycans expressed on correctly processed host glycoproteins (*67*, *68*).

The relative pro- and anti-viral effects of the presence of oligomannose-type glycans are specific to the viral pathogen. It is also important to note that the necessity of glycans as invasion factors can vary greatly, and whilst a wide spectrum of viruses have been shown to interact with lectins, that the majority of viruses for example HIV (*210*), arenaviruses (*208*), influenza (*217*), Hepatitis C (*218*), and coronaviruses (*211*, *219*), are recognised by host lectins on immune cells but do not utilise lectins as obligate receptors. However, as in the case of HIV, these lectin interactions have been shown to expand and enhance infectivity

routes. A comprehensive table of references of viruses and associated lectin interactions can be found in the review by Van Breedam et al. (*220*).

Although many viruses utilise both host proteins and lectins during infection, some viruses use lectins as obligate receptors. Alphaviruses and Phleboviruses have been reported to employ DC-SIGN as the primary receptor (*213*, *214*) that recognises oligomannose-type glycans on the viral surfaces (*52*, *221*). Glycosylation analysis of the envelope glycoproteins of a prototypic alphavirus, Semliki Forest virus (SFV), revealed near-exclusive oligomannose-type glycan populations on the E2 attachment glycoprotein, but more complex-type glycosylation on the membrane-proximal E1 fusion protein (*52*). Similarly, phleboviruses of the Phenuiviridae family, such as Rift Valley fever virus and other members of the Bunyavirales order, such as severe fever with thrombocytopenia syndrome virus (SFTSV) (*222*), display oligomannose-type glycans (*223*), which are required for DC-SIGN dependent cellular attachment and entry into mammalian dendritic cells (*214*). Although the exact composition of the glycans at each of the sites on the Gn and Gc glycoproteins is not understood, it has been shown that more than one site can be used as an attachment site at spatially distinct sites on the virion envelope (*223*, *224*). A glycomic study into understanding the post-translational modifications on the Gn and Gc glycoproteins of Uukuniemi virus, a relative of Rift Valley fever virus, revealed significant populations of oligomannose-type glycans, predominantly on the Gc glycoprotein of Uukuniemi virus (*221*). However, the dependency of DC-SIGN and other C-type lectins (*225*) for infection across phleboviruses is still not fully understood, especially considering that positions of N-linked glycan sites on Gn and Gc glycoproteins on the virion envelope are not well-conserved across the family (*226*).

Dengue virus is another pathogen that utilises both the macrophage mannose receptor (*227*) and DC-SIGN (*209, 228, 229*) as putative receptors to infect macrophages and dendritic cells respectively. Structural data using cryo-EM of Dengue in complex with the CRD of DC-SIGN revealed binding of N-linked glycans residues at N67 on two neighbouring E proteins by a single CRD (*228*). Binding of DC-SIGN CRD does not result in any significant conformational changes, suggesting that DC-SIGN is an attachment receptor that mediates initial binding, prior to membrane fusion, which is triggered by pH-dependent rearrangements (*230*). Nevertheless, DC-SIGN has been shown to be indispensable for Dengue infection of dendritic cells (*209, 229, 231*). C-type lectin usage by flaviviruses is not limited to infection of mammals; both West Nile virus and Dengue appear to employ C-type lectins in Aedes aegypti called mosquito galactose specific lectins (mosGCTL) as ligands to promote infection of these invertebrate vectors (*232*, *233*). An important question remains with regards to flavivirus E protein glycosylation and their usage of lectins as receptors during viral pathogeny. Does the compositional variation in glycosylation between insect and mammalian expression systems determine the variable interactions of these lectins during different stages of infection?

The dense glycan shield of LASV that confers its immunological resistance against the immune system (*13*), leads to the generation of specific oligomannose-type glycan clusters across the side of the GPC spike (*140*). These glycans have been shown to play an advantageous role for the virus in infecting human dendritic cells, via DC-SIGN mediated recognition (*208*). LASV infection of macrophages and dendritic cells is thought to be crucial to viral pathogenesis, as the virus can be propagated in these cells while also not inducing their activation, suggesting a mechanism of avoiding immune surveillance (*234*). Thus, whilst DC-SIGN may not be the primary receptor for LASV, the oligomannose-type

glycans on the GPC do act as attachment factors and positively influence infection of immune cells. A similar phenomenon has been observed for HIV-1 Env, where recognition of oligomannose-type glycans by DC-SIGN has been shown to augment infection of T cells (*235*). This DC-SIGN-mediated enhancement of infection of target cells via trans-infection has also been observed across other viruses, including SARS (*236*). A wide range of other membrane-associated lectins besides DC-SIGN and the mannose receptor such as, hepatic asialoglycoprotein receptor, liver/lymph node sinusoidal endothelial cell C-type lectin, siglecs, and macrophage Gal/GalNAc-specific C-type lectin have been implicated to have pro-viral effects (*220*).

A growing body of research indicates that membrane-associated lectin binding of many viruses augments infection and is advantageous for pathogenesis. Whether these paradoxical consequences are due to lectin functions to tackle non-viral pathogens such as fungi and bacteria, it would seem likely that immune cells exhibiting these lectins, can utilise them to combat viral infection using downstream functions, such as antigen presentation (*237*). A prominent example of anti-viral lectin activity includes oligomannose-type glycan recognition on HIV-1 Env by langerin, a C-type lectin expressed on Langerhans cells, which results in virus internalisation and degradation (*238*). As such, it seems feasible that membrane-bound lectins constitute an important part of the innate immune response against other oligomannose glycan-bearing viruses, perhaps by also aiding in antigen presentation (*239*).

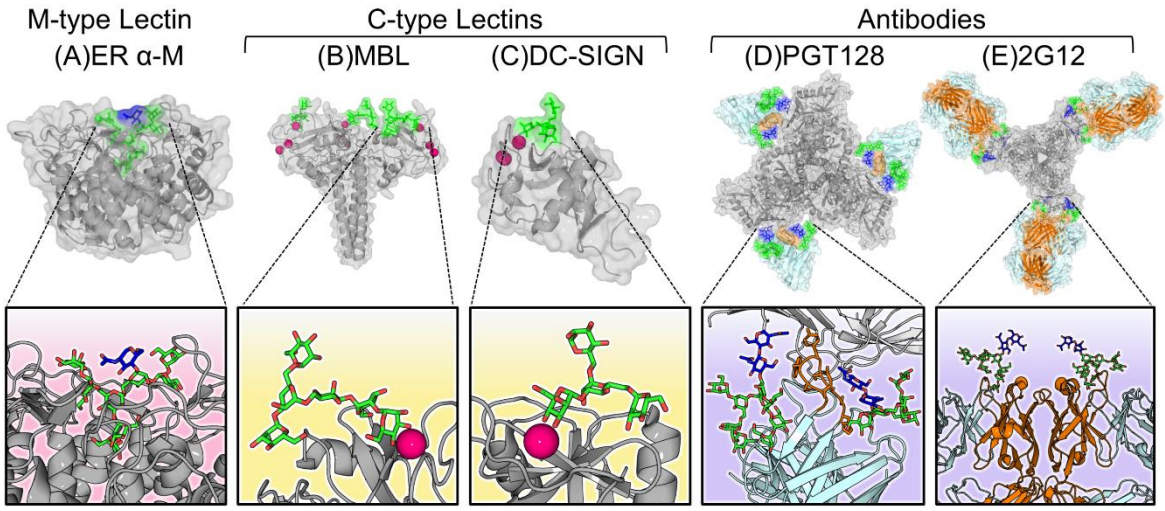


Figure 1.4. Diverse modes of oligomannose-type glycan recognition. (A) The glycan processing enzyme, ER α-mannosidase. Notice the deep binding pocket of the protein that nearly encapsulates the entire Man9GlcNAc2 glycan (PDB ID: 5KIJ) (*240*). **(B)** The collagen-containing C-type lectin, mannose binding lectin (MBL), that recognises oligomannose-type glycans via a carbohydrate recognition domain containing a calcium ion (pink), which is responsible for mediating the primary interactions to bind the sugar (PDB ID: 1KX1) (*241*). **(C)** The membrane bound C-type lectin receptor, DC-SIGN recognises oligomannose-type glycans via a Ca2+ ion and initiates phagocytosis of the pathogen (PDB ID: 1SL4) (*215*). **(D)** An anti-HIV-1 broadly neutralising antibody, PGT128, that recognises conserved oligomannose-type glycans on Env using an extended CDR loop (orange) that penetrates the glycan shield (PDB ID: 5ACO) (*242*). **(E)** The unique anti-oligomannose antibody, 2G12, featuring its unique "domain-exchanged" architecture where the heavy chains (orange) of the opposite Fab domain are swapped over (PDB ID: 6N2X) (*243, 244*).

1.6 Host glycans as attachment factors

Glycan binding properties are not limited to host proteins, viral protein can also possess glycan-binding properties. Some viral glycoproteins are capable of specifically recognizing distinct glycan motifs on the host cell surface and thereby mediate viral entry, infection, and tropism. Depending on the virus, host cell glycans can act as primary receptors, co-receptors, and/or attachment factors.

Perhaps the most well-characterised example is the hemagglutinin of influenza A viruses (*245, 246*). The ability of HA to recognise and bind specific glycan moieties via the

receptor binding site has led to it being regarded as a viral lectin (*247*). The binding event between HA and its glycan receptor leads to the endocytic internalisation of the virion, subsequent pH-dependent viral-endosomal membrane fusion, and the infection of the target cell. Remarkably, cross-species tropism is determined by preferential binding of HAs to glycan receptors with a single change in sialic acid linkage to the penultimate galactose residue; Neu5Ac-α(2,3)-Gal that is primarily expressed in bird and pig gastro-intestinal and respiratory tract cells or Neu5Ac-α(2,6)-Gal that is the predominant structure found in human upper respiratory epithelial cells (*248–252*). Sialic acid and host glycan recognition is not limited to influenza viruses; many pathogens such as paramyxoviruses (*102*), rotaviruses (*253*), noroviruses (*254*), polyomaviruses (*255*), and coronaviruses (*256*, *257*) also possess glycoproteins with sialic acid binding capabilities that facilitate host cell entry. Glycans recognised by viruses are not solely presented on glycoproteins. These glycan epitopes can also be found on glycolipids, which are composed of oligosaccharides linked to ceramide lipid molecules, which are widely found on host-cell surfaces (*258*). Furthermore, interactions between glycolipids on the viral envelope and cellular receptors have been implicated to contribute to viral pathogenesis, for example sialyllactose-containing glycolipids in the HIV-1 viral membrane can be bound by Siglec-1, a lectin found on dendritic cells, to mediate trans-infection of T cells (*259*).

GPCs of Old World arenaviruses, including the important human pathogens, lymphocytic choriomeningitis virus, LASV, and Clade C of New World arenaviruses also utilise a specific host glycan motif to mediate infection. Initial host cell entry is mediated by GPC-mediated attachment to an unusual O-mannosyl class glycan composed of a tri-saccharide core with xylose-glucuronic acid repeats, presented on the cell surface receptor, α-dystroglycan (*260–263*). Once the GPC recognises this so called matriglycan,

arenaviruses can enter the endocytic pathway, where the virions are internalised into endosomal compartments (*264*). In the case of LASV, the associated lowered pH induces a conformational change of the GPC that leads to binding to lysosomal-associated membrane protein 1 (LAMP1) (*200*, *262*). The subsequent dissociation of GP1 from the GPC triggers viral envelope-endosomal host membrane fusion. It has been suggested that glycosylation is key not only in the primary binding event of GPC but also in the following step of arenavirus viral fusion. Specifically, the sialylated N-linked glycan at position Asn76 on human LAMP1 has been demonstrated to be crucial for LASV GPC recognition (*119*, *262*). In any case, glycosylation of specific host proteins is critical for Old World arenaviral attachment and likely for viral membrane fusion.

Aside from specific host-glycan binding capabilities of viral envelope proteins, broader interactions between host glycosaminoglycans (GAGs) present on the target cell surface, and viruses, including HIV (*265*), herpes simplex virus-1 (*266*), and Dengue (*267*) have been shown to occur and promote viral attachment independent of cognate receptor binding. Contact with GAGs often constitute the initial interaction between a virus and the target host cell. In the case of herpesviruses, glycoproteins C (gC) and B (gB) are known to initially bind to the GAG, heparan sulphate (HS), which is a proteoglycan consisting of glucuronic acid (GlcA) and GlcNAc disaccharide repeats with various sulphate groups on the saccharide residue (*266*, *268*). This primary interaction of herpes simplex virus-1 to HS proteoglycans is critical and removal of HS from the cell surface, or the use of HS-deficient mutant cell lines renders the cells resistant to infection (*266*). Herpes simplex virus-1 interaction with GAGs is not limited to HS; chondroitin sulfate another GAG found in the extracellular matrix, which is composed of alternating repeats of GalNAc and GlcA carbohydrates with sulphate groups, was revealed to be efficiently bound by herpes simplex

virus-1, indicating multiple binding specificities to sulphated GAGs (*269*). Interestingly, the mucin-like domain of HSV-1 Gc has been shown to modulate binding to GAGs, highlighting the complex interplay between viral and host glycosylation, which can be an important determinant in viral infectivity (*270*).

1.7 Soluble lectins of the innate immune system and complement activation

The presence of oligomannose-type glycans is an uncommon feature on mature secreted and cell-surface host glycoproteins, and as such readily triggers the host innate immune system (*271*). As pathogen-associated molecular patterns (PAMPs), they can be recognised by a variety of soluble lectins, for example, langerin, surfactant protein A and D (SPA and SPD), and mannose-binding lectin (MBL) (**Figure 1.4.B**). MBL is a trimeric, soluble C-type lectin of the collectin family that constitutively circulates in the bloodstream (*272*). Each protomer of the trimer possesses a C-terminal CRD, a coiled coil neck domain, a collagen-like domain, and a cysteine-rich N-terminal domain. MBL specifically binds to equatorial 3- and 4-hydroxyl groups on terminal mannose sugars and GlcNAc residues. Whilst individual CRD binding is relatively weak (K_D of approximately 1 mM), the ability of collectins to form multi-trimeric oligomers significantly enhances glycan binding affinity via avidity effects resulting in K_D values in the nM range (*273*, *274*). Once MBL binds to viral glycoproteins, it recruits mannose-binding lectin-associated serine proteases (MASPs), which trigger the lectin pathway of the complement system (*275–277*). Furthermore, collagen-like domains can interact with collectin receptors found on phagocytic immune cells to promote clearance of pathogens. Ficolins, another member of collagenous soluble lectin family found in serum specifically recognize GlcNAc moieties (*278*). These lectins contribute toward a functional complement system that is vital in combating viruses. MBL has been shown to recognise N-

linked glycans on Dengue (*279*), HIV (*280*), Marburg virus (*281*), Ebola (*281*), influenza (*282*), and SARS coronavirus (*283*) and neutralize them by mechanisms including recruitment of complement, promoting clearance, blocking viral fusion, and interfering with DC-SIGN mediated trans-infection.

In addition to these soluble lectins found in sera, SPA and SPD, which share the basic structure of other collectins, recognize oligomannose-type glycans on viral particles in the lungs (*284*). The mechanisms of SPA and SPD activity in combating influenza virus infection, whether by inhibition of hemagglutinin activity (*285*, *286*), neuraminidase activity (*287*), or promoting opsonisation of virion by alveolar macrophages (*288*) have been investigated. Interestingly, the gradual addition of N-linked glycan sites on HAs of H3N2 influenza viruses has been thought to attenuate viral pathogenicity, partly due to increased levels of SPD mediated clearance from the lungs (*289*). Other respiratory viruses including coronaviruses (*290*), and respiratory syncytial virus (*291*) have been shown to be targeted by these surfactant proteins.

Galectins are a class of small soluble, so called S-type, lectins that bind to galactose and galactose-containing glycoconjugates. Unlike C-type lectins, glycan binding by the CRD is independent of calcium binding. Galectin-1 has been shown to bind to the envelope fusion glycoprotein (F) of Nipah (*292–294*), Hendra (*292*), and HA of influenza (*295*) viruses and inhibit membrane fusion. However, galectin-1 has also been shown to promote HIV infection of T cells by cross-linking the virus to host cells (*296*, *297*). The varied pro- and anti-viral consequences of soluble lectin interactions highlights the diverse, at times, paradoxical roles that they play in the innate immune system.

1.8 Glycans as antibody epitopes

Self-glycans are by their very nature, poorly immunogenic, which is an important feature for how glycan shields function. There are very few examples where a host antibody response readily recognises a glycan component of viral glycoproteins. However, there are contexts where such phenomena have been observed. The two most characterised examples, HIV-1 and Dengue, reveal varied mechanisms to how these glycan-binding antibodies can arise. In the case of HIV-1 the chronic nature of infection enables, the eventual evolution of antibodies, capable of recognising conserved glycan features on the envelope spike. Whereas in Dengue virus, antibodies have been isolated that target structurally integral glycans. In both cases the challenge when exploiting these potential vulnerabilities in vaccine design is that precursor B-cells exhibiting the required glycan specificities are negatively selected.

1.8.1 HIV-1 envelope glycoprotein

A subset of patients infected with HIV-1 develop broadly neutralising antibodies capable of recognising glycan structures on Env. Due to the immense genetic diversity across HIV-1, many broadly neutralising antibodies target conserved features across the envelope spike, namely the glycan shield. Many such antibodies have been characterised for HIV-1, that not only target regions of dense of glycosylation that generate mannose patches (*145*, *159–163*, *243*, *298–301*), but also hybrid-type (*302*), and tri- and tetra-antennary complex type glycans (*300*).

Due to the intrinsically weak immunogenic nature of host-cell derived glycans, many anti-HIV bnAbs that target glycans often adopt unusual architectures to overcome epitope masking. For example, bnAbs PGT128, 145, and 151 display long heavy chain complementarity determining region-3 (HCDR3) loops that penetrate the glycan shield to

make protein-protein contacts (*160*) (**Figure 1.4.D**), and 2G12 that features a unique domain-exchange phenomenon (*243, 303*), where the variable domains from the two heavy chains are exchanged, giving rise to a compact dual Fab architecture (**Figure 1.4.E**). Since numerous anti-HIV-1 Env bnAbs specifically recognise areas of the glycan shield, the compositional conservation of glycans on HIV-1 Env has significant implications in immunogen design as any vaccine candidate would have to emulate the native glycosylation of infectious virions (*168*), in order to elicit these bnAbs.

1.8.2 Dengue virus envelope protein

Broadly neutralising antibodies with epitopes comprised of glycans have also been characterised against Dengue virus E proteins. Specifically, these bnAbs are able to cross-neutralise all four Dengue virus serotypes by binding to the conserved so-called E dimer epitope (EDE) (*304*). Dengue E proteins are presented on the mature virion surface as 90 repeating dimers, each of which contains the EDE that bridges the two monomeric subunits with two conserved N-linked glycosylation sites (N67 and N153). These EDE antibodies are divided into two sub-classes called EDE1, which do not require the conserved glycan at N153 for binding, and EDE2 antibodies, which utilises the sugar at N153 for stronger binding as part of the neutralising epitope. Beyond the fact that these EDE antibodies possess broadly neutralising capabilities across multiple serotypes (*305*), these glycan-binding EDE2 antibodies are able to also bind partially immature viral particles as well as the fully mature virions (*304*). As such, the use of immunogens that elicit EDE antibodies has been proposed as an alternative route for next-generation vaccines due to their broadly neutralising nature (*306*). An important consideration of these vaccines will be the effect of antibody-dependent enhancement of infection due to the cross-reactive nature of these antibodies (*305, 307*). In any case, it is likely that glycan compositions of any immunogen

to combat Dengue virus will have to be carefully considered, especially when trying to elicit antibodies that target the EDE.

1.9 Concluding remarks

The ability of enveloped viruses to hijack host cell glycosylation machinery and adorn their own glycoproteins with host-derived glycans is vital for multiple facets of viral pathogenesis. The recent advances in the field of glycosylation analysis have provided greater insights into the roles that glycans play in protein trafficking and folding, viral attachment, and immune responses to infection. Often these viral glycoproteins are sole antigens expressed on the viral surface, and as such constitute crucial vaccine targets. Since antigenic mimicry is fundamental to most licensed vaccines (*168*); it is important that the glycosylation of immunogens is representative of that observed on the virus, as the elicitation of antibodies against epitopes that are occluded on the virus, and against non-native glycoforms is undesirable. Moreover, glycosylation of immunogens can play central roles in innate immune recognition to enhance humoral immunity (*308*). The understanding of glycan structures, modes of recognition, and their functionality have also resulted in the development of several therapeutics to combat a wide array of deadly pathogens (*93*, *105*, *309–313*). It is proposed that a growing understanding of viral glycobiology will provide further opportunities to rationally develop novel therapeutics and vaccines.

1.10 Mapping the glycan shields of enveloped viruses

Viral envelope proteins are often extensively glycosylated. The high density of glycans can impose steric constraints on the host cell's glycan processing enzymes, which leads to the presentation of oligomannose-type glycans. The glycans on these envelope proteins can play crucial roles in the viral lifecycle, including the protection of immunogenic protein surface. The glycans themselves can however result in being targeted by both the innate and adaptive immune systems. This thesis utilises an established mass spectrometric workflow initially used to investigate the glycosylation of HIV-1 Env immunogens, to study other viral envelope glycoproteins.

Chapter 3 of this thesis focuses on the structure of the glycan shield of the Old World arenavirus, Lassa virus, and how it protects the GPC from the immune system. It also examines and compares the glycosylation of trimeric immunogen candidates to the native-like virus.

Chapter 4 reveals how despite the extensive glycosylation on coronavirus spike proteins there are vulnerabilities throughout the sparse shield. It also provides a comparison of the global glycan shield density of coronavirus spikes with other viral proteins including the densely shielded HIV-1 Env protein. It also examines the glycosylation of the newly emergent SARS-CoV-2, the causative agent of COVID-19 which can be used as a benchmark to compare spike immunogens used for vaccination and serological testing.

Chapter 5 describes how the evolution of the H3N2 influenza hemagglutinin glycan shield has resulted in the emergence of a conserved carbohydrate epitope, which has resulted in an HIV-1 Env antibody, 2G12, being able to neutralize recent H3N2 influenza viruses.

2. Materials and Methods

2.1 DNA plasmids constructs

The pDCE expression plasmid encoding His-tagged H3N2 HAs were provided by Prof. Ian Wilson (Scripps Research, La Jolla, USA). The 2G12 light and heavy chain antibody expression plasmids were provided by Prof. Dennis Burton (Scripps Research, La Jolla, USA). 2P-stabilised SARS-CoV-1, SARS-CoV-2, MERS-CoV, and HKU1-CoV spike pHLSec expression plasmids were provided by Prof. Jason McLellan (The University of Texas at Austin). All DNA preps were performed using the Miniprep or Plasmid Maxi Kits (Qiagen) according to the manufacturer's instructions.

2.2 Recombinant protein expression and purification

Numerous glycoproteins were analysed throughout this DPhil; the constructs and the laboratory of origin is summarised in Table 2.1.

Table 2.1. Summary of analysed glycoproteins.

Construct	Cell	Lab	Chapter
2G12 IgG	HEK293F	Crispin	Apdx. A
2G12 I19R IgG	HEK293F	Crispin	Apdx. A
LASV GPC from VLPs	MDCK-II	Bowden	3
LASV GPC NPs	HEK293F	Sanders	3
MERS-CoV S	HEK293F	Crispin	4
SARS-CoV-1 S	HEK293F	Crispin	4
SARS-CoV-2 S	HEK293F	Crispin/McLellan	4
HKU1-CoV S	HEK293F	Crispin	4
MERS S ΔN155A	HEK293F	Crispin	4

MERS S ΔN166A	HEK293F	Crispin	4
MERS S ΔN236A	HEK293F	Crispin	4
Influenza H3N2 Hemagglutinins	HEK293F	Crispin/Wilson	5
EEEV E proteins	BHK/C6/36	Rossmann	Apdx B.
DENV 1-4 NS1 proteins	HEK293T	NAC	Apdx B.
DENV 1-4 E proteins	HEK293T	NAC	Apdx B.
ZIKV NS1 protein	HEK293T	NAC	Apdx B.
ZIKV E protein	HEK293T	NAC	Apdx B.

2.2.1 Recombinant protein expression in HEK cells

Proteins were expressed transiently in HEK 293F suspension cell cultures in FreeStyle Expression Medium (ThermoFisher Scientific). For transfection, 200 μL of FreeStyle Max transfection reagent (ThermoFisher Scientific) and 200 μg DNA were incubated in 10 mL of serum-free OptiPro medium (ThermoFisher Scientific) for 15 min. This was then added to a 200 mL culture at a concentration of 1 x 10^6 cells/mL. The cells were maintained at 37 °C, 8% CO_2 with shaking at 125 rpm. Cultures were incubated for 5–7 days prior to harvesting. Supernatant was clarified by centrifugation and sterile filtered through a 0.22 μm membrane (Merck Millipore).

2.2.2 Expression and purification of LASV VLPs

Madin-Darby Canine Kidney-II (MDCK-II) cells stably expressing LASV GPC (Josiah strain, GenBank ID code AY628203) were cultured in Dulbecco's Modified Eagle Media (DMEM) supplemented with 10% Foetal Calf Serum (FCS) for 96 hours. The medium was replaced with DMEM with 2% FCS for VLP expression as described by Schlie et al. (*314*). After 96 hours, the cell supernatant was cleared by centrifugation (4,000 g for 30 mins).

VLPs were pelleted through 10 mL of 20% sucrose cushion by ultracentrifugation (170,000 g for 3 hours). The pellets were resuspended in SPG buffer at pH 8 for 12 hours at 4 ºC.

2.2.3 Ni^{2+} affinity purification

His-tagged glycoproteins were purified using a 5 mL HisTrap column (GE Healthcare). Column equilibration and washing was performed using a 50 mM $NaPO_4$, 0.3 M NaCl, 10 mM imidazole buffer. Column loading was performed at a flow rate of 1 mL/min. Env proteins were eluted in 50 mM $NaPO_4$, 0.3 M NaCl, 150 mM imidazole. Eluted proteins were immediately buffer exchanged and concentrated using 50 kDa cut-off Vivaspin columns (Sartorius).

2.2.4 Size-exclusion chromatography

A Superdex 200 16 600 column was washed with PBS at a rate of 1 mL/min. After 2 hours, 1 mL of the nickel affinity purified material was injected into the column. Fractions separated by SEC were pooled according to their corresponding peaks on the Size Exclusion chromatograms. The target fraction was concentrated in 3, 10, 50, 100 kDa vivaspin (GE healthcare) tubes to ~1 mL.

2.3 Analysis of total glycan profiles and compositions

2.3.1 In-gel release of N-linked glycans

N-linked glycans were enzymatically released from viral glycoproteins via in-gel digestion. Purified proteins were resolved by pre-cast NuPAGE 4-12% Bis-Tris polyacrylamide gel (Invitrogen) and stained with Coomassie Blue. Following destaining, the corresponding bands were excised and washed three times, alternating between acetonitrile and water. The gel bands were incubated with PNGase F (New England Biolabs) overnight at 37 °C. Released N-linked glycans were eluted with water and dried in a SpeedVac.

2.3.2 Fluorescent labelling of N-linked glycans

Aliquots of released glycans were fluorescently labelled with procainamide or 2-aminobenzoic acid (2-AA) in the following solutions: 110 mg/mL procainamide hydrochloride (Abcam), 60 mg/mL sodium cyanoborohydride, dissolved in 30% dimethyl sulfoxide, 70% acetic acid; or 30 mg/mL 2-AA, 45 mg/mL sodium cyanoborohydride dissolved in a solution of 4% (w/v) sodium acetate trihydrate, 2% (w/v) boric acid in methanol. An 80 – 100 μL aliquot of labelling mixture was added to the glycan sample (dissolved in 30 μL water), vortexed and incubated at 65 °C for 4 hours or 80 °C for 1 hour, respectively. Excess label and PNGase F were removed using Spe-ed Amide 2 cartridges (Applied Separations).

2.3.3 HILIC-UPLC analysis

Glycans were analysed on a Waters Acquity H-Class UPLC instrument with a Glycan BEH Amide column (2.1 mm x 100 mm, 1.7 μm; Waters) and the following gradient: time (t) = 0: 22% A, 78% B (flow rate = 0.5 mL/min); t = 38.5: 44.1% A, 55.9% B (0.5 mL/min); t = 39.5: 100% A, 0% B (0.25 mL/min); t = 44.5: 100% A, 0% B (0.25 mL/min); t = 46.5: 22% A, 78% B (0.5 mL/min), where solvent A was 50 mM ammonium formate, pH 4.4 (Waters) and B was acetonitrile. Fluorescence was measured at an excitation wavelength of 310 nm and an emission wavelength of 370 nm for procainamide, or 250 nm and 428 nm for 2-AA. Data were processed using Empower 3 software (Waters).

2.3.4 Glycosidase digestions of labelled glycans

The relative abundances of different N-glycan structures were determined by digesting fluorescently labelled glycans with glycosidases overnight at 37 °C; these include: Endo H, α2-3, 6, 8 neuraminidase, α2-3 neuraminidase, β1-4 galactosidase, β-*N*-Acetylglucosaminidase (all New England Biolabs), and α-L-fucosidase (Sigma Aldrich).

Glycans were repurified using a PVDF protein-binding membrane (Merck Millipore). Digested glycans were analysed by HILIC-UPLC, as before. Glycans were quantified by integrating the peaks before and after glycosidase digestion, following normalisation of the chromatograms.

2.3.5 Ion-mobility mass spectrometry analysis of released N-linked glycans

To generate glycan libraries in order to aid in the subsequent assignment of glycopeptides, an unlabelled aliquot of PNGase F released glycans were analysed by ion-mobility electrospray ionisation mass spectrometry (IM-ESI MS). The glycan sample was cleaned with a Nafion membrane for approximately 2 hours, and then dissolved in a solution of methanol-water (1:1 v/v), containing a trace amount of ammonium phosphate to promote phosphate adduct formation. Glycans were analysed by nano-electrospray with direct infusion using a Synapt G2Si instrument (Waters) with the following settings: capillary voltage, 0.8–1.0 kV; sample cone, 100 V; extraction cone, 25 V; cone gas, 40 L/h; source temperature, 150 °C; trap collision voltage, 4–160 V; transfer collision voltage, 4 V; trap direct current bias, 35–65 V; IMS wave velocity, 450 m/s; IMS wave height, 40 V; trap gas flow, 2 mL/min; IMS gas flow, 80 mL/min. Data were acquired and processed with MassLynx v4.1 and Driftscope version 2.8 software (Waters).

2.4 Site-specific glycan analysis

2.4.1 Reduction, alkylation and proteolytic digestion

Approximately 50 μg of viral glycoproteins were denatured, reduced, and alkylated by sequential 1 hour incubations at room temperature in the following solutions: 50 mM Tris-HCl, pH 8.0 buffer containing 6 M urea and 5 mM DTT, followed by the addition of 20 mM iodacetamide (IAA) for a further hour at room temperature in the dark, and then additional DTT (20 mM), to eliminate residual IAA. The alkylated polypeptides were buffer

exchanged into 50 mM Tris-HCl, pH 8.0 using Vivaspin columns and digested with trypsin/chymotrypsin/alpha-lytic protease/Glu-C/subtilisin (Mass Spectrometry Grade, Promega) at a ratio of 1:30 (w/w) overnight at 37 ºC. Reaction mixtures were dried and glycopeptides were extracted using C18 ZipTip (Merck Millipore), following the manufacturer's protocol.

2.4.2 Liquid chromatography-mass spectrometry of glycopeptides

The peptides were dried again, re-suspended in 0.1% formic acid and analyzed by nanoLC-ESI MS with an Easy-nLC 1200 (Thermo Fisher Scientific) system coupled to a Fusion mass spectrometer (Thermo Fisher Scientific) using higher energy collision-induced dissociation (HCD) fragmentation. Peptides were separated using an EasySpray PepMap RSLC C18 column (75 µm × 75 cm). A trapping column (PepMap 100 C18 3µM 75µM x 2cm) was used in line with the LC prior to separation with the analytical column. The LC conditions were as follows: 275 minute linear gradient consisting of 0-32% acetonitrile in 0.1% formic acid over 240 minutes followed by 35 minutes of 80% acetonitrile in 0.1% formic acid. The flow rate was set to 200 nL/min. The spray voltage was set to 2.7 kV and the temperature of the heated capillary was set to 40 °C. The ion transfer tube temperature was set to 275 °C. The scan range was 400−1600 m/z. The HCD collision energy was set to 50%, appropriate for fragmentation of glycopeptide ions. Precursor and fragment detection were performed using an Orbitrap at a resolution MS1= 100,000. MS2= 30,000. The AGC target for MS1=4e5 and MS2=5e4 and injection time: MS1=50ms MS2=54ms.

Glycopeptide fragmentation data were extracted from the raw file using ByonicTM (Version 3.5) and ByologicTM software (Version 3.5; Protein Metrics Inc.). The glycopeptide fragmentation data were evaluated manually for each glycopeptide; the peptide was scored as true-positive when the correct b and y fragment ions were observed along with oxonium

ions corresponding to the glycan identified. The MS data was searched using the Protein Metrics N-glycan library. The relative amounts of each glycan at each site as well as the unoccupied proportion were determined by comparing the extracted chromatographic areas for different glycotypes with an identical peptide sequence. All charge states for a single glycopeptide were summed. The precursor mass tolerance was set at 4 ppm and 10 ppm for fragments. A 1% false discovery rate (FDR) was applied. The relative amounts of each glycan at each site as well as the unoccupied proportion were determined by comparing the extracted ion chromatographic areas for different glycopeptides with an identical peptide sequence. Glycans were categorized according to the composition detected. HexNAc(2)Hex(9−5) was classified as M9 to M5. HexNAc(3)Hex(5−6)X was classified as Hybrid with HexNAc(3)Fuc(1)X classified as Fhybrid. Complex-type glycans were classified according to the number of processed antenna and fucosylation. If all of the following compositions have a fucose they are assigned into the FA categories. HexNAc(3)Hex(3-4)X is assigned as A1, HexNAc(4)X is A2/A1B, HexNAc(5)X is A3/A2B, and HexNAc(6)X is A4/A3B. As this fragmentation method does not provide linkage information compositional isomers are group, so for example a triantennary glycan contains HexNAc 5 but so does a biantennary glycans with a bisect. Any glycan containing at least one sialic acid was counted as sialylated.

For O-linked glycan analysis, trypsin and alpha lytic protease-generated glycopeptides were treated with PNGase F prior to analysis to remove N-linked glycans. This was performed on a single biological replicate using an HCD energy of 27%. The MS data was searched using the Protein Metrics 70 common O-linked glycan library.

Table 2.2. Peptide modifications for site-specific glycan analysis

Modification	MW	Frequency
Carbamidomethylation of Cys	+57.021464	Fixed
Oxidation of Met	+15.994915	Rare
Glu→pryo-Glu at N-terminus Glu	-18.010565	Rare
Gln→pryo-Gln at N-terminus Gln	-17.026549	Rare
N-glycan at N-glycan sequon	n/a	Common

A maximum of two common and one rare modification were permitted per peptide.

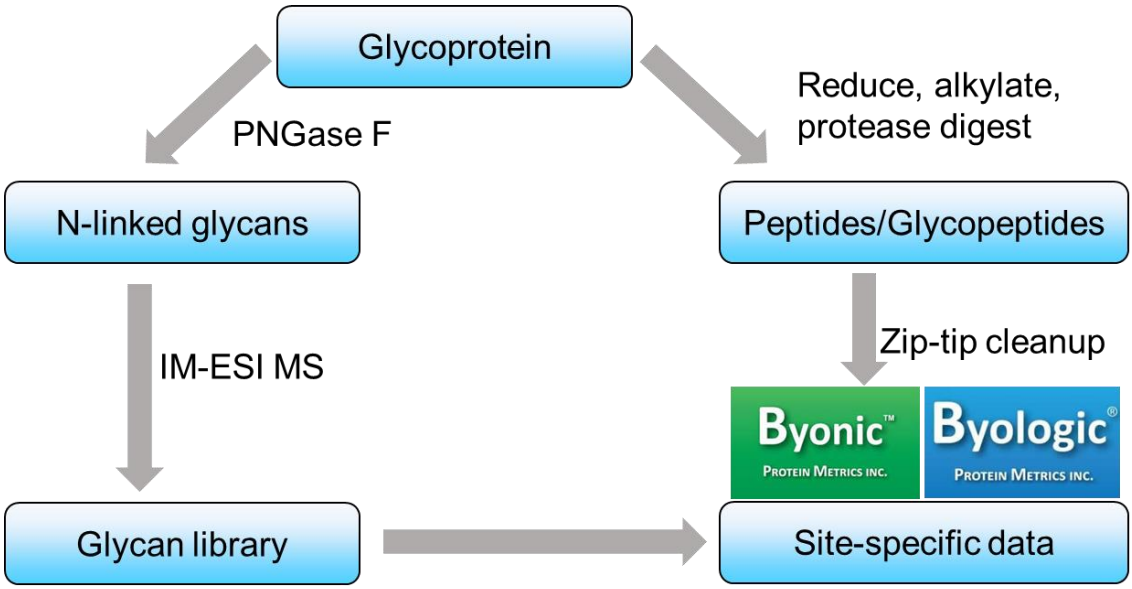


Figure 2.1 Summary of LC-ESI MS site-specific analysis workflow. A glycan library is generated by IM-ESI MS analysis of enzymatically cleaved N-linked glycans. A separate aliquot of glycoprotein is used for LC-ESI MS analysis. Briefly, glycoproteins are denatured, reduced and alkylated prior to proteolytic digestion. Peptides and glycopeptides are extracted by C18 ZipTip. Data analysis is performed using Byonic™ and Byologic® software.

2.5 Immunoassays

2.5.1 Enzyme-linked immunosorbent assay (ELISA)

ELISAs were performed using 96-well Ni-NTA His Sorb plates (Qiagen). Plates were incubated overnight at 4°C with 10μg of purified viral glycoproteins. Plates were washed four times with 0.5% PBS/Tween and blocked with 5% skim milk/PBS for1 h at room temperature. Serial dilutions of antibodies in 5% skim milk/PBS were incubated for an hour. Unbound antibody was removed by washing as described above. Horseradish peroxidase conjugated antihuman goat IgG (ThermoFisher Scientific) was added at a 1:3000 dilution for 1h. The chromogen tetramethylbenzidine was added for 5 min and then neutralized using 2 M sulfuric acid. Absorbance was measured at 450 nm.

2.5.2 Western blot

Proteins were resolved by SDS-PAGE gel and transferred onto a PVDF or nitrocellulose membrane using the Trans-Blot® Turbo™ Transfer system (BioRad). Membranes were blocked overnight at 4 °C or for 1 hour at room temperature in 5% milk in PBS + 0.5% Tween. Membranes were washed in 0.5% Tween-PBS and the primary antibody (1:1'000 – 3'000) was incubated in 0.5% Tween-PBS for 1 hour at room temperature. Membranes were washed again and incubated with the secondary antibody (goat anti-human IgG-HRP, 1:2'000; Abcam) in 0.5% Tween-PBS for another hour. Proteins of interest were visualised with Pierce ECL Western Blotting Substrate (Thermo Scientific) and images were captured with the Fuji Intelligent Dark Box ii and Image Reader 1000 Pro software.

2.6 Model building

The model of a fully glycosylated viral glycoproteins throughout this thesis were created using X-ray/cryo-EM structures detailed in **Table 2.3**. The most dominant glycoform presented at each site was modelled onto the N-linked carbohydrate attachment sites in Coot.

Table 2.3. Structures used for model building.

Viral Glycoprotein	PDB ID
SARS-CoV-1 S	5X58 (*315*)
SARS-CoV-2 S	6VSB (*316*)
LASV GPC	5VK2 (*117*)
HIV-1 Env	4ZMJ (*143*)
SIV Env	6OHY (*317*)
MERS-CoV S	5X59 (*315*)
HKU1- CoV S	5I08 (*205*)
H3N2 HK68 HA	4FNK (*318*)
H3N2 Vic11 HA	4O5N (*7*)
NL63-CoV	5SZS (*8*)
OC43-CoV	6OHW (*319*)
229E-CoV	6U7H (*320*)
EBOV GP	5JQ3 (*141*)
NIPV F	5EVM (*144*)

2.7 Clustering analysis of viral glycan shields

Solvent-accessible residues and interactions between N-linked glycans and amino-acid residues were calculated using Proteins, Interfaces, Structures and Assemblies (PISA) European Bioinformatics Institute (EBI) (*321*). Glycan shield density was calculated by the number of amino-acid residues interacting with glycans divided by the total number of solvent-accessible amino-acid residues.

3. The structure of the Lassa virus glycan shield provides a model for immunological resistance

Lassa virus (LASV), an arenavirus endemic to rodent populations in West Africa, causes severe haemorrhagic fever upon transmission to humans, with an estimated 300,000 infections and several thousand deaths each year (*322*). To date, no licensed vaccine exists against LASV and there are no approved therapeutics for treatment, though the compassionate use of the antiviral drug ribavirin alone, or in combination with favipiravir, has shown efficacy if administered early in infection (*323*). The inconsistent induction of potent LASV-specific antibody immunity, both during natural infection and by vaccination attempts (*324–328*), is thought to be partly due to the extensive glycosylation presented on the surface of the LASV glycoprotein complex (GPC) (*13*). While the architecture of the protein components of LASV GPC is well understood (*117*, *200*, *329*, *330*), structural knowledge of the immunologically important glycans displayed on the GPC surface has remained elusive.

The arenaviral GPC is encoded by the S segment of the single-stranded, bi-segmented RNA genome. Following expression of a single polyprotein precursor, the GPC is proteolytically processed by the host cell subtilase SKI-1/S1P (*331*) and displayed on the lipid bilayer surface of the mature virion as a trimer of heterotrimers (*200*, *314*). Each heterotrimer consists of a receptor-binding GP1 domain (*116*, *117*, *197*, *198*, *332*, *333*), a GP2 class I membrane fusion protein (*117*, *196*, *333*, *334*), and a retained myristoylated stable signal peptide (SSP), which is required for GPC processing and function (*335–337*). Host cell entry of Old World arenaviruses and Clade C New World arenaviruses is initiated by GPC-mediated attachment to O-mannose glycans containing xylose-glucuronic acid sugar repeats presented on the cell surface receptor, α-dystroglycan (α-DG) (*199*, *260*, *263*, *338*). Factors

including the lowered-pH associated with entry into the endocytic pathway, lysosome-associated membrane protein 1 (LAMP1) recognition, and dissociation of GP1 from the GPC, are responsible for triggering fusion of the viral envelope and endosomal host cell membrane (*200*, *262*, *339*).

The eleven potential N-linked glycosylation sites (PNGs) found on each SSP-GP1-GP2 protomer accounts for nearly 30% of the total mass of the LASV GPC (*117*, *340*). It has been shown that LASV glycans promote evasion from the neutralizing antibody response and are required for viral fitness (*13*). Additionally, under-processed oligomannose-type glycans on LASV GPC augment infection through interaction with the C-type lectin, dendritic cell-specific ICAM-3-grabbing nonintegrin (DC-SIGN) (*208*). However, the relative abundance and distribution of these under-processed glycans and fine structure of the LASV glycome have yet to be determined.

Here, using an established virus-like particle (VLP) system (*200*, *314*), a global and site-specific analysis of the N-linked glycosylation presented on LASV GPC is provided. The analysis reveals extensive global heterogeneity, ranging from highly processed complex-type glycosylation to under-processed oligomannose-type glycans. Mapping of these glycans onto the structure of the LASV GPC ectodomain reveals that some of these carbohydrates form a dense shield consisting of clusters of oligomannose-type glycans that are likely to be utilized during DC-SIGN-mediated entry. Sequence analysis of LASV isolates reveals a higher incidence of amino acid variation on the surface of the GPC in regions less occluded by N-linked glycosylation. Together, these data reveal how host cell-derived glycosylation renders LASV an immunologically challenging target.

3.1. Glycan processing of trimeric LASV GPC

LASV encodes a large number of N-linked glycosylation sequons on both the GP1 and GP2 subcomponents of the GPC (**Figure. 3.1.A**). I sought to characterize the composition of the carbohydrate structures displayed on the mature LASV GPC spike using a previously established virus-like-particle production and purification strategy, which displays LASV GPC in the full native assembly (*200, 314, 341*). Western blot analysis of secreted VLPs using an anti-LASV GP1 (*314*) monoclonal antibody and anti-LASV GP2 polyclonal antibody (*342*) confirmed the presence and maturation of the GPC into GP1 and GP2 subunits (**Figure 3.1.B**). Cryo-electron microscopy further verified the expected display of globular GPC spikes on the surface of the purified VLPs (**Figure 3.1.C**).

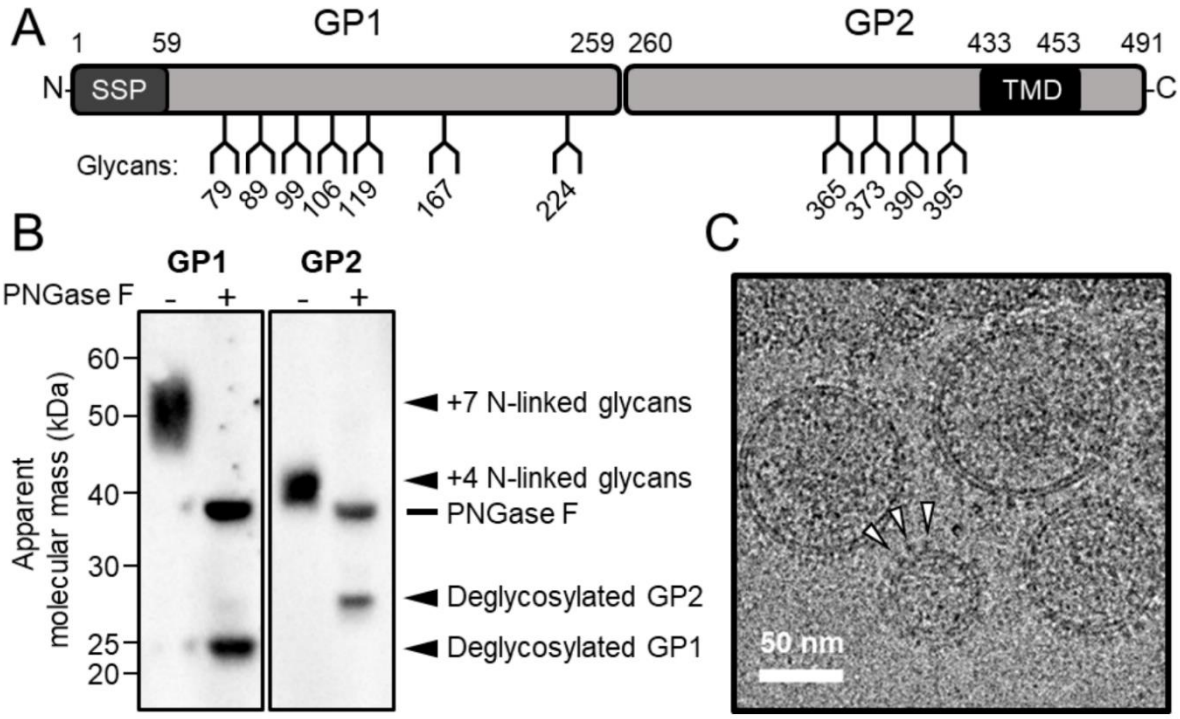


Figure 3.1. Preliminary characterization of LASV VLPs. (A) Schematic representation of LASV GPC, showing the position of N-linked glycosylation amino acid sequons (NXT/SX, where X ≠ P), SSP, GP1 attachment glycoprotein, GP2 fusion glycoprotein, and transmembrane domain (TMD). **(B)** Western blot analysis of purified LASV VLPs performed using anti-GP1 (*314*) and anti-GP2 (*342*) antibodies, against native and deglycosylated LASV GPC. Blots show LASV GP1 and GP2 before and after PNGase F

treatment. **(C)** Electron cryomicroscopy image of VLPs purified from MDCK-II cells. White arrows indicate the positions of prominent LASV GPC spikes. (Scale bar, 50 nm.). The VLPs were made and imaged by Sai Li at the Division of Structural Biology, University of Oxford using a method originated from the Strecker Lab (*341*).

To quantitatively assess the composition of the LASV GPC glycosylation, enzymatically released N-linked glycans were fluorescently labelled, and subjected to hydrophobic interaction chromatography-ultra-performance liquid chromatography (HILIC-UPLC) analysis. Cleavage of the released glycan pool with endoglycosidase H (Endo H) revealed an abundance (49%) of oligomannose-type glycans (**Figure 3.2.A**), particularly $Man_{6-9}GlcNAc_2$ glycoforms. I observed only a minor population of $Man_5GlcNAc_2$, suggesting the limited processing by Golgi-resident α-mannosidases to convert $Man_6GlcNAc_2$ to $Man_5GlcNAc_2$ at specific sites. The high proportion of oligomannose-type glycans on the LASV GPC is consistent with previous lectin-binding and glycosidase digestion studies (*343*, *344*), which revealed under-processed glycans on recombinant LASV GP1 constructs, albeit to varying levels.

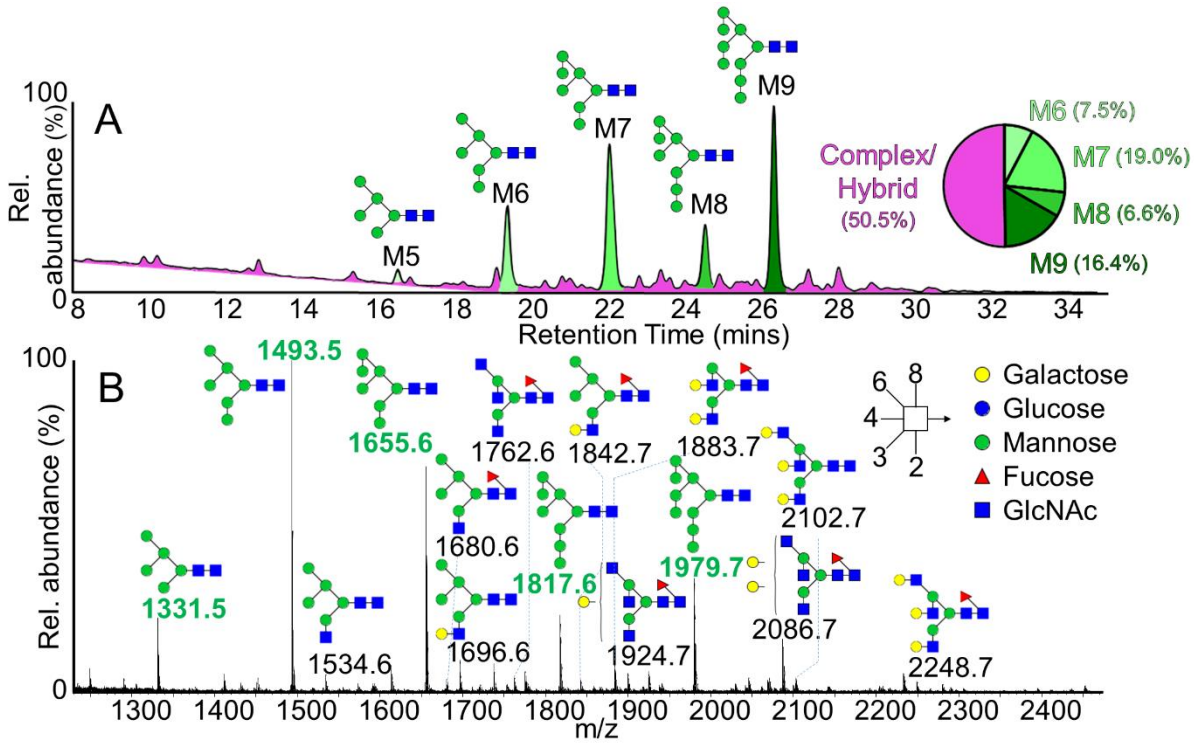


Figure 3.2. Compositional analysis of LASV GPC glycosylation. (A) HILIC-UPLC profile of fluorescently labelled N-linked glycans from LASV GPC produced in VLPs. Oligomannose-type glycans (M5 to M9; $Man_5GlcNAc_2$-$Man_9GlcNAc_2$) (green) and complex-type glycans (pink) were identified by Endo H digestion, with quantification of major glycan types summarized as a pie chart. **(B)** Negative-ion electrospray spectrum of N-linked glycans from the GPC. Peaks are annotated with the corresponding compositions, using Consortium for Functional Glycomics symbolic nomenclature and Oxford system linkages (*31*), as per the key. Oligomannose-type glycan m/z values are labelled in green.

I ascertained the precise structure of each of the glycans within the released pools by negative-ion mobility-electrospray ionization mass spectrometry (IM-ESI MS) (**Figure 3.2.B**). Consistent with the UPLC data, IM-ESI MS confirmed a dominant oligomannose-type glycan population, lacking the level of sialylation characteristic to most host-cell surface glycoproteins (*345*, *346*).

To confirm the composition of these oligomannose-type glycans, fragmentation by collision-induced dissociation was performed. This analysis reveals the expected array of under-processed $Man_{5\text{-}9}GlcNAc_2$ species that form following processing by endoplasmic reticulum (ER)-resident α-glucosidases I and II (SI Appendix, Fig. S1) (*54*). Consistent with

the biological preference of ER α-mannosidase I to remove the 3-branched mannose of the 6-antenna (D2) from $Man_9GlcNAc_2$ during N-linked glycan processing (*347*), MSMS of $Man_8GlcNAc_2$ exhibits a single set of ions derived from a particular (D1, D3) isomer (**Figure 3.3.B**). I observed two $Man_7GlcNAc_2$ isomers, with the seventh mannose located on either the 6-antenna (D3) or 3-antenna (D1) arm (**Figure 3.3.C**). These isomers have also been observed in HIV-1 (gp120) and Semliki Forest virus E1 and E2 glycoproteins (*29*, *52*). It is likely that the existence of high levels of oligomannose glycans amongst such pathobiologically diverse viruses arises from a requirement for conserved immune evasion and receptor recognition functionality, respectively.

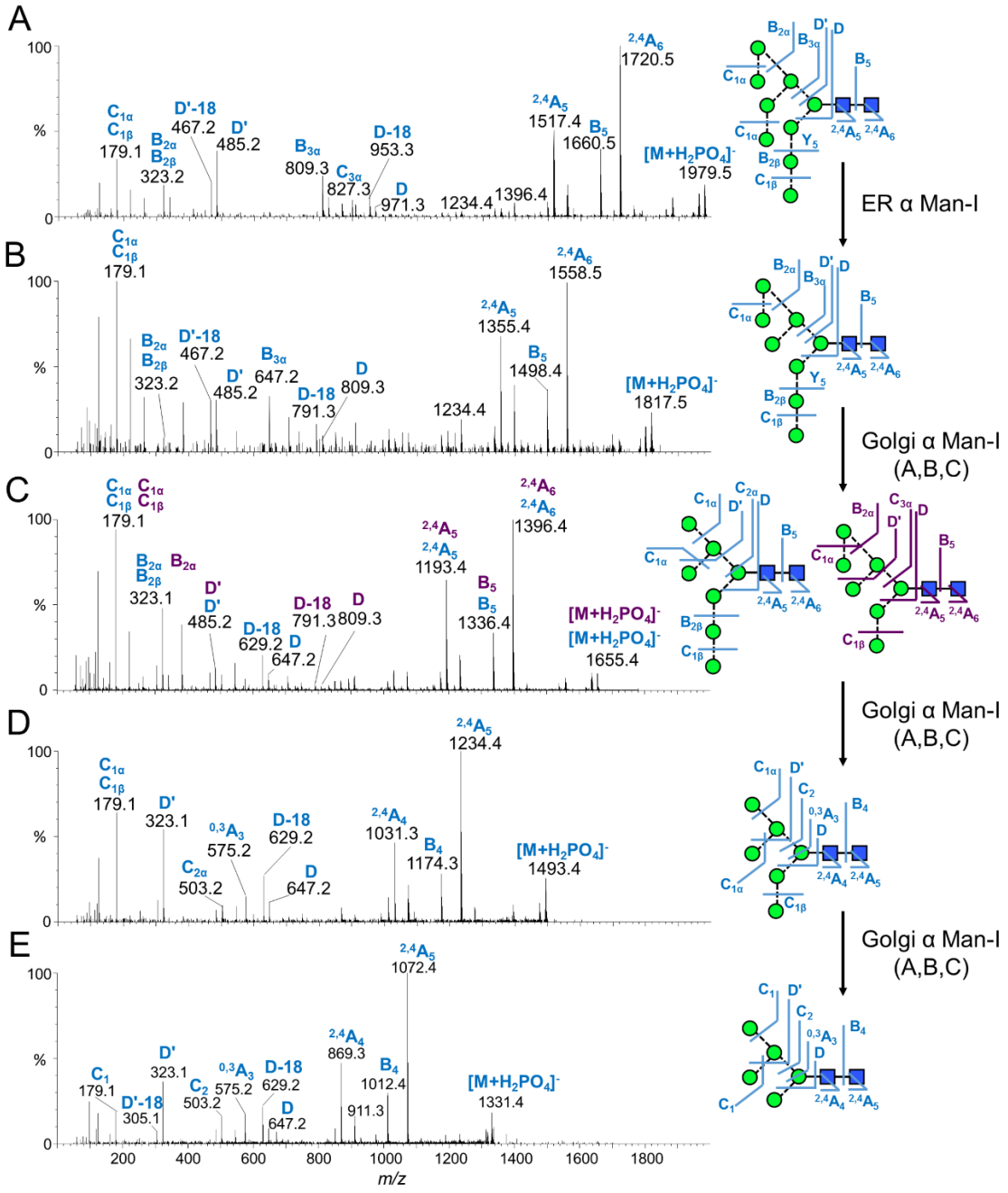


Figure 3.3. Mobility-extracted negative-ion collision induced dissociation tandem MS spectra of oligomannose-type glycans from LASV GPC. (A) $Man_9GlcNAc_2$ **(B)** $Man_8GlcNAc_2$ **(C)** $Man_7GlcNAc_2$ **(D)** $Man_6GlcNAc_2$ **(E)** $Man_5GlcNAc_2$. Arrows indicate the direction of biological glycan processing.

3.2. Structural clustering of under-processed glycans on the GPC

It has been previously shown that oligomannose-type glycans displayed on the LASV GPC mediate host cell attachment to DC-SIGN presented on monocyte-derived dendritic cells (*208*). I sought to identify the possible location(s) of this interaction using an integrated site-specific compositional and structural approach. LASV GPC glycopeptides were generated by digestion with trypsin, chymotrypsin, and GluC and subjected to in-line liquid chromatography−mass spectrometry. This analysis revealed that each site presents a differential level of oligomannose, hybrid, and complex-type glycan populations (**Figure 3.4.A**). Consistent with the UPLC analysis (Fig. 2A), I observed that a number of these sites ($Asn79_{GP1}$, $Asn89_{GP1}$, $Asn99_{GP1}$, $Asn365_{GP2}$, and $Asn373_{GP2}$) were predominantly of the oligomannose type. The level of mannosylation varies widely across these sites, where the glycans at $Asn79_{GP1}$ and $Asn365_{GP2}$ present a dominant population of $Man_9GlcNAc_2$ and $Asn89_{GP1}$, $Asn99_{GP1}$, and $Asn373_{GP2}$ exhibit less restrictive processing and display $Man_6GlcNAc_2$ and $Man_7GlcNAc_2$.

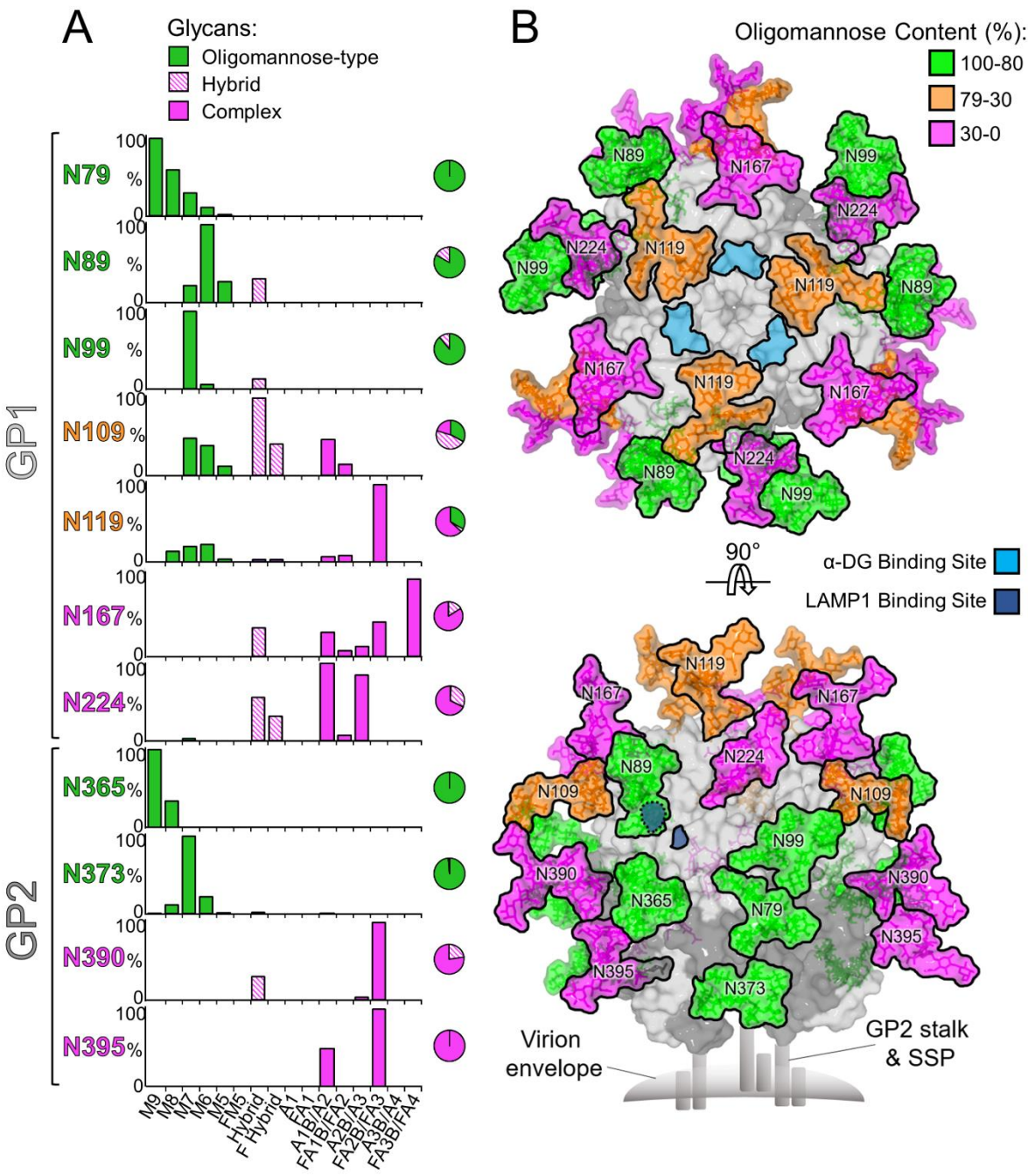


Figure 3.4. Compositional analysis and structure-based mapping of LASV GPC N-linked glycans. (A) Quantitative site-specific N-linked glycan analysis of LASV GPC. Purified LASV GPC was digested with trypsin, chymotrypsin, and GluC, then analyzed by LC-ESI MS. Glycan compositions are based on the glycan library generated from negative-ion mass spectrometry of released N-glycans. The bar graphs represent the relative quantities of each glycan group with oligomannose-type glycan series (M9 to M5; $Man_9GlcNAc_2$ to $Man_5GlcNAc_2$) (green), afucosylated and fucosylated hybrid glycans (Hybrid & F Hybrid) (dashed pink), and complex glycans grouped according to fucosylation and number of antennae (A1 to FA4) (pink). The pie charts summarize the quantification of these glycans. **(B)** Modelling experimentally observed glycosylation onto the crystal structure of the

trimeric LASV GPC (PDB ID code 5VK2) (*117*). The glycans are coloured according to the oligomannose content, as defined by the upper-right-hand key. The locations of α-DG and LAMP1 binding sites have been previously proposed (*116*, *119*, *199*, *200*) and are annotated in cyan and dark blue, respectively. GP1 and GP2 are coloured light grey and dark grey, respectively.

Using the crystal structure of the trimeric LASV GP1−GP2 ectodomain [Protein Data Bank (PDB) ID code 5VK2 (*117*)], I determined the distribution of the observed glycan populations in a structural context. I generated a model of the fully glycosylated LASV GP1−GP2 ectodomain by overlaying the experimentally determined glycan structures onto crystallographically observed N-linked glycosylation sites (**Figure 3.4.B**). This analysis reveals how N-linked glycosylation envelopes the majority of the GPC ectodomain and provides a structure-based model for understanding glycan-mediated shielding of the proteinous LASV GPC surface. At a more detailed level, this integrated structural approach also indicates the existence of a high mannose cluster, which spans GP1 and GP2 subunits. This cluster is located on the side of the GPC trimer and includes $Asn79_{GP1}$, $Asn89_{GP1}$, $Asn99_{GP1}$, $Asn365_{GP2}$, and $Asn373_{GP2}$. It is suggested that the dominant oligomannose (94%) composition observed in this region is likely due to the high spatial density of N-linked glycans, which limit the accessibility of glycan processing enzymes to these sites. The existence of such a high mannose cluster has precedence and is reminiscent of the "mannose patches" observed on the glycan shield of the HIV-1 envelope glycoprotein (*151*, *152*, *156*, *348*). Further examination reveals that the proposed LAMP1 binding site is partially occluded by this oligomannose cluster. In particular, the glycan extending from Asn89 shields the histidine triad (His92, His93, and His230) of LASV GP1 thought to be a region critical for this interaction (*262*, *339*). The occlusion of this binding site is consistent with the proposed mechanism of LASV GPC−LAMP1 recognition (*116*, *200*, *339*), which requires pH-dependent conformational rearrangements of the GPC spike upon exposure to

the late endosomes. Indeed, modelling indicates that the formation of the low-pH LASV GP1 conformation redirects the glycan extending from N89 to create a LAMP1-accessible recognition site (**Figure 3.5**).

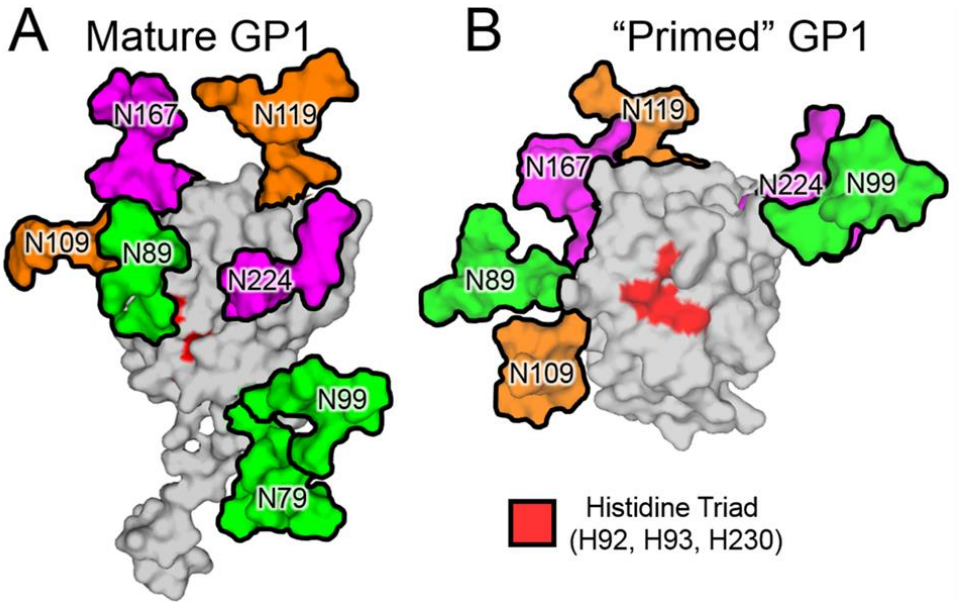


Figure 3.5. The glycan extending from N89 partially obstructs the putative histidine triad on LASV GP1 in the prefusion state and is made accessible upon 'priming' (*116*) **of the glycoprotein. (A)** Occlusion of the LAMP-1-binding histidine triad (red) by N89 in the LASV prefusion state (PDB ID: 5VK2 (*117*)). **(B)** N-linked glycans mapped onto low-pH conformation of LASV GP1 (PDB ID: 4ZJF (*116*)).

Restricted glycan processing also occurs at Asn119, albeit to a lesser extent (33% oligomannose composition), at the membrane-distal apex of the trimer (**Figure 3.4.B**). Interestingly, Asn119 is located near, but does not occlude, residues proposed to be required for α-DG binding (His141, Asn146, Phe147, and Tyr150) (27), and a lymphocytic choriomeningitis virus (LCMV) GPC N119Q site-directed mutation revealed that the Asn119 glycan protects the α-DG receptor binding site from antibody-mediated neutralization (*13*). The use of N-linked glycosylation to obstruct immunodominant receptor-binding sites has been observed for other highly glycosylated viruses, such as the

CD4 binding site on the envelope spike of HIV-1 (*187*) and the sialic acid binding site on the HA of influenza virus (*188*).

3.3. Amino acid sequence diversification occurs at antibody-accessible sites on the GPC

The absence of an effective antibody response is a characteristic feature of patients who succumb to LASV infection (*324–328*). Indeed, extensive affinity maturation is thought to be required to generate tightly binding antibodies capable of targeting and neutralizing the highly glycosylated GPC (*349*). We sought to quantify the steric role that GPC-displayed glycans play in shielding the GPC surface. Using publicly available LASV GPC gene sequences, we performed a comparative nonsynonymous to synonymous nucleotide substitutions (i.e., dN/dS ratio) analysis of the two major lineages, predominantly found in Nigeria and Sierra Leone (**Figure 3.6 and Figure 3.7**).

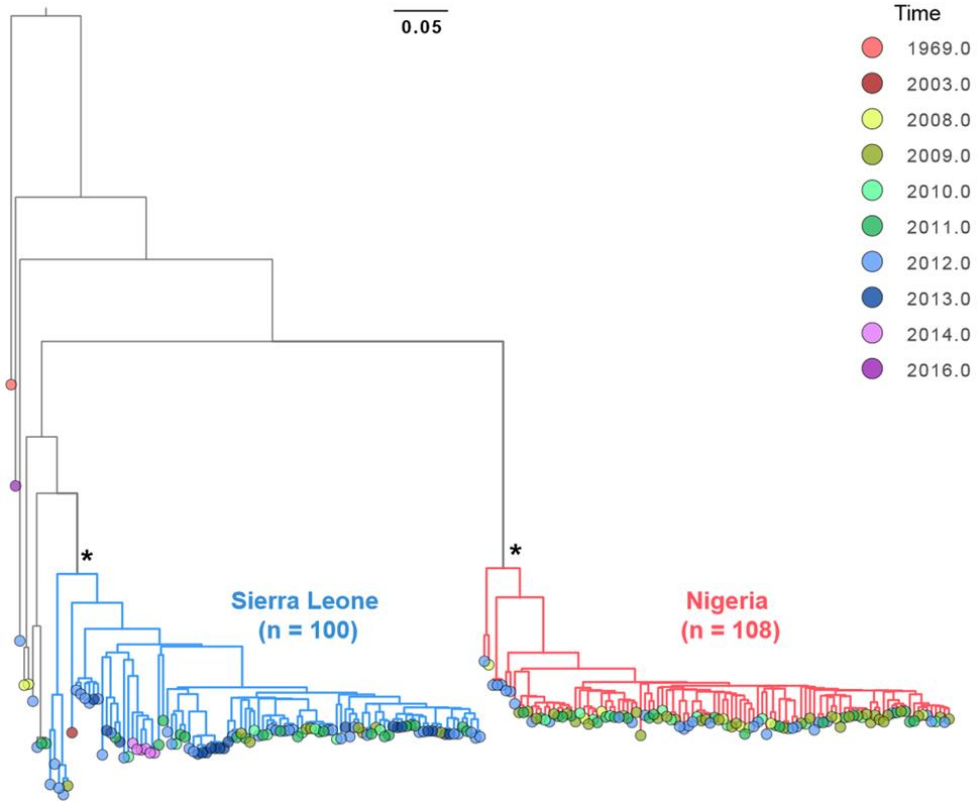


Figure 3.6. Maximum likelihood phylogeny of Lassa virus using GPC gene sequences (n=217). Two main lineages are observed, one predominantly found in Nigeria (Lineage II, red), while the other is mainly found in Sierra Leone (Lineage IV, blue). This evolutionary analysis was performed by Jayna Raghwani at the Big Data Institute, University of Oxford.

Consistent with a recent dN/dS analysis on LASV GPC (*350*), the mean dN/dS ratios for the Nigeria and Sierra Leone clades were estimated at 0.060 and 0.063, respectively. Using the crystal structure of LASV GPC, it was revealed that solvent-accessible residues were characterized by significantly higher dN/dS (mean dN/dS ratios estimated at 0.070 and 0.080 for the Nigeria and Sierra Leone lineages, respectively), compared with buried residues (mean dN/dS ratios estimated at 0.015 and 0.028 for the Nigeria and Sierra Leone lineages, respectively) (**Figure 3.7.B**). Interestingly, when mapped onto the structure, amino acids corresponding to nucleotides with the greatest relative number of nonsynonymous substitutions colocalized to regions of the GPC surface with lower levels of glycan density (**Figure 3.7.C**), distal from the functionally required α-DG binding site (*351*). These data provide a structural rationale for how protein surfaces occluded by glycan density are shielded from the humoral antibody response of the host and also rationalize previous suggestions that immune selection is a predominant driver of nonsynonymous substitutions for accessible regions of the LASV GPC (*350*).

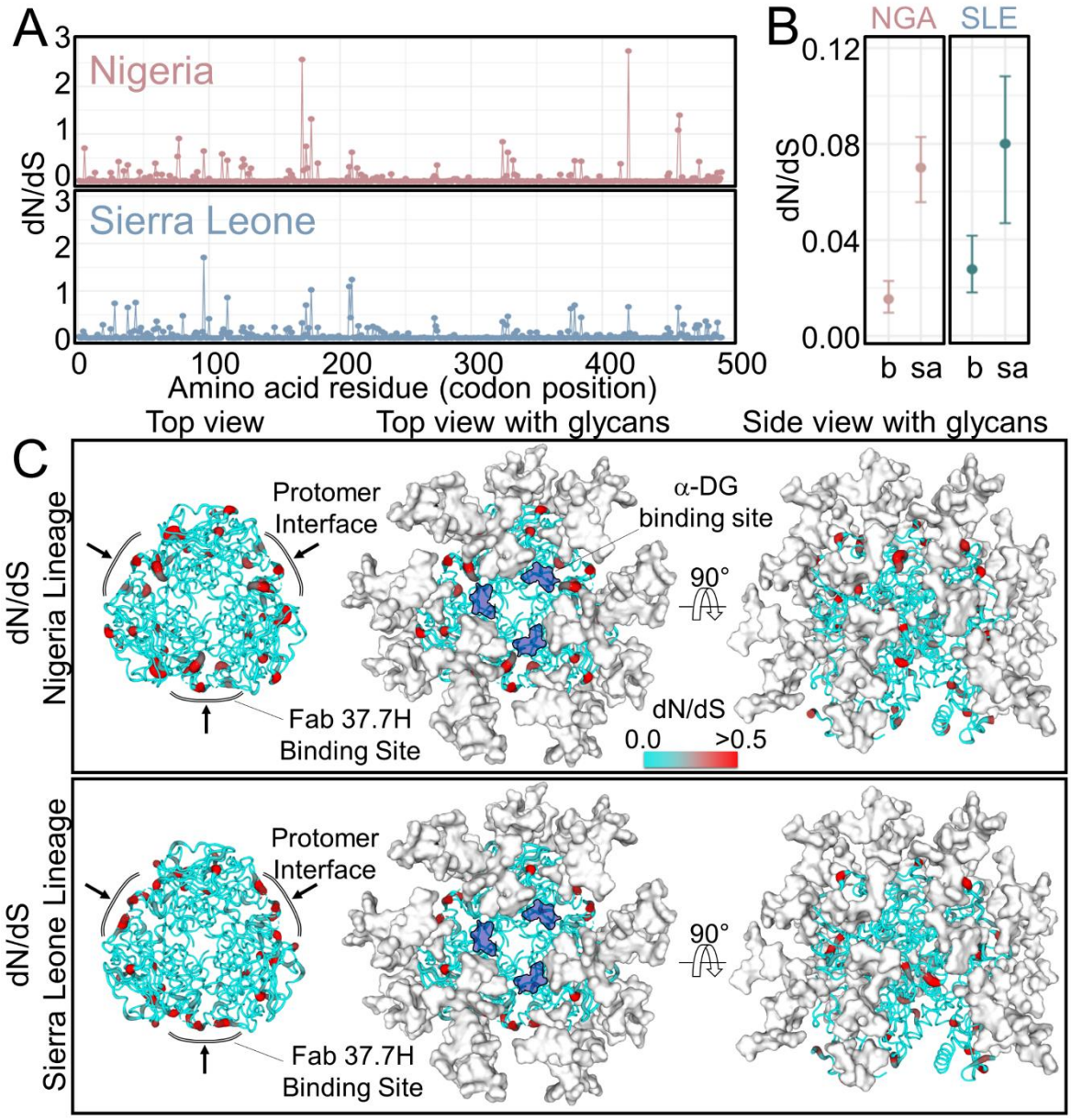


Figure 3.7. Amino acid sequence diversification across the LASV GPC. (A) Site-wise dN/dS analysis of LASV GPC gene sequences from the Nigeria (red, lineage II) and Sierra Leone (blue, lineage IV) lineages. **(B)** Comparison of dN/dS values between buried (b) and solvent-accessible (sa) residues on the LASV GPC for Nigeria (NGA) and Sierra Leone (SLE). The error bars correspond to the 95% highest posterior density intervals, while circles indicate mean dN/dS values. **(C)** Mapping of per residue dN/dS values presented in A onto the crystal structure of LASV GPC (PDB ID code 5VK2) (*117*). LASV GPC is presented as a cartoon with residues coloured according to dN/dS values. Residues with elevated dN/dS values are coloured in red, and N-linked glycans are presented as white surfaces. The putative α-DG binding site is shown in dark blue (*199*). The interprotomer epitope of Fab 37.7H on LASV GPC is also shown. The evolutionary analysis in **(A)** was performed by Jayna Raghwani at the Big Data Institute, University of Oxford.

On a broader level, we note the stringent conservation of LASV GPC N-linked glycosylation sequons across Old World arenaviruses, including the five glycan sites that constitute the LASV mannose cluster (**Figure 3.8.A**), suggesting that mannose patches may be inherent features of Old World arenaviral GPCs. In contrast, the glycan sites constituting the GP1 component of the mannose patch are less prevalent in New World arenaviral GPCs. This juxtaposition may be due to contrasting functional restraints (for example, the requirement to use transferrin receptor rather than α-DG). It is suggested that such differential levels of N-linked glycosylation site conservation on the GP1 may at least partially account for the contrasting locations of immunodominant neutralizing epitopes on New World (the GP1 subunit) and Old World (GP1−GP2 interfaces) GPCs (*117*, *197*, *352*, *353*).

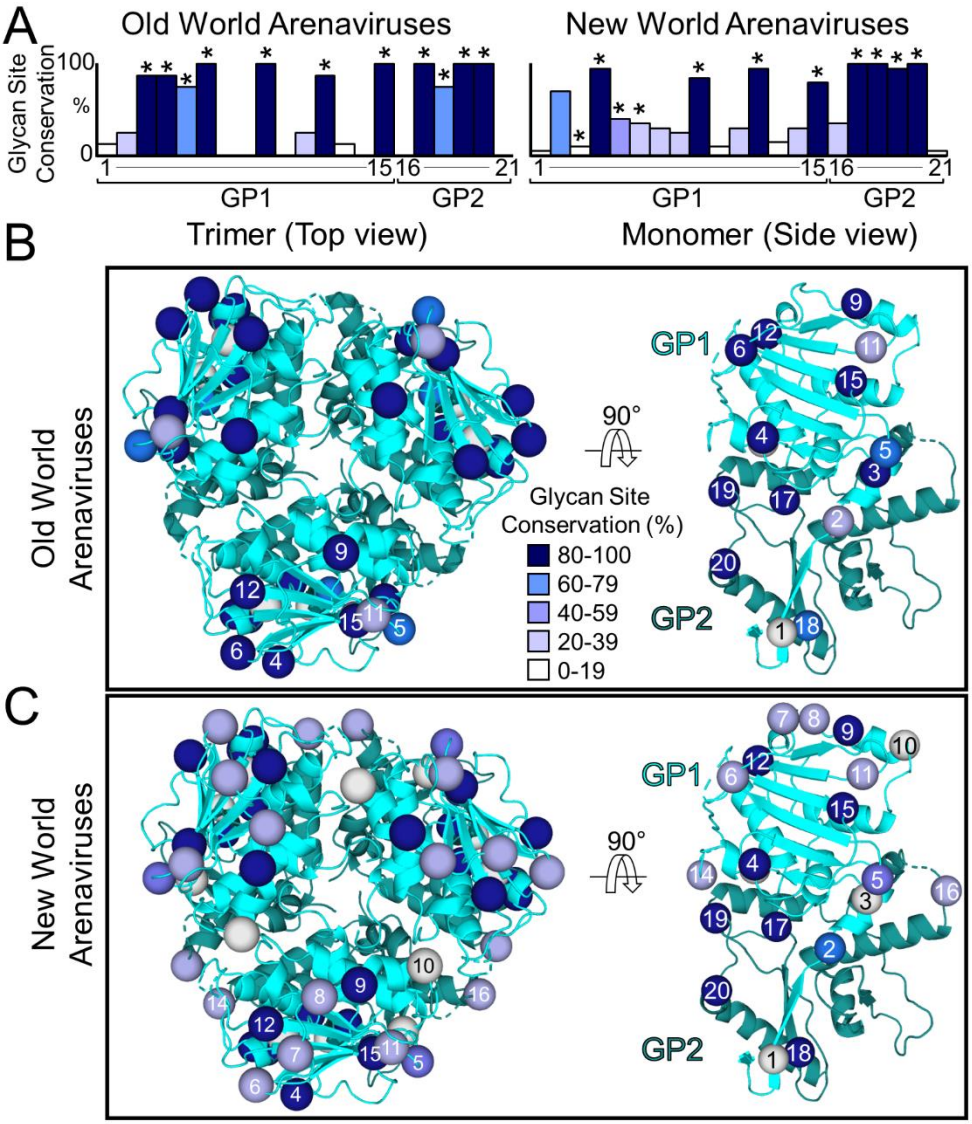


Figure 3.8. N-linked glycosylation site conservation across Old and New World arenaviruses. (A) Glycan site conservation across arenaviruses following sequence alignment with Jalview (*354*). Glycan sites are numbered according to the nomenclature established by Sommerstein et al. (*13*), with those present on LASV GPC labelled with asterisks. (B and C) The positions of **(B)** Old World and **(C)** New World arenavirus N-linked glycosylation sequons mapped onto the structure of LASV GPC (PDB ID code 5VK2) (*117*). Spheres are coloured according to the level of conservation of each glycosylation site.

3.4. Glycosylation of Lassa virus immunogens

As the main target of the humoral immune response, the LASV GPC constitutes the main focus for the development of vaccine development. Engineering trimeric recombinant

LASV GPC ectodomains has been extremely challenging, seemingly due to the distance between the stalks of the trimers. Indeed, when the crystal structure of the trimeric LASV GPC (PDB ID: 5VK2) was solved, GP1-GP2 protomers were trimerized using 37.7H Fabs that binds at the protomer interfaces of the GPC (*117*). Our collaborators from AMC were able to engineer trimeric LASV GPCs using a two-component nanoparticle (NP) system (*355–357*) of two LASV strains, Josiah (JOS) and Nigeria (NIG). In order to ascertain whether the candidate immunogens had a native-like structure, and to investigate whether the glycosylation was virus-like, global and site-specific glycan analyses were performed on these engineered GPCs

HILIC-UPLC analysis revealed extremely similar oligomannose-type glycan populations and overall profile to the GPCs derived from VLPs (49.5% oligomannose), with the JOS and NIG NPs presenting 49.18% and 47.47% oligomannose-type glycans, respectively (**Figure 3.9**). Since glycans are sensitive reporters of protein architecture, these results indicated the native-like trimeric structure of the GPCs.

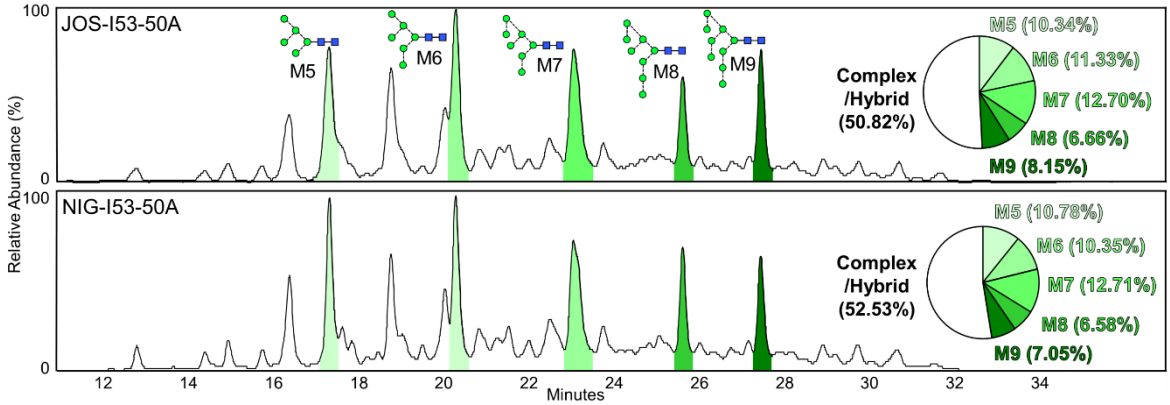


Figure 3.9. HILIC-UPLC profile of fluorescently labelled N-linked glycans from recombinant JOS and NIG LASV GPCs expressed in HEK-293F cells for incorporation into NPs. Oligomannose-type glycans (M5 to M9; $Man_5GlcNAc_2$-$Man_9GlcNAc_2$) (green) and complex-type glycans (white) were identified by Endo H digestion, with quantification of major glycan types summarized as a pie chart.

Site-specific glycan analysis on the proteins was subsequently performed to probe the precise carbohydrate structures presented at each N-linked glycan site (**Figure 3.10**). Similar to the HILIC-UPLC analysis, the glycan processing states at each site was remarkably conserved to the glycosylation of the LASV GPC from VLPs. In particular, the conservation of the oligomannose-type glycan cluster on the side of the trimer composed of the glycans at N79, N89, N99, N365 and N373, which spans both the GP1 and GP2 subunits indicates the native-like structural integrity of these engineered glycoproteins. These immunogens are currently being tested in animals.

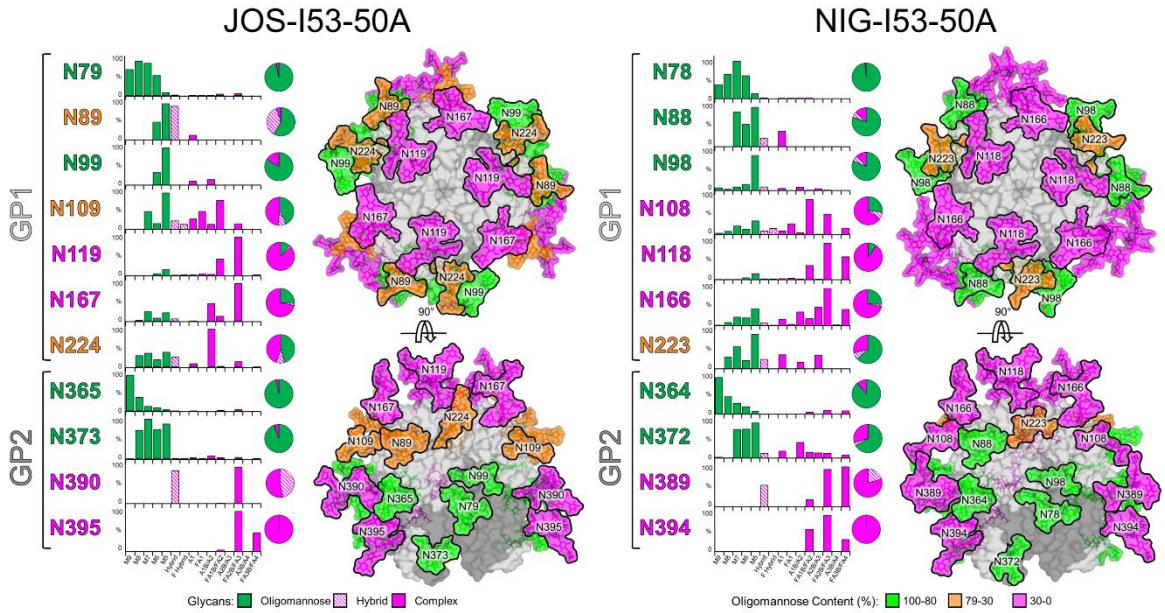


Figure 3.10. Compositional analysis and structure-based mapping of JOS and NIG LASV GPC N-linked glycans. The bar graphs represent the relative quantities of each glycan group with oligomannose-type glycan series (M9 to M5; $Man_9GlcNAc_2$ to $Man_5GlcNAc_2$) (green), afucosylated and fucosylated hybrid glycans (Hybrid & F Hybrid) (dashed pink), and complex glycans grouped according to fucosylation and number of antennae (A1 to FA4) (pink). The pie charts summarize the quantification of these glycans. Modelling experimentally observed glycosylation onto the crystal structure of the trimeric LASV GPC (PDB ID code 5VK2) (*117*). The glycans are coloured according to the oligomannose content, as defined by the key.

3.5 Discussion

While the LASV GPC constitutes a key therapeutic target, vaccine design efforts have been hindered by the host-derived glycosylation that encompasses the protein surface (*13*). Here, using an established VLP expression strategy, a comprehensive compositional investigation of the LASV glycome was performed. The LASV GPC was produced in MDCK-II cells and forms a native-like conformation on the surface of the VLP (**Figure 3.1. B & C**) (*200*, *314*, *341*). Although MDCK-II cells do not represent a natural host cell type, due to the stringent conservation of the N-linked glycan biosynthesis processing pathway (*54*) across mammalian cell types (*358*, *359*), only limited variations in the composition and abundance of the N-linked glycosylation of LASV GPC is expected. Additionally, it has been shown that the HIV-1 glycome is determined by structural constraints and is compositionally well conserved when produced in varied mammalian cell types (*155*). It is suggested that future studies on the glycosylation state of circulating viruses in LASV-infected patients should corroborate these findings.

In this chapter, I present a structure-based model for rationalizing glycan-mediated shielding of LASV GPC from the humoral host response, revealing a cluster of underprocessed glycans that spans both the GP1 and GP2 subunits of the trimeric spike complex (**Figure 3.4**). While the presence of mannose-rich glycosylation is unusual for cellular proteins, it has often been observed on enveloped viruses, such as orthomyxoviruses, phleboviruses, alphaviruses, and flaviviruses (*220*). The principles rationalizing the extent of glycan processing of viral proteins have yet to be fully elucidated and should be considered in the context of the route of egress from the host cell. In the case of LASV, however, it is suggested that the formation of underprocessed moieties is likely enabled by the local structural environment and that the proximity of glycans extending from $Asn79_{GP1}$,

Asn89$_{GP1}$, Asn99$_{GP1}$, Asn365$_{GP2}$, and Asn373$_{GP2}$ sterically impede accessibility to glycan-processing enzymes (**Figure 3.9**).

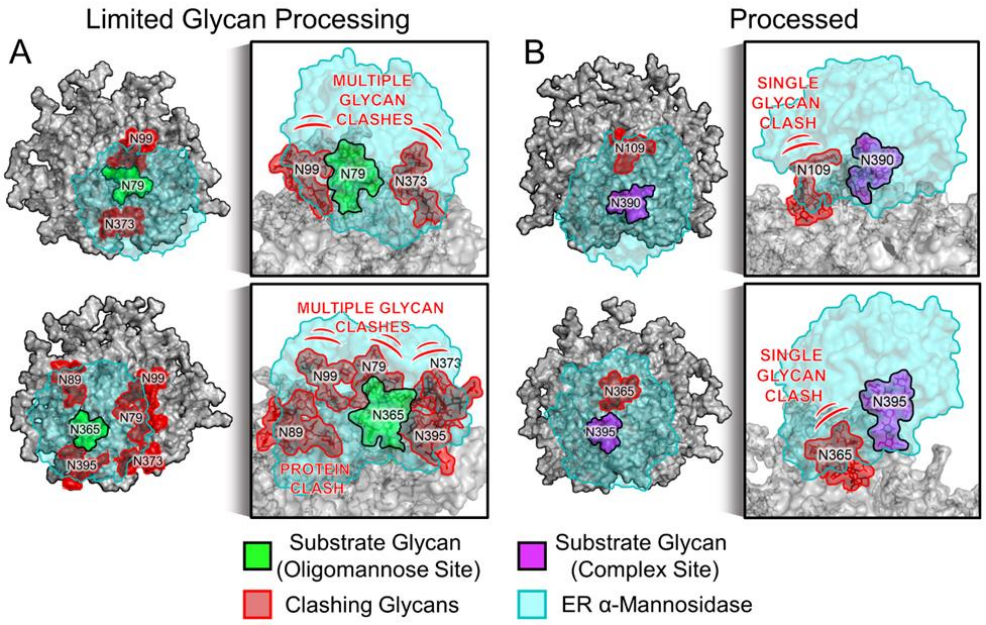


Figure 3.9. A model for rationalizing enzymatic resistance to glycan processing on the LASV GPC. (A) The crystal structure (PDB ID: 5KIJ)(*240*) of ER α1,2-mannosidase I (cyan) was modelled onto the $Man_9GlcNAc_2$ substrate glycans (green) of N79 and N365 of LASV GPC (PDB: 5VK2)(*117*). Neighbouring glycan sites that sterically clash with the enzyme are highlighted in red. **(B)** Modelling of ER α1,2-mannosidase I (cyan) onto $Man_9GlcNAc_2$ at positions N390 and N395 (pink) revealed only partial clashes with a single neighbouring glycan.

Oligomannose-type glycans were also observed at sites outside of this cluster, albeit at lower levels. The presence of oligomannose at multiple locations across the GPC is suggestive of a promiscuous model of DC-SIGN usage, where numerous N-linked glycans may contribute as attachment factors for LASV entry.

The existence of a large population of oligomannose-type structures on LASV GPC has important consequences in the development and production of recombinant vaccine candidates. On recombinant glycoproteins, oligomannose-type glycans are considered to impart elevated clearance rates and may influence immunogenicity (*360*, *361*). In addition, from immunogen design efforts for HIV, it is known that the levels of oligomannose-type

glycans on recombinant mimics of the envelope spike are highly sensitive to the structural constraints imposed by native-like trimeric oligomeric architecture (*152*, *155*). Given the importance of both glycan processing states and native quaternary architecture, it is likely that the current recombinant expression technologies for LASV GP1 (*116*, *343*, *344*) and GPC (*117*) monomeric ectodomains may not reproduce native-like glycosylation. We envisage that the next generation of full-length LASV GPC ectodomain immunogens will both exhibit trimeric architecture and suppress the exposure of natively inaccessible epitopes through the presentation of more-native-like glycosylation.

This study also reveals that amino acid diversification occurs primarily at glycan-devoid regions on the LASV GPC (**Figure 3.7**), providing important clues to what sites may be most vulnerable to the antibody immune response. By analogy to template-based vaccinology approaches against "evasion-strong" pathogens (*165*), such as HIV-1, it is possible that these regions are viable targets for the development of immunogens capable of effectively neutralizing LASV.

Continued emergence and high pathogenicity render LASV an important human pathogen and underscore the necessity for reagents capable of preventing and treating infection. Given the prominence of N-linked glycosylation on the LASV surface, it is suggested that the compositional and structural data presented here will be integral for the creation of a humoral immunity-based vaccine capable of mimicking the mature LASV virion.

4. Vulnerabilities in coronavirus glycan shields despite extensive glycosylation

Coronaviruses (CoVs) are enveloped pathogens responsible for multiple respiratory disorders of varying severity in humans (*362*). Certain CoVs represent a significant threat to global human health, as illustrated by outbreaks of severe acute respiratory syndrome coronavirus (SARS-CoV) in 2003 (*363*), Middle East respiratory syndrome coronavirus (MERS-CoV) in 2012 (*364*), and most recently of SARS-CoV-2 (*365*). Given their mortality rates, the current lack of targeted treatments and licensed vaccines, and their capacity to transmit between humans and across species barriers (*366*, *367*), there is an urgent need for effective countermeasures to combat these pathogens. Ongoing vaccine development efforts focus on the spike (S) proteins that protrude from the viral envelope and constitute the main target of neutralizing antibodies (*368*, *369*).

These trimeric S proteins mediate host-cell entry with the S1 and S2 subunits responsible for binding to the host cell receptor and facilitating membrane fusion, respectively (*205*, *315*, *370*). MERS S binds to dipeptidyl-peptidase 4 (DPP4) (*371*), whereas SARS S (*372*) and SARS-CoV-2 (*316*, *373*) utilize angiotensin-converting enzyme 2 (ACE2) as a host cellular receptor. CoV S proteins are the largest class I viral fusion proteins known (*205*), and are extensively glycosylated, with SARS and MERS S glycoproteins both encoding 69 N-linked glycan sequons per trimeric spike with SARS-CoV-2 containing 66 sites. These modifications often mask immunogenic protein epitopes from the host humoral immune system by occluding them with host-derived glycans (*8*, *186*, *374*). This phenomenon of immune evasion by molecular mimicry and glycan shielding has been well characterised across other viral glycoproteins, such as HIV-1 envelope protein

(Env) (*150, 375, 376*), influenza hemagglutinin (HA) (*171, 177*) and Lassa virus glycoprotein complex (LASV GPC) (*13, 140, 377*).

Previous analyses of viral glycan shields have revealed the presence of underprocessed oligomannose-type glycans that seemingly arise due to steric constraints that prevent access of glycan processing enzymes to substrate glycans (*140, 151, 156*), especially when the viral glycoprotein has evolved to mask immunogenic epitopes with a particularly dense array of host-derived glycans (*50, 377–382*). Restricted access to these glycan sites or interference with surrounding protein surface or neighbouring glycan residues can render glycan processing enzymes ineffective in specific regions (*67, 151, 156*). Glycan processing on soluble glycoproteins has also been shown to be a strong reporter of native-like protein architecture and thus immunogen integrity (*2, 3, 155*); and glycan processing on a successful immunogen candidate should therefore mimic, as closely as possible, the structural features observed on the native virus (*51, 168*).

Here, I provide global and site-specific analyses of N-linked glycosylation on soluble SARS, MERS and HKU1 CoV S glycoproteins and reveal extensive heterogeneity, ranging from oligomannose-type glycans to highly-processed complex-type glycosylation. The structural mapping of glycans of trimeric S proteins revealed that some of these glycans contribute to the formation of a cluster of oligomannose-type glycans at specific regions of high glycan density on MERS-CoV S. Molecular evolution analysis of SARS and MERS S genes also reveals a higher incidence of amino-acid diversity on the exposed surfaces of the S proteins that are not occluded by N-linked glycans. Additionally, a comparison of the structures of the respective glycan coats of SARS and HIV-1 envelope proteins is provided using cryo-electron microscopy (cryo-EM) and computational modelling, which delineate a sparse glycan shield exhibited on SARS S compared to other viral glycoproteins.

Subsequently, a comparative analysis of viral glycan shields from characterized class I fusion proteins was undertaken to highlight how glycosylation density influences oligomannose-type glycan abundance, and the relationship between effective glycan shields and viral evasion ability. Together, these data underscore the importance of glycosylation in viral immune evasion.

4.1 Glycan Processing of Trimeric SARS and MERS Spike proteins

To generate a soluble mimic of the viral S proteins, I expressed the 2P stabilised native-like SARS and MERS S protein antigens, the design and structures of which have been described previously by Pallesen et al. (*192*). SARS, MERS and HKU1 S genes encode many N-linked glycan sequons; 23, 23 and 29, respectively (**Figure 4.1 A**). I initially sought to quantitatively assess the composition of the carbohydrate structures displayed on the S glycoproteins. N-linked glycans were enzymatically released, fluorescently labelled, and subjected to hydrophilic interaction chromatography-ultra-performance liquid chromatography (HILIC-UPLC). Treatment with endoglycosidase H (Endo H) revealed a population (SARS 32.2%; MERS 33.8%, HKU1 25.0%) of under-processed oligomannose-type glycans (**Figure 4.1 B**). This observation of both complex and oligomannose-type glycans reveals that the majority of N-linked glycans can be processed, although there is limited processing at specific sites across the S proteins. It is also interesting to note that the distribution of oligomannose-type glycans was broad, with $Man_5GlcNAc_2$ to $Man_9GlcNAc_2$ glycans all present, without one particular dominant peak, as is the case for some viral glycoproteins, such as HIV-1 Env (*3*). The proportion of oligomannose-type glycans on recombinant coronavirus S proteins is consistent with previous studies performed on virally derived MERS and SARS coronavirus S proteins (*10, 186*). Coronaviruses have been previously been reported to form virions by budding into the lumen of endoplasmic reticulum-Golgi intermediate compartments (ERGIC) (*25, 383*). Observations of hybrid- and complex-type glycans on virally derived material (*10, 186*) would, however, suggest that it is likely that coronavirus virions travel through the Golgi apparatus after virion formation in the ERGIC en route to the cell surface, thus supporting recombinant immunogens as models of viral glycoproteins.

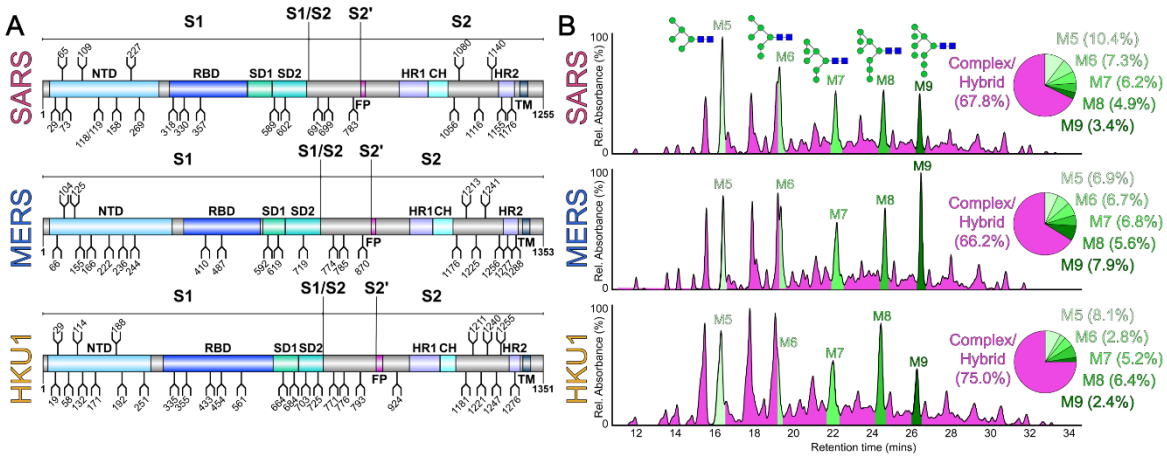


Figure 4.1. Compositional analysis of SARS, MERS and HKU1 glycans. (A) Schematic representation of SARS, MERS and HKU1 coronavirus S glycoproteins, showing the positions of N-linked glycosylation amino-acid sequons (NXS/T, where X ≠ P) shown as branches. The domains of the S glycoproteins are illustrated: N-terminal domain (NTD), receptor-binding domain (RBD), sub-domain 1/2 (SD1/2), fusion peptide (FP), heptad repeat 1/2 (HR1/2), central helix (CH), and transmembrane domain (TM). **(B)** HILIC-UPLC chromatograms of fluorescently labelled N-linked glycans from SARS, MERS and HKU1 S. Oligomannose-type glycans (M5 to M9; $Man_5GlcNAc_2$-$Man_9GlcNAc_2$) (green) and complex-type glycans (magenta) were identified by Endo H digestion, with quantification of major glycan types summarised as a pie chart. Oligomannose-type glycans are schematically annotated with mannose residues as green circles and GlcNAc residues as blue squares.

To ascertain the precise structures of N-linked glycans, glycan pools of each coronavirus S protein were analysed by negative-ion ion-mobility-electrospray ionisation mass spectrometry (IM-ESI MS) (**Figure 4.2**). Consistent with the UPLC data, IM-ESI MS confirmed an array of complex-type glycans ranging from mono- to tetra-antennary, but also oligomannose- and hybrid-type glycans. The glycan compositions characterised in the spectra were largely invariant among the coronaviruses with no major structural differences observed.

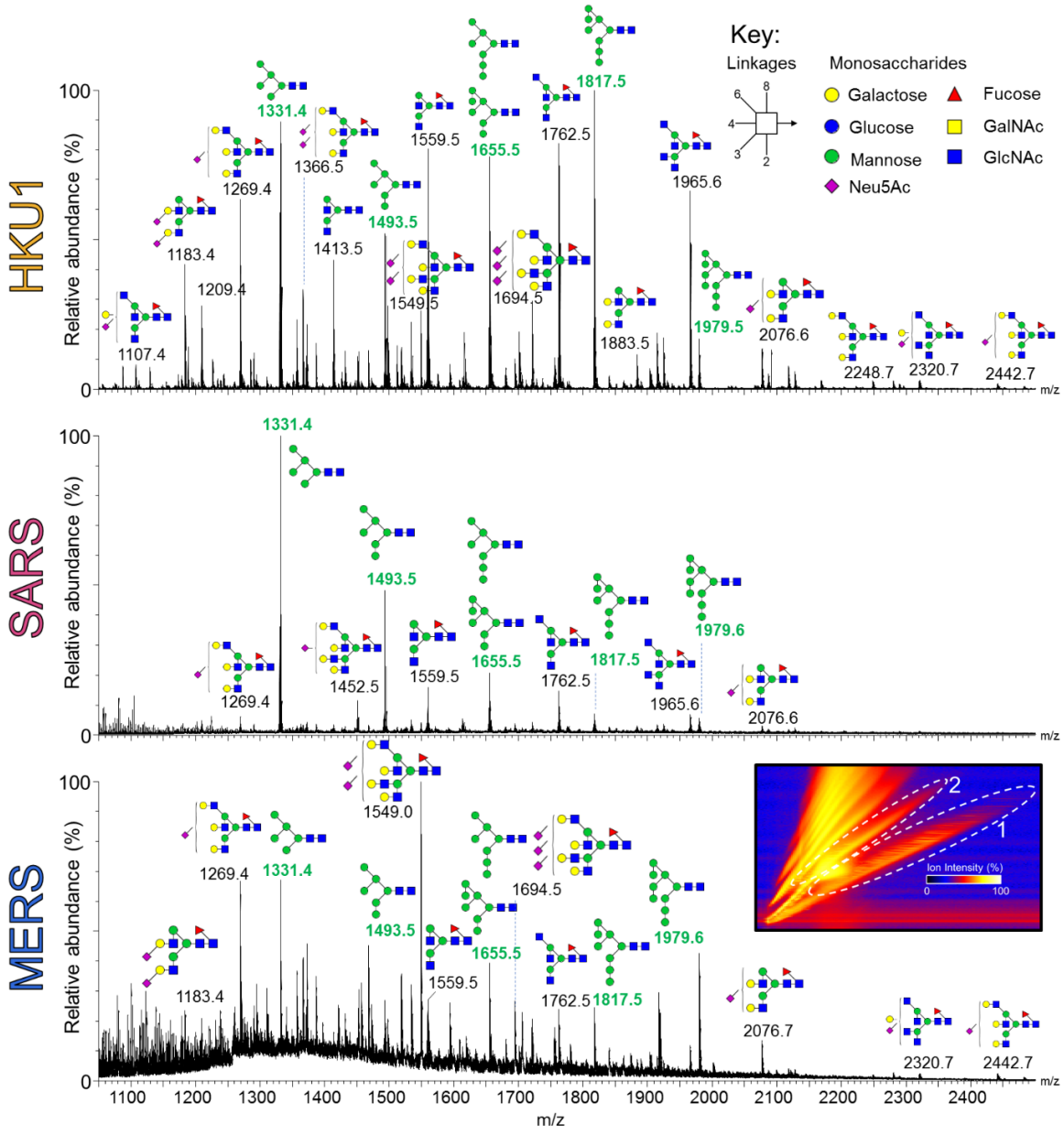


Figure 4.2. Ion mobility-extracted mass spectra of singly- and doubly- charged N-linked glycan ions from HKU1, SARS and MERS S glycoproteins. Peaks are annotated with the corresponding compositions, using Consortium for Functional Glycomics symbolic nomenclature and Oxford system linkages (*31*), as per the key. Oligomannose-type glycan *m/z* values are labelled in green.

4.2 Structural Clustering of Underprocessed Glycans on MERS S.

I subsequently performed glycopeptide analysis to ascertain the compositions of glycans at all the potential N-linked glycosylation sites (PNGs). MERS, SARS and HKU1 recombinant

S proteins were reduced, alkylated and digested with an assortment of proteases to yield glycopeptides, which were subjected to in-line liquid-chromatography mass spectrometry (LC-MS). This revealed differential levels of oligomannose, hybrid, and complex-type glycan populations (**Figure 4.3**).

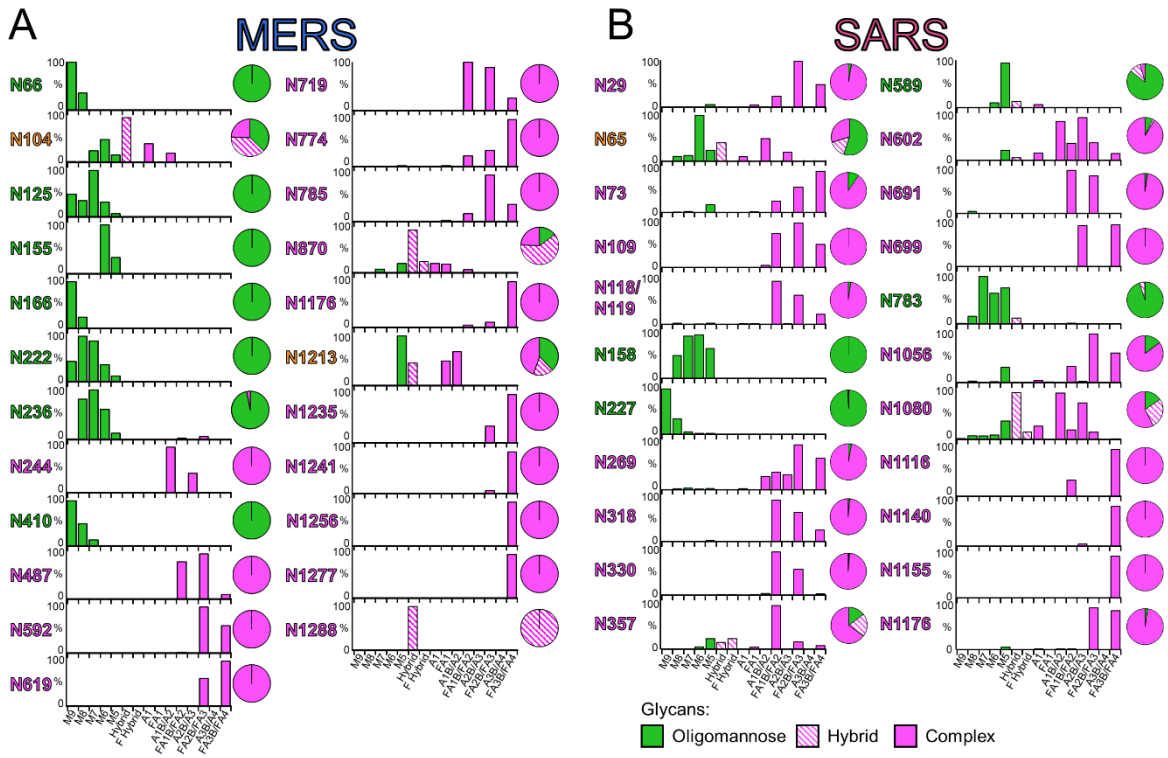


Figure 4.3. Quantitative site-specific N-linked glycan analysis of **(A)** MERS and **(B)** SARS S glycoproteins. Purified S proteins were digested with trypsin, chymotrypsin, alpha-lytic protease, Glu-C, and trypsin plus chymotrypsin, then analysed by LC-ESI MS. Glycan compositions are based on the glycan library generated from negative-ion mass spectrometry of released N-glycans. The bar graphs represent the relative quantities of each glycan group with oligomannose-type glycan series (M9 to M5; $Man_9GlcNAc_2$ to $Man_5GlcNAc_2$) (green), afucosylated and fucosylated hybrid glycans (Hybrid & F Hybrid) (dashed pink), and complex glycans grouped according to the number of antennae and presence of core fucosylation (A1 to FA4) (pink). Left to right; least processed to most processed. The pie charts summarise the quantification of these glycans.

Using structures of the trimeric MERS and SARS S proteins (PDB ID: 5X59 and 5X58, respectively), I generated models of fully glycosylated coronavirus spikes using experimentally determined glycan compositions (**Figure 4.4**). This revealed that

oligomannose-type glycans on MERS S co-localize to specific clusters on the head of the S protein, consisting of glycans at Asn155, Asn166, and Asn236 (**Figure 4.4 A**).

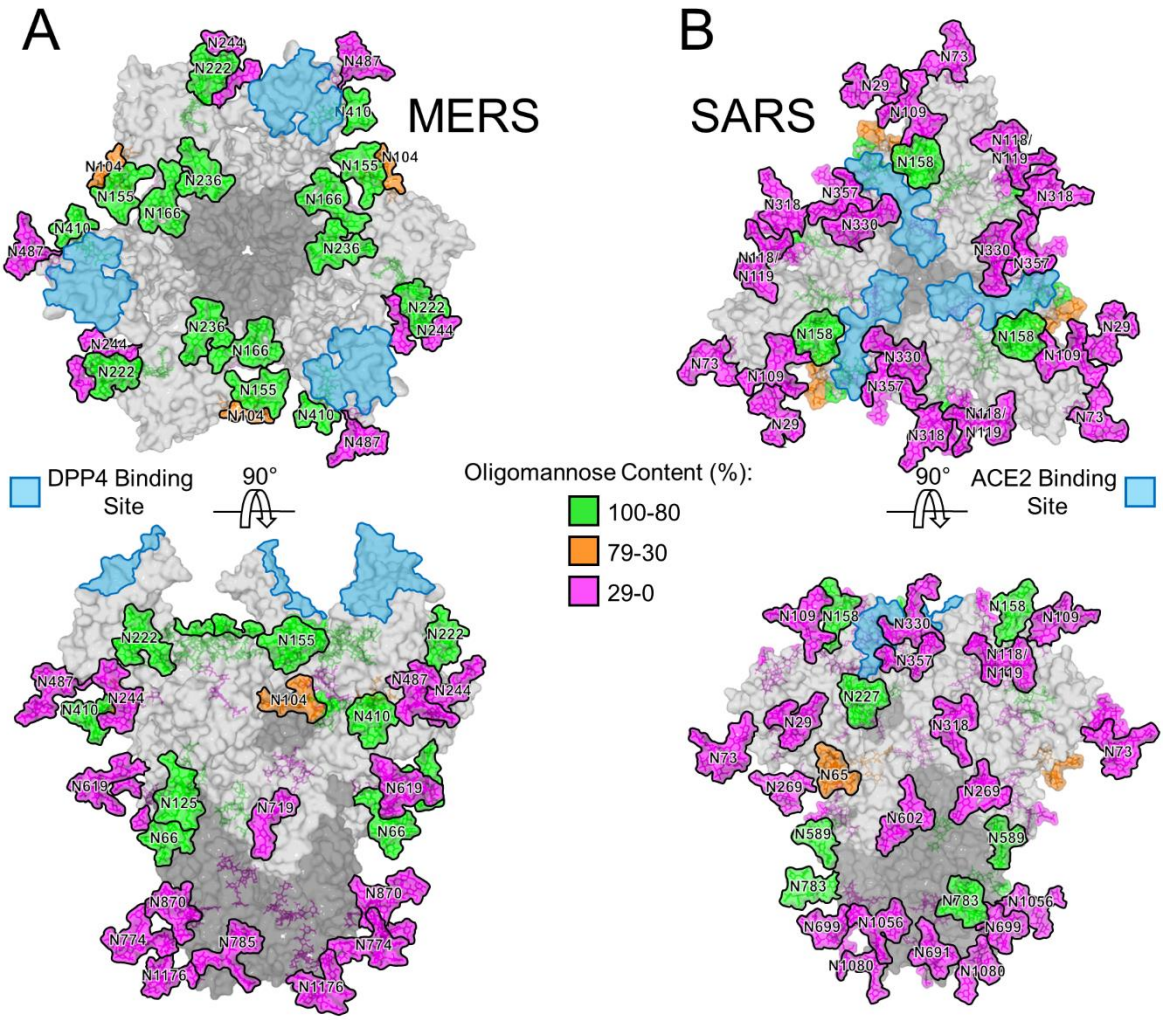


Figure 4.4. Structural-based mapping of N-linked glycans on **(A)** MERS and **(B)** SARS S proteins. The modelling of the experimentally observed glycosylation is illustrated on the pre-fusion structure of trimeric MERS S (PDB ID 5X59) (*315*) and SARS S (PDB ID 5X58) (*315*) glycoproteins. The glycans are colored according to oligomannose content, as defined by the key. DPP4 receptor binding sites and ACE2 receptor binding sites for MERS and SARS, respectively, are indicated in light blue. The S1 and S2 subunits are colored light grey and dark grey, respectively.

It was hypothesized that the fully oligomannose-type glycan population in this cluster arises due to the hindered accessibility of glycan processing enzymes to access the substrate glycan (*151*). As such, I performed mutagenesis to knock out glycosylation sites

with N155A, N166A, and N236A mutations. Site-specific analysis of these glycan-KO mutants revealed enhanced trimming of mannose residues, i.e. increased processing, when glycan clustering was reduced (**Figure 4.5**). The presence of clustered oligomannose-type glycans is reminiscent of that found on other viral glycoproteins, including HIV-1 Env and LASV GPC (*3*, *140*, *152*, *153*, *379*, *382*).

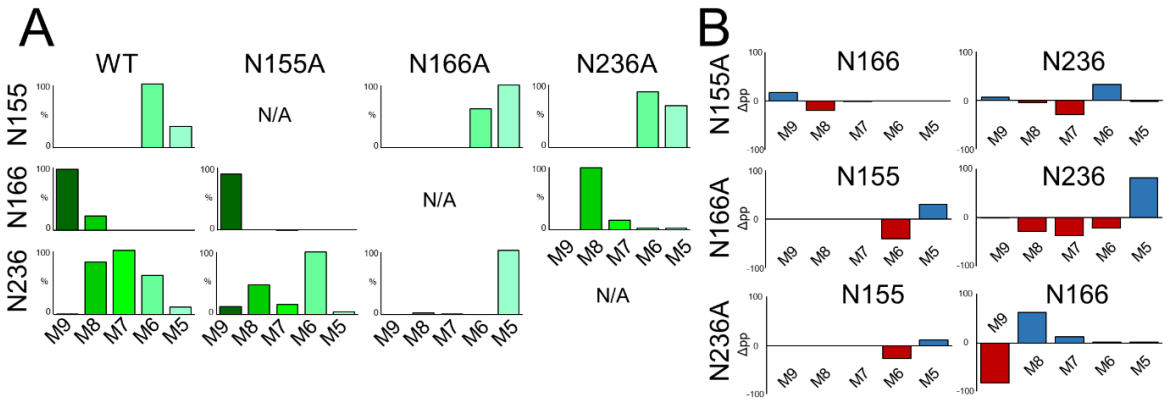


Figure 4.5. Glycan deletion increases mannose trimming of N-linked glycans on MERS S oligomannose patch. (A) Relative quantitation of glycans in the mannose patch sites (N155, N166, N236) on MERS S. M9 to M5; ($Man_9GlcNAc_2$ to $Man_5GlcNAc_2$) (dark green to pale green). (B) Percentage point differences in the abundance of oligomannose-type glycans at mannose patch sites in the glycan knockout mutants compared to WT MERS. Decreased and increased abundances are colored red and blue, respectively.

Interestingly, SARS (**Figure 4.4 B**) and HKU1 (**Figure 4.6 B**) S proteins did not exhibit specific mannose clusters that contribute to the overall mannose abundance, but only isolated glycans were underprocessed. It is hypothesised that the oligomannose-type glycans here arise from protein-directed inhibition of glycan processing, as opposed to the glycan-influenced processing observed on MERS. Importantly, oligomannose-type glycans has also been implicated in innate immune recognition of coronaviruses by lectins (*212*, *283*) that recognise these underprocessed glycans as pathogen-associated molecular patterns.

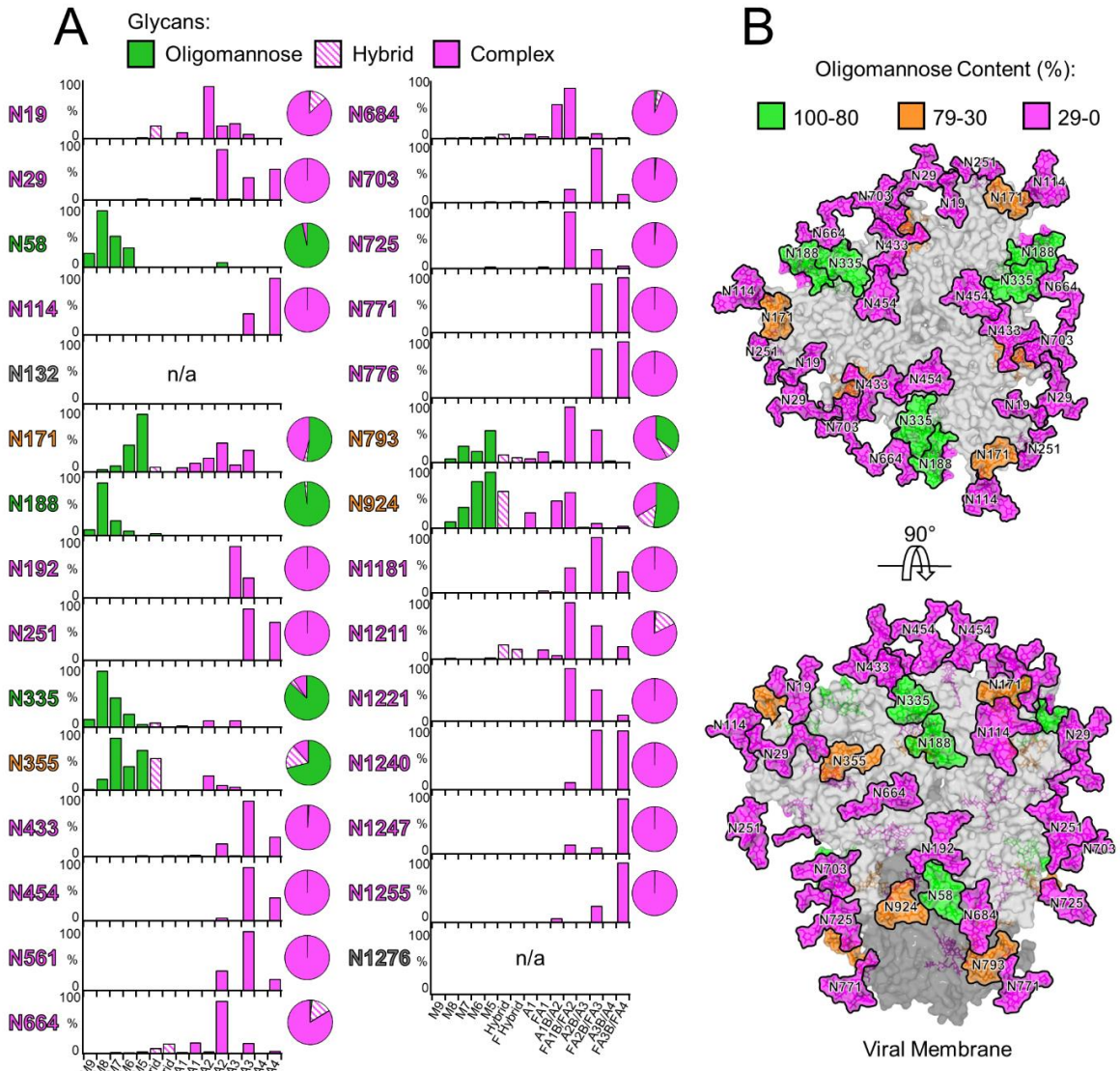


Figure 4.6. Compositional analysis and structure-based mapping of HKU1 S N-linked glycans. **(A)** Quantitative site-specific N-linked analysis of HKU1 S. Purified HKU1 S was digested with trypsin, chymotrypsin, and trypsin + chymotrypsin, then analysed by LC-ESI MS. Glycan compositions are based on the glycan library generated from negative-ion mass spectrometry of released N-glycans. The bar graphs represent the relative quantities of each glycan group with oligomannose-type glycan series (M9 to M5; $Man_9GlcNAc_2$ to $Man_5GlcNAc_2$) (green), afucosylated and fucosylated hybrid glycans (Hybrid & F Hybrid) (dashed pink), and complex glycans grouped according to the number of antennae and fucosylation (A1 to FA4) (pink). Left to right; least-processed to most processed. The pie charts summarise the quantification of these glycans. **(B)** Modelling of experimentally observed glycosylation onto the pre-fusion structure of trimeric HKU1 S (PDB ID code 5I08) (*205*). The glycans are coloured according to oligomannose content, as defined by the upper right-hand key. S1 and S2 subunits coloured light grey and dark grey, respectively.

Given that the receptor binding domain is the main target of neutralising antibodies (*369*), it is surprising that the DPP4 receptor binding site of MERS S was not occluded by glycans (**Figure 4.4 A**), as observed for other receptor-binding sites of class I viral fusion proteins, including SARS S (**Figure 4.4 B**), HIV-1 Env (*187*), LASV GPC (*140*), and influenza HA (*189*). It is suggested that this is likely due to the intrinsic functionality of the receptor-binding domain of MERS S, that would be sterically hindered by the presence of N-linked glycans, whereas other viruses are able to accommodate the post-translational modifications, without greatly perturbing functionality.

4.3 Sequence Diversification Occurs at Antibody-accessible Regions of CoV spikes

It was hypothesized that solvent-accessible, amino-acid residues on S proteins would be undergoing higher rates of mutations compared to buried residues and regions that are occluded by glycans, which are unable to be targeted by host immune responses. To that end, an evaluation of amino-acid diversification on a residue-specific level was performed, using publicly available gene sequences of SARS and MERS S, which was calculated as the number of observed pairwise differences divided by the total number of pairwise comparisons. Firstly, we found that amino-acid diversity was elevated at known epitopes targeted by neutralizing antibodies, such as the N-terminal domain and the receptor binding domains, and reduced in the regions in the S2 domain, such as the fusion peptide, heptad repeat one, and the central helix domains, which are likely subject to greater functional constraints (**Figure 4.7 A**).

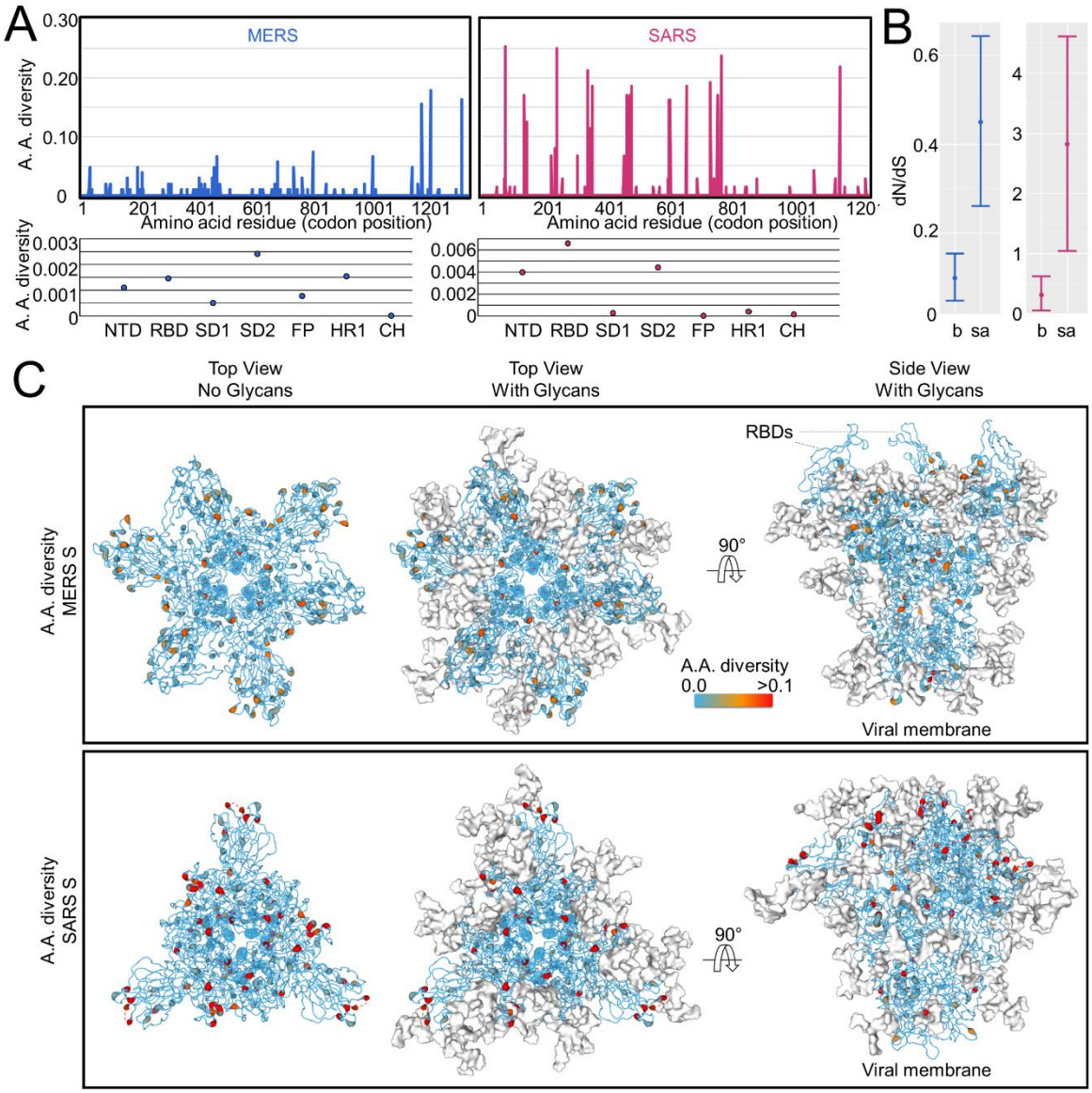


Figure 4.7. Amino-acid sequence diversification across SARS and MERS spikes. **(A)** Amino-acid diversity in SARS and MERS S gene sequences. Averaged values for each domain are also shown below. **(B)** Comparison of dN/dS values between buried and exposed residues across SARS and MERS S (n=70 and 100 for SARS and MERS, respectively). The error bars correspond to the 95% highest posterior density intervals while the circles indicate mean dN/dS values. **(C)** Mapping of the per residue amino-acid diversity shown in **A** onto the structures of SARS and MERS S (PDB ID 5X58 and 5X59, respectively) (*315*). S proteins are presented as backbone traces with residues colored according to amino-acid diversity. Residues with elevated diversity are colored in red, and N-linked glycans are presented as white surfaces. The evolutionary analysis in **(A)** was performed by Jayna Raghwani at the Big Data Institute, University of Oxford.

Analysis of the relative ratio of non-synonymous to synonymous nucleotide substitutions (i.e. dN/dS ratios) revealed that exposed residues exhibited significantly higher dN/dS values (**Figure 4.7 B**). Buried residues on SARS had mean dN/dS ratios of 0.31 compared to 2.82 for exposed resides. Likewise, the buried residues on MERS had a calculated dN/dS ratio of 0.10 compared to exposed residues with a value of 0.45. Furthermore, when per-site amino-acid diversities were mapped onto the fully glycosylated structural model of the respective CoV S proteins (**Figure 4.7 C**), hotspots of mutations were highlighted on the protein surface throughout the trimer revealing extensive vulnerabilities permeating through the glycan shield of SARS and MERS CoVs. It is interesting to note the lack of amino-acid diversity on the receptor binding domains of MERS S proteins that protrude away from the glycans. It is suggested that this may result from the intrinsic receptor binding functionality of these domains.

Although dN/dS estimates are comparable within each viral outbreak, they are not directly comparable between viral families as they can only be considered in the environment in which they are measured (i.e. multiple differences in transmission ecology and host-virus interactions disallow meaningful comparisons). For example, differences in the epidemic behaviour and host immune environment of MERS and SARS outbreaks likely contribute to the observed genetic diversity and thus dN/dS. MERS was characterized by repeated spillover events from camels into humans, where it circulated transiently. In contrast, the SARS outbreak corresponded to a single zoonotic event followed by extensive human-to-human transmission. Consequently, inferring the degree of selection acting upon MERS and SARS from dN/dS analysis is extremely difficult. Importantly, while similar analyses of SARS-CoV-2 is desirable, due to the low genetic variation among the current SARS-CoV-2 sequences (as of 17th March 2020), which likely include deleterious mutations

that will be removed by selection over time, the resulting bioinformatic analyses would be unreliable.

4.4 Visualising the HIV-1 and SARS glycan shields by cryo-EM

HIV-1 Env is a prototypic viral class I fusion protein that exhibits extensive surface glycosylation, resulting in an effective glycan shield to aid evasion from the host adaptive immune response (*376, 379*). In order to visualize the structure of the respective glycan "shields" of HIV-1 and SARS coronavirus we used single-particle cryo-electron microscopy (cryo-EM). The results for HIV-1 Env were reproduced directly from Berndsen et al. (*384*) while the previously published SARS 2P dataset (*385*) was reprocessed for this study. Although cryo-EM datasets of fully glycosylated MERS S (*192*) and chimpanzee simian immunodeficiency virus (SIVcpz) (*317*) are also available, only the HIV and SARS data were of sufficient quality (**Figure 4.8**).

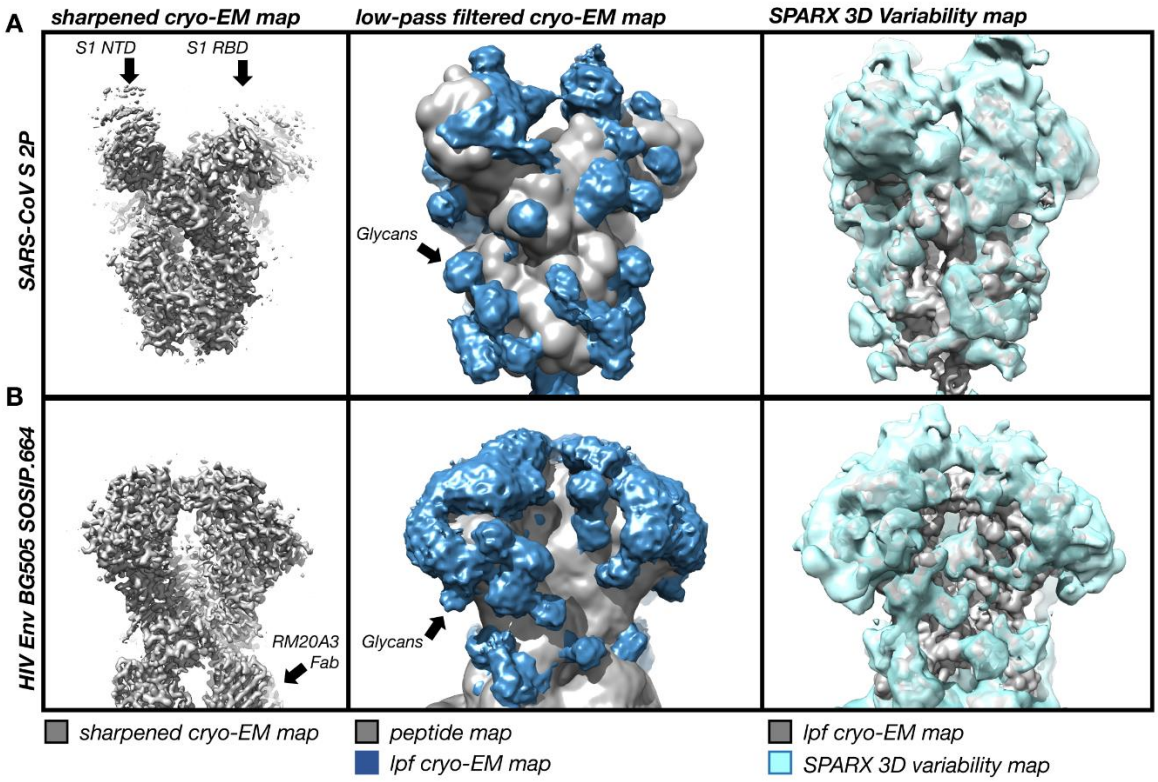


Figure 4.8. Comparative cryo-EM analysis of SARS S and HIV-1 Env glycan shields. **(A)** Left panel: Sharpened 3.2Å-resolution C3-symmetric cryo-EM map of SARS S 2P ectodomain (*385*) visualized at a high contour level with disordered S1 receptor binding and N-terminal domains extending out from the central core. Middle panel: Low-pass filtered (lpf) cryo-EM map of the glycoprotein visualised at a low contour level along with a simulated peptide-only map overlaid. Right panel: SPARX 3D variability map (*384*). **(B)** Same as in **(A)** but for HIV-1 Env BG505 SOSIP.664 construct in complex with 3 copies of RM20A3 base-specific Fabs (*384*). This work was performed by Zachary Berndsen at the Scripps Research Institute.

It has previously been shown that dynamics in surface exposed glycans HIV-1 Env leads to an extensive network of interactions that drive higher-order structuring in the glycan shield (*384*). This structure defines diffuse boundaries between buried and exposed surface protein surface, which can serve to define potential sites of vulnerability. Cryo-EM captures the ensemble-average structure of biomolecules and therefore glycan dynamics results in blurred density at the resolutions necessary for building atomic structure. However, a simple combination of low-pass filtering and auto-thresholding, as well as 3D variability analysis, can reveal the previously hidden structure of the SARS glycan shield and compare it with

the HIV-1 Env glycan shield (*384*) (**Figure 4.8**). We observe the nearly all-encompassing glycan density on HIV-1 Env and evidence for extensive glycan-glycan interactions, especially in the oligomannose patch regions, whereas the glycans on SARS S appear more isolated and lack the wide-ranging glycan networks that are the hallmark of an effective glycan shield (*386*, *387*). The 3D variability maps are more sensitive to low intensity signal and reveal additional glycan-glycan interactions in both maps, however the S1 receptor binding domains in the SARS dataset were shown to exist in both up and down conformations (*385*), leading to poor resolution and significant 2D-variability which is convolved with the variability coming from glycans and limits the interpretability of glycan shielding effects in this region of the map.

4.5 Comparison of Viral Glycosylation Reveals Disparate Shielding Efficacies

Viral envelope proteins are glycosylated to varying degrees, but depending on their overall mass, surface area, and volume, the overall density of glycan shielding may differ significantly. For example, both LASV GPC and coronavirus S proteins consist of 25% glycan by molecular weight. However, given the significantly larger protein surface area and volume of coronavirus S proteins, coverage of the glycan "shield" over the proteinaceous surface is considerably sparser in comparison to the smaller LASV GPC, which occludes a far greater proportion of the protein surface with fewer glycans. To demonstrate that the presence of glycosylation plays a major role in the immune response to these different glycoproteins, I studied the glycome of several biomedically important coronaviruses and compared their glycan compositions in a structural context.

I then investigated the glycan shield densities of seven viral class I fusion proteins using a global structural approach which was calculated by dividing the number of amino-acids that interact with glycans by the number of solvent-accessible amino-acid residues of each respective glycoprotein and plotted this against oligomannose abundance. A strong correlation was observed (**Figure 4.9**) and viruses historically classified as "evasion strong" (*165*) had significantly elevated glycan shield densities and oligomannose abundance, which underscores the importance of glycan shielding in immune evasion.

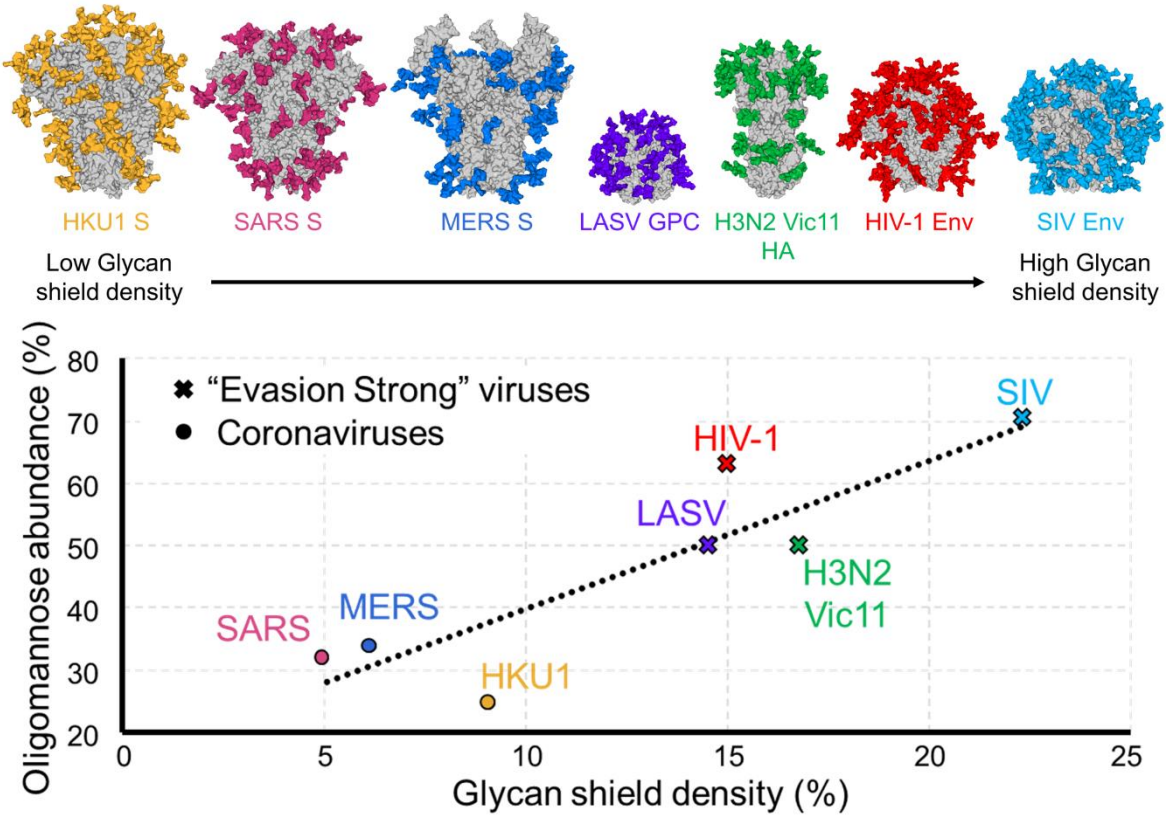


Figure 4.9. Comparison of the glycan shields of viral class I fusion proteins. Glycan shield densities were calculated using Proteins, Interfaces, Structures and Assemblies (PISA)(*321*) analyses of fully glycosylated models of SARS S, MERS S, HKU1 S, LASV GPC, HIV-1 Env (BG505), Influenza H3N2 hemagglutinin (Victoria 2011), SIV Env (PDB ID 5X58, 5X59, 5I08, 5VK2, 4ZMJ, 4O5N, 6OHY, respectively) (*7*, *117*, *143*, *205*, *315*, *317*). Oligomannose abundances of viral glycoproteins were ascertained by HILIC-UPLC analysis of PNGase F released N-linked glycans that were fluorescently labelled with procainamide (*140*, *152*, *317*)**.** The number of amino-acid residues interacting with N-linked glycans was divided by the number of solvent-accessible amino-acid residues of the glycoprotein as a measure for global glycan shield density. All viral glycoproteins analysed

were expressed as trimers in HEK 293F cells apart from LASV GPC, which was derived from virus-like particles from Madin-Darby canine kidney II cells.

Whether the restricted glycan shielding observed on coronaviruses is linked to the zoonosis of the pathogens is unknown. However, it is tempting to speculate, for example, that MERS has not evolved a dense shield since it would not offer as much of a protective advantage against camel nanobodies (also known as single-domain antibodies) which could more easily penetrate it. Investigation of the host immune response to viruses in their natural reservoirs may offer a route to understanding why coronavirus glycosylation does not reach the density of other viruses such as HIV-1. Additionally, it may be that functional constraints, such as maintaining flexibility of the receptor binding domains, limit the accretion of glycans on coronavirus spikes, which would render it incapable of performing its primary functions, including receptor binding and membrane fusion. This phenomenon has been observed on other viral glycoproteins, including influenza HAs, where there is a limit to the accumulation of glycosylation sites that can be incorporated *in vivo* (*182*, *388*), compared to *in vitro* (*389*), with H3N2 and H1N1 HAs replacing existing PNGs rather than continually adding them upon the glycoprotein (*171*, *388*). The importance of glycosylation in modulation of viral infectivity and immune responses have also been investigated during influenza vaccine research (*171, 390*) and should be considered in coronavirus vaccine research.

Although it is difficult to directly compare viruses in terms of immunogenic responses, on the one hand, SARS and MERS coronaviruses readily elicit neutralizing antibodies following infection or immunization (*391–394*). Indeed, many potential MERS CoV vaccine candidates are able to elicit high titres of serum IgG upon immunization but fail to produce sufficient mucosal immunity (*394*). In contrast, the high mutation rate (*395*)

and the evolving glycan shield of HIV-1 (*51, 150*), which firmly exemplifies it as "evasion strong" virus, hinders the development of broadly neutralizing antibodies (*396*).Viruses classified as "evasion strong" (*165, 377*) may then differ due to varied efficacies of protein surface shielding by glycans.

Overall, this study adds further evidence suggesting that extensive N-linked glycan modifications of SARS and MERS CoV S proteins do not constitute an effective shield, in comparison to glycan shields of certain other viruses, which is reflected by the overall structure, density and oligomannose abundance across the corresponding trimeric glycoproteins. It is also demonstrated that amino-acid diversification indeed occurs at antibody accessible regions on the trimer, which confirms that glycans play a role in occluding specific regions if vulnerability on the glycoprotein. Furthermore, comparisons between glycan shields from a number of viruses highlight the importance of a glycan shield in immune evasion and reveal structural principles that govern glycosylation status.

4.6 Site-specific glycan analysis of the SARS-CoV-2 Spike

Severe acute respiratory syndrome coronavirus-2 (SARS-CoV-2), the causative pathogen of COVID-19 (*365, 397*), induces fever, severe respiratory illness and pneumonia. SARS-CoV-2 utilizes an extensively glycosylated spike (S) protein that protrudes from the viral surface to bind to angiotensin-converting enzyme 2 (ACE2) to mediate host-cell entry (*398*). The S protein is trimeric class I fusion protein, composed of two functional subunits, responsible for receptor binding (S1 subunit) and membrane fusion (S2 subunit) (*316, 399*). Remarkably, the surface of the envelope spike is dominated by host-derived glycans with each trimer displaying 66 N-linked glycosylation sites. The S protein is a key target in vaccine design efforts (*400*), and understanding the glycosylation of recombinant viral

spikes can reveal fundamental features of viral biology and guide vaccine design strategies (*153*, *154*).

Viral glycosylation has wide-ranging roles in viral pathobiology, including mediating protein folding and stability, and shaping viral tropism (*377*). Glycosylation sites are under selective pressure as they facilitate immune evasion by shielding specific epitopes from antibody neutralization. However, due to the low mutation rate of SARS-CoV-2, there have been no observed mutations to N-linked glycosylation sites (*401*). Surfaces with an unusually high density of glycans can also enable immune recognition (*377*, *402*, *403*). The role of glycosylation in camouflaging immunogenic protein epitopes has been studied for other coronaviruses (*186*, *374*, *401*). Coronaviruses form virions by budding into the lumen of endoplasmic reticulum-Golgi intermediate compartments (ERGIC) (*25*, *404*). However, observations of complex-type glycans on virally derived material suggests that the viral glycoproteins are subjected to Golgi-resident processing enzymes (*10*, *186*).

High viral glycan density and local protein architecture can sterically impair the glycan maturation pathway. Impaired glycan maturation resulting in the presence of oligomannose-type glycans can be a sensitive reporter of native-like protein architecture (*154*), and site-specific glycan analysis can be used to compare different immunogens and monitor manufacturing processes (*405*). Additionally, glycosylation can influence the trafficking of recombinant immunogen to germinal centers (*308*).

To resolve the site-specific glycosylation of SARS-CoV-2 S protein and visualize the distribution of glycoforms across the protein surface, I expressed and purified three biological replicates of recombinant soluble material in an identical manner to that which was used to obtain the high-resolution cryo-electron microscopy (cryo-EM) structure, albeit without glycan processing blockade using kifunensine (*316*). This variant of the S protein

contains all 22 glycans on the SARS-CoV-2 S protein (**Figure 4.10 A**). Stabilization of the trimeric prefusion structure was achieved using the "2P" stabilizing mutations (*192*) at residues 986 and 987, a "GSAS" substitution at the furin cleavage site (residues 682–685), and a C-terminal trimerization motif. This helps to maintain quaternary architecture during glycan processing. Prior to analysis, supernatant containing the recombinant SARS-CoV-2 S was purified by size-exclusion chromatography ensure only native-like trimeric protein was analyzed (**Figure 4.10 B**). The trimeric conformation of the purified material was validated using negative-stain electron microscopy (**Figure 4.10 C**).

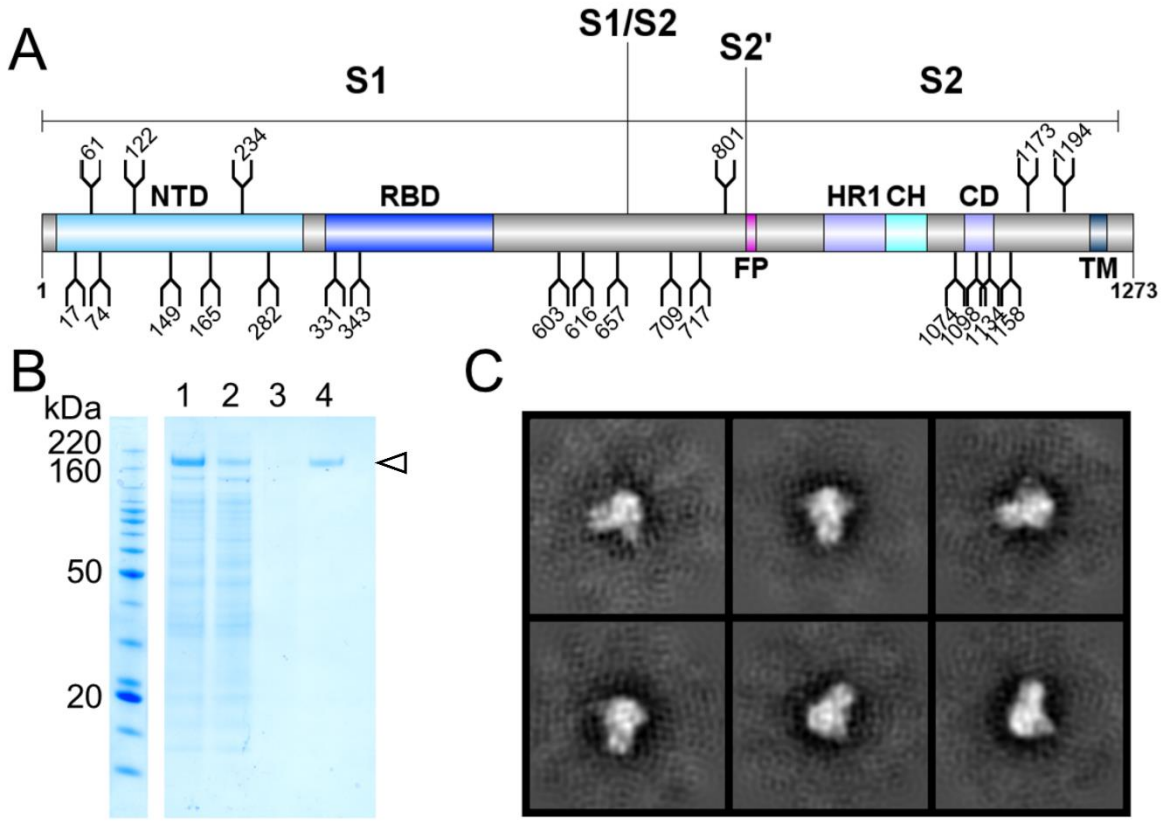


Figure 4.10. Expression and validation of SARS-CoV-2 S glycoprotein. (A) Schematic representation of SARS-CoV-2 S glycoprotein. The positions of N-linked glycosylation sequons (N-X-S/T, where X≠P) are shown as branches. Protein domains are illustrated: N-terminal domain (NTD), receptor-binding domain (RBD), fusion peptide (FP), heptad repeat 1 (HR1), central helix (CH), connector domain (CD), and transmembrane domain (TM). **(B)** SDS-PAGE analysis of SARS-CoV-2 S protein expressed in human embryonic kidney 293F cells. Lane 1: filtered supernatant from transfected cells; lane 2: flow-through from StrepTactin resin; lane 3: wash from StrepTactin resin; lane 4: elution from StrepTactin

resin. **(C)** Negative-stain EM 2D class averages of the SARS-CoV-2 S protein. 2D class averages of the SARS-CoV-2 S protein are shown, confirming that the protein adopts the trimeric prefusion conformation matching the material used to determine the structure (*316*).

To determine the site-specific glycosylation of SARS-CoV-2 S, I employed trypsin, chymotrypsin, and alpha-lytic protease to generate three glycopeptide samples. These proteases were selected to generate glycopeptides that contain a single N-linked glycan sequon. The glycopeptides were analyzed by liquid-chromatography-mass spectrometry (LC-MS), and the glycan compositions were determined for all 22 N-linked glycan sites (**Figure 4.11**). To convey the main processing features at each site, the abundances of each glycan are summed into oligomannose-, hybrid- and categories of complex-type glycosylation based on branching and fucosylation.

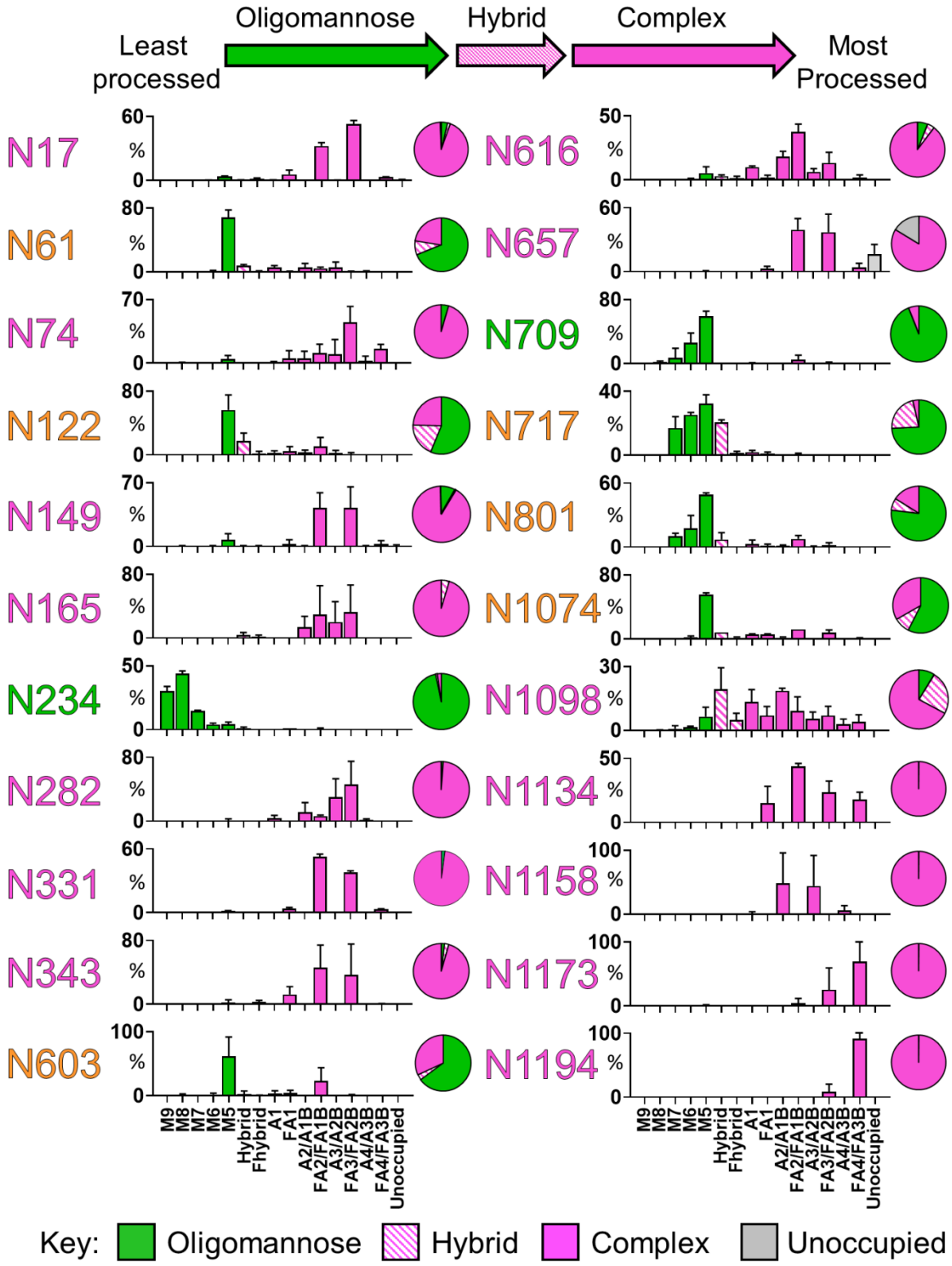


Figure 4.11: Site-specific N-linked glycosylation of SARS-CoV-2 S glycoprotein. The schematic illustrates the color code for the principal glycan types that can arise along the maturation pathway from oligomannose-, hybrid- to complex-type glycans. The graphs summarize quantitative mass spectrometric analysis of the glycan population present at individual N-linked glycosylation sites simplified into categories of glycans. The

oligomannose-type glycan series (M9 to M5; $Man_9GlcNAc_2$ to $Man_5GlcNAc_2$) is colored green, afucosylated and fucosylated hybrid-type glycans (Hybrid & F Hybrid) dashed pink, and complex glycans grouped according to the number of antennae and presence of core fucosylation (A1 to FA4) and are colored pink. Unoccupancy of an N-linked glycan site is represented in grey. The pie charts summarize the quantification of these glycans. Glycan sites are colored according to oligomannose-type glycan content with the glycan sites labelled in green (80−100%), orange (30−79%) and pink (0−29%). The bar graphs represent the mean quantities of three biological replicates with error bars representing the standard error of the mean.

There are two sites on SARS-CoV-2 S that are principally oligomannose-type: N234 and N709. The predominant oligomannose-type glycan structure observed across the protein, with the exception of N234, is $Man_5GlcNAc_2$, which demonstrates that these sites are largely accessible to α1,2-mannosidases but are poor substrates for GlcNAcT-I, which is the gateway enzyme in the formation of hybrid- and complex-type glycans in the Golgi apparatus. The stage at which processing is impeded is a signature related to the density and presentation of glycans on the viral spike. For example, the more densely glycosylated spikes of HIV-1 Env and Lassa virus GPC exhibit numerous sites dominated by $Man_9GlcNAc_2$ (*3*, *4*, *140*, *152*).

A mixture of oligomannose- and complex-type glycans can be found at sites N61, N122, N603, N717, N801 and N1074 (**Figure 4.11**). Of the 22 sites on the S protein, 8 contain significant populations of oligomannose-type glycans, highlighting how the processing of the SARS-CoV-2 S glycans is divergent from host glycoproteins (*68*). The remaining 14 sites are dominated by processed, complex-type glycans.

Although unoccupied glycosylation sites were detected on SARS-CoV-2 S, when quantified they were revealed to form a very minor component of the total peptide pool (**Figure 4.12**). In HIV-1 immunogen research, the holes generated by unoccupied glycan sites have been shown to be immunogenic and potentially give rise to distracting epitopes

(*406*). The high occupancy of N-linked glycan sequons of SARS-CoV-2 S indicates that recombinant immunogens will not require further optimization to enhance site occupancy.

Figure 4.12. Glycoform abundances observed across SARS CoV-2 S protein. The upper table shows the categorized glycan compositions at each N-linked glycan site with the reported value the mean of three biological replicates. The global averages are shown in the right-hand table. The lower table further categorizes the glycan compositions into

	N17	N61	N74	N122	N149	N165	N234	N282	N331	N343	N603	N616	N657	N709	N717	N801	N1074	N1098	N1134	N1158	N1173	N1194
M9	0	0	0	0	0	0	30	0	0	0	0	0	0	0	0	0	0	0	0	0	0	0
M8	0	0	0	0	0	0	44	0	0	0	1	0	0	2	0	0	0	0	0	0	0	0
M7	0	0	0	0	0	0	14	0	0	0	0	0	0	7	17	10	0	1	0	0	0	0
M6	0	1	0	0	0	0	4	0	0	0	2	1	0	26	25	17	2	2	0	0	0	0
M5	3	68	4	56	7	0	4	1	1	2	62	5	0	59	32	49	55	6	0	0	1	0
Hybrid	0	8	0	17	0	3	1	0	0	0	3	3	0	0	21	7	8	19	0	0	0	0
Fhybrid	2	1	0	2	0	1	0	0	0	2	0	1	0	0	1	0	1	5	0	0	0	0
A1	0	5	1	3	0	0	0	4	0	0	4	10	0	0	2	3	5	14	0	1	0	0
FA1	6	1	5	5	3	0	1	0	4	12	4	2	3	0	1	1	5	7	15	0	0	0
A2/A1B	0	6	5	3	0	14	0	11	0	0	0	18	0	0	0	1	2	19	0	48	0	0
FA2/FA1B	32	4	11	10	42	29	1	6	53	46	23	37	39	5	1	8	12	9	44	0	4	0
A3/A2B	0	6	10	3	0	20	0	30	0	0	0	6	0	0	0	0	0	5	0	44	0	0
FA3/FA2B	53	1	45	1	42	32	0	46	38	37	1	13	37	1	0	2	8	7	23	0	25	8
A4/A3B	0	0	3	0	0	0	0	2	0	0	0	0	0	0	0	0	0	3	0	6	0	0
FA4/FA3B	3	0	16	0	3	0	0	0	3	0	0	2	4	0	0	0	1	4	18	0	70	92
Unoccupied	1	0	0	0	1	0	0	0	0	0	0	0	16	0	0	0	0	0	0	0	0	0

Total	
M9	1
M8	2
M7	2
M6	4
M5	19
Hybrid	4
Fhybrid	1
A1	2
FA1	3
A2/A1B	6
FA2/FA1B	19
A3/A2B	6
FA3/FA2B	19
A4/A3B	1
FA4/FA3B	10
Unoccupied	1

%	N17	N61	N74	N122	N149	N165	N234	N282	N331	N343	N603	N616	N657	N709	N717	N801	N1074	N1098	N1134	N1158	N1173	N1194
Mannose	4	69	4	56	8	0	97	1	2	2	65	6	0	94	74	77	57	9	0	0	1	0
Hybrid	2	9	0	19	1	5	1	0	0	3	3	4	0	0	22	7	9	24	0	0	0	0
Complex	94	22	96	25	91	95	2	99	98	96	32	90	83	6	4	16	33	67	100	100	99	100
Unoccupied	1	0	0	0	1	0	0	0	0	0	0	0	16	0	0	0	0	0	0	0	0	0
Fucosylation	95	6	77	18	91	63	2	52	98	98	29	56	83	5	3	11	27	31	100	0	99	100
Sialylation	20	4	18	5	33	18	0	14	22	4	0	1	2	0	2	5	6	30	7	39	4	100

Total	
Mannose	28
Hybrid	5
Complex	66
Unoccupied	1
Fucosylation	52
Sialylation	15

oligomannose-, hybrid-, and complex-type as well as the percentage of glycan compositions containing at least one fucose or one sialic acid residue.

Using the cryo-EM structure of the trimeric SARS-CoV-2 S protein (PDB ID 6VSB) (*316*), the glycosylation status of the coronavirus spike mimetic was mapped onto the experimentally determined 3D structure (**Figure 4.13**). This combined mass spectrometric and cryo-EM analysis reveals how the N-linked glycans occlude distinct regions across the surface of the SARS-CoV-2 spike.

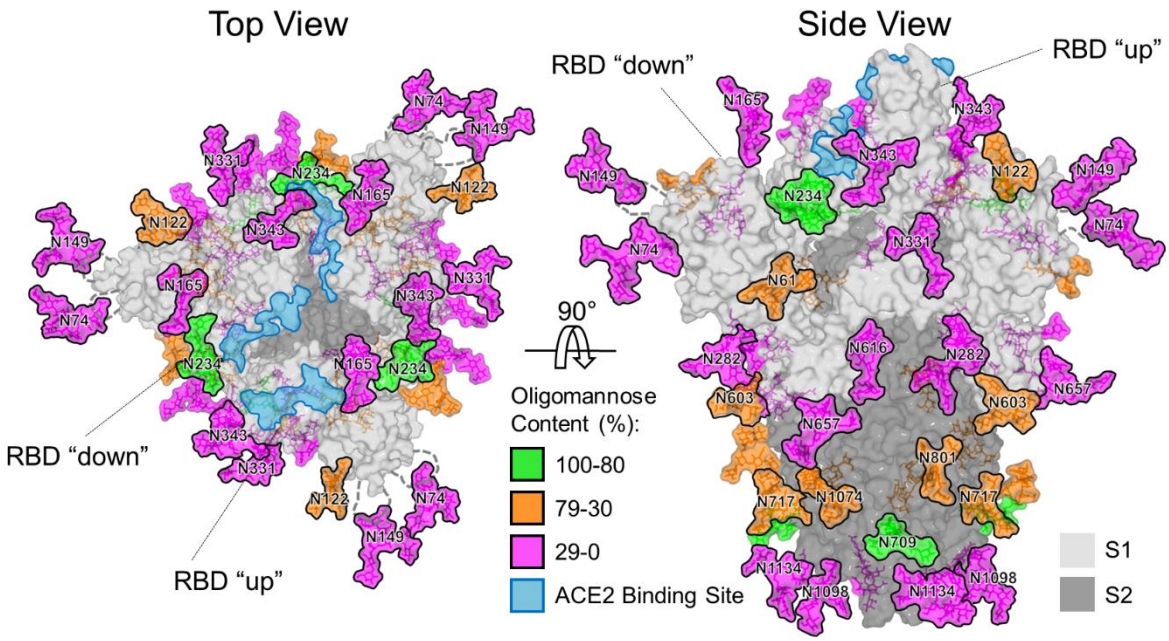


Figure 4.13. Structure-based mapping of SARS-CoV-2 S N-linked glycans. Representative glycans are modelled onto the prefusion structure of trimeric SARS-CoV-2 S glycoprotein (PDB ID 6VSB) (*316*), with one RBD in the "up" conformation and the other two RBDs in the "down" conformation. The glycans are colored according to oligomannose content as defined by the key. ACE2 receptor binding sites are highlighted in light blue. The S1 and S2 subunits are rendered with translucent surface representation, colored light and dark grey, respectively. Note that the flexible loops on which N74 and N149 glycan sites reside are represented as dashed lines with glycan sites on the loops mapped at their approximate regions.

Shielding of the receptor binding sites on the SARS-CoV-2 spike by proximal glycosylation sites (N165, N234, N343) can be observed, especially when the receptor binding domain is in the "down" conformation. The shielding of receptor binding sites by glycans is a common feature of viral glycoproteins, as observed on SARS-CoV-1 S (*186*, *401*), HIV-1 Env (*187*), influenza HA (*188*, *189*), and LASV GPC (*140*). Given the functional constraints of receptor binding sites and the resulting low mutation rates of these residues, it is likely that there is selective pressure to utilize N-linked glycans to camouflage one of the most conserved and potentially vulnerable areas of their respective glycoproteins (*50*, *150*).

It is interesting to note the dispersion of oligomannose-type glycans across both the S1 and S2 subunits. This is in contrast to other viral glycoproteins, for example the dense glycan clusters in several strains of HIV-1 Env induce oligomannose-type glycans that are recognized by antibodies (*375*, *407*). In SARS-CoV-2 S the oligomannose-type structures are likely protected by the protein component, as exemplified by the N234 glycan which is partially sandwiched between the N-terminal and receptor-binding domains (**Figure 4.13**).

The N-linked glycans on extended flexible loop structures (N74 and N149) and at the membrane-proximal C-terminus (N1158, N1173, N1194) that were not resolved in the cryo-EM maps (*316*) were also characterized. These were determined to be complex-type glycans, consistent with steric accessibility of these residues.

Whilst the oligomannose-type glycan content (28%) (**Figure 4.12**) is above that observed on typical host glycoproteins, it is lower than other viral glycoproteins. For example, one of the most densely glycosylated viral spike proteins is HIV-1 Env, which exhibits ~60% oligomannose-type glycans (*2*, *3*). This suggests that SARS-CoV-2 S protein is less densely glycosylated and that the glycans form less of a shield compared with other viral glycoproteins including HIV-1 Env and LASV GPC, which may be beneficial for the elicitation of neutralizing antibodies.

Additionally, the processing of complex-type glycans is an important consideration in immunogen engineering, especially considering that epitopes of neutralizing antibodies against SARS-CoV-2 S can contain fucosylated glycans at N343 (*408*). Across the 22 N-linked glycosylation sites, 52% are fucosylated and 15% of the glycans contain at least one sialic acid residue (**Figure 4.12** & **Figure 4.14**). The analysis reveals that N343 is highly fucosylated with 98% of detected glycans bearing fucose residues. Glycan modifications can be heavily influenced by the cellular expression system utilized. It has previously

demonstrated for HIV-1 Env glycosylation that the processing of complex-type glycans is driven by the producer cell but that the levels of oligomannose-type glycans were largely independent of the expression system and is much more closely related to the protein structure and glycan density (*29*).

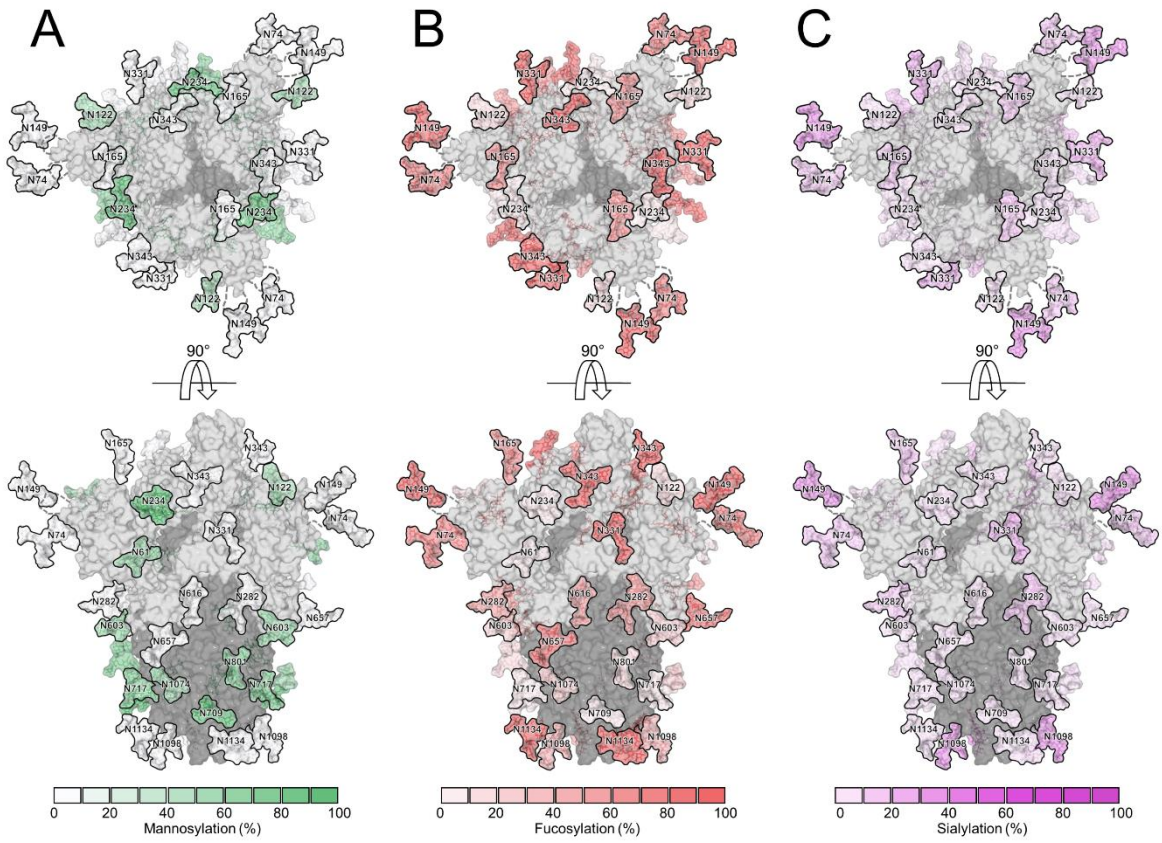


Figure 4.14. Glycosylated model of SARS-CoV-2 S glycoprotein highlighting different glycan modifications. The experimentally determined quantities of mannosylation, fucosylation and sialylation presented in **Figure 4.12** were used to color the glycosylated model of SARS-CoV2 S protein presented in **Figure 4.13**. Glycans are highlighted according to mannosylation **(A)**, fucosylation **(B)** and sialylation **(C)** levels as denoted in the keys. S1 and S2 subunits are colored light grey and dark grey, respectively.

Highly dense glycan shields, such as those observed on LASV GPC and HIV-1 Env, feature so-called mannose clusters (*140*, *152*) on the protein surface (**Figure 4.15**). Whilst small mannose-type clusters have been characterized on the S1 subunit of Middle East respiratory syndrome (MERS) CoV S (*401*), no such phenomenon has been observed for

SARS-CoV-1 or SARS-CoV-2 S proteins. The site-specific glycosylation analysis reported here suggests that the glycan shield of SARS-CoV-2 S is consistent with other coronaviruses and similarly exhibits numerous vulnerabilities throughout the glycan shield (*401*).

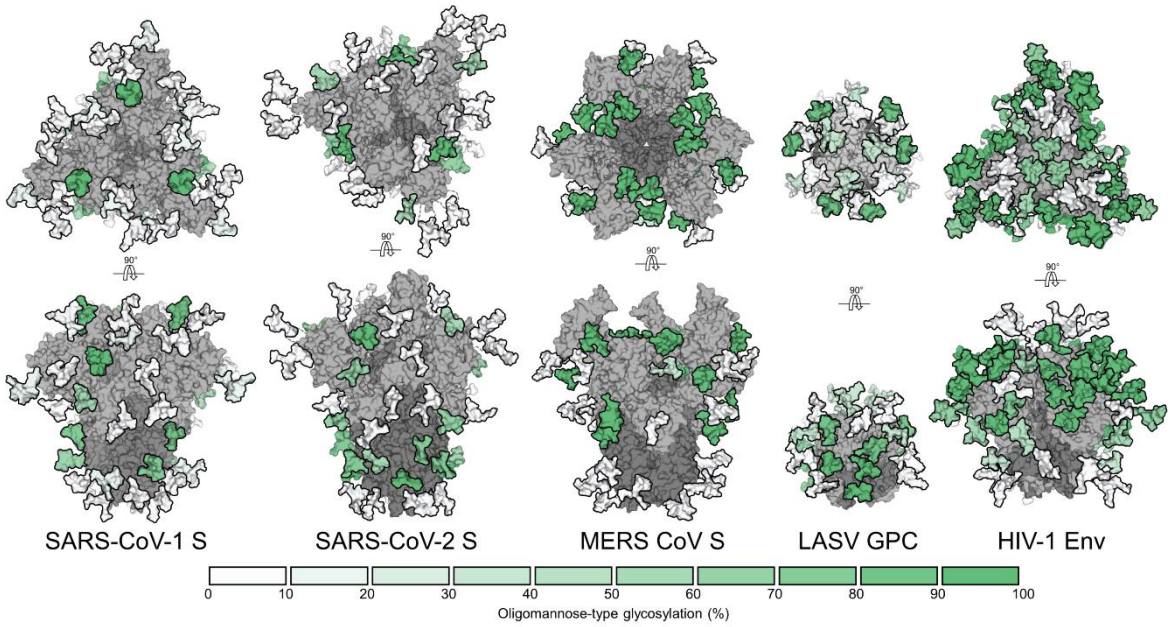


Figure 4.15. Under-processing of viral glycan shields. Left to Right: MERS-CoV S (*401*), SARS-CoV-1 S (*401*), SARS-CoV-2 S, LASV GPC (*140*), HIV-1 Env (*3*, *154*). Site-specific N-linked glycan oligomannose quantifications are colored according to the key. All glycoproteins were expressed as soluble trimers in HEK 293F cells apart from LASV GPC, which was derived from virus-like particles from Madin-Darby canine kidney II cells.

Finally, trace levels of O-linked glycosylation were detected at T323/S325 with over 99% of these sites unmodified (**Figure 4.16**) suggesting that O-linked glycosylation of this region is minimal when the structure is native-like.

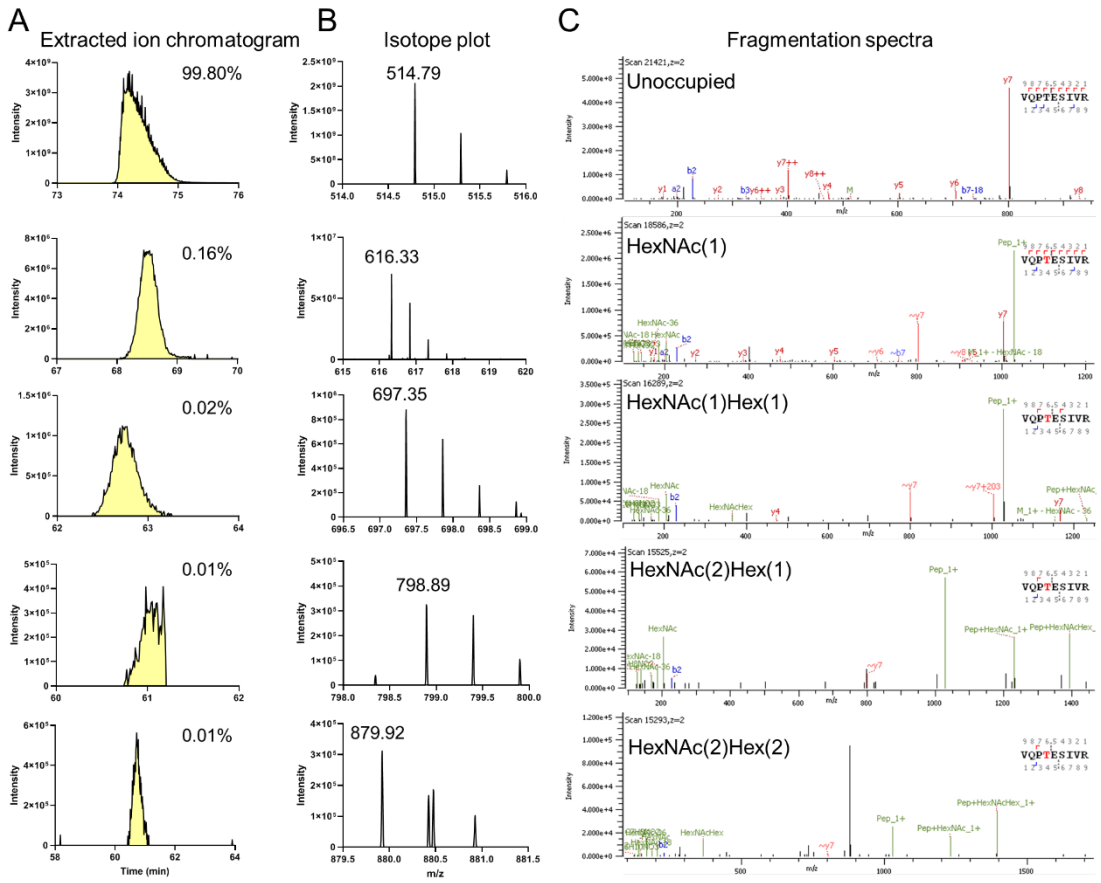


Figure 4.16. Detection of low levels of mucin-type O-linked glycosylation at T323/S325 of SARS-CoV-2 S. O-linked glycan compositions were observed at T323/S325. This analysis was performed on a single biological replicate. For each peptide/glycopeptide detected the extracted ion chromatogram (XIC) **(A)**, isotope distribution **(B)**, and fragmentation spectrum **(C)** is shown. The monoisotopic peak *m/z* is labelled in **(B)**. Fragment ions are colored blue and red for b- and y-ions, respectively. Oxonium ions are colored in green.

The glycosylation analysis of SARS-CoV-2 offers a detailed benchmark of site-specific glycan signatures characteristic of a natively folded trimeric spike. As an increasing number of glycoprotein-based vaccine candidates are being developed, their detailed glycan analysis offers a route for comparing immunogen integrity and will also be important to monitor as manufacturing processes are scaled for clinical use. Glycan profiling will therefore also be an important measure of antigen quality in the manufacture of serological

testing kits. Finally, with the advent of nucleotide-based vaccines, it will be important to understand how those delivery mechanisms impact immunogen processing and presentation.

5. Anti-HIV-glycan antibody 2G12 broadly neutralizes human H3N2 influenza viruses during natural evolution of the hemagglutinin glycan shield

The discovery of broadly neutralizing antibodies (bnAbs) from infected HIV-1 patients has contributed to the design and development of HIV-1 vaccine candidates and therapies (*161, 409–414*). Many of these antibodies have demonstrated remarkable potency and breadth against diversified HIV-1 strains and subtypes (*158, 415*). One unusual class is anti-carbohydrate antibodies that exclusively target the glycan shield on the HIV-1 Env glycoprotein (*158, 415, 416*). Although the glycan shield of HIV-1 Env acts as a protective barrier that prevents or hinders recognition of the immunogenic protein surface of Env by the humoral immune system, the overly dense glycan shield on HIV-1 compared to host proteins results in the glycans themselves being targeted by antibodies (*160, 161, 243, 409, 411*). Such anti-carbohydrate antibodies have been rarely seen against other viral pathogens (*304, 417*).

HIV-1 is not the only heavily glycosylated viral pathogen. Since causing the 1968 pandemic, human seasonal H3N2 influenza viruses have gradually become more heavily glycosylated due to the accumulation of N-linked glycosylation sites on its major surface antigen, hemagglutinin (HA) (*7, 171, 418*). These newly acquired N-linked glycan sites are mainly located on the receptor binding domain (RBD) of the HA globular head, which contains the major antigenic sites (*7, 173, 388, 418*). N-linked glycans can help mask or redefine epitopes and lead to antigenic drift (*172*). The relentless antigenic drift of both glycan and protein components in the HA necessitates annual updates of the seasonal influenza vaccine.

Previous studies have nevertheless indicated that accumulation of underprocessed oligomannose-type glycans on the HA would be a target for mannose binding lectin, thereby facilitating virus inhibition both in vitro and vivo (*282*, *419–421*).

These glycan modifications therefore raised the question whether anticarbohydrate antibodies could now neutralize human seasonal H3N2 influenza viruses. Anti-carbohydrate antibody, 2G12, was one of the first handful of neutralising antibodies to be discovered against HIV-1 and was isolated from pooled sera of HIV-1 patients (*409*, *410*). 2G12 neutralizes HIV-1 by binding to an oligomannose-type glycan cluster on the gp120 subunit of Env, around a site that is now known as the N332/V3 base epitope (*160*, *298*, *422*). 2G12 is an extremely unusual antibody that forms a domain-swapped dimer between the heavy chain variable regions of its two Fab arms and can, therefore, bind to the Manα1-2Man disaccharide residues at the tips of up to four different oligomannose glycans on the gp120 surface, without any observable contacts to amino acids (*243*, *244*, *423*). In this study, we demonstrate the ability of 2G12 to neutralize human seasonal H3N2 viruses over the last three decades and investigate the mechanism of neutralization by structural biology, mass spectrometry, and evolutionary analyses of N-linked glycans on viral and recombinant HA proteins. A conserved and a newly acquired oligomannose N-linked glycosylation nearby the HA RBS both contribute to this broad neutralizing activity of 2G12 on influenza viruses.

5.1 N-linked glycosylation sites accumulate on human H3N2 HA during evolution

The HA glycoprotein is formed by three homoprotomers, each composed of HA1 and HA2 from the cleavage of HA0 by host cell proteases (*246*). The evolution of glycosylation sites on the HA since the emergence of the H3N2 1968 pandemic was analysed (**Figure 5.1)**. The

number of N-linked glycosylation sites per HA protomer was six (five conserved and one non-conserved) when A/Hong Kong/1/1968 (HK68) first appeared in the human population in the 1968 H3N2 pandemic. Non-conserved N-linked glycan sites have since accumulated from one to seven during five decades of H3N2 virus evolution. The increased number and density of glycans on the HA during natural evolution from the 1968 pandemic suggests the presence of oligomannose-type glycans on HAs.

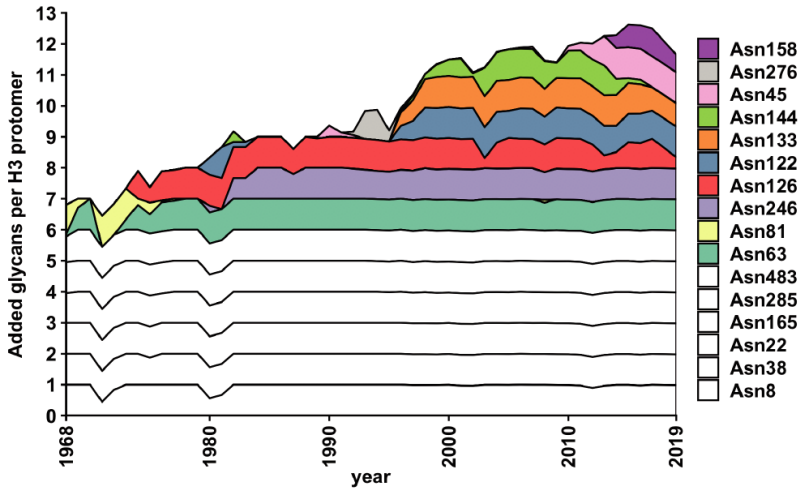


Figure 5.1. Evolution of N-linked glycosylation sites on H3 HAs. The number of non-conserved N-linked glycosylation sites on HA has evolved from one in 1968 to seven in 2019 on HA1, as shown in the stack chart. Then glycan sites are cumulatively involved, where some are retained, and others are substituted from 1968 to 2019. The six completely conserved N-linked glycan sites in human H3N2 viruses (N8, N22, N38, N165, N285in HA1, and N154 in HA2, which corresponds to N483 in HA0) are shown in white. This figure was made by Nicholas Wu at the Scripps Research Institute.

5.2 2G12 broadly neutralizes human H3N2 viruses from the past thirty years

To test our hypothesis that human H3N2 viruses have acquired sufficient oligomannose-type glycans to be a target for 2G12, the neutralization activity of 2G12 was tested on panel of human H3N2 strains spanning from 1968 to 2016. 2G12 was able to neutralize most strains in the panel except for early isolates, such as HK68 and Bk79 (**Figure 5.2 A**). Two

strains from clinical isolates were also tested and were revealed to be sensitive to neutralization by 2G12 (**Figure 5.2 B**).

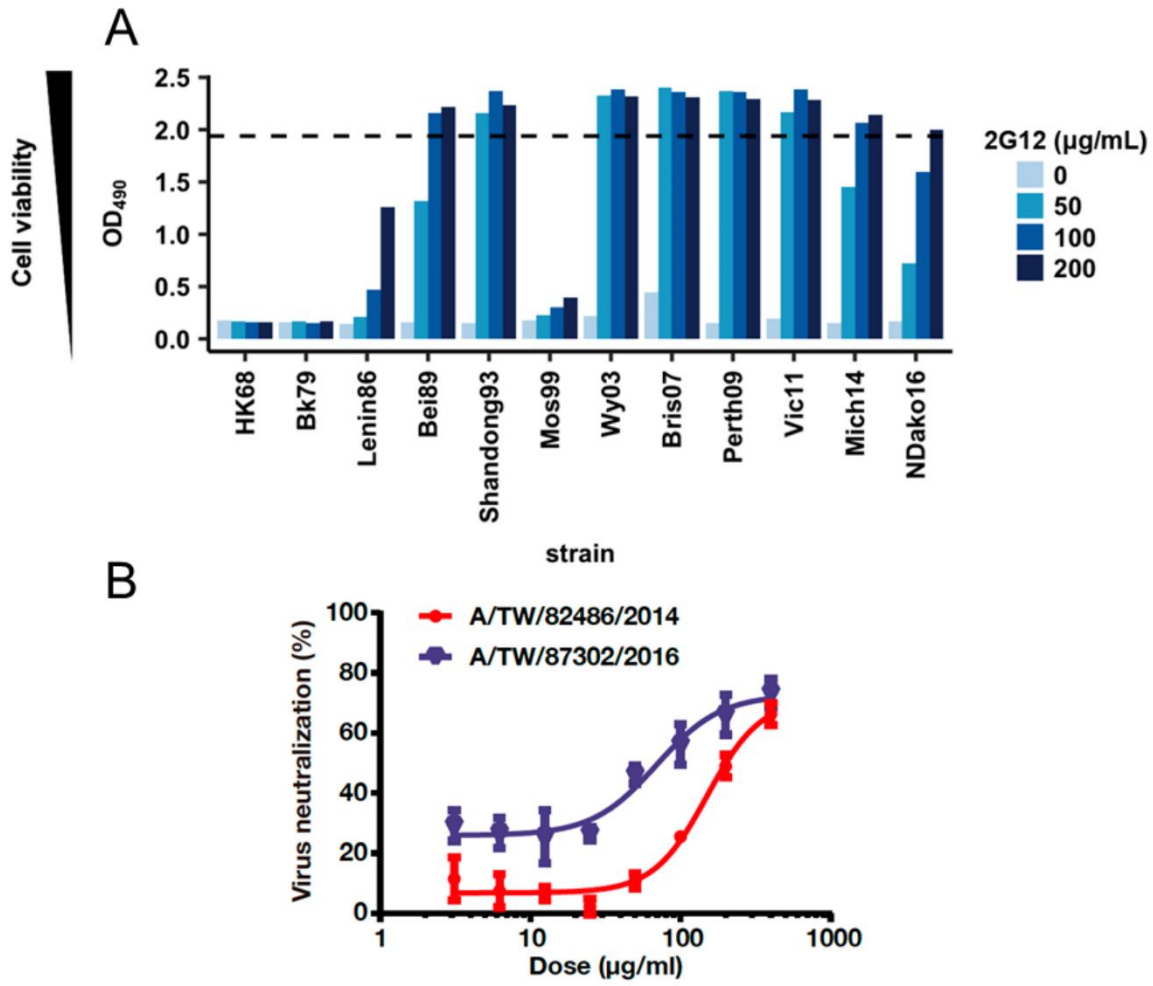


Figure 5.2. Broad Neutralization of H3N2 viruses by anti-glycan antibody 2G12 after 1980. (A) Neutralization activity of 2G12 IgG with different H3N2 strains was measured by a cell viability assay at four different antibody concentrations. The OD_{490} value is proportional to the cell density. The dashed line represents the OD for cell only control with no virus. **(B)** Neutralisation activity of 2G12 IgG against two clinical isolates. The IC_{50} values of 2G12 to A/TW/82486/2014 and A/TW/87302/2016 are 151 and 69 μg/ml respectively. The error bars on each value are the standard deviation of three technical replicates. The neutralization assays were performed by David Lee at the Scripps Research Institute.

5.3 Oligomannose-type glycans are enriched on the HA head in more recent H3N2 viruses

We subsequently profiled the glycoforms present on the HAs of different H3N2 viruses. Site-specific glycan compositions were delineated by liquid chromatography-mass spectrometry (LC-MS) of glycopeptides from recombinant HAs expressed in Expi293F cells (**Figure 5.3**). HA samples were proteolytically digested using trypsin, chymotrypsin and Glu C, and the resulting glycopeptides were analysed by LC-MS. Five out of six glycosylation sites on HK68 displayed significant population of both oligomannose- and complex-type glycans, except for N38, which was fully complex. Interestingly, glycosylation sites on subsequent H3N2 strains diverged to either predominantly oligomannose- or complex-type sites. These experimentally observed glycans were used to model fully glycosylated models of recombinant HAs of HK68 and Vic11 using crystal structures and glycan compositions revealed by the mass spectrometric analysis (**Figure 5.4**). Increased occlusion of the HA protein surface by glycans has emerged since 1968, especially in the immunogenic globular head, with an oligomannose-type glycan cluster appearing at N165 and N246.

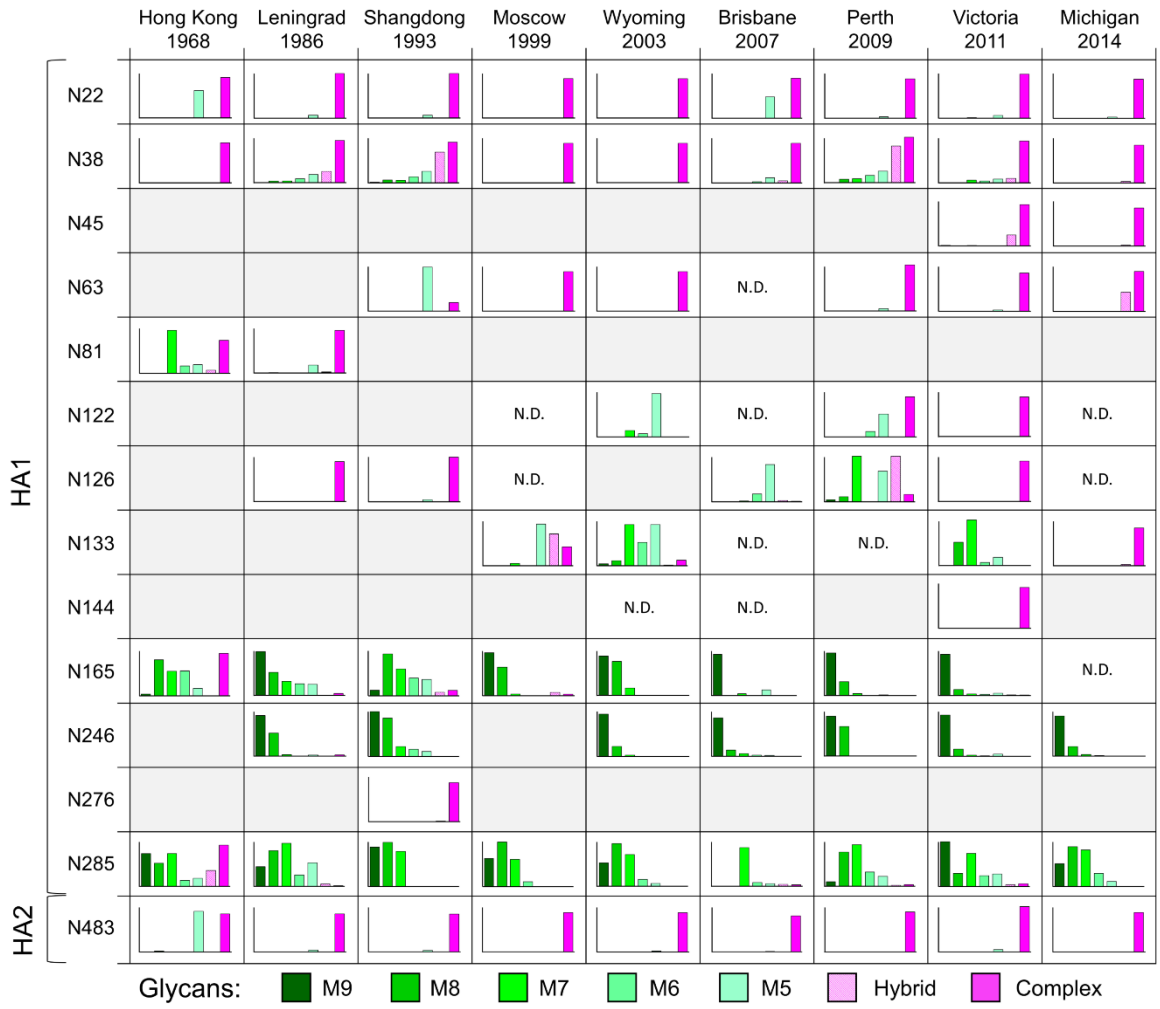


Figure 5.3. Site-specific N-linked glycosylation of H3N2 HA glycoproteins. Recombinant H3N2 HA glycoproteins were proteolytically digested and analysed by LC-MS. Each graph summarises the quantitative mass spectrometric analysis of the glycan populations at each individual N-linked glycosylation site, which are simplified into glycan categories. These categories are coloured according to glycan compositions as per the key. The oligomannose-type glycoforms (M9 to M5; $Man_9GlcNac_2$ to $Man_5GlcNac_2$) are indicated in shades of green, hybrid-type glycans in dashed pink, and complex-type glycans in pink. Glycosylation sites that are not present on individual HAs are shaded in grey, and sites where the glycosylation site is encoded, but the glycan compositions could not be determined, are labelled as not determined (N.D.).

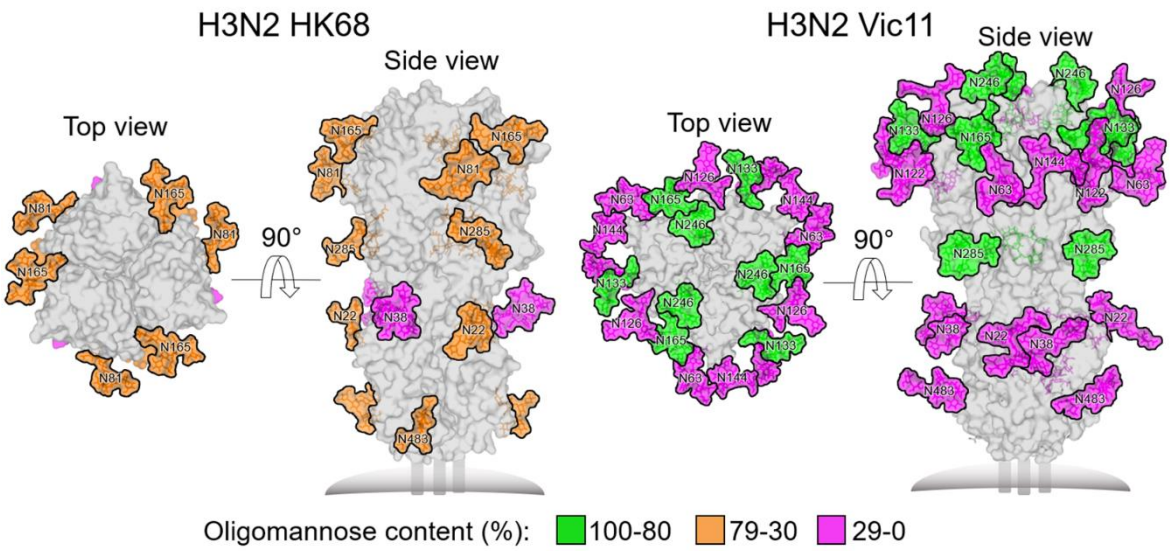


Figure 5.4. Models of fully glycosylated HK68 and Vic 11 HAs. Experimentally observed glycans shown in **Figure 5.3.** are modelled onto the prefusion structure of trimeric HA from HK68 (PDB ID: 4FNK) (*318*) and Vic11 (PDB ID: 4O5N) (*7*). Glycans are coloured according to the oligomannose-type glycan content as per the key, with the protein shown in grey.

We also sought to quantitatively assess the total compositions of the carbohydrate structures displayed on H3N2 HAs. Enzymatically released glycans were fluorescently labelled and subjected to HILIC-UPLC analysis (**Figure 5.5).** Treatment with endoglycosidase H revealed the presence of underprocessed oligomannose-type glycans across the all the glycan sites. This analysis confirmed the abundance of trimmed oligomannose-type gycans on HK68, while more recent strains display the $Man_{8/9}GlcNAc_2$ 2G12 epitope.

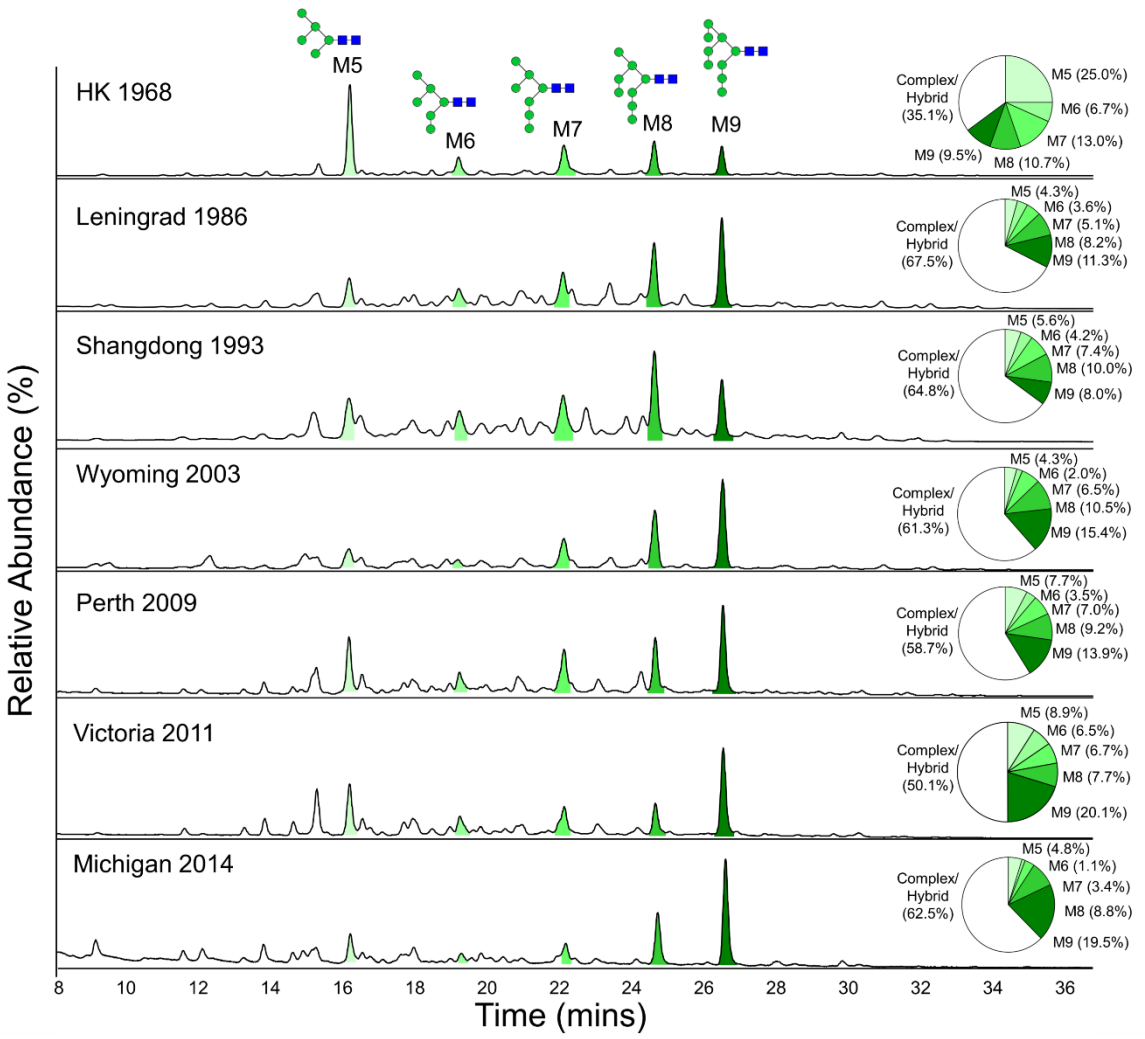


Figure 5.5. HILIC-UPLC N-linked glycan analysis of H3N2 HAs. Chromatograms of fluorescently labelled N-linked glycans on HAs from H3N2 strains: HK68, Leningrad86, Shangdong93, Wyoming03, Perth09, Victoria11, and Michigan14. Note the dominant peak of $Man_5GlcNAc_2$ on HK68, whereas the 2G12 sensitive strains have prominent $Man_{8/9}GlcNAc_2$ peaks.

In order to ensure that the recombinant HAs recapitulated the glycans found on virally derived HAs, site-specific glycan analysis was also performed on HAs from HK68 and Vic11 viruses, grown in MDCK-SIAT1 cells, which represent 2G12-insensitive and 2G12-sensitive strains, respectively (**Figure 5.6**). The site-specific glycan profiling from recombinant HAs corresponded well to the viral HAs. The oligomannose-type glycans were particualry conserved between virus and recombinant material, with HAs of HK68

predominantly exhibiting the lower order oligomannose-type glycans ($Man_{5-7}GlcNac_2$) and HAs of Vic11 presenting predominantly $Man_9GlcNAc_2$ on N165 and N246.

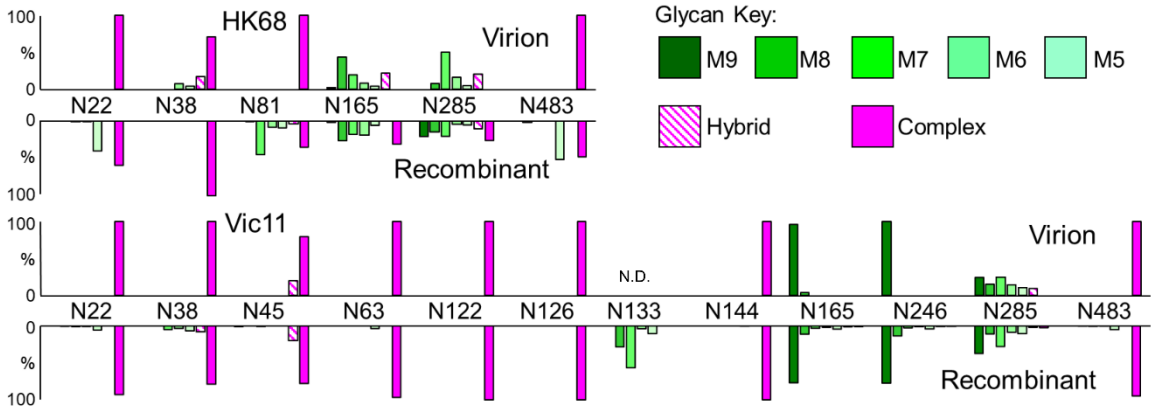


Figure 5.6. Site-specific N-linked glycosylation of viral and recombinant H3N2 HA glycoproteins. HAs from HK68 and Vic11 were expressed recombinantly in MDCK-SIAT1 cells and their glycans analysed by LC-MS. Glycans are coloured according to the key

5.4 The glycoform at N165 depends on the presence of N246

The contribution of these two N-linked glycan sites for 2G12 specificity and neutralization was investigated on another 2G12-sensitive virus, Bris07. N165A, N246K, and N165A/N246K double mutants of Bris07 HA were constructed. We further examined the glycoforms at residues 165 and 246 of the wild type and N165A of Bris07 to delineate how they may functionally interact. LC-MS analysis revealed that wild type Bris07 HA presented predominantly $Man_9GlcNAc_2$ on both N165 and N246, whereas the N165A phenotype presented mainly $Man_8GlcNAc_2$ on N246. Likewise, the N246K mutant resulted in $Man_8GlcNAc_2$ being predominantly displayed on N165 (**Figure 5.7.**). Interestingly, the N165A mutant virus could not be neutralised by 2G12 (data not shown).

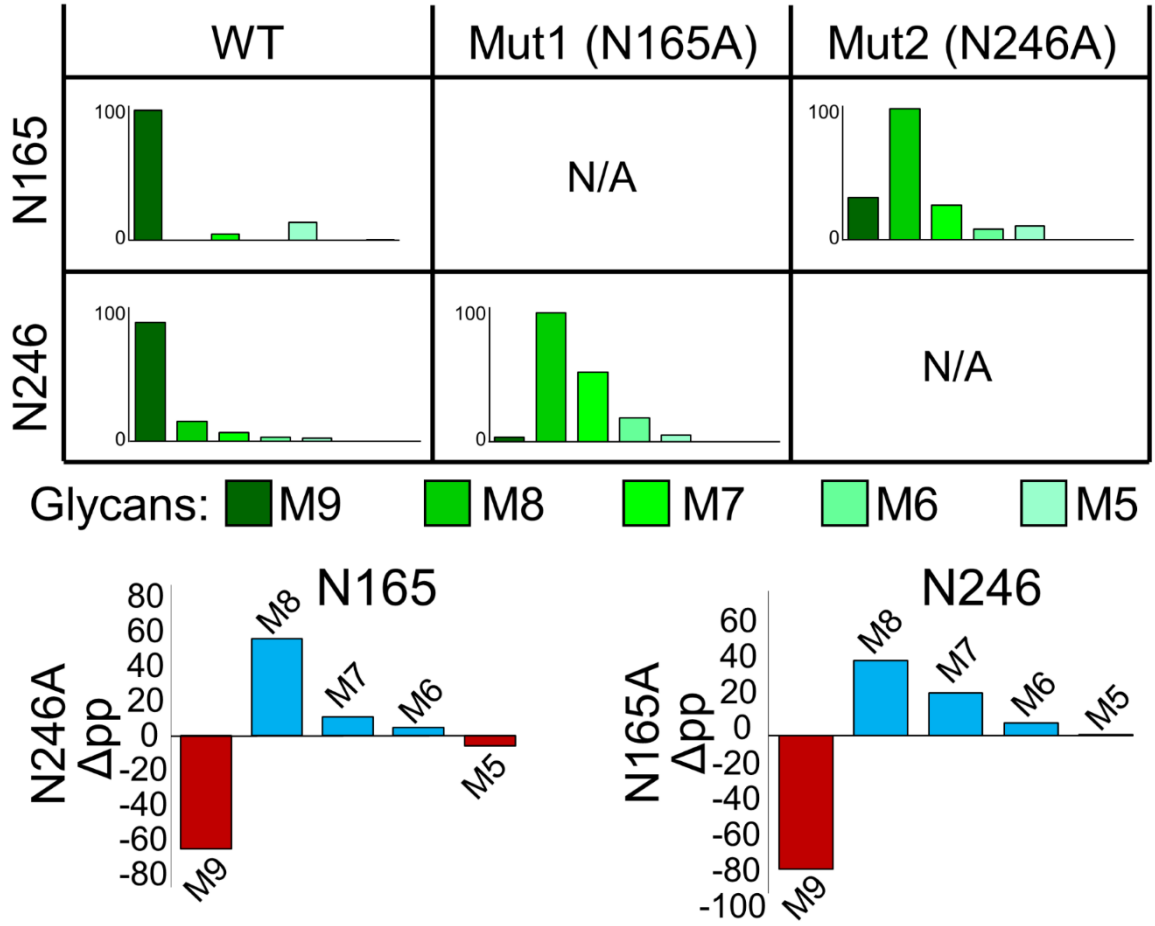


Figure 5.7. Site-specific glycosylation analysis of Bris07 HA glycan knockout mutants at N165 and N246. Percentage point differences in abundance of oligomannose-type glycans between glycan knockout mutants and WT Bris07 HA are also illustrated with decreased and increased abundance coloured in red and blue, respectively.

This enhanced trimming of mannose residues, when proximal glycan sites are knocked out, reveals the structural constraints on the glycan-processing enzymes by the neighbouring glycan site. This feature is reminiscent of that found not only on HIV-1 Env, but also LASV GPC and MERS spike protein (*140*, *423*, *424*). Furthermore, all of the 2G12-sensitive strains presented mainly $Man_9GlcNAc_2$ with some $Man_8GlcNAc_2$ on both N165 and N246 (**Figure 5.3**). These data suggested both the presence of N165 and N246, and particular oligomannose glycoforms presented at these sites, are crucial for neutralisation by 2G12.

5.5 Structural analysis of the 2G12 neutralization mechanism

We next investigated why 2G12 could neutralize wild type Bris07 virus but not the N165A mutant, using negative-stain electron microscopy (nsEM). The nsEM analysis revealed that one to two 2G12 domain-swapped Fab dimers bound per wild type HA trimer (**Figure 5.8.**). Notably, there were two major binding modes for this interaction on the globular head of the HA: one binding mode was to the apex of the HA trimer, whereas the other was to the lateral face of the trimer next to the RBS. There were also two major poses of 2G12 on the HA apex, with one being parallel to and the other tilted relative to the flat apex surface (**Figure 5.8.B**). In contrast, 2G12 bound only to the apex of the HA N165A mutant in the parallel and slightly tilted binding modes (**Figure 5.8.C**). As there was a visible gap between 2G12 and HA in the class averages, 2G12 likely recognises HA exclusively through antibody-carbohydrate interactions without involving the protein component of HA.

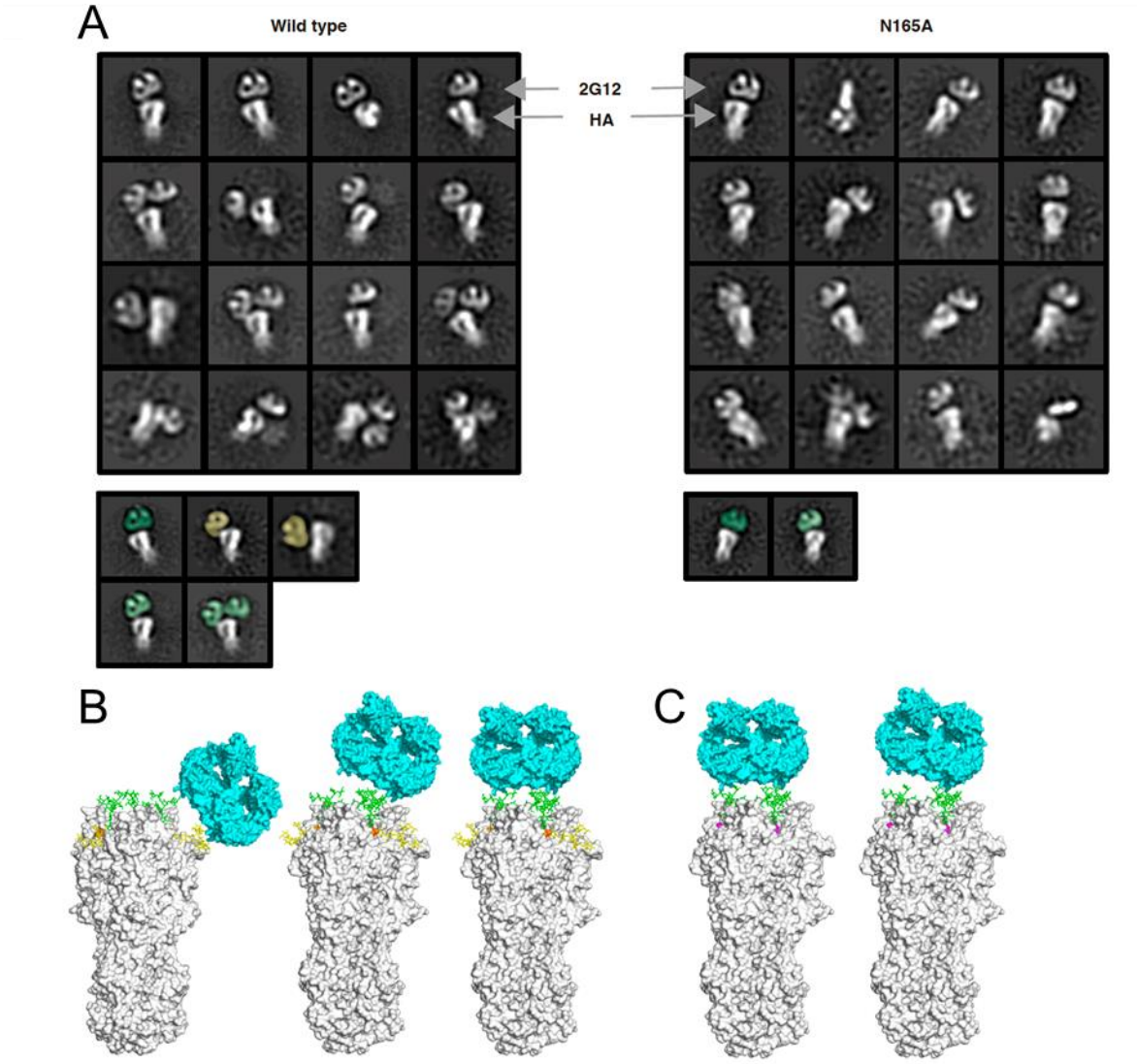


Figure 5.8. 2G12 binding mode to HA wildtype and glycan mutants. (A) Negative-stain electron microscopy (nsEM) images show the different modes of 2G12 recognition of Bris07 wild type (left panel) and N165A mutant (right panel) HA. Fab 2G12, as a domain-swapped dimer, and the HA trimer are indicated by arrows. 2G12 Fab involved in binding to two N246 glycans, one N246 glycan, and one N165 and possibly one N246 glycan are shown in green, light green, and yellow, respectively. **(B)** Front view of A/Brisbane/10/07 (H3N2) HA trimer (PDB 6AOV, in grey) (*425*). Man9GlcNAc2 on N165 and N246 were modelled onto Bris07 wild type HA with Charmm-Gui (*426*). 2G12 (PDB 6N2X, in cyan) (*243*) is shown bound to the lateral side (left panel) and apex of trimer in parallel (middle panel) or tilted (right panel) binding mode from the nsEM data in Fig. 5C. Man9GlcNAc2 on N165 and N246 are in yellow and green, respectively. **(C)** Same as **(B)**, but N165A is shown in magenta. N246 was modelled with Man8GlcNAc2. 2G12 is shown bound to the apex of Bris07 N165A trimer as in the nsEM reconstruction. The Man8GlcNAc2 at N246 is in green.

Scrutinization of the spatial distribution N165 and N246 on H3 HA trimer surface, revealed that both are located on adjacent strands of an antiparallel β-sheet with a distance the C_α's of 4.6 Å within each protomer (**Figure 5.9.**). Interestingly, the same secondary structural feature and C_α distances were observed for two of the N-linked glycan sites on HIV-1 Env (N295 and N332, Figure XXXX) which are involved in 2G12 recognition (*243*, *409*, *423*). The distances between the ends of the flexible Man9GlcNAc2 on N165 and N246 within the same protomer was about 26 Å to 29 Å. In addition, on the apex of HA trimer, the distance of Man9GlcNAc2 on N246 of one protomer to the next protomer was 14 Å (D1 to D1) and 44 Å (D3 to D3) (Data not shown).

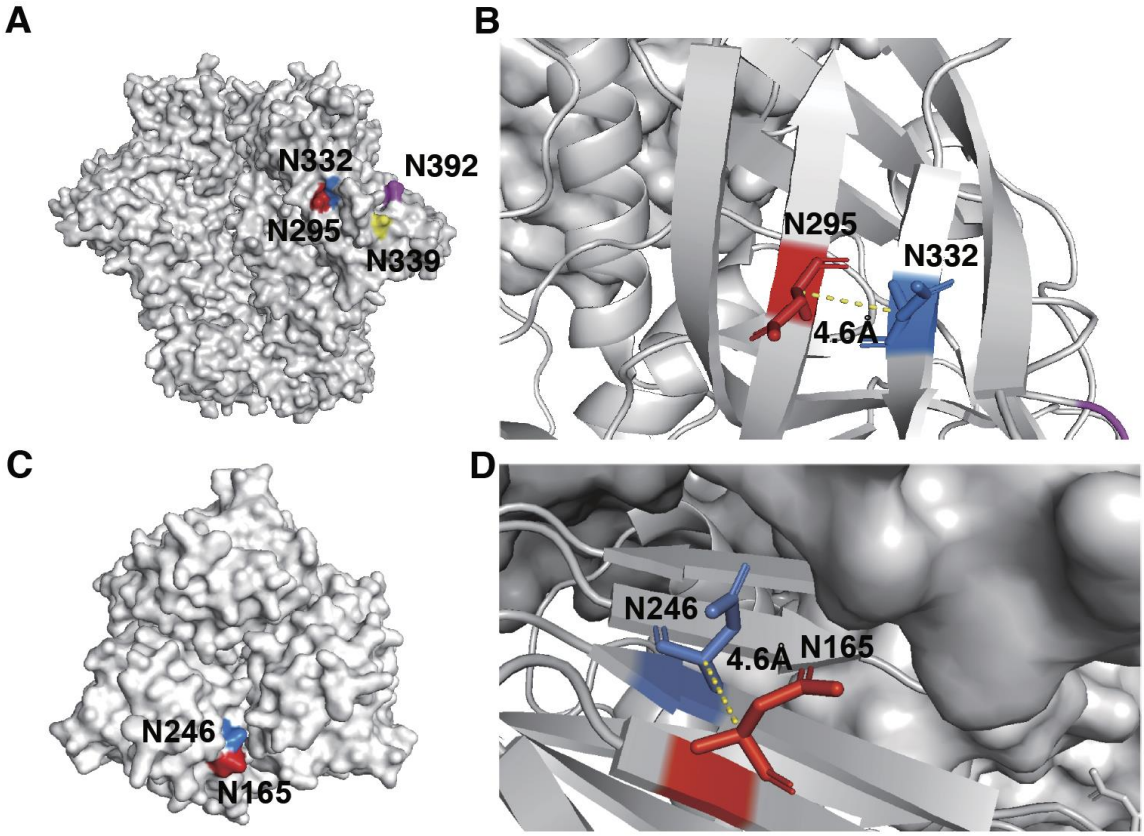


Figure 5.9. The spatial distribution of N-glycosylation sites involved in 2G12 recognition on the HIV-1 Env trimer and influenza H3 hemagglutinin. (A) Front view of the HIV-1 Env trimer (PDB: 4ZMJ) (*143*). Oligomannose on four N-glycosylation sites, N295 (red), N332 (marine), N339 (yellow), and N392 (purple) are involved in 2G12 recognition (*168*)s. (B) Close-up view of N295 and N332 on HIV-1 Env. The distance between the Cα's of N295 and N332 is 4.6Å (yellow dashed line). (C) Top view of the H3 hemagglutinin trimer (PDB:

6AOV) (*425*). Oligomannose on two N-glycosylation sites, N165 (red) and N246 (marine), are involved in recognition by 2G12. (D) Close-up view of H3 hemagglutinin trimer around N165 and N246. The distance between Cα of N165 and N246 on adjacent strands of a beta-sheet is also 4.6Å (yellow dashed line).

Overall, the distance between each $Man_9GlcNAc_2$ on N165 to N246 in the same protomer or from $Man_9GlcNAc_2$ on N246 in different protomers matched the 2G12-$Man_9GlcNAc_2$ binding distances on gp120 (*243*). By modelling 2G12 binding to the HA in the nsEM reconstructions (**Figure 5.8.**), we can conclude that N165 and N246 on the same protomer constitute the lateral binding pose (**Figure 5.8.B**). This interaction is lost in the N165A mutant, where binding is now only seen to the apex and mainly in the parallel pose (**Figure 5.8.C**). Thus, we surmise that 2G12 in this mode binds to the high mannose glycans at N246 in different promoters of the trimer. The final pose is the more tilted apex orientation, where one or two glycans at N246 are involved, perhaps in a different combination to the parallel pose. The loss of 2G12 neutralization of N165A mutant HA suggests that the lateral interaction with both N1645 and N246 is key for neutralization through blocking receptor binding compared to the apex only interaction. We further suggest that weaker overall binding to the apex in N165A is not sufficient for 2G12 to neutralize the virus compared to the additional lateral interaction in wild-type, but this is still not completely answered and may also depend on the exact glycoforms present in each case. In conclusion, during the natural evolution of human H3N2 influenza viruses from 1968 to present, the conserved N165 and emergent N246 formed a high-mannose cluster that conferred neutralizing activity of 2G12 on influenza virus.

5.6 Discussion

The addition, removal or substitution of N-linked glycosylation sites of the glycan shield are a common strategy for RNA viruses to evade recognition by antibodies (*172*, *203*, *377*, *427*).

Here, we demonstrate that 2G12, despite being an anti-HIV antibody, also has the ability to broadly neutralize human H3N2 influenza viruses that have evolved over the past five decades. Through comprehensive and evolutionary trajectory-based site-specific glycoproteomics, mutagenesis, and nsEM imaging, we reveal that neutralization is achieved through binding to two oligomannose-type glycans present at N165 and N246, which are proximal to the HA RBS. 2G12 then represents the first neutralizing antibody against human influenza viruses that solely recognises a glycan epitope on HA. The emergence of N246 around 1980 endows H3N2 viruses with an oligomannose cluster at N165 and N246 that can be recognised by 2G12. Escape mutants at these sites are then likely to have a high fitness cost, since the abolition of the conserved N165 site decreases viral fitness, as shown here and in a previous study (*289*), whereas the abolition of the N246 site could not be rescued in recent viruses.

The similarity of the glycosylation profiles of virally-derived antigens to recombinant proteins is a significant issue for vaccine design (*2*, *3*, *360*, *428*). For example, differences in glycoforms of soluble and viral HIV-1 Env have been shown to affect neutralisation and elicitation of bnAbs (*2*, *3*). From our data on H3N2 influenza viruses, the site-specific oligomannose-type glycans between recombinant HA from 293F cells and viral HAs derived from MDCK-SIAT1 cells are conserved. This finding also implies that soluble recombinant HAs could be used as immunogens in an attempt to elicit anti-carbohydrate antibodies. Although self-glycans are poorly immunogenic, in high enough density on viral glycoproteins, they have become the focus of immune responses by antibodies that interact with both glycan and protein epitopes (*161*, *301*, *376*, *429*). Multivalent binding to the high mannose glycans contributes to a potent IC_{50} of 2G12 against HIV-1. Notably, 2G12 exhibited neutralization (IC_{50} from 1 to 10 μg/ml) of sensitive HIV-1 viral strains through

the involvement of four N-linked glycan sites that constitute the mannose patch on Env (*298*, *430*). 2G12 neutralises sensitive H3N2 strains only at sub-micromolar IC_{50}'s through targeting the mannose cluster derived from only two N-linked glycans. Therefore, the 1 to 2-log difference seems to result from the fewer oligomannose-sites in the cluster of HA compared to HIV-1 Env.

Besides HIV-1 and influenza viruses, many enveloped viral pathogens, such as Ebola, Hepatitis C, LASV and coronaviruses, including SARS-COV-2 are highly glycosylated and present oligomannose on their surface antigens (**Figure 5.10**) (*26*, *140*, *428*, *431*). Indeed, besides H3N2 HAs and HIV-1 Env, 2G12 has been purported to bind SARS-CoV-2 S by recognising oligomannose-type glycans on the S2 subunit (*432*). Oligomannose clusters on surface antigens can also be recognised or captured by various lectins, such as human mannose binding lectin (MBL) or DC-SIGN (*433–435*). Similar to our finding of oligomannose glycans near the RBS on H3 HAs, some oligomannose-type glycans are also found near the RBS of the LASV GPC (*140*, *428*). Based on our findings, it is possible that other high-mannose clusters are presented near critical functional sites of highly glycosylated viruses, which could be targeted by 2G12. 2G12 could then be a potential candidate for passive immunotherapy against these viruses, especially as no adverse effects were reported during a phase I clinical trial (*436*).

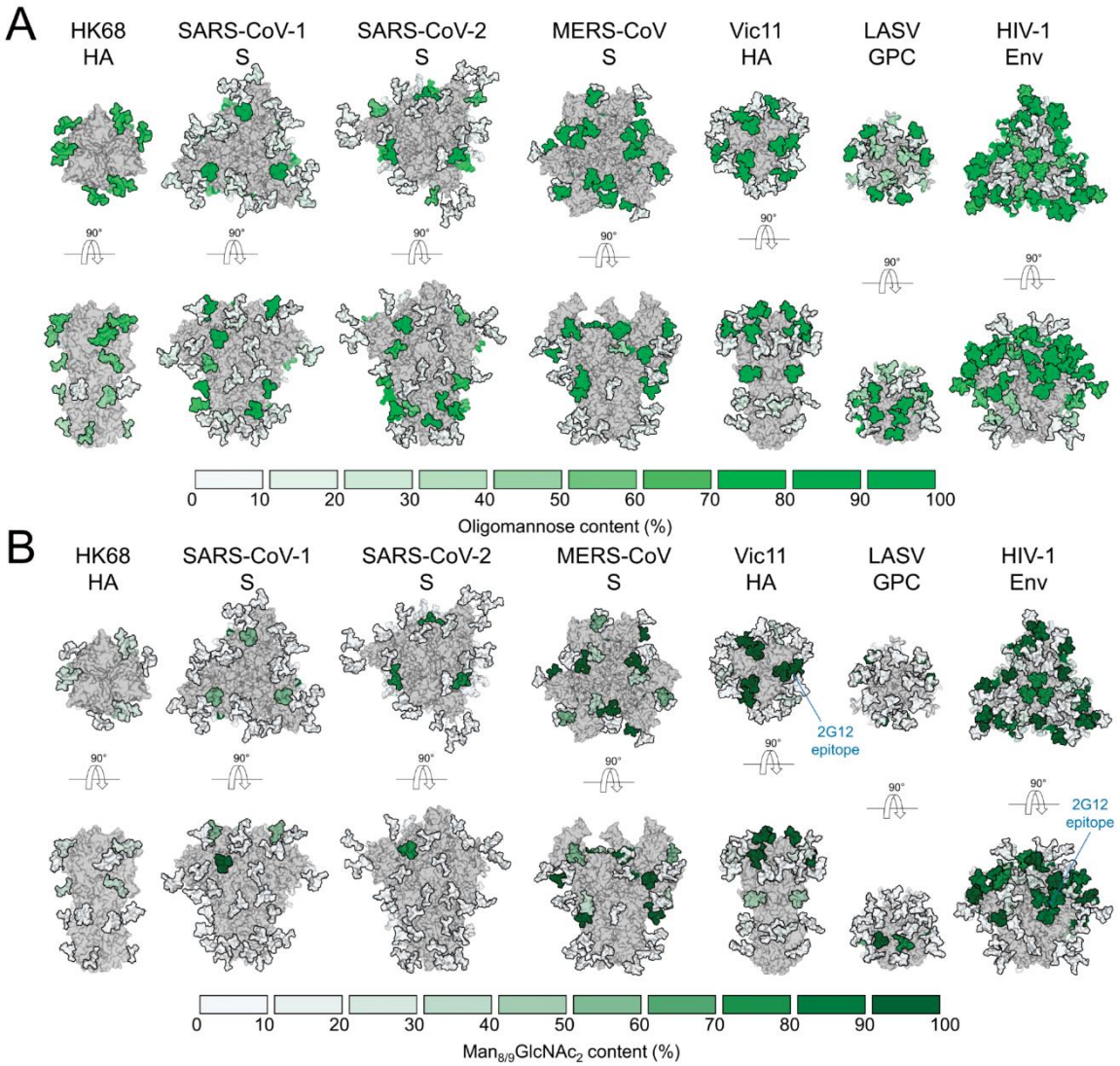


Figure 5.10. Differential under-processing of viral glycan shield (A) From left to right, HK68 HA, SARS-CoV-1 S, SARS-CoV-2 S, MERS-CoV S, Vic11 HA, LASV GPC, HIV-1 Env (PDB ID: 4FNK, 5X58, 6VSB, 5X59, 4O5N, 5VK2, 5ACO, respectively) (*7*, *117*, *242*, *315*, *316*, *318*). Glycans are coloured according to site-specific oligomannose-type glycan content (*140*, *424*, *428*), as per the key. **(B)** Glycans are coloured according to $Man_{8/9}GlcNAc_2$ content (2G12 epitopes), as per the key. Note that the HIV-1 Env 2G12 epitope consists of 4 N-linked glycans.

In toto, we reveal that 2G12 can neutralise human H3N2 viruses due to the emergence of an N246 glycosylation site approximately 30-35 years ago during the evolution of H3N2 viruses from the 1968 pandemic. As 2G12 also binds to oligomannose-type glycan epitopes on HIV-1 Env, this raises the question whether such carbohydrates can act as a universal epitope on enveloped RNA viruses. The ontogeny of 2G12 has not been documented and

most anti-carbohydrate antibodies to date have been found in patients with chronic HIV-1 infection. Thus, 2G12 recognition of carbohydrates on H3N2 influenza viruses suggests that it could be used in passive immunisation against influenza. The use of 2G12 in combination with other antibodies to generate more potent bi- or tri-specific antibodies could also be effective and more difficult for viruses to escape from (*437*).

6. Concluding remarks and perspectives

In this thesis, a quantitative site-specific mass spectrometric methodology was employed to investigate the glycan shields of numerous class I viral fusion proteins.

We reveal that on a number of viruses, such as the newly emergent coronaviruses (SARS-CoV-1, SARS-CoV-2, MERS-CoV), the glycan modifications do not constitute an efficacious glycan shield that can effectively thwart the humoral immune response in comparison to glycan shields of other more densely glycosylated viruses. This thesis also demonstrates that amino-acid diversification occurs at antibody-accessible regions of viral glycoproteins which underscores the role of glycosylation as an immune evasion strategy used by viruses.

Furthermore, while the presence of oligomannose-type glycosylation is an unusual feature for mature host cellular proteins, it appears to be a common feature on class I viral fusion proteins arising from the introduction of N-linked glycan sequons. This thesis also investigates the structural principles leading towards the generation of oligomannose-type clusters on viruses via the use of glycan knockout mutants on MERS-CoV S and influenza H3N2 HAs. I show that the local glycan density limits glycan processing as hypothesised by *Behrens et al.* (*156*), and in a similar manner to N-linked glycans on HIV-1 Env (*423*). Since glycans are also sensitive reporters of local protein architecture, it is a useful tool to guide immunogen design. Indeed, the LASV GPC glycosylation data has aided the creation of a recombinant-protein based vaccine candidate against this pathogen.

This thesis also follows the evolution of H3N2 influenza viruses which has continuously accumulated N-linked glycosylation sites on HA during antigenic drift. This

accretion of glycans in order to shield immunogenic epitopes on the head region of HA, has led to the induction of carbohydrate-epitopes which arise from improper processing of glycans. This has led to recent H3N2 viruses being susceptible to neutralisation by the anti-HIV antibody 2G12. It will be of great interest to observe whether antibodies isolated against not only influenza HAs, but also arenavirus GPCs and coronavirus S proteins will exhibit glycan-binding properties as the viruses evolve.

Overall, this thesis highlights the importance of glycan shielding as an immune evasion strategy for viruses and offers novels therapeutic avenues to target conserved epitopes found on many viruses. I hypothesise that a drug that is able to target the glycan shield would be advantageous with regards to the potential development of anti-drug resistance, since it would be targeting epitopes that make the virus more evasive. It is however important to note that since glycans are inherently "self" molecules, and the carbohydrate-binding affinities are generally low, any therapeutic would have significant challenges to overcome.

List of Abbreviations

2-AA	2-aminobenzoic acid
α-Glu I/II	α-glucosidase I/II
α-DG	α-dystroglycan
α-Man I/II	α-mannosidase I/II
Ab	Antibodies
AIDS	Acquired immunodeficiency syndrome
BEAST	Bayesian evolutionary analysis and sampling trees
bnAbs	Broadly neutralising antibodies
bp	Base pair
bsAb	Bispecific antibodies
CCR5	C-C chemokine receptor 5
CCS	Collision cross section
CDR	Complementarity-determining region
CD4	Cluster of differentiation 4
CFG	Centre for Functional Glycomics
CIU	Collision-induced unfolding
CNX/CLN	Calnexin/calreticulin
CoV	Coronavirus
CRD	Carbohydrate recognition domains
CXCR4	C-X-C chemokine receptor 4
DC-SIGN	Dendritic cell-specific intercellular adhesion molecule-3-grabbing non-integrin
DENV	Dengue virus
DMEM	Dulbecco's Modified Eagle Media
DSC	Differential Scanning Calorimetry
DTT	Dithiothreitol
dN/dS	Nonsynonymous to synonymous substitutions ratio
E	Envelope protein
EBOV	Ebola virus
EDE	E dimer epitope
EEEV	Eastern equine encephalitis virus
ELISA	Enzyme-linked immunosorbent assay
EM	Electron microscopy
Endo H	Endoglycosidase H
Env	Envelope spike
ER	Endoplasmic reticulum
ER α-M	Endoplasmic reticulum α-mannosidase I
ESI	Electrospray ionisation
Fab	Fragment antigen binding
Fc	Fragment crystallisable
FCS	Foetal Calf Serum
FP	Fusion peptide
FT	Fucosyltransferase
Fuc	Fucose
GAGs	Glycosaminoglycans
Gal	Galactose

GalNAc	*N*-Acetylgalactosamine
Glc	Glucose
GlcA	Glucuronic acid
GlcN	Glucosamine
GlcNAc	*N*-Acetylglucosamine
GnT-I	*N*-Acetylglucosaminyltransferase I
GP	Glycoprotein
GPC	Glycoprotein complex
HA	Hemagglutinin
HCD	Higher energy collisional dissociation
HCDR3	Heavy chain complementarity determining region-3
HEK	Human embryonic kidney
Hex	Hexose
HexNAc	*N*-Acetylhexosamine
HILIC-UPLC	Hydrophilic interaction chromatography-Ultra performance liquid chromatography
HIV-1	Human immunodeficiency virus, type 1
HN	Hemagglutinin-neuraminidase
HS	Heparan sulfate
HSV	Herpes simplex virus
IAA	Iodoacetamide
IdeS	IgG degrading enzyme from *Streptococcus pyogenes*
IgG	Immunoglobulin G
IM	Ion mobility
IMP	Intrinsic mannose patch
kb	kilobase
kDa	kilodalton
LAMP-1	lysosomal-associated membrane protein-1
LASV	Lassa virus
LC-ESI MS	Liquid chromatography-electrospray ionisation mass spectrometry
MALDI	Matrix assisted laser desorption ionisation
Man	Mannose
MBL	Mannose binding lectin
MDCK-II	Madin-Darby canine kidney-II
MERS	Middle eastern respiratory syndrome
MosGCTL	Mosquito galactose specific lectins
MPER	Membrane proximal external regions
MS	Mass spectrometry/spectrum
MW	Molecular weight
NA	Neuraminidase
NB-DNJ	*N*-butyl-deoxynojirimycin
Neu5Ac	*N*-acetylneuraminic acid/sialic acid
Nipah G	Nipah Attachment glycoprotein
Nipah F	Nipah Fusion glycoprotein
NS1	Non-structural protein-1
OST	Oligosaccharyltransferase
PAMPs	Pathogen-associated molecular patterns
PBS	Phosphate buffered saline
PDB	Protein data bank

PISA	Protein, Interfaces, Structures and Assemblies
PNGase A	Peptide-*N*-glycosidase A
PNGase F	Peptide-*N*-glycosidase F
PNGS	Potential *N*-linked glycosylation site
ppGalNAcT	Polypeptide *N*-acetylgalactosaminetransferases
RAxML	Randomised axelerated maximum likelihood
RBS	Receptor binding site
RMSD	Root-mean-squared-deviation
RT	Reverse transcriptase
S	Spike protein
SARS	Severe acute respiratory syndrome
SDS-PAGE	Sodium dodecyl sulphate-polyacrylamide gel electrophoresis
SEC	Size exclusion chromatography
SFV	Semliki Forest virus
SFTSV	Severe fever with thrombocytopenia syndrome virus
SIV	Simian immunodeficiency virus
sGP	Secreted glycoprotein
SOSIP.664	Stabilising mutation, including disulphide bond (“SOS”) and Ile to Pro point mutation (“IP”), truncation at residue 664
SPA/D	Surfactant protein A/D
ssG	secreted glycoprotein G
ssGP	small secreted glycoprotein
SSP	Stable signal peptide
TAMP	Trimer associated mannose patch
TM	Transmembrane region
TW	Travelling wave
UGGT	UDP-glucose:glycoprotein glucosyltransferase
VLP	Virus-like particle
XIC	Extracted ion chromatograms
ZIKV	Zika virus

Appendix A: Signature of antibody domain exchange by native mass spectrometry and collision-induced unfolding

Abstract

The development of domain-exchanged antibodies offers a route to high-affinity targeting to clustered multivalent epitopes, such as those associated with viral infections and many cancers. One strategy to generate these antibodies is to introduce mutations into target antibodies to drive domain exchange using the only known naturally occurring domain-exchanged anti-HIV IgG1 antibody, 2G12, as a template. Here, we show that domain exchange can be sensitively monitored by ion-mobility mass spectrometry and gas-phase collision-induced unfolding. Using native 2G12 and a mutated form that disrupts domain exchange such that it has a canonical IgG1 architecture (2G12 I19R), we show that the two forms can be readily distinguished by their unfolding profiles. Importantly, the same signature of domain exchange is observed for both intact antibody and isolated Fab fragments. The development of a mass spectrometric method to detect antibody domain exchange will enable rapid screening and selection of candidate antibodies engineered to exhibit this and other unusual quaternary antibody architectures.

Introduction

Antibodies (Ab) have emerged as the leading format for biotherapeutics because of their fine target specificity and their ability to recruit immune effector functions (*438*). Most immunoglobulin-based therapeutics are based on the IgG format whereby target recognition is mediated through the variable domains of the fragment antigen binding (Fab) and the

fragment crystallizable (Fc) domain mediates immune effector functions via complement activation and/or binding to cellular Fcγ receptors (*439–441*).

The Fc activity can be fine-tuned or silenced by both protein and glycan engineering (*442–445*). In this way, therapeutic antibodies can be designed that either have minimal immunological effector can exhibit elevated immune recruitment for maximal cell killing. In contrast, much less attention has been paid to exploring enhancing the target selectivity beyond that achieved by a natural Fab architecture. One approach to circumvent this limitation has been the development of bispecific antibodies (bsAb) where target selectivity is enhanced by Fabs of differing specificity (*446–448*). A further underexplored architecture is the use of domain-exchanged IgG whereby the Variable domains from the two heavy chains (VH and VH′) are exchanged, leading to a compact dual Fab (*243*). This architecture was discovered during the epitope mapping of 2G12, an antibody that is capable of neutralizing a broad range of human immunodeficiency virus (HIV) isolates (**Figure A.1.A**) (*298*). This Ab is unusual in that the epitope consists of the dense cluster of N-linked glycans on the outer domain of the HIV attachment glycoprotein, gp120 (*298, 449*). 2G12 specifically recognizes terminal Manα1-2Man-linked moieties predominantly found on $Man_8GlcNAc_2$ and $Man_9GlcNAc_2$ (*298, 450, 451*). Domain exchange is critical for effective binding as the target glycans for the canonical Fab binding sites are only 20 Å apart (*450*). In addition, domain exchange may generate a new glycan binding surface at the V_H/V_H' interface, which further enhances binding (*243, 244*).

Domain exchange of 2G12 has been verified by X-ray crystallography of the isolated $(Fab)_2$ domain and also size-exclusion chromatography, analytical ultracentrifugation, and electron microscopy (*243, 244*). A single-point mutation, I19R, completely results in the un domain-exchanged, classical IgG format, and X-ray crystallography of the resulting isolated

Fab was shown to exhibit identical V_H/V_L structure compared to the parental domain-exchanged form (*452*) (**Figure A.1.B**). It has been suggested that domain-exchange architecture on antibodies could be used to target multivalent ligands in tumours and pathogens by providing binding specificities that go beyond the classical Fab paradigm. However, identifying domain-exchanged antibodies by aforementioned techniques is low throughput and requires considerable amounts of protein.

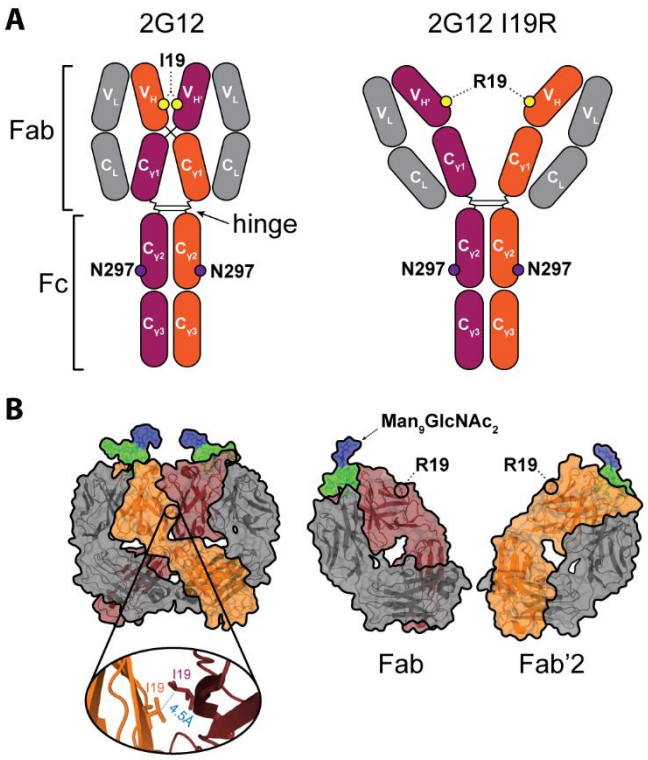


Figure A.1. (A) Cartoon structures of domain-exchanged 2G12 and2G12 I19R antibodies showing the location of Fab, hinge, and Fc regions (domains are labelled with white text). Light chains are grey and heavy chains are coloured dark red and orange. The location of amino acid I19/R19 on both heavy chains is labelled yellow and the conserved Asn297 N-linked glycosylation site is purple. **(B)** Crystal structures of 2G12 (PDB: 1OM3) and 2G12 I19R (PDB: 3OAU) Fab domains with a single Man9GlcNAc2glycan bound to each antigen binding site. Mannose, green. GlcNAc, blue.

Using native ion-mobility mass spectrometry (IM-MS), which separates ions not only by their mass-to-charge ratio but also by their three-dimensional shape, and collision-

induced unfolding (CIU), which activates selected ions prior to IM separation, we sought to explore whether domain-exchanged antibody architecture of 2G12 could be distinguished. Compared to other MS-based approaches, native MS maintains proteins in their intrinsically folded state and is an emerging method for biotherapeutic analysis (*453–456*). IM-MS has proven useful to study thermal stability (*457*), dynamics (*458*, *459*), interactions (*460*), and biosimilarity (*461*) of intact monoclonal antibodies. CIU experiments utilize both collision activation to induce protein unfolding and IM separation which is based on the rotationally averaged collision cross section (CCS) of the ion (*462–464*). CIU of protein complexes is an efficient tool to detect various protein features, including discriminating IgG glycosylation and disulphide bonding (*465*). Additionally, native IM-MS has proven capable of characterizing antibody drug conjugates, specifically assigning drug-to-antibody ratio of trastuxumab emtansine (*466*).

With antibodies at the forefront of biotherapeutics, a high-throughput analytical technique for the assessment of their structural properties is desirable (*467*). Here we continue the development of IM-MS and CIU as an analytical technique and show that gas-phase methods offer a route to rapid and sensitive screening of unusual quaternary architectures that arise from antibody engineering. We examine the CIU profiles of 2G12 and 2G12 I19R Abs and confirm that the specific footprints are determined solely by the domain-exchanged architecture of 2G12.

Experimental Section

Antibody Expression and Purification

Plasmids encoding antibody heavy and light chains of 2G12 and 2G12 I19R, b12, and trastuzumab were transiently expressed in HEK 293Fcells at a density of 1×10^6 cells/mL. Transfection was done with a 1:2 construct ratio (heavy to light chain) and cells were grown

for 5 days. Cells were pelleted and the supernatant was loaded onto a HiTrap Protein A column (GE Healthcare) using the manufacturer's protocol. The binding buffer was 20 mM sodium phosphate, pH 7.5, and the elution buffer was 0.1 M citric acid, pH 3. Antibodies were immediately neutralized with1 M Tris-HCl, pH 9, prior to buffer exchange into phosphate buffered saline (PBS) using a 50 kDa cut-off Vivaspin column (Sartorius). Antibodies were stored at 4°C until prior to analysis.

Enzyme-Linked Immunosorbent Assay

ELISAs were performed using 96-well Ni-NTA His Sorb plates (Qiagen). Plates were incubated overnight at 4°C with 10μg of HIVgp120, expressed as described (*468*). Plates were washed four times with 0.5% PBS/Tween and blocked with 5% skim milk/PBS for1 h at room temperature. Serial dilutions of 2G12 and 2G12I19R antibodies in 5% skim milk/PBS were incubated for an hour. Unbound antibody was removed by washing as described above. Horseradish peroxidase conjugated antihuman goat IgG (ThermoFisher Scientific) was added at a 1:3000 dilution for 1h. The chromogen tetramethylbenzidine was added for 5 min and then neutralized using 2 M sulfuric acid. Absorbance was measured at 450 nm.

IdeS Expression and Purification

Recombinant IdeS was expressed in Escherichia coliBL21 (DE3) cells. Then 500 mL of MagicMedia (Invitrogen) containing carbenicillin (100μg/mL) was inoculated with the 12.5 mL of an overnight seed culture. Cells were grown at 30°C with shaking at 300 rpm for 7 h and then at 25°C for an additional 24 h. Cells were harvested by centrifugation at 4000gfor 30 min. Bacterial lysis was performed by sonication at 4°C in a lysis buffer of 30 mM sodium phosphate, 300 mM NaCl, and pH 8. After centrifugation at 30 000g for 40 min, the filtered supernatant was loaded onto a HisTrap column (GE Healthcare) with a binding

buffer of 100 mM HEPES, 150 mM NaCl at pH 7.5. Sequential elutions of IdeS were performed using increasing concentrations of imidazole from 20 to 300 mM.

IdeS Cleavage

2G12 and 2G12 I19R were incubated for 2h at 37°C with IdeS (IdeS-to-antibody ratio of 1:100) to generate intact Fc and Fab antibody fragments.

Ion-Mobility Mass Spectrometry and Collision-Induced Unfolding

Samples were buffer-exchanged into 200mM ammonium acetate, pH 6.9, with Bio-Spin 6 columns (Bio-Rad). Additional desalting was accomplished by three sequential washes of 200 mM ammonium acetate using 50kDa molecular weight cut-off (MWCO) centrifugal spin filters (GE Healthcare). Samples were diluted to 10μM and analysed with a Synapt G2Si mass spectrometer (Waters, Manchester, UK). A nanoelectrospray (nESI) ion source was used with gold-coated borosilicate glass capillaries prepared in-house. Instrument settings were as follows: capillary voltages, 1.4−1.8kV; source temperature, 30°C; sampling cone, 10 kV; trap direct current bias, 20 V; trap gas flow, 5 mL/min; helium cell gas flow, 5 mL/min; IMS gas flow, 30 mL/min; trap wave velocity, 311 m/s; trap wave height, 4 V. Data acquisition and processing were carried out using MassLynx v4.11 and Driftscope version 2.8 software (Waters, Manchester, UK).

For CIU experiments, collision energy was applied in the trap region prior to IM. The collision voltage was increased from 4 to 200 V in 10 V increments. IM data were collected for 1 min at each collision voltage. Unfolding plots were created using PULSAR software, available from http://pulsar.chem.ox.ac.uk. (*469*). Mass fitter was utilized using the following parameters: mass, 150 kDa; Z_{avg}= 24; Z_{width}= 1.5; resolution, 900; and maximum intensity, 1. Experiments were grouped according to hierarchy based on collision voltages.

Drift time data were extracted using Driftscope version 2.8(Waters, Manchester, UK), and statistical analysis was performed using python2.7 version of CIUSuite package (*470*). Root-mean-squared-deviation (RMSD) values were calculated using CIUSuite stats and compare modules between 2G12 and 2G12 I19R variants.

Differential Scanning Calorimetry (DSC)

Antibody samples were prepared at a concentration of 20μM in 400μL of PBS. DSC measurements were performed on a Malvern VP Capillary DSC (Malvern), with an unfolding temperature range of 30−110°C.

Glycan Analysis

N-Linked glycans were enzymatically cleaved from SDS-PAGE gels using PNGase F prepared in-house. Released N-glycans were fluorescently labelled with 2-aminobenzoic acid (2-AA) for analysis by hydrophilic interaction chromatography ultra-high-performance liquid chromatography (HILIC-UPLC) with a Waters Acquity UPLC instrument, as previously described (*155*). Glycan compositions were determined using traveling wave (TW) IM-MS measurements performed on a Synapt G2Si instrument (Waters, Manchester, UK). For each analysis 2 μL of sample was cleaned with a Nafion 117 membrane and directly infused by nanoelectrospray ionization (nano-ESI) from gold-coated borosilicate glass capillaries as previously described (*451, 471*). Instrument settings were as follows: capillary voltage, 0.8−1.0 kV; sample cone, 100 V; extraction cone, 25 V; cone gas, 40 L/h; source temperature, 150°C; trap collision voltage, 4−160 V; transfer collision voltage, 4 V; trap direct current bias, 35−65 V; IMS wave velocity, 450 m/s; IMS wave height, 40 V; trap gas flow, 2 mL/min; IMS gas flow, 80 mL/min. Data were acquired and processed with MassLynx v4.1 and Driftscope version 2.8software (Waters, Manchester, UK).

Results and Discussion

Functional ELISA to Characterize Domain Exchange.

Prior to IM-MS and CIU experiments, an ELISA was used to confirm the impact of each 2G12 antibody architecture on function. The monovalent I19R variant is able to recognize HIV gp120 monomers but with a lower affinity to the divalent domain-exchanged 2G12 (*450*). Wells were coated with gp120 (BG505 clade A strain) which has 24 N-glycosylation sites and binding was measured from serial dilutions of the antibodies. Expectedly, binding to gp120, which displays the oligomannose-type glycans of the 2G12 epitope (*29*, *151*, *152*), differs between 2G12 and 2G12 I19R (**Figure A.2**). These data are consistent with the expected 2G12 and 2G12 I19R architectures and the material was suitable for subsequent MS experiments.

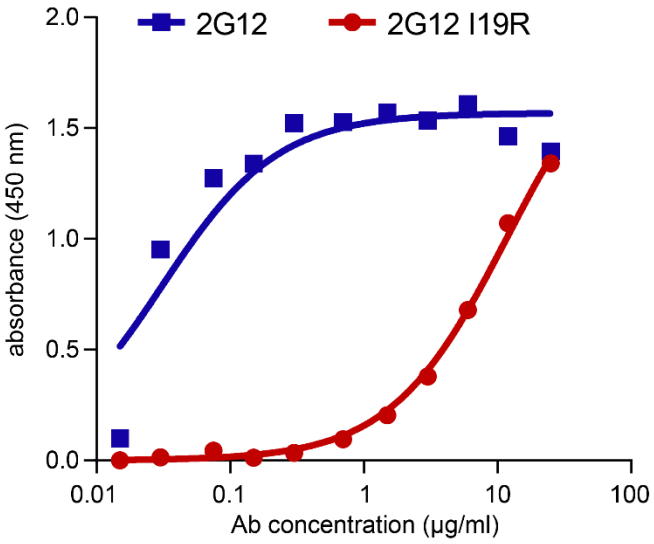


Figure A.2. Binding assay of 2G12 (blue) and 2G12 I19R (red) to recombinant HIV gp120. ELISAs were performed with Ni^{+} immobilised gp120 and serial Ab dilutions.

Differential Scanning Calorimetry of 2G12 and 2G12 I19R

Differential scanning calorimetry (DSC), a technique that measures unfolding in solution because of heat denaturation, was used to explore the potential for different thermodynamic properties between 2G12 mAbs. DSC revealed that 2G12 I19R unfolded in the manner

previously observed for typical IgG1 antibodies (*472*, *473*), with three transitions: first, CH2 domain unfolding (T_m= 61.0°C), followed by Fab unfolding (T_m= 72.9°C) and unfolding of the CH3 domain (T_m= 86.0°C) (**Figure A.3**). The domain-exchanged 2G12 yielded only two transitions, with the first unfolding state occurring at 73.7°Cand the second at 86.0°C. The CH2 domain and the Fab region of 2G12 unfolds at the same temperature, possibly because of the domain-exchanged architecture, while the CH3 domain unfolds at the same temperature as 2G12 I19R. Importantly DSC unfolding profiles can range significantly among typical IgGs (*472*, *474*) but these results point to different stability properties between 2G12 and 2G12 I19R.

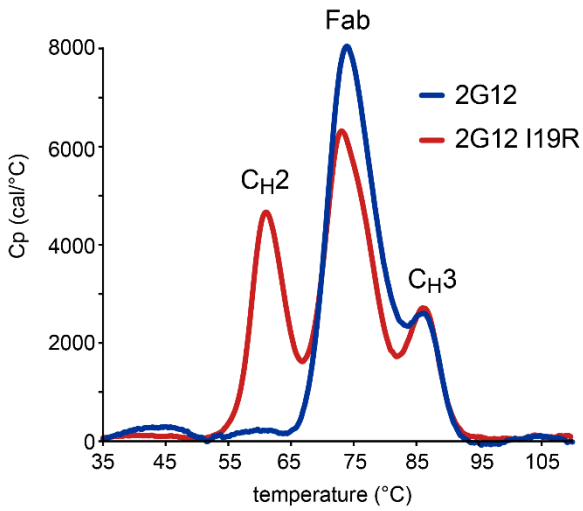


Figure A.3. DSC of 2G12 (blue) and 2G12 I19R (red). Cp, specific heat capacity. Peaks are labelled based on previously reported IgG1 assignments (*472*, *473*).

Native Mass Spectrometry and Ion Mobility of 2G12 and 2G12 I19R.

We next tested gas-phase separation of both antibodies by ion-mobility MS. The native MS spectra of 2G12 and 2G12 I19R were characteristic of an intact folded IgG1with charge states ranging between 22^+–26^+ (2G12) and 21^+–25^+ (2G12 I19R) (**Figure A.4.A**). The 2G12 charge-state distribution was slightly higher with 24^+ as the major charge state, whereas for 2G12 I19R the 23^+ charge state was foremost, followed closely by 24^+. In

principle, the difference in distribution of charge could be attributed to differences in available surface area (during electrospray desolvation) exhibited by undomain-exchanged (2G12 I19R) or domain-exchanged (2G12) Fab architectures. Interestingly, the IM drift times of 2G12 were greater between all charge states (22^+–25^+) which directly infers a larger CCS compared to the canonical undomain-exchanged IgG (2G12 I19R) architecture (**Figure A.4.B**). Although subtle, the intact MS analysis indicates differences exist between 2G12 and 2G12 I19R; however, these data alone are inconclusive to recognize domain exchange among unknown IgGs.

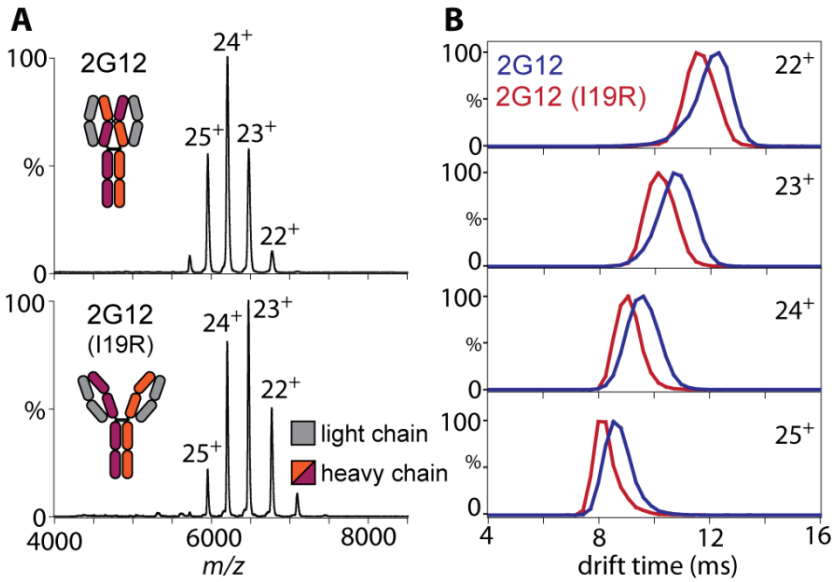


Figure A.4. (A) Native mass spectra of 2G12 and 2G12 I19R. **(B)** Arrival time distributions of 2G12 (blue) and 2G12 I19R (red) 22^+-25^+ charge states.

Collision-Induced Unfolding Signatures of Domain-Exchanged Antibodies

We next assessed CIU differences between 2G12 and 2G12 I19R (**Figure A.5**). In a CIU experiment the unfolding of a protein (induced by increased collision voltages) is monitored as a function of drift time. The resulting two-dimensional data follow the progressive unfolding or change in size from the initial folded protein ion. The relative abundance of each transition is presented (**Figure A.5, blue line**) over the course of each applied voltage.

From the initial folded state, the CIU plot follows unfolded intermediates, sometimes referred to as transitions, and represents gas-phase stability of a protein complex.

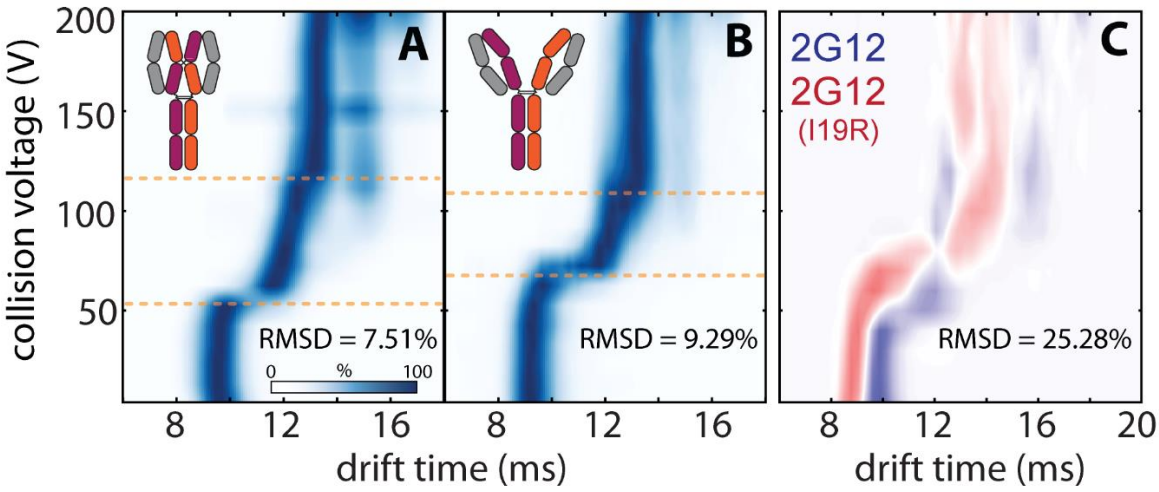


Figure A.5. Collision-induced unfolding profiles of the 24^+ charge state of 2G12 **(A)** and 2G12 I19R **(B)**. The orange dotted lines indicate the collision voltage at the two observed transition states. The blue gradient represents normalised ion intensities for each voltage scan. **(C)** Difference overlay of 2G12 (blue) and 2G12 I19R (red) CIU profiles.

The CIU profiles of 2G12 and 2G12 I19R 24^+charge state revealed differences in gas-phase unfolding with 2G12 under-going its first unfolding transition at a lower collision voltage (50 V) (**Figure A.5.A**), whereas 2G12 I19R started to unfold at 70V (**Figure A.5.B**). The second 2G12 unfolded intermediate was maintained to 120 V compared to 2G12 I19R which unfolded earlier (110 V). Consistent with **Figure A.2**, the drift times of the initial folded state differed (2G12 I19R = 9.1 ms, 2G12 = 9.6ms), but interestingly, the drift times of the second intermediate were similar for both Abs (~12.5 ms). This could be interpreted as both 2G12s unfolding toward a similar configuration or unfolding of the Fab domain during firs transition. A third unfolded state was observed for the 24^+ with some low-intensity signal detected which may correspond to a fourth state (~16 ms). The choice of charge state used for antibody CIU experiments has been previously described (*467*) and influences the amount and features of transitions. This differential behaviour between

domain-exchanged and non-exchanged antibodies of the 24^+ charge state showed clear differences in gas-phase stability and unfolding existed between the two Ab forms. CIU experiments were performed using two biological replicates (two separate Ab expressions) for both 2G12 antibodies, and the root-mean-squared deviation (RMSD) values were calculated using the CIUSuite software (*470*). The RMSD values were 7.51% and 9.29% for 2G12 and 2G12 I19R, respectively, suggesting minimal differences within each replicate (*465*). The RMSD value for the difference plot was much greater (RMSD = 25.28%), revealing the considerable differences between the two 2G12 Abs (**Figure A.5.C**).

Glycosylation Analysis of 2G12 and 2G12 I19R.

Antibody glycosylation has been shown to affect CIU fingerprinting of antibodies (*465*, *467*) and may account for different unfolding profiles observed for the 2G12-based architectures. Although 2G12 and 2G12 I19R differ by a single amino acid substitution, it is conceivable that Fc glycosylation may account for CIU discrepancies, yet any glycan-specific-induced stability effects in the gas phase is unclear. To confirm the glycosylation status of both 2G12 and 2G12 I19R, N-glycans were released by PNGase F digestion and analysed by HILIC-UHPLC (**Figure A.6**). UHPLC analysis of fluorescently labelled glycans provided relative amounts of each glycan and no major differences were observed between 2G12 antibodies. Both2G12 and 2G12 I19R glycans were equivalent and also similar to typical IgG1s with the fucosylated a-, mono-, and digalactosylated biantennary glycans being the most dominant (*475*). However, 2G12 exhibited slightly more $Man_5GlcNAc_2$ glycan than 2G12 I19R but no previous influence on this glycan on CIU has been reported. Individual glycan structures were further characterized by IM-MS (**Figure A.7.**).

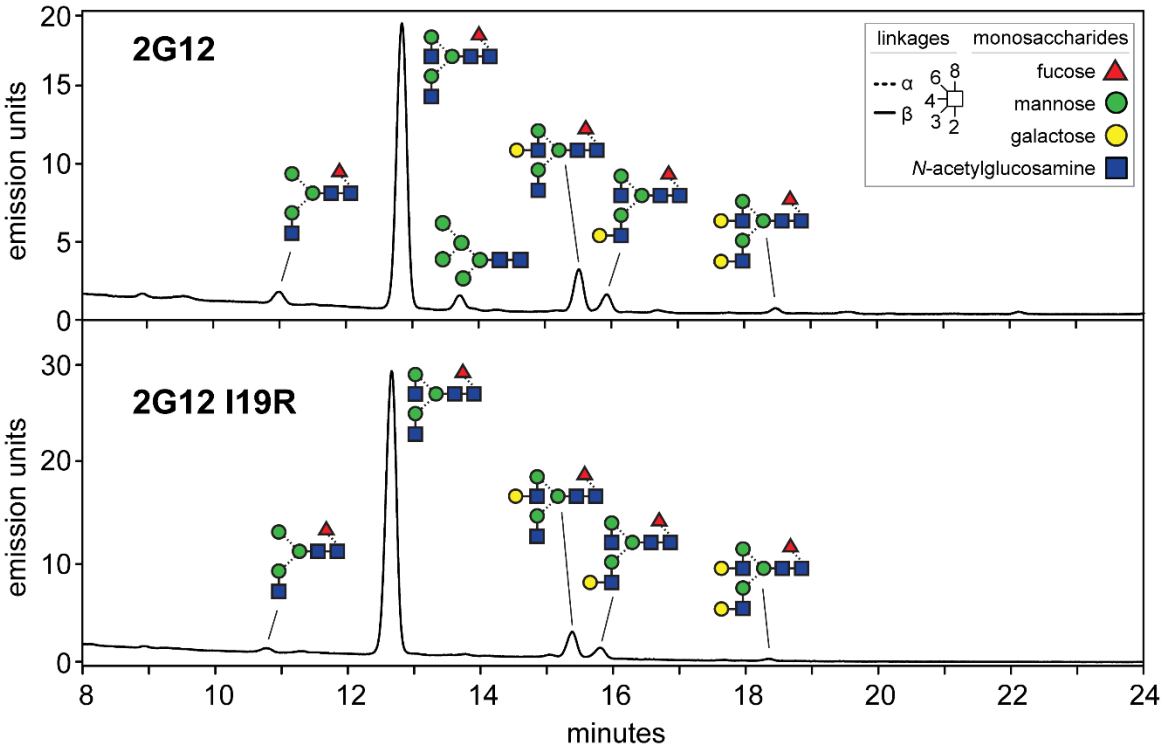


Figure A.6. Glycan analysis by HILIC-UHPLC of 2AA-labelled N-linked glycans from 2G12 and 2G12 I19R. Peaks were labelled accordingly to previous assignments (*476*).

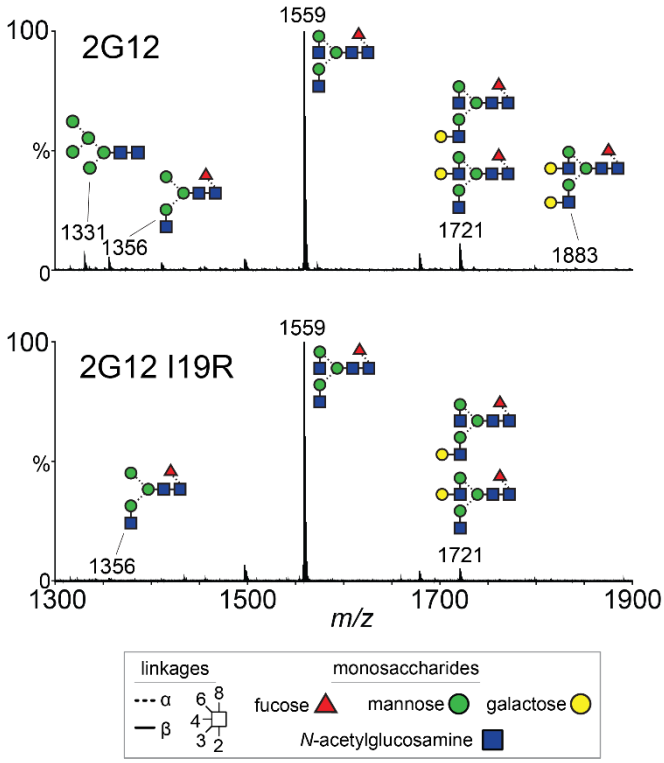


Figure A.7. Ion mobility mass spectra of 2G12 and 2G12 I19R N-linked glycans. N-linked glycans were detected as negative ion phosphate adducts $[M+H2PO4]^-$.

Collision Induced Unfolding of 2G12 and 2G12 I19R Fab and Fc domains.

To confirm that the observations made from the CIU profiles in Figure 5 were solely due to the domain-exchanged architecture rather than other factors, an IgG degrading enzyme from Streptococcus pyogenes (IdeS) cleavage was used to isolate the two regions. IdeS specifically cleaves IgGs between the Fc and Fab at a single site at the lower hinge region leaving both fragments intact (*477*). After incubation with IdeS, the Fab and Fc regions were unfolded as before, with the Fc domains of both 2G12 and 2G12 I19R unfolding in an identical manner (**Figure A.8**). However, CIU of the Fab regions differed and were analogous to the intact CIU results. Overall three unfolded states were observed, and the domain exchanged 2G12 Fab unfolded first (55V) whilst the 2G12 I19R Fab unfolded at a higher collision energy (70V). Unfolding to the third state occurred at 125V and 150V for 2G12 and 2G12 I19R, respectively. On the whole, CIU pro-files of both the domain-exchanged intact antibody and isolated Fabs unfolded at lower collision voltages than the non-domain-exchanged IgGs.

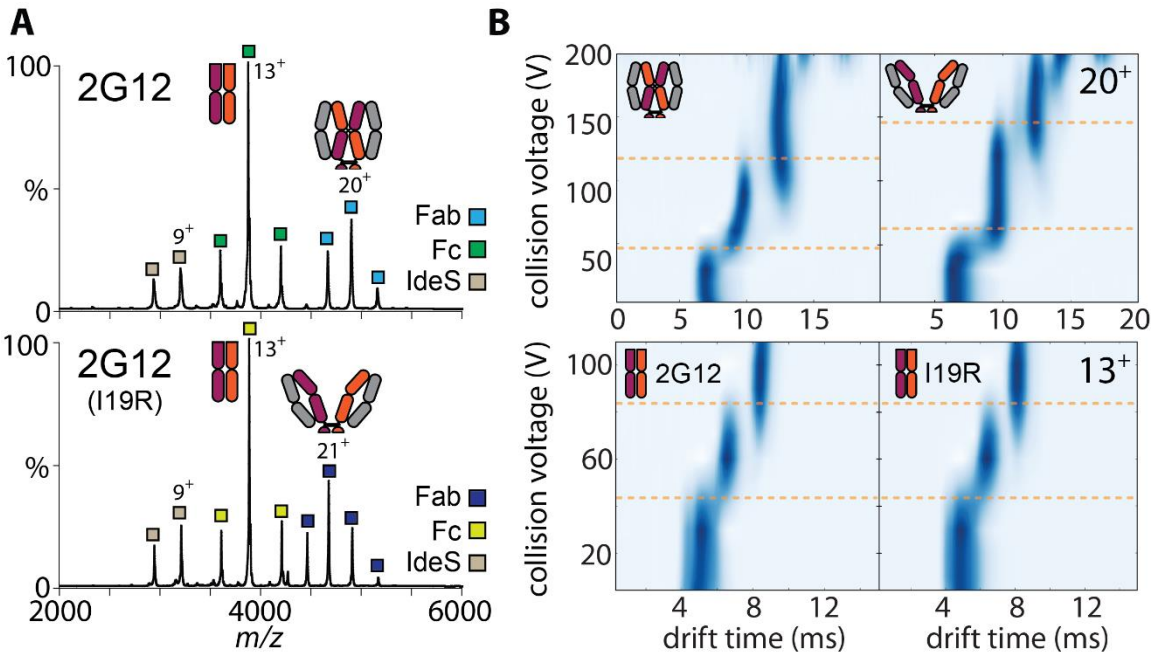


Figure A.8. (A) Native mass spectra of 2G12 and 2G12 I19R treated with IdeS. **(B)** Unfolding plots of 2G12 Fab domains (20^+ charge state) and Fc domains (13^+ charge state). The orange dotted lines indicate the collision voltage at each observed transition states.

Collision Induced Unfolding of 2G12 I19R is equivalent to standard IgG antibodies.

To confirm that the CIU profiles of 2G12 I19R were consistent with other IgG1 antibodies, two representative anti-bodies were tested. The first is the well-known IgG1 therapeutic antibody, trastuzumab, and the other is an HIV-neutralising IgG1 antibody, b12 (*478*, *479*) (**Figure A.9**). The CIU profiles of the 24^+ charge states were similar with trastuzumab, b12 and 2G12 I19R unfolding first at a collision voltage of 70 V. The second transition occurred at a collision voltage of 120 V. The unfolding patterns of b12, trastuzumab and 2G12 I19R was observed across all other major charge states (22^+, 23^+, 25^+) (**Figure A.10**) and differed to 2G12. As discussed above, charge state selection for CIU fingerprinting is an important factor when comparing antibodies.

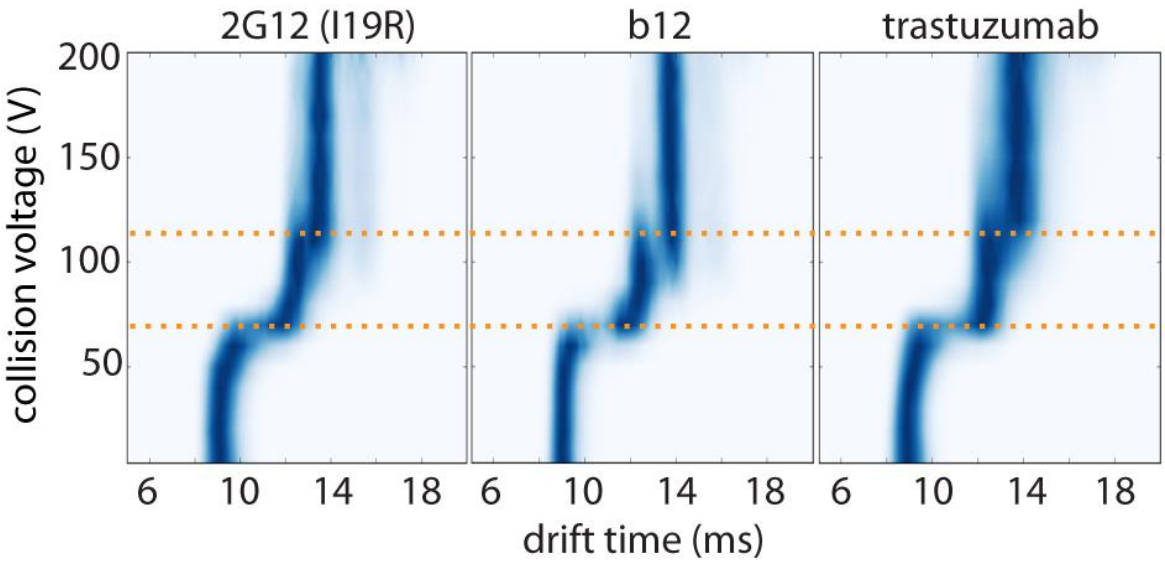


Figure A.9. Collision-induced unfolding profiles of convention-al IgG1 antibodies b12 and trastuzumab alongside 2G12 I19R (24^+ charge state). The dashed orange lines represent the un-folding transitions.

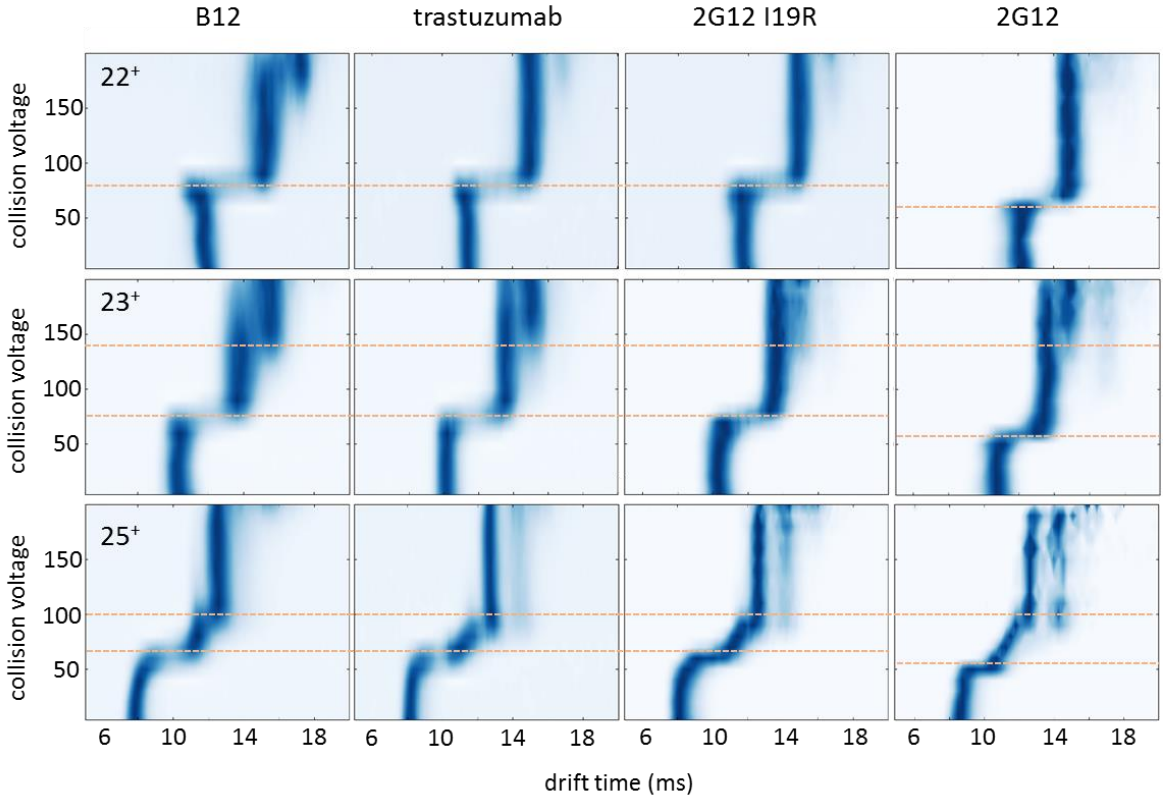


Figure A.10. Collision-induced unfolding of b12, trastuzumab, 2G12 I19R and 2G12 antibodies (charge states 22^+, 23^+ and 25^+). The dashed orange lines represent the unfolding transitions.

Conclusions

Identification of Ab structural features has generally been approached by classical techniques including X-ray crystallography and electron microscopy. Further structural details have been investigated using thermodynamic, hydrodynamic, scat-tering, and other spectroscopic and mass spectrometric meth-odologies. Here, we demonstrate that native mass spectrome-try and collision-induced unfolding can complement these established methods by rapidly and sensitively distinguish between domain-exchanged and non-exchanged antibody architectures. We further demonstrate that the change in gas-phase unfolding is localized to Fab domains, identified specif-ically after IdeS cleavage. The characteristics of the full-length antibody CIU profiles are consistent between canonical IgG1 structures thereby providing a benchmark for screening for antibody features, including domain-exchanged architectures, extended CDRs, and potentially the correct assembly of multi-specific antibodies. The applications for CIU in charac-terisation of unusual antibody architectures offers the poten-tial for this technique to become a high-throughput screening tool during the development of macromolecular drugs.

Appendix B: Glycan analysis of class II viral fusion proteins

B.1. Glycan variation of eastern equine encephalitis virus expressed in insect vs mammalian cell lines

Alphaviruses are enveloped pathogens that cause arthritis and encephalitis. In this project, the glycosylation of eastern equine encephalitis virus (EEEV), grown in both mammalian and insect cells, was investigated (*480*).

The N-linked glycans on the E1E2 had been purported as potential binding sites for cell surface lectins such as DC-SIGN and L-SIGN (*213*). Our collaborators wished to determine the glycan compositions on the E1E2 protein from EEEV. To evaluate the glycan structures present on the envelope protein a comparative hydrophilic interaction chromatography ultra-performance liquid chromatography (HILIC-UPLC) analysis was performed using virus cultivated in *Aedes albopictus* C6/36 or mammalian BHK-15 cells (**Figure B.1.1**)

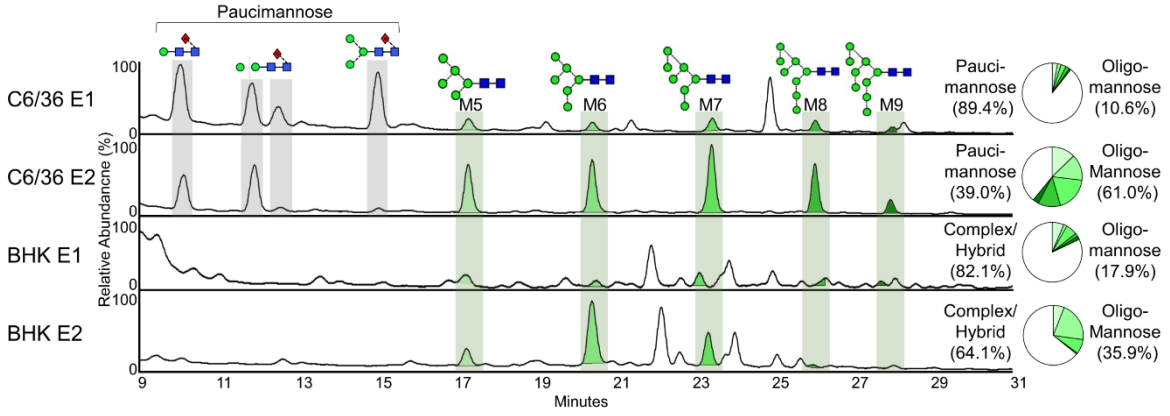


Figure B.1.1. Quantitative and compositional analysis of EEEV glycosylation. HILIC-UPLC profiles of fluorescently labelled N-linked glycans from EEEV- derived E1 and E2 glycoproteins from C6/36 and BHK-15 cells. Oligomannose-type glycans (M5-M9; $Man_5GlcNAc_2$-$Man_9GlcNAc_2$) (green) were identified by Endo H digestion with quantification of major glycan types summarised in the pie charts.

The E1 glycan, which is exposed and protrudes from the protein surface, consisted of predominantly pauci-mannose carbohydrates in the C6/36 cell-derived virus and complex-type glycans in the BHK-15 cell-derived virus, but not the oligomannose-type glycans which are required for efficient interactions with DC-SIGN and L-SIGN. Therefore, even though EEEV contains and exposed glycan on the E1 ectodomain, the glycan compositions of the invertebrate-derived glycan suggests that interactions with these lectins are unlikely. This was confirmed by a flow cytometric assay which showed insufficient binding of DC-SIGN and L-SIGN to EEEV for infection (*480*).

B.2. Mapping the site-specific glycosylation of recombinant Dengue and Zika antigens used in serological monitoring

Abstract

Dengue and Zika flaviviruses pose a major threat to global public health. The flavivirus genome encodes several glycoproteins including the envelope (E) glycoprotein that is solely responsible for viral membrane fusion and infection of host cells, and the enigmatic non-structural protein 1 (NS1). Dengue and Zika viruses can employ carbohydrate binding proteins of the host innate immune system, such as macrophage mannose receptor and DC-SIGN, facilitating infection. With the importance of glycosylation of any potential immunogen and its impact on serological studies, we sought to benchmark the glycan processing states of the two major antigenic proteins of flaviviruses, E and NS1. Here using both a global and site-specific N-linked glycosylation analysis approach, we investigate the structural glycan compositions across these flavivirus glycoproteins and reveal the conservation of distinct glycan-processing states on NS1 across the four dengue serotypes and Zika, but variations across the recombinant E proteins and VLPs. As glycans are known to be sensitive reporters of protein structure and configuration, detailed glycan and glycopeptide analysis provides a parameter for the comparison and interpretation of antigenicity and immunogenicity studies.

Introduction

The *Flavivirus* genus of positively-stranded RNA viruses include the important human pathogens Dengue virus (DENV) (serotypes 1-4) and Zika virus, which are primarily spread through mosquito vectors (*481*). The flavivirus genome encodes a single polyprotein that is cleaved by cellular and virally encoded proteases into the capsid, the prM and envelope (E)

glycoproteins, and seven non-structural (NS) proteins: NS1, NS2A, NS2B, NS3, NS4A, NS4B and NS5 (*482–484*).

As obligate parasites, flaviviruses exploit host-cell machinery including the glycan processing enzymes to modify their own proteins during replication. The N-linked glycosylation of flavivirus E protein has been demonstrated to be imperative for viral pathogenesis, not only in terms of correct glycoprotein expression that is essential for infection, but also in terms of facilitating receptor recognition (*14*, *15*). It has previously been shown, through mutagenesis studies where the N67 and N153 glycosylation site knockouts of DENV E proteins that both DENV E glycosylation sites are essential for efficient replication, secretion and infectivity (*14*). Furthermore, the use of glucosidase inhibitors has been shown to disrupt proper protein folding and trafficking resulting in decreased infectivity. This highlights not only the importance of glycosylation for viral pathogenesis but also therapeutic avenues targeting viral glycosylation (*90*, *92*).

The putative receptors for DENV, dendritic cell-specific ICAM-3-grabbing nonintegrin (DC-SIGN) (*209*, *228*, *229*) and macrophage mannose receptor (MMR) (*227*), which recognise under-processed oligomannose-type glycans presented on E protein, are thought to mediate virus attachment to target and infect immune cells. Many other viruses have been proposed to take advantage of the specificity of DC-SIGN to under-processed oligomannose-type glycans, which are seldom found on mature host glycoproteins (*67*, *68*). Some pathogens utilise DC-SIGN as either an obligate receptor, or to facilitate *trans*-infection of immune cells (*208*, *210–214*). In addition, C-type lectin usage by flaviviruses is not limited to infection of mammals; both West Nile virus (WNV) (*232*) and DENV (*233*) employ lectins in *Aedes aegypti* called mosquito galactose specific lectins (mosGCTL) as receptors to promote infection of invertebrate vectors. This broad employment of lectins

underscores the biological importance of the compositional state of glycosylation in flaviviral pathogenesis. Glycosylation is not only important in DENV pathology but also ZIKV. Recent research into the glycosylation of ZIKV E protein revealed that non-glycosylated viruses were attenuated and exhibited lower infectivity (*485*). It has been proposed that the single glycosylation site on ZIKV E facilitates attachment and infection of immune cells via DC-SIGN and DC-SIGNR akin to the mechanism of DENV infection(*15*, *486*). Historical strains of ZIKV do not possess glycans on E protein, thereby suggesting a mechanism for the increased virulence of recent ZIKV strains (*485*). These examples underscore the importance of glycosylation in efficient pathogenesis of these flaviviruses.

Flavivirus NS1 proteins, which exist in their active state as a noncovalently bound hexameric oligomer formed of three dimeric subunits (*16*, *487*, *488*), have been implicated in many viral functions including enhancing infection, RNA replication, particle assembly and immune evasion. DENV NS1 encodes two N-linked glycosylation sequons at N130 and N207 which play roles in protein stability and facilitate secretion, respectively (*489*). It has also been shown via mutagenesis studies that the N-linked glycans are essential for hexamer formation and modulating protein stability (*120*). NS1 is one of the major antigenic proteins of flaviviruses and antibodies against NS1 are routinely found in patient sera, indicating that it may contribute towards immune evasion by subverting the humoral immune system against this secreted protein, thereby acting as a decoy.

Broadly neutralising antibodies (bnAbs) with epitopes comprised of glycans have been characterised against Dengue virus E proteins (*305*). Specifically, these bnAbs are able to cross-neutralise all four DENV serotypes by binding to the conserved so-called E dimer epitope (EDE). DENV E proteins are presented on the mature virion surface as 90 repeating

dimers, each of which contains the EDE that bridges the two monomeric subunits with two conserved N-linked glycosylation sites (N67 and N153). These EDE antibodies are divided into two sub-classes called EDE1, which do not require the conserved glycan at N153 for binding, and EDE2 antibodies, which utilises the sugar at N153 for stronger binding as part of the neutralising epitope. Beyond the fact that these EDE antibodies possess broadly neutralising capabilities across multiple serotypes, these glycan-binding EDE2 antibodies are able to also bind partially immature viral particles as well as the fully mature virions. As such, the use of immunogens that elicit EDE antibodies has been proposed as an alternative route for vaccines due to their broadly neutralising nature. Due to the importance of glycosylation as part of the neutralising epitope, it is likely that glycan compositions of any next-generation subunit vaccine, attempting to elicit EDE antibodies, will have to be carefully considered, in order to accurately mimic the epitopes presented on virion particles. Furthermore, glycosylation compositions will likely differ depending on the organism in which the virus replicates. For example, virion particles derived from the insect vector will likely portray paucimannose-type glycosylation (*52*, *480*, *490*)

Here, we characterise the processing states of flavivirus E proteins from virus-like particles, and NS1 glycoproteins from the 4 DENV serotypes and Zika virus produced in HEK293 cells, the most common human cell line used for production of recombinant proteins. As glycans are known to be sensitive reporters of protein architecture and configuration, we sought to benchmark glycosylation on native-like flavivirus glycoproteins used for serological studies. We reveal variations in the glycan processing states of the E protein, but strict conservation of glycan compositions in NS1. These findings provide insights into the enzyme accessibility and activity that shapes glycosylation, which can have vast immunological consequences.

Materials and Methods

VLP and NS1 production

Recombinant DENV and ZIKV NS1 (NCBI accession numbers: DENV1: P17763.2, AA752-1127; DENV2: P29990.1, AA752-1127; DENV3: YP_001621843.1, AA750-1125; DENV4: P09866.2 ,AA751-1126; ZIKV NS1: A0A024B7W1.1, AA794-1148, an alternative signal sequence was used) proteins and VLPs were purchased from The Native Antigen Company (Kidlington, UK).

In short, NS1 proteins were C-terminally His-tagged and expressed in HEK293 cells by transient transfection. 3 days post transfection culture supernatant was cleared by centrifugation. Cleared supernatants were 0.2um filtered and concentrated using tangential flow filtration. NS1 proteins were purified by immobilised metal affinity chromatography followed by ion exchange chromatography and/or size exclusion chromatography (SEC). The multimerization state of NS1 proteins was then analysed using calibrated SEC.

Recombinant DENV and ZIKV VLPs (DENV1: AAQ19665.2, AA114-676; DENV2: AAP06252.1, AA114-676; DENV3: YP_001621843.1, AA114-675; DENV4: P09866.2, AA114-679; ZIKV: A0A024B7W1.1, AA123-819; for DEN and ZIKV VLPs alternative signal sequences were used; For all DENV VLPs the C-terminus of the Envelope proteins were replaced with their homologous Japanese encephalitis virus sequences) were expressed in HEK293 cells by transient transfection. 3 days post transfection culture supernatant was cleared by centrifugation, and cleared supernatants were 0.2um filtered. For DENV VLPs production supernatant was concentrated by tangential flow filtration, and VLPs were floated on a sucrose density gradient. Floated VLPs were then subjected to ion exchange chromatography followed by buffer exchange. To produce ZIKV VLPs cleared supernatants were precipitated using polyethylene glycol-6000 (PEG). The precipitates were

resuspended, and VLPs floated on a sucrose gradient. The floated VLPs were then concentrated by PEG precipitation and subjected to glycerol-tartrate ultracentrifugation followed by buffer exchange.

Ion-mobility mass spectrometry of released glycans

Excised flavivirus glycoprotein gel bands were washed alternately with acetonitrile and water before drying in a vacuum centrifuge. Bands were rehydrated with 100 µl of water and incubated with PNGase F at 37 ºC overnight. Ion mobility-electrospray ionisation (IM-ESI) mass spectrometry and tandem MS was performed on a Synapt G2Si instrument (Waters) as previously described. Glycans were purified on a Nafion® 118 membrane (Sigma-Aldrich) prior to injection. Data acquisition and processing were carried out using MassLynx v4.11 and Driftscope version 2.8 software (Waters)

Glycan Analysis by HILIC-UPLC

Released N-linked glycans were procainamide labelled using a 100 µl aliquot of labelling mixture comprised of 100 mg/ml procainamide, 60 mg/ml sodium cyanoborohydrate in 70% DMSO and 30% glacial acetic acid. The labelling mixture was added to dried N-linked glycans and incubated at 65 ºC for 4 hours. Labelled glycans were purified using Spe-ed Amide 2 columns (Applied Separations) as previously described (REF).Procainamide labelled glycans were analysed using a 2.1 mm x 10 mm Acquity BEH Glycan column (Waters) on a Waters Acquity H-Class UPLC instrument as performed previously (REF), with wavelength of λex = 310 nm and λem = 370 nm. Endo H digestions of labelled glycans were used to quantify the abundance of oligomannose-type glycans.

Glycopeptide liquid chromatography-mass spectrometry

Aliquots of 150ug to 200 ug of flaviviral proteins were denatured, reduced and alkylated by sequential 1 hour incubations using 50mM Tris/HCl, pH 8.0 buffer containing 6 M urea and 5 mM dithiothreitol (DTT), followed by the addition of 20 mM iodoacetamide (IAA) for a further 1 hour in the dark, and finally addition of 20 mM DTT. The alkylated proteins were buffer-exchanged into 50 mM Tris/HCl, pH 8.0 and subsequently digested using trypsin (Mass spectrometry grade, Promega) at a ratio of 1:30 (w/w). Reaction mixtures were dried and glycopeptides extracted using C18 zip-tip (Merck Milipore) following the manufacturer's protocol.

Eluted Glycopeptides were dried and resuspended in 0.1% formic acid prior to analysis on an Orbitrap Fusion Tribrid mass spectrometer (Thermo Fisher Scientific) coupled to an EASY-Spray nano-LC system (Thermo Fisher Scientific). MS data were acquired with XCalibur 4.0 (Thermo Fisher Scientific) as previously described (*152*). Glycopeptides were fragmented using higher-energy collisional dissociation. Data analysis and glycopeptide identification were performed using Byonic and Byologic software (Protein Metrics), with glycopeptide fragmentation data evaluated manually for each glycopeptide. Chromatographic areas for each assigned glycopeptide, with the same amino acid sequence, were compared to provide relative quantitation of specific glycoforms at each N-linked glycosylation site.

Results

Virus-like particles were purified, and their structural integrity was previously verified using electron microscopy to ensure proper particle formation, which revealed the efficient display of conformational and quaternary structure-dependent antibody epitopes (*491*). In order to study the glycome of flavivirus envelope glycoproteins, gel bands corresponding to the E and prM proteins from DENV 1-4 and ZIKV were treated with PNGase F to enzymatically release N-linked glycans. The released glycans were fluorescently labelled with procainamide and subjected to quantitative analysis by HILIC-UPLC (**Figure B.2.1**), Cleavage of the release glycan pools with endoglycosidase H revealed an abundance of complex-type N-linked glycans, with 80.6-89.0% of N-linked glycans being processed on the DENV serotypes and 92.1% complex-type glycans on ZIKV. Oligomannose-type glycans were also detected although in significantly smaller quantities (9.8-19.4%). The most prevalent oligomannose-type across the four DENV serotypes is the $Man_6GlcNAc_2$ glycoform; we speculate that this results from a block in the enzymatic processing by Golgi mannosidases at one more of the glycosylation sites of E. However the overall paucity of oligomannose-type glycans was surprising due to the well-characterised usage of these glycoforms to act as ligands to putative DENV receptors, namely DC-SIGN and MMR (*227*, *228*). Nevertheless, we highlight the divergence of glycosylation between the DENV serotypes and ZIKV VLPs.

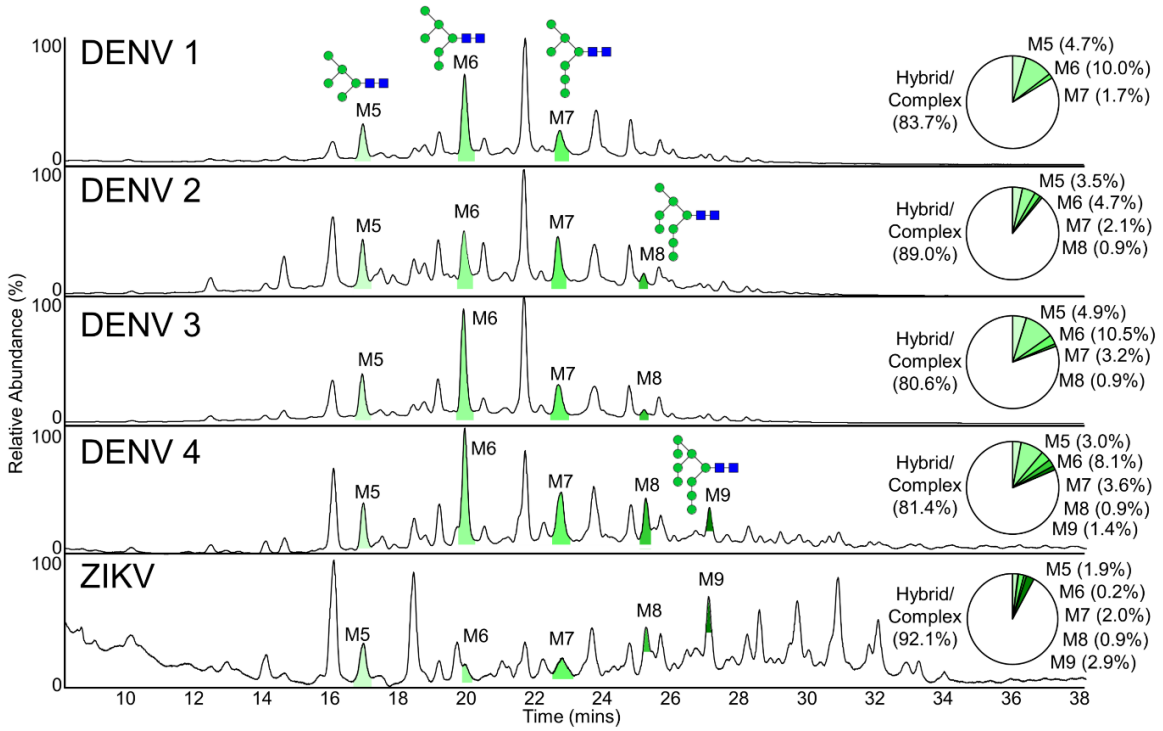


Figure B.2.1: Compositional analysis of flavivirus VLP glycome. HILIC-UPLC profiles of fluorescently labelled N-linked glycans from DENV serotypes 1-4 and ZIKV VLPs consisting of E, prM and M protein produced in HEK293 cells. Peaks corresponding to oligomannose-type glycans (green) were identified by Endo H digestion, with quantification of major glycan types summarized as a pie chart.

Variation of Glycan Processing States across Flavivirus E proteins

We subsequently sought to investigate the site-specific glycosylation on these antigenically relevant flaviviruses proteins LC-MS analysis was performed on enzymatically cleaved glycopeptides (**Figure B.2.2**). The four Dengue serotypes encode two conserved N-linked glycan sites on the mature E protein at N67 and N153. It also encodes a glycosylation site on the prM subunit, at N69 on the pr peptide which is cleaved from prM upon maturation of VLPs. Perhaps surprisingly glycopeptides corresponding to prM were identified, however with approximately 30% of virion particles containing immaturely processed prM proteins, due to inefficient cleavage by furin (*492*, *493*), this is somewhat expected. No major differences in glycan compositions on the N67 glycan site of E can be observed, with all four DENV serotypes exhibiting oligomannose-type glycans at this site. These glycans on the N67 site are proposed to be responsible for DC-SIGN and MMR receptor binding, therefore the presence of oligomannose-type glycans are expected. The glycosylated E proteins were fitted into the cryo-EM maps of immature and mature viruses (**Figure B.2.3**)

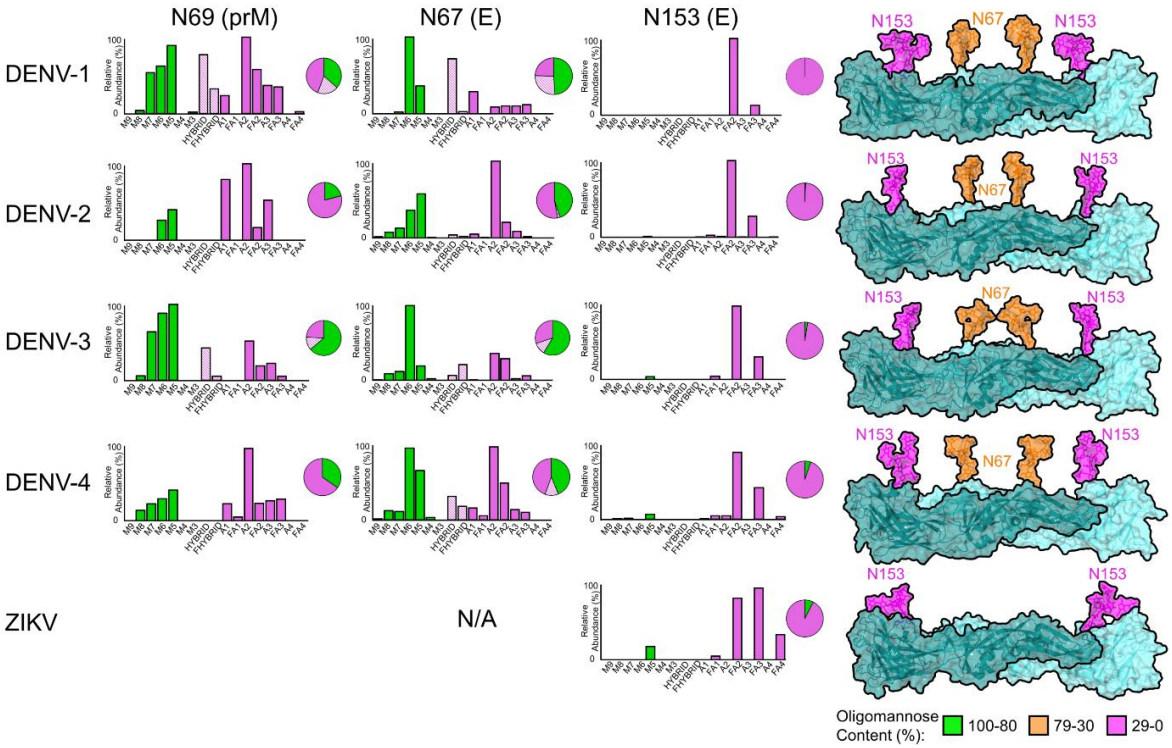


Figure B.2.2: Quantitative site-specific glycosylation analysis and structure-based mapping of flavivirus E protein N-linked glycans. The bar graphs represent the relative quantities of each glycan group with oligomannose-type glycan series (M9 to M3; Man9GlcNAc2 to Man3GlcNAc2) (green), afucosylated and fucosylated hybrid glycans (Hybrid & F Hybrid) (dashed pink), and complex glycans grouped according to fucosylation and number of antennae (A1 to FA4) (pink). Modelling of experimentally observed glycans onto crystal structures of DENV-1 and ZIKV E glycoproteins (PDB ID: 4UT6(*304*), 3J2P(*494*), 5LBV(*495*)) with glycans coloured according to oligomannose content.

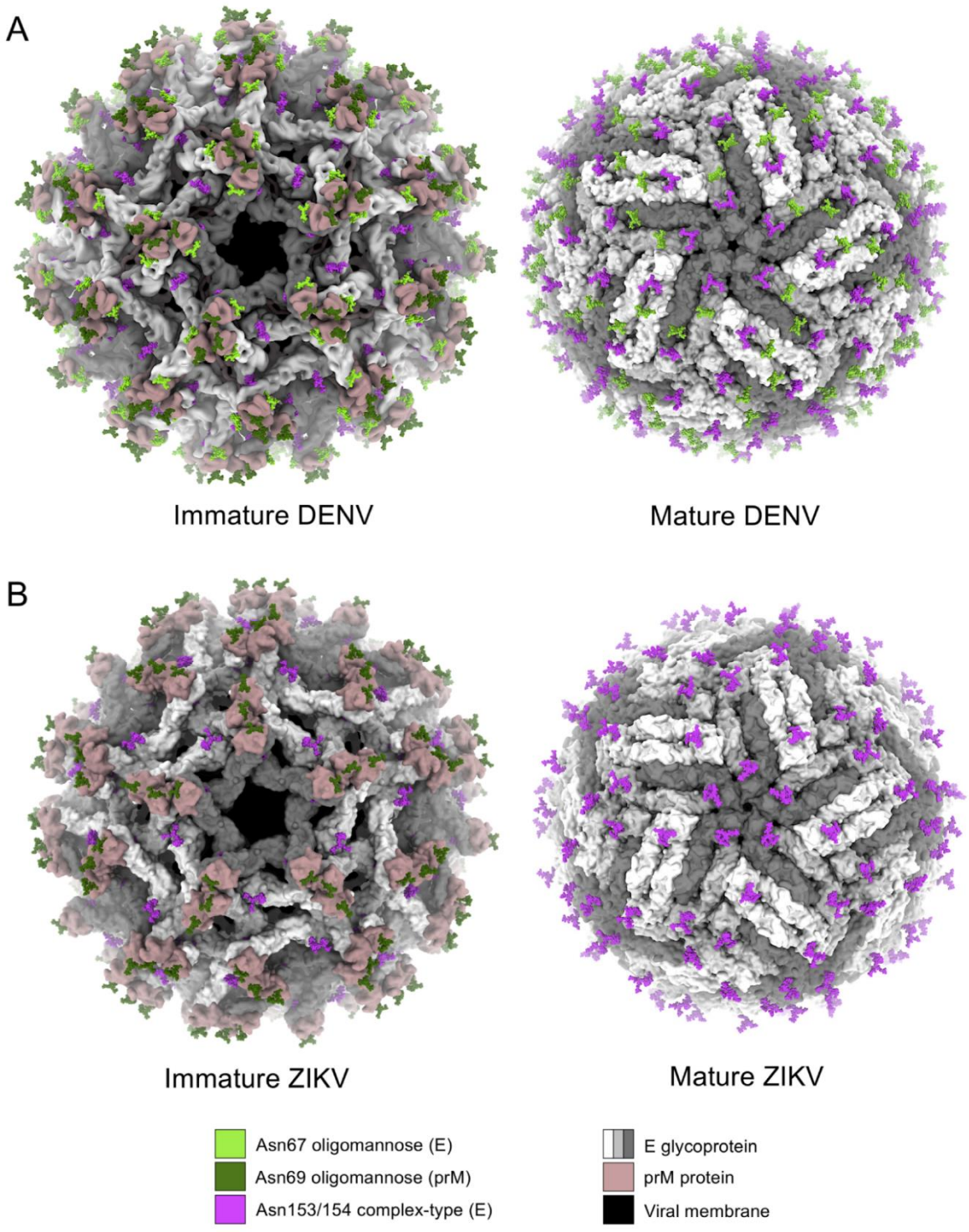


Figure B.2.3: Whole virion models of glycosylated DENV and ZIKV in its immature and mature states. The crystal structures of DENV/ZIKV E and prM proteins (PDB ID 3C6E, 4UT6, 5LBV, 5U4W) were fitted into the corresponding cryo-EM maps. E proteins are shown in grey. Oligomannose-type glycans on E or prM are coloured in green as per the key, with complex-type glycans at N153/154 coloured in pink. This figure was made by Weng Ng, Division of Structural Biology, University of Oxford.

Conservation of glycan-processing across flavivirus non-structural protein 1 (NS1).

We also sought to characterise glycosylation states of the other major antigenic protein of flaviviruses, NS1. Previous N-linked glycosylation analysis using enzymatic digests coupled with electrophoretic analysis have been performed on DENV NS1 proteins showing that N130 is complex and N207 is oligomannose-type (*120*). Here, we quantitatively ascertained the precise N-linked glycan compositions at each N-linked glycosylation site and reveal that across the DENV serotypes and ZIKV NS1 glycoproteins. The processing states of the glycans are conserved, with N130 and N207 exhibiting predominantly complex-type fucosylated tetra-antennary glycans and oligomannose-type sugars respectively (**Figure B.2.4**). We hypothesise that these conserved states arise from the inaccessibility of N207 to glycan processing enzymes such as ER alpha mannosidase and other Golgi mannosidases, due to its location in a nook of the protein dimer leading to steric protein-protein clashes between NS1 and glycan processing enzymes. Whereas N130 is located at an accessible site that allows docking of the enzyme onto the substrate glycan.

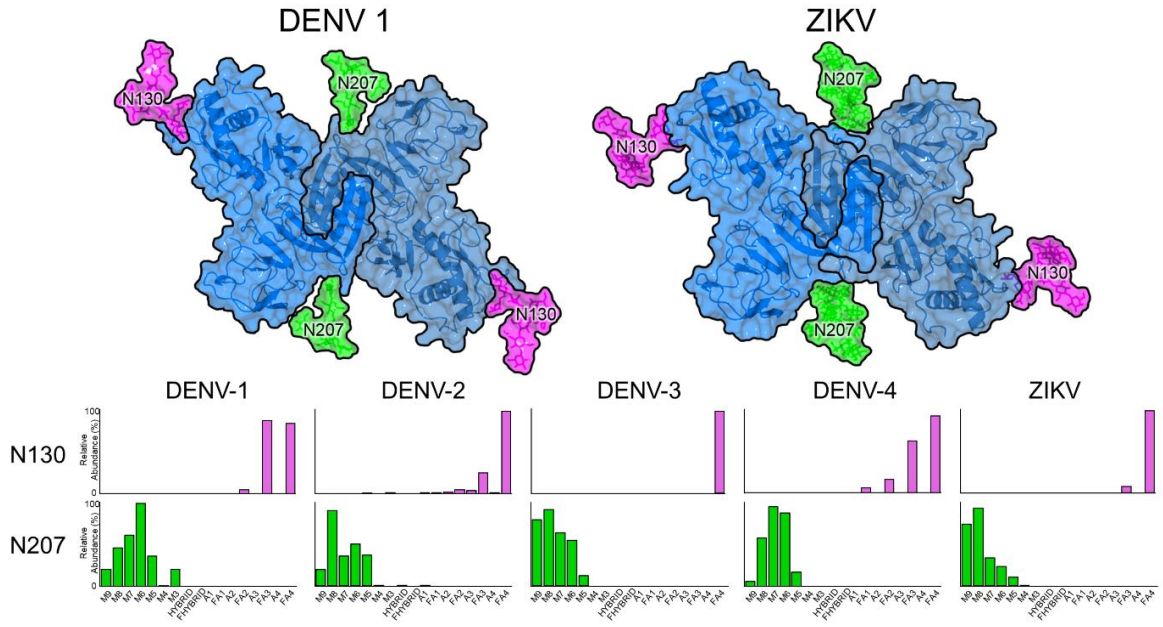


Figure B.2.4: Quantitative site-specific glycosylation analysis and structure-based mapping of flavivirus NS1 N-linked glycans. The bar graphs represent the relative quantities of each glycan group with oligomannose-type glycan series (M9 to M3; $Man_9GlcNAc_2$ to $Man_3GlcNAc_2$) (green), afucosylated and fucosylated hybrid glycans (Hybrid & F Hybrid) (dashed pink), and complex glycans grouped according to fucosylation and number of antennae (A1 to FA4) (pink). Modelling of experimentally observed glycans onto crystal structures of DENV-1 and ZIKV NS1 glycoproteins (PDB ID: 4O6B and 5K6K)(*487*, *496*) with glycans coloured according to oligomannose content.

Here, we characterize glycosylation of antigenic proteins from dengue and Zika flavivirus used in serological studies at a global and site-specific level to benchmark flaviviral glycosylation recombinant glycoproteins. On one hand, we show that the E proteins found on the surface of viruses are more prone to differences in glycan processing whereas glycan compositions of NS1 proteins are more conserved.

Due to the importance of protein folding for viral protein function, certain sugar mimetics, namely iminosugars, have been investigated for their antiviral activity. Iminosugars inhibit ER alpha-glucosidase activity, resulting in the generation of unfolded, non-functional viral glycoproteins. The antiviral activity of iminosugars has been tested on a diverse spectrum of viruses including HIV, influenza viruses, EBOV, arenaviruses, and flaviviruses. A variety of iminosugar compounds have been shown to potently inhibit the release of infectious virion particles and the number of infected cells. The inhibition of DENV pathogeny by these compounds demonstrates the importance of glycosylation in DENV glycoprotein folding and virulence.

DENV non-structural protein-1 (NS1) is an intriguing glycoprotein that is secreted from infected cells. NS1 binds to heparin sulphate and chondroitin sulphate glycosaminoglycans on the surface of various cells. NS1 has been shown to play a role in both viral replication and immune evasion, and it has been hypothesised that immune recognition of NS1 on endothelial cell surfaces may facilitate vascular leakage during severe DENV infection. The use of secreted/shed GPs in order to subvert the immune system and/or enhance infectivity appears to be a common phenomenon utilised by viruses.

The presence of oligomannose-type glycans on NS1 may be linked to its potential role in acting as a decoy to subvert the immune response. For example, secreted NS1 has been demonstrated to protect DENV from mannose binding-lectin mediated neutralisation (*124*).

Overall the data presented here will aid in the understanding of serological test results for which these viral proteins are used.

Appendix C: List of publications

n=15, Citations=321, h-index=10 (as of August 18th, 2020)

Blundell PA, Le NPL, Allen J, **Watanabe Y**, Pleass RJ. J Biol Chem. 2017. Engineering the fragment crystallizable (Fc) region of human IgG1 multimers and monomers to fine-tune interactions with sialic acid-dependent receptors.

Watanabe Y, Vasiljevic S, Allen JD, Seabright GE, Duyvesteyn HME, Doores KJ, Crispin M, Struwe WB. Anal Chem. 2018. Signature of antibody domain exchange by native mass spectrometry and collision-induced unfolding.

Harvey DJ, **Watanabe Y**, Allen JD, Rudd P, Pagel K, Crispin M, Struwe WB. J Am Soc Mass Spectrom. 2018. Collision cross sections and ion mobility separation of fragment ions from complex N-glycans.

Watanabe Y, Raghwani J, Allen JD, Seabright GE, Li S, Moser F, Huiskonen JT, Strecker T, Bowden TA, Crispin M. Proc Natl Acad Sci U S A. 2018. Structure of the Lassa virus glycan shield provides a model for immunological resistance.

Struwe WB, Chertova E, Allen JD, Seabright GE, **Watanabe Y**, Harvey DJ, Medina-Ramirez M, Roser JD, Smith R, Westcott D, Keele BF, Bess JW Jr, Sanders RW, Lifson JD, Moore JP, Crispin M. Cell Rep. 2018. Site-specific glycosylation of virion-derived HIV-1 Env is mimicked by a soluble trimeric immunogen.

Iliopoulou M, Nolan R, Alvarez L, **Watanabe Y**, Coomer CA, Jakobsdottir GM, Bowden TA, Padilla-Parra S. Nat Struct Mol Biol. 2018. A dynamic three-step mechanism drives the HIV-1 pre-fusion reaction.

Hasan SS, Sun C, Kim AS, **Watanabe Y**, Chen CL, Klose T, Buda G, Crispin M, Diamond MS, Klimstra WB, Rossmann MG. Cell Rep. 2018. Cryo-EM structures of Eastern equine encephalitis virus reveal mechanisms of virus disassembly and antibody neutralisation.

Pryce R, Ng WM, Zeltina A, **Watanabe Y**, El Omari K, Wagner A, Bowden TA. J Virol. 2018. Structure-based classification defines the discrete conformational classes adopted by the arenaviral GP1.

Watanabe Y, Bowden TA, Wilson IA, Crispin M. Biochim Biophys Acta 2019. Exploitation of glycosylation in enveloped virus pathobiology.

Seabright GE, Cottrell CA, D'Addabbo A, van Gils MJ, **Watanabe Y**, Behrens AJ, Allen JD, Vasiljevic S, Sanders R, Ward A, Crispin M. Structure. 2020. Networks of HIV-1 envelope glycans maintain antibody epitopes in the face of glycan additions and deletions.

Watanabe Y, Berndsen ZT, Raghwani J, Seabright GE, Allen JD, McLellan JS, Wilson IA, Bowden TA, Ward AB, Crispin M. Nat. Commun. 2020. Vulnerabilities in coronavirus glycan shields despite extensive glycosylation.

Watanabe Y, Allen JD, Wrapp D, McLellan JS, Crispin M. Science. 2020. Site-specific glycan analysis of the SARS-CoV-2 spike.

Shields AM, Faustini SE, Perez-Toledo M, Jossi S, Aldera EL, Allen JD, Al-Taei S, Backhouse C, Bosworth A, Dunbar L, Ebanks D, Emmanuel B, Grey J, Kidd IM, McGinnel G, McLoughlin D, Morley G, O'Neill J, Papakonstantinou D, Pickles O, Poxon C, Richter M, Walker E, Wanigasooriya K, **Watanabe Y**, Whalley C, Zielinska AE, Crispin M, Wraith DC, Beggs AD, Cunningham AF, Drayson MT, Richter AG. Thorax. 2020. SARS-CoV-2 seroconversion in health care workers.

Perez-Toledo M, Faustini SE, Jossi SE, Shields A, Kanthimathinathan HK, Allen JD, **Watanabe Y**, Goodall M, Wraith DC, Veenith TV, Drayson MT, Jyothish D, Al-Abadi E, Chikermane A, Welch S, Masilamani K, Hackett S, Crispin M, Scholefield B, Cunningham AF, Richter AG. MedRxiv. 2020. Serology confirms SARS-CoV-2 infection in PCR-negative children presenting with Paediatric Inflammatory Multi-System Syndrome.

Perez-Toledo M, Faustini SE, Jossi SE, Shields A, Kanthimathinathan HK, Allen JD, **Watanabe Y**, Goodall M, Wraith DC, Veenith TV, Drayson MT, Jyothish D, Al-Abadi E, Chikermane A, Welch S, Masilamani K, Hackett S, Crispin M, Scholefield B, Cunningham AF, Richter AG. MedRxiv. 2020. Serology confirms SARS-CoV-2 infection in PCR-negative children presenting with Paediatric Inflammatory Multi-System Syndrome.

References

1. K. E. Jones, N. G. Patel, M. A. Levy, A. Storeygard, D. Balk, J. L. Gittleman, P. Daszak, Global trends in emerging infectious diseases. *Nature*. **451**, 990–993 (2008).

2. L. Cao, M. Pauthner, R. Andrabi, K. Rantalainen, Z. Berndsen, J. K. Diedrich, S. Menis, D. Sok, R. Bastidas, S.-K. R. Park, C. M. Delahunty, L. He, J. Guenaga, R. T. Wyatt, W. R. Schief, A. B. Ward, J. R. Yates, D. R. Burton, J. C. Paulson, Differential processing of HIV envelope glycans on the virus and soluble recombinant trimer. *Nat. Commun.* **9**, 3693 (2018).

3. W. B. Struwe, E. Chertova, J. D. Allen, G. E. Seabright, Y. Watanabe, D. J. Harvey, M. Medina-Ramirez, J. D. Roser, R. Smith, D. Westcott, B. F. Keele, J. W. Bess, R. W. Sanders, J. D. Lifson, J. P. Moore, M. Crispin, Site-specific glycosylation of virion-derived HIV-1 Env Is mimicked by a soluble trimeric immunogen. *Cell Rep.* **24**, 1958-1966.e5 (2018).

4. M. Panico, L. Bouché, D. Binet, M.-J. O'Connor, D. Rahman, P.-C. Pang, K. Canis, S. J. North, R. C. Desrosiers, E. Chertova, B. F. Keele, J. W. Bess, J. D. Lifson, S. M. Haslam, A. Dell, H. R. Morris, Mapping the complete glycoproteome of virion-derived HIV-1 gp120 provides insights into broadly neutralizing antibody binding. *Sci. Rep.* **6**, 32956 (2016).

5. Y. Kobayashi, Y. Suzuki, Evidence for N-glycan shielding of antigenic sites during evolution of human influenza A virus hemagglutinin. *J. Virol.* **86**, 3446–51 (2012).

6. K. Wanzeck, K. L. Boyd, J. A. McCullers, Glycan shielding of the Influenza virus hemagglutinin contributes to immunopathology in mice. *Am. J. Respir. Crit. Care Med.* **183**, 767–773 (2011).

7. P. S. Lee, N. Ohshima, R. L. Stanfield, W. Yu, Y. Iba, Y. Okuno, Y. Kurosawa, I. A. Wilson, Receptor mimicry by antibody F045-092 facilitates universal binding to the H3 subtype of influenza virus. *Nat. Commun.* **5**, 3614 (2014).

8. A. C. Walls, M. A. Tortorici, B. Frenz, J. Snijder, W. Li, F. A. Rey, F. DiMaio, B.-J. Bosch, D. Veesler, Glycan shield and epitope masking of a coronavirus spike protein observed by cryo-electron microscopy. *Nat. Struct. Mol. Biol.* **23**, 899–905 (2016).

9. X. Xiong, M. A. Tortorici, J. Snijder, C. Yoshioka, A. C. Walls, W. Li, A. T. McGuire, F. A. Rey, B.-J. Bosch, D. Veesler, Glycan shield and fusion activation of a deltacoronavirus spike glycoprotein fine-tuned for enteric infections. *J. Virol.* **92** (2018), doi:10.1128/JVI.01628-17.

10. G. Ritchie, D. J. Harvey, F. Feldmann, U. Stroeher, H. Feldmann, L. Royle, R. A. Dwek, P. M. Rudd, Identification of N-linked carbohydrates from severe acute respiratory syndrome (SARS) spike glycoprotein. *Virology*. **399**, 257–69 (2010).

11. G. Ritchie, D. J. Harvey, U. Stroeher, F. Feldmann, H. Feldmann, V. Wahl-Jensen, L. Royle, R. A. Dwek, P. M. Rudd, Identification of N-glycans from Ebola virus glycoproteins by matrix-assisted laser desorption/ionisation time-of-flight and negative ion electrospray tandem mass spectrometry. *Rapid Commun. Mass Spectrom.* **24**, 571–85 (2010).

12. J. E. Lee, M. L. Fusco, A. J. Hessell, W. B. Oswald, D. R. Burton, E. O. Saphire, Structure of the Ebola virus glycoprotein bound to an antibody from a human

survivor. *Nature*. **454**, 177–182 (2008).

13. R. Sommerstein, L. Flatz, M. M. Remy, P. Malinge, G. Magistrelli, N. Fischer, M. Sahin, A. Bergthaler, S. Igonet, J. ter Meulen, D. Rigo, P. Meda, N. Rabah, B. Coutard, T. A. Bowden, P.-H. Lambert, C.-A. Siegrist, D. D. Pinschewer, Arenavirus glycan shield promotes neutralizing antibody evasion and protracted infection. *PLoS Pathog.* **11**, e1005276 (2015).

14. J. A. Mondotte, P.-Y. Lozach, A. Amara, A. V Gamarnik, Essential role of dengue virus envelope protein N glycosylation at asparagine-67 during viral propagation. *J. Virol.* **81**, 7136–48 (2007).

15. C. R. Fontes-Garfias, C. Shan, H. Luo, A. E. Muruato, D. B. A. Medeiros, E. Mays, X. Xie, J. Zou, C. M. Roundy, M. Wakamiya, S. L. Rossi, T. Wang, S. C. Weaver, P.-Y. Shi, Functional analysis of glycosylation of Zika virus envelope protein. *Cell Rep.* **21**, 1180–1190 (2017).

16. M. Flamand, F. Megret, M. Mathieu, J. Lepault, F. A. Rey, V. Deubel, Dengue virus type 1 nonstructural glycoprotein NS1 is secreted from mammalian cells as a soluble hexamer in a glycosylation-dependent fashion. *J. Virol.* **73**, 6104–10 (1999).

17. G. S. Mohan, W. Li, L. Ye, R. W. Compans, C. Yang, Antigenic subversion: a novel mechanism of host immune evasion by Ebola virus. *PLoS Pathog.* **8**, e1003065 (2012).

18. S. Gorander, J. Mbwana, E. Lyamuya, T. Lagergard, J.-A. Liljeqvist, Mature glycoprotein G Presents high performance in diagnosing Herpes Simplex Virus type 2 infection in sera of different Tanzanian cohorts. *Clin. Vaccine Immunol.* **13**, 633–639 (2006).

19. M. E. Taylor, K. Drickamer, *Introduction to glycobiology* (Oxford University Press, 2011).

20. A. Varki, P. Gagneux, *Biological functions of glycans* (Cold Spring Harbor Laboratory Press, 2015).

21. R. G. Spiro, Protein glycosylation: nature, distribution, enzymatic formation, and disease implications of glycopeptide bonds. *Glycobiology*. **12**, 43R-56R (2002).

22. A. Varki, *Essentials of glycobiology* (Cold Spring Harbor Laboratory Press, 2009).

23. B. Korber, B. Gaschen, K. Yusim, R. Thakallapally, C. Kesmir, V. Detours, Evolutionary and immunological implications of contemporary HIV-1 variation. *Br. Med. Bull.* **58**, 19–42 (2001).

24. J. Jäntti, P. Hildén, H. Rönkä, V. Mäkiranta, S. Keränen, E. Kuismanen, Immunocytochemical analysis of Uukuniemi virus budding compartments: role of the intermediate compartment and the Golgi stack in virus maturation. *J. Virol.* **71**, 1162–72 (1997).

25. S. Stertz, M. Reichelt, M. Spiegel, T. Kuri, L. Martínez-Sobrido, A. García-Sastre, F. Weber, G. Kochs, The intracellular sites of early replication and budding of SARS-coronavirus. *Virology*. **361**, 304–315 (2007).

26. K. Bayer, C. Banning, V. Bruss, L. Wiltzer-Bach, M. Schindler, Hepatitis C Virus is released via a noncanonical secretory route. *J. Virol.* **90**, 10558–10573 (2016).

27. K. J. Doores, C. Bonomelli, D. J. Harvey, S. Vasiljevic, R. A. Dwek, D. R. Burton, M. Crispin, C. N. Scanlan, Envelope glycans of immunodeficiency virions are almost entirely oligomannose antigens. *Proc. Natl. Acad. Sci. U. S. A.* **107**, 13800–5 (2010).

28. C. Bonomelli, K. J. Doores, D. C. Dunlop, V. Thaney, R. A. Dwek, D. R. Burton, M. Crispin, C. N. Scanlan, The glycan shield of HIV is predominantly oligomannose independently of production system or viral clade. *PLoS One*. **6**, e23521 (2011).

29. L. K. Pritchard, D. J. Harvey, C. Bonomelli, M. Crispin, K. J. Doores, Cell- and protein-directed glycosylation of native cleaved HIV-1 envelope. *J. Virol.* **89**, 8932–44 (2015).

30. P. Gluschankof, I. Mondor, H. R. Gelderblom, Q. J. Sattentau, Cell membrane vesicles are a major contaminant of gradient-enriched human immunodeficiency virus type-1 preparations. *Virology*. **230**, 125–133 (1997).

31. D. J. Harvey, A. H. Merry, L. Royle, M. P. Campbell, R. A. Dwek, P. M. Rudd, Proposal for a standard system for drawing structural diagrams of N- and O-linked carbohydrates and related compounds. *Proteomics*. **9**, 3796–3801 (2009).

32. A. Halim, G. Brinkmalm, U. Rüetschi, A. Westman-Brinkmalm, E. Portelius, H. Zetterberg, K. Blennow, G. Larson, J. Nilsson, Site-specific characterization of threonine, serine, and tyrosine glycosylations of amyloid precursor protein/amyloid beta-peptides in human cerebrospinal fluid. *Proc. Natl. Acad. Sci. U. S. A.* **108**, 11848–53 (2011).

33. C. Steentoft, S. Y. Vakhrushev, H. J. Joshi, Y. Kong, M. B. Vester-Christensen, K. T.-B. G. Schjoldager, K. Lavrsen, S. Dabelsteen, N. B. Pedersen, L. Marcos-Silva, R. Gupta, E. Paul Bennett, U. Mandel, S. Brunak, H. H. Wandall, S. B. Levery, H. Clausen, Precision mapping of the human O-GalNAc glycoproteome through SimpleCell technology. *EMBO J.* **32**, 1478–1488 (2013).

34. I. Nishikawa, Y. Nakajima, M. Ito, S. Fukuchi, K. Homma, K. Nishikawa, Computational prediction of O-linked glycosylation sites that preferentially map on intrinsically disordered regions of extracellular proteins. *Int. J. Mol. Sci.* **11**, 4991–5008 (2010).

35. I. Bagdonaite, R. Nordén, H. J. Joshi, S. Dabelsteen, K. Nyström, S. Y. Vakhrushev, S. Olofsson, H. H. Wandall, A strategy for O-glycoproteomics of enveloped viruses—the O-glycoproteome of Herpes Simplex virus type 1. *PLoS Pathog.* **11**, e1004784 (2015).

36. I. Bagdonaite, R. Nordén, H. J. Joshi, S. L. King, S. Y. Vakhrushev, S. Olofsson, H. H. Wandall, Global mapping of O-glycosylation of Varicella Zoster virus, human Cytomegalovirus, and Epstein-Barr virus. *J. Biol. Chem.* **291**, 12014–28 (2016).

37. M. B. Iversen, L. S. Reinert, M. K. Thomsen, I. Bagdonaite, R. Nandakumar, N. Cheshenko, T. Prabakaran, S. Y. Vakhrushev, M. Krzyzowska, S. K. Kratholm, F. Ruiz-Perez, S. V Petersen, S. Goriely, B. M. Bibby, K. Eriksson, J. Ruland, A. R. Thomsen, B. C. Herold, H. H. Wandall, S. Frische, C. K. Holm, S. R. Paludan, An innate antiviral pathway acting before interferons at epithelial surfaces. *Nat. Immunol.* **17**, 150–158 (2016).

38. O. Martinez, L. Tantral, N. Mulherkar, K. Chandran, C. F. Basler, Impact of Ebola mucin-like domain on antiglycoprotein antibody responses induced by Ebola virus-

like particles. *J. Infect. Dis.* **204 Suppl**, S825-32 (2011).

39. R. Nordén, A. Halim, K. Nyström, E. P. Bennett, U. Mandel, S. Olofsson, J. Nilsson, G. Larson, O-Linked glycosylation of the mucin domain of the Herpes Simplex virus type 1-specific glycoprotein gC-1 is temporally regulated in a seed-and-spread manner. *J. Biol. Chem.* **290**, 5078–5091 (2015).

40. J. S. McLellan, W. C. Ray, M. E. Peeples, Structure and function of respiratory syncytial virus surface glycoproteins. *Curr. Top. Microbiol. Immunol.* **372**, 83–104 (2013).

41. K. B. Luther, A. J. Hülsmeier, B. Schegg, S. A. Deuber, D. Raoult, T. Hennet, Mimivirus collagen is modified by bifunctional lysyl hydroxylase and glycosyltransferase enzyme. *J. Biol. Chem.* **286**, 43701–9 (2011).

42. Y. Xiang, U. Baxa, Y. Zhang, A. C. Steven, G. L. Lewis, J. L. Van Etten, M. G. Rossmann, Crystal structure of a virus-encoded putative glycosyltransferase. *J. Virol.* **84**, 12265–73 (2010).

43. N. Markine-Goriaynoff, L. Gillet, J. L. Van Etten, H. Korres, N. Verma, A. Vanderplasschen, Glycosyltransferases encoded by viruses. *J. Gen. Virol.* **85**, 2741–2754 (2004).

44. F. Piacente, C. De Castro, S. Jeudy, M. Gaglianone, M. E. Laugieri, A. Notaro, A. Salis, G. Damonte, C. Abergel, M. G. Tonetti, The rare sugar N-acetylated viosamine is a major component of Mimivirus fibers. *J. Biol. Chem.* **292**, 7385–7394 (2017).

45. R. O'Flaherty, I. Trbojević-Akmačić, G. Greville, P. M. Rudd, G. Lauc, The sweet spot for biologics: recent advances in characterization of biotherapeutic glycoproteins. *Expert Rev. Proteomics*. **15**, 13–29 (2018).

46. M. Thaysen-Andersen, N. H. Packer, Advances in LC–MS/MS-based glycoproteomics: Getting closer to system-wide site-specific mapping of the N- and O-glycoproteome. *Biochim. Biophys. Acta - Proteins Proteomics*. **1844**, 1437–1452 (2014).

47. H. Xiao, F. Sun, S. Suttapitugsakul, R. Wu, Global and site-specific analysis of protein glycosylation in complex biological systems with mass spectrometry. *Mass Spectrom. Rev.* (2019), doi:10.1002/mas.21586.

48. D. F. Smith, X. Song, R. D. Cummings, Use of glycan microarrays to explore specificity of glycan-binding proteins. *Methods Enzymol.* **480**, 417–444 (2010).

49. C. D. Rillahan, J. C. Paulson, Glycan microarrays for decoding the glycome. *Annu. Rev. Biochem.* **80**, 797–823 (2011).

50. M. Zhang, B. Gaschen, W. Blay, B. Foley, N. Haigwood, C. Kuiken, B. Korber, Tracking global patterns of N-linked glycosylation site variation in highly variable viral glycoproteins: HIV, SIV, and HCV envelopes and influenza hemagglutinin. *Glycobiology*. **14**, 1229–1246 (2004).

51. K. Wagh, E. F. Kreider, Y. Li, H. J. Barbian, G. H. Learn, E. Giorgi, P. T. Hraber, T. G. Decker, A. G. Smith, M. V. Gondim, L. Gillis, J. Wandzilak, G.-Y. Chuang, R. Rawi, F. Cai, P. Pellegrino, I. Williams, J. Overbaugh, F. Gao, P. D. Kwong, B. F. Haynes, G. M. Shaw, P. Borrow, M. S. Seaman, B. H. Hahn, B. Korber, Completeness of HIV-1 envelope glycan shield at transmission determines

neutralization breadth. *Cell Rep.* **25**, 893-908.e7 (2018).

52. M. Crispin, D. J. Harvey, D. Bitto, C. Bonomelli, M. Edgeworth, J. H. Scrivens, J. T. Huiskonen, T. A. Bowden, Structural plasticity of the Semliki Forest Virus glycome upon interspecies transmission. *J. Proteome Res.* **13**, 1702–1712 (2014).

53. H. Shelton, G. Ayora-Talavera, J. Ren, S. Loureiro, R. J. Pickles, W. S. Barclay, I. M. Jones, Receptor binding profiles of avian influenza virus hemagglutinin subtypes on human cells as a predictor of pandemic potential. *J. Virol.* **85**, 1875–80 (2011).

54. R. Kornfeld, S. Kornfeld, Assembly of asparagine-linked oligosaccharides. *Annu. Rev. Biochem.* **54**, 631–664 (1985).

55. N. Y. Kim, W.-W. Jung, Y.-K. Oh, T. Chun, H.-Y. Park, H.-T. Lee, I.-K. Han, J. M. Yang, Y. B. Kim, Natural protection from zoonosis by alpha-gal epitopes on virus particles in xenotransmission. *Xenotransplantation*. **14**, 104–111 (2007).

56. A. Antonopoulos, S. J. North, S. M. Haslam, A. Dell, Glycosylation of mouse and human immune cells: insights emerging from N-glycomics analyses. *Biochem. Soc. Trans.* **39**, 1334–1340 (2011).

57. U. Galili, Natural anti-carbohydrate antibodies contributing to evolutionary survival of primates in viral epidemics? *Glycobiology*. **26**, 1140–1150 (2016).

58. I. Brockhausen, Pathways of O-glycan biosynthesis in cancer cells. *Biochim. Biophys. Acta*. **1473**, 67–95 (1999).

59. S. J. D. Neil, A. McKnight, K. Gustafsson, R. A. Weiss, HIV-1 incorporates ABO histo-blood group antigens that sensitize virions to complement-mediated inactivation. *Blood*. **105**, 4693–4699 (2005).

60. L. Cooling, Blood groups in infection and host susceptibility. *Clin. Microbiol. Rev.* **28**, 801–70 (2015).

61. R. M. Seymour, M. J. Allan, A. Pomiankowski, K. Gustafsson, Evolution of the human ABO polymorphism by two complementary selective pressures. *Proceedings. Biol. Sci.* **271**, 1065–72 (2004).

62. M. Matrosovich, A. Tuzikov, N. Bovin, A. Gambaryan, A. Klimov, M. R. Castrucci, I. Donatelli, Y. Kawaoka, Early alterations of the receptor-binding properties of H1, H2, and H3 avian influenza virus hemagglutinins after their introduction into mammals. *J. Virol.* **74**, 8502–12 (2000).

63. K. Shinya, M. Ebina, S. Yamada, M. Ono, N. Kasai, Y. Kawaoka, Influenza virus receptors in the human airway. *Nature*. **440**, 435–436 (2006).

64. J. M. Nicholls, A. J. Bourne, H. Chen, Y. Guan, J. S. M. Peiris, Sialic acid receptor detection in the human respiratory tract: evidence for widespread distribution of potential binding sites for human and avian influenza viruses. *Respir. Res.* **8**, 73 (2007).

65. U. Kumlin, S. Olofsson, K. Dimock, N. Arnberg, Sialic acid tissue distribution and influenza virus tropism. *Influenza Other Respi. Viruses*. **2**, 147–54 (2008).

66. X. Shi, D. L. Jarvis, Protein N-glycosylation in the baculovirus-insect cell system. *Curr. Drug Targets*. **8**, 1116–25 (2007).

67. M. D. Crispin, G. E. Ritchie, A. J. Critchley, B. Paul Morgan, I. A. Wilson, R. A.

Dwek, R. B. Sim, P. M. Rudd, Monoglucosylated glycans in the secreted human complement component C3: implications for protein biosynthesis and structure. *FEBS Lett.* **566**, 270–274 (2004).

68. I. Loke, D. Kolarich, N. H. Packer, M. Thaysen-Andersen, Emerging roles of protein mannosylation in inflammation and infection. *Mol. Aspects Med.* **51**, 31–55 (2016).

69. D. N. Hebert, L. Lamriben, E. T. Powers, J. W. Kelly, The intrinsic and extrinsic effects of N-linked glycans on glycoproteostasis. *Nat. Chem. Biol.* **10**, 902–10 (2014).

70. M. R. Wormald, R. A. Dwek, Glycoproteins: glycan presentation and protein-fold stability. *Structure*. **7**, R155-60 (1999).

71. X. Shi, K. Brauburger, R. M. Elliott, Role of N-linked glycans on bunyamwera virus glycoproteins in intracellular trafficking, protein folding, and virus infectivity. *J. Virol.* **79**, 13725–34 (2005).

72. X. Shi, R. M. Elliott, Analysis of N-linked glycosylation of hantaan virus glycoproteins and the role of oligosaccharide side chains in protein folding and intracellular trafficking. *J. Virol.* **78**, 5414–22 (2004).

73. S. Li, M. M. van Oers, J. M. Vlak, S. Shen, Z. Hu, M. Wang, I. Braakman, H. Wang, X. Li, F. Deng, Mutational and functional analysis of N-linked glycosylation of envelope fusion protein F of *Helicoverpa armigera* nucleopolyhedrovirus. *J. Gen. Virol.* **97**, 988–999 (2016).

74. E. Lee, R. C. Weir, L. Dalgarno, Changes in the Dengue virus major envelope protein on passaging and their localization on the three-dimensional structure of the protein. *Virology*. **232**, 281–290 (1997).

75. F. Guirakhoo, A. R. Hunt, J. G. Lewis, J. T. Roehrig, Selection and partial characterization of Dengue 2 virus mutants that induce fusion at elevated pH. *Virology*. **194**, 219–223 (1993).

76. J. Dubuisson, L. Cocquerel, A. Fournillier, J. C. Meunier, A. Cahour, A. Choukhi, C. Wychowski, Analysis of the glycosylation sites of hepatitis C virus (HCV) glycoprotein E1 and the influence of E1 glycans on the formation of the HCV glycoprotein complex. *J. Gen. Virol.* **80**, 887–896 (1999).

77. M. Moll, A. Kaufmann, A. Maisner, Influence of N-glycans on processing and biological activity of the Nipah virus fusion protein. *J. Virol.* **78**, 7274–7278 (2004).

78. S. Luo, K. Hu, S. He, P. Wang, M. Zhang, X. Huang, T. Du, C. Zheng, Y. Liu, Q. Hu, Contribution of N-linked glycans on HSV-2 gB to cell–cell fusion and viral entry. *Virology*. **483**, 72–82 (2015).

79. W. Wang, J. Nie, C. Prochnow, C. Truong, Z. Jia, S. Wang, X. S. Chen, Y. Wang, A systematic study of the N-glycosylation sites of HIV-1 envelope protein on infectivity and antibody-mediated neutralization. *Retrovirology*. **10**, 14 (2013).

80. K. O. François, J. Balzarini, The highly conserved glycan at asparagine 260 of HIV-1 gp120 is indispensable for viral entry. *J. Biol. Chem.* **286**, 42900–42910 (2011).

81. L. Kong, I. A. Wilson, P. D. Kwong, Crystal structure of a fully glycosylated HIV-1 gp120 core reveals a stabilizing role for the glycan at Asn262. *Proteins*. **83**, 590–6 (2015).

82. X. Wang, X. Liu, D. Yang, S. Chen, D. Peng, X. Zhang, J. Zhu, Role of stem glycans attached to haemagglutinin in the biological characteristics of H5N1 avian influenza virus. *J. Gen. Virol.* **96**, 1248–1257 (2015).

83. R. A. Gruters, J. J. Neefjes, M. Tersmette, R. E. Y. de Goede, A. Tulp, H. G. Huisman, F. Miedema, H. L. Ploegh, Interference with HIV-induced syncytium formation and viral infectivity by inhibitors of trimming glucosidase. *Nature*. **330**, 74–77 (1987).

84. G. W. J. Fleet, A. Karpas, R. A. Dwek, L. E. Fellows, A. S. Tyms, S. Petursson, S. K. Namgoong, N. G. Ramsden, P. W. Smith, J. C. Son, F. Wilson, D. R. Witty, G. S. Jacob, T. W. Rademacher, Inhibition of HIV replication by amino-sugar derivatives. *FEBS Lett.* **237**, 128–132 (1988).

85. M. A. Fischl, L. Resnick, R. Coombs, A. B. Kremer, J. C. Pottage, R. J. Fass, K. H. Fife, W. G. Powderly, A. C. Collier, R. L. Aspinall, S. L. Smith, K. G. Kowalski, C.-B. Wallemark, The safety and efficacy of combination N-butyl-deoxynojirimycin (SC-48334) and zidovudine in patients with HIV-1 infection and 200-500 CD4 cells/mm3. *J. Acquir. Immune Defic. Syndr.* **7**, 139–47 (1994).

86. S. Hussain, J. L. Miller, D. J. Harvey, Y. Gu, P. B. Rosenthal, N. Zitzmann, J. W. McCauley, Strain-specific antiviral activity of iminosugars against human influenza A viruses. *J. Antimicrob. Chemother.* **70**, 136–52 (2015).

87. R. Datema, P. A. Romero, G. Legler, R. T. Schwarz, Inhibition of formation of complex oligosaccharides by the glucosidase inhibitor bromoconduritol. *Proc. Natl. Acad. Sci. U. S. A.* **79**, 6787–91 (1982).

88. J. L. Miller, S. G. Spiro, S. D. Dowall, I. Taylor, A. Rule, D. S. Alonzi, A. C. Sayce, E. Wright, E. M. Bentley, R. Thom, G. Hall, R. A. Dwek, R. Hewson, N. Zitzmann, Minimal in vivo efficacy of iminosugars in a lethal Ebola virus guinea pig model. *PLoS One*. **11**, e0167018 (2016).

89. J. Chang, T. K. Warren, X. Zhao, T. Gill, F. Guo, L. Wang, M. A. Comunale, Y. Du, D. S. Alonzi, W. Yu, H. Ye, F. Liu, J.-T. Guo, A. Mehta, A. Cuconati, T. D. Butters, S. Bavari, X. Xu, T. M. Block, Small molecule inhibitors of ER α-glucosidases are active against multiple hemorrhagic fever viruses. *Antiviral Res.* **98**, 432–40 (2013).

90. A. C. Sayce, D. S. Alonzi, S. S. Killingbeck, B. E. Tyrrell, M. L. Hill, A. T. Caputo, R. Iwaki, K. Kinami, D. Ide, J. L. Kiappes, P. R. Beatty, A. Kato, E. Harris, R. A. Dwek, J. L. Miller, N. Zitzmann, Iminosugars inhibit Dengue virus production via inhibition of ER alpha-glucosidases—not glycolipid processing enzymes. *PLoS Negl. Trop. Dis.* **10**, e0004524 (2016).

91. J. L. Miller, R. Lachica, A. C. Sayce, J. P. Williams, M. Bapat, R. Dwek, P. R. Beatty, E. Harris, N. Zitzmann, Liposome-mediated delivery of iminosugars enhances efficacy against dengue virus in vivo. *Antimicrob. Agents Chemother.* **56**, 6379–86 (2012).

92. S.-F. Wu, C.-J. Lee, C.-L. Liao, R. A. Dwek, N. Zitzmann, Y.-L. Lin, Antiviral effects of an iminosugar derivative on flavivirus infections. *J. Virol.* **76**, 3596–604 (2002).

93. D. S. Alonzi, K. A. Scott, R. A. Dwek, N. Zitzmann, Iminosugar antivirals: the therapeutic sweet spot. *Biochem. Soc. Trans.* **45**, 571–582 (2017).

94. J. L. Kiappes, M. L. Hill, D. S. Alonzi, J. L. Miller, R. Iwaki, A. C. Sayce, A. T. Caputo, A. Kato, N. Zitzmann, ToP-DNJ, a selective inhibitor of endoplasmic

reticulum α-glucosidase II exhibiting antiflaviviral activity. *ACS Chem. Biol.* **13**, 60–65 (2018).

95. I. Bagdonaite, H. H. Wandall, Global aspects of viral glycosylation. *Glycobiology*. **28**, 443–467 (2018).

96. Y. A. Shtyrya, L. V Mochalova, N. V Bovin, Influenza virus neuraminidase: structure and function. *Acta Naturae*. **1**, 26–32 (2009).

97. N. M. Bouvier, P. Palese, The biology of influenza viruses. *Vaccine*. **26 Suppl 4**, D49-53 (2008).

98. P. Palese, R. W. Compans, Inhibition of Influenza virus replication in tissue culture by 2-deoxy-2,3-dehydro-N-trifluoroacetylneuraminic acid (FANA): mechanism of action. *J. Gen. Virol.* **33**, 159–163 (1976).

99. M. N. Matrosovich, T. Y. Matrosovich, T. Gray, N. A. Roberts, H.-D. Klenk, Neuraminidase is important for the initiation of Influenza virus infection in human airway epithelium. *J. Virol.* **78**, 12665–12667 (2004).

100. M. N. Waxham, D. C. Merz, J. S. Wolinsky, Intracellular maturation of mumps virus hemagglutinin-neuraminidase glycoprotein: conformational changes detected with monoclonal antibodies. *J. Virol.* **59**, 392–400 (1986).

101. R. Xu, S. G. Palmer, M. Porotto, L. M. Palermo, S. Niewiesk, I. A. Wilson, A. Moscona, Interaction between the Hemagglutinin-Neuraminidase and Fusion glycoproteins of Human Parainfluenza virus type III regulates viral growth in vivo. *mBio*. **4**, e00803-13 (2013).

102. H. Connaris, T. Takimoto, R. Russell, S. Crennell, I. Moustafa, A. Portner, G. Taylor, Probing the sialic acid binding site of the hemagglutinin-neuraminidase of Newcastle disease virus: identification of key amino acids involved in cell binding, catalysis, and fusion. *J. Virol.* **76**, 1816–24 (2002).

103. A. Zeltina, T. A. Bowden, B. Lee, Emerging Paramyxoviruses: receptor tropism and zoonotic potential. *PLoS Pathog.* **12**, e1005390 (2016).

104. M. von Itzstein, The war against influenza: discovery and development of sialidase inhibitors. *Nat. Rev. Drug Discov.* **6**, 967–974 (2007).

105. G. Taylor, S. Crennell, T. Takimoto, A. Portner, Crystal structure of the multifunctional paramyxovirus hemagglutinin-neuraminidase. *Nat. Struct. Biol.* **7**, 1068–1074 (2000).

106. Y.-Q. Chen, T. J. Wohlbold, N.-Y. Zheng, M. Huang, Y. Huang, K. E. Neu, J. Lee, H. Wan, K. T. Rojas, E. Kirkpatrick, C. Henry, A.-K. E. Palm, C. T. Stamper, L. Y.-L. Lan, D. J. Topham, J. Treanor, J. Wrammert, R. Ahmed, M. C. Eichelberger, G. Georgiou, F. Krammer, P. C. Wilson, Influenza infection in humans induces broadly cross-reactive and protective neuraminidase-reactive antibodies. *Cell*. **173**, 417-429.e10 (2018).

107. J. E. Crowe, Antibody determinants of influenza immunity. *J. Infect. Dis.* (2019), doi:10.1093/infdis/jiz010.

108. Y. Desheva, I. Sychev, T. Smolonogina, A. Rekstin, N. Ilyushina, V. Lugovtsev, A. Samsonova, A. Go, A. Lerner, Anti-neuraminidase antibodies against pandemic A/H1N1 influenza viruses in healthy and influenza-infected individuals. *PLoS One*.

13, e0196771 (2018).

109. J. C. Trefry, S. E. Wollen, F. Nasar, J. D. Shamblin, S. J. Kern, J. J. Bearss, M. A. Jefferson, T. B. Chance, J. R. Kugelman, J. T. Ladner, A. N. Honko, D. J. Kobs, M. Q. S. Wending, C. L. Sabourin, W. D. Pratt, G. F. Palacios, M. L. M. Pitt, Ebola virus infections in nonhuman primates are temporally influenced by glycoprotein poly-U editing site populations in the exposure material. *Viruses*. **7**, 6739–54 (2015).

110. T. Maruyama, P. W. H. I. Parren, A. Sanchez, I. Rensink, L. L. Rodriguez, A. S. Khan, C. J. Peters, D. R. Burton, Recombinant human monoclonal antibodies to Ebola virus. *J. Infect. Dis.* **179**, S235–S239 (1999).

111. C. Druar, S. S. Saini, M. A. Cossitt, F. Yu, X. Qiu, T. W. Geisbert, S. Jones, P. B. Jahrling, D. I. H. Stewart, E. J. Wiersma, Analysis of the expressed heavy chain variable-region genes of Macaca fascicularis and isolation of monoclonal antibodies specific for the Ebola virus' soluble glycoprotein. *Immunogenetics*. **57**, 730–738 (2005).

112. J. D. Cook, J. E. Lee, The secret life of viral entry glycoproteins: moonlighting in immune evasion. *PLoS Pathog.* **9**, e1003258 (2013).

113. E. O. Saphire, S. L. Schendel, M. L. Fusco, K. Gangavarapu, B. M. Gunn, A. Z. Wec, P. J. Halfmann, J. M. Brannan, A. S. Herbert, X. Qiu, K. Wagh, S. He, E. E. Giorgi, J. Theiler, K. B. J. Pommert, T. B. Krause, H. L. Turner, C. D. Murin, J. Pallesen, E. Davidson, R. Ahmed, M. J. Aman, A. Bukreyev, D. R. Burton, J. E. Crowe, C. W. Davis, G. Georgiou, F. Krammer, C. A. Kyratsous, J. R. Lai, C. Nykiforuk, M. H. Pauly, P. Rijal, A. Takada, A. R. Townsend, V. Volchkov, L. M. Walker, C.-I. Wang, L. Zeitlin, B. J. Doranz, A. B. Ward, B. Korber, G. P. Kobinger, K. G. Andersen, Y. Kawaoka, G. Alter, K. Chandran, J. M. Dye, Viral Hemorrhagic Fever Immunotherapeutic Consortium, Systematic analysis of monoclonal antibodies against Ebola virus GP defines features that contribute to protection. *Cell*. **174**, 938-952.e13 (2018).

114. L. M. Branco, R. F. Garry, Characterization of the Lassa virus GP1 ectodomain shedding: implications for improved diagnostic platforms. *Virol. J.* **6**, 147 (2009).

115. L. M. Branco, J. N. Grove, L. M. Moses, A. Goba, M. Fullah, M. Momoh, R. J. Schoepp, D. G. Bausch, R. F. Garry, Shedding of soluble glycoprotein 1 detected during acute Lassa virus infection in human subjects. *Virol. J.* **7**, 306 (2010).

116. H. Cohen-Dvashi, N. Cohen, H. Israeli, R. Diskin, Molecular mechanism for LAMP1 recognition by Lassa virus. *J. Virol.* **89**, 7584–7592 (2015).

117. K. M. Hastie, M. A. Zandonatti, L. M. Kleinfelter, M. L. Heinrich, M. M. Rowland, K. Chandran, L. M. Branco, J. E. Robinson, R. F. Garry, E. O. Saphire, Structural basis for antibody-mediated neutralization of Lassa virus. *Science*. **356**, 923–928 (2017).

118. R. Pryce, W. M. Ng, A. Zeltina, Y. Watanabe, K. El Omari, A. Wagner, T. A. Bowden, Structure-based classification defines the discrete conformational classes adopted by the arenaviral GP1. *J. Virol.* **93**, e01048-18 (2019).

119. H. Israeli, H. Cohen-Dvashi, A. Shulman, A. Shimon, R. Diskin, F. Chevenet, Mapping of the Lassa virus LAMP1 binding site reveals unique determinants not shared by other old world arenaviruses. *PLoS Pathog.* **13**, e1006337 (2017).

120. P. Somnuke, R. E. Hauhart, J. P. Atkinson, M. S. Diamond, P. Avirutnan, N-linked glycosylation of dengue virus NS1 protein modulates secretion, cell-surface expression, hexamer stability, and interactions with human complement. *Virology*. **413**, 253–264 (2011).

121. P. Avirutnan, L. Zhang, N. Punyadee, A. Manuyakorn, C. Puttikhunt, W. Kasinrerk, P. Malasit, J. P. Atkinson, M. S. Diamond, Secreted NS1 of Dengue virus attaches to the surface of cells via interactions with heparan sulfate and chondroitin sulfate. *PLoS Pathog.* **3**, e183 (2007).

122. P. Scaturro, M. Cortese, L. Chatel-Chaix, W. Fischl, R. Bartenschlager, Dengue virus non-structural protein 1 modulates infectious particle production via interaction with the structural proteins. *PLoS Pathog.* **11**, e1005277 (2015).

123. P. Avirutnan, R. E. Hauhart, P. Somnuke, A. M. Blom, M. S. Diamond, J. P. Atkinson, Binding of Flavivirus nonstructural protein NS1 to C4b binding protein modulates complement activation. *J. Immunol.* **187**, 424–433 (2011).

124. S. Thiemmeca, C. Tamdet, N. Punyadee, T. Prommool, A. Songjaeng, S. Noisakran, C. Puttikhunt, J. P. Atkinson, M. S. Diamond, A. Ponlawat, P. Avirutnan, Secreted NS1 protects Dengue virus from mannose-binding lectin–mediated neutralization. *J. Immunol.* **197**, 4053–4065 (2016).

125. P. R. Beatty, H. Puerta-Guardo, S. S. Killingbeck, D. R. Glasner, K. Hopkins, E. Harris, Dengue virus NS1 triggers endothelial permeability and vascular leak that is prevented by NS1 vaccination. *Sci. Transl. Med.* **7**, 304ra141 (2015).

126. A. Bukreyev, L. Yang, J. Fricke, L. Cheng, J. M. Ward, B. R. Murphy, P. L. Collins, The secreted form of Respiratory Syncytial Virus G glycoprotein helps the virus evade antibody-mediated restriction of replication by acting as an antigen decoy and through effects on Fc receptor-bearing leukocytes. *J. Virol.* **82**, 12191–12204 (2008).

127. M. E. Ressing, D. van Leeuwen, F. A. W. Verreck, S. Keating, R. Gomez, K. L. M. C. Franken, T. H. M. Ottenhoff, M. Spriggs, T. N. Schumacher, L. M. Hutt-Fletcher, M. Rowe, E. J. H. J. Wiertz, Epstein-Barr Virus gp42 Is posttranslationally modified to produce soluble gp42 that mediates HLA class II immune evasion. *J. Virol.* **79**, 841–852 (2005).

128. E. K. Hoebe, T. Y. S. Le Large, N. Tarbouriech, D. Oosterhoff, T. D. De Gruijl, J. M. Middeldorp, A. E. Greijer, Epstein-Barr virus-encoded BARF1 protein is a decoy receptor for macrophage colony stimulating factor and interferes with macrophage differentiation and activation. *Viral Immunol.* **25**, 461–70 (2012).

129. P. L. Moore, E. T. Crooks, L. Porter, P. Zhu, C. S. Cayanan, H. Grise, P. Corcoran, M. B. Zwick, M. Franti, L. Morris, K. H. Roux, D. R. Burton, J. M. Binley, Nature of nonfunctional envelope proteins on the surface of human immunodeficiency virus type 1. *J. Virol.* **80**, 2515–2528 (2006).

130. Q. J. Sattentau, J. P. Moore, Human immunodeficiency virus type 1 neutralization is determined by epitope exposure on the gp120 oligomer. *J. Exp. Med.* **182**, 185–96 (1995).

131. R. W. Sanders, R. Derking, A. Cupo, J.-P. Julien, A. Yasmeen, N. de Val, H. J. Kim, C. Blattner, A. T. de la Peña, J. Korzun, M. Golabek, K. de los Reyes, T. J. Ketas, M. J. van Gils, C. R. King, I. A. Wilson, A. B. Ward, P. J. Klasse, J. P. Moore, A next-

generation cleaved, soluble HIV-1 Env trimer, BG505 SOSIP.664 gp140, expresses multiple epitopes for broadly neutralizing but not non-neutralizing antibodies. *PLoS Pathog.* **9**, e1003618 (2013).

132. S. W. de Taeye, G. Ozorowski, A. Torrents de la Peña, M. Guttman, J.-P. Julien, T. L. G. M. van den Kerkhof, J. A. Burger, L. K. Pritchard, P. Pugach, A. Yasmeen, J. Crampton, J. Hu, I. Bontjer, J. L. Torres, H. Arendt, J. DeStefano, W. C. Koff, H. Schuitemaker, D. Eggink, B. Berkhout, H. Dean, C. LaBranche, S. Crotty, M. Crispin, D. C. Montefiori, P. J. Klasse, K. K. Lee, J. P. Moore, I. A. Wilson, A. B. Ward, R. W. Sanders, Immunogenicity of stabilized HIV-1 envelope trimers with reduced exposure of non-neutralizing epitopes. *Cell*. **163**, 1702–1715 (2015).

133. F. Helle, G. Vieyres, L. Elkrief, C.-I. Popescu, C. Wychowski, V. Descamps, S. Castelain, P. Roingeard, G. Duverlie, J. Dubuisson, Role of N-linked glycans in the functions of hepatitis C virus envelope proteins incorporated into infectious virions. *J. Virol.* **84**, 11905–15 (2010).

134. M. Lavie, X. Hanoulle, J. Dubuisson, Glycan shielding and modulation of Hepatitis C virus neutralizing antibodies. *Front. Immunol.* **9**, 910 (2018).

135. R. Julithe, G. Abou-Jaoudé, C. Sureau, Modification of the hepatitis B virus envelope protein glycosylation pattern interferes with secretion of viral particles, infectivity, and susceptibility to neutralizing antibodies. *J. Virol.* **88**, 9049–59 (2014).

136. B. G. Bradel-Tretheway, Q. Liu, J. A. Stone, S. McInally, H. C. Aguilar, Novel functions of Hendra virus G N-glycans and comparisons to Nipah virus. *J. Virol.* **89**, 7235–47 (2015).

137. S. Samal, S. K. Khattar, S. Kumar, P. L. Collins, S. K. Samal, Coordinate deletion of N-glycans from the heptad repeats of the fusion F protein of Newcastle disease virus yields a hyperfusogenic virus with increased replication, virulence, and immunogenicity. *J. Virol.* **86**, 2501–11 (2012).

138. D. L. Sodora, G. H. Cohen, R. J. Eisenberg, Influence of asparagine-linked oligosaccharides on antigenicity, processing, and cell surface expression of herpes simplex virus type 1 glycoprotein D. *J. Virol.* **63**, 5184–93 (1989).

139. B. Machiels, C. Lété, A. Guillaume, J. Mast, P. G. Stevenson, A. Vanderplasschen, L. Gillet, Antibody evasion by a gammaherpesvirus O-glycan shield. *PLoS Pathog.* **7**, e1002387 (2011).

140. Y. Watanabe, J. Raghwani, J. D. Allen, G. E. Seabright, S. Li, F. Moser, J. T. Huiskonen, T. Strecker, T. A. Bowden, M. Crispin, Structure of the Lassa virus glycan shield provides a model for immunological resistance. *Proc. Natl. Acad. Sci.* **115**, 7320–7325 (2018).

141. Y. Zhao, J. Ren, K. Harlos, D. M. Jones, A. Zeltina, T. A. Bowden, S. Padilla-Parra, E. E. Fry, D. I. Stuart, Toremifene interacts with and destabilizes the Ebola virus glycoprotein. *Nature*. **535**, 169–172 (2016).

142. Y. An, J. A. McCullers, I. Alymova, L. M. Parsons, J. F. Cipollo, Glycosylation analysis of engineered H3N2 Influenza A virus hemagglutinins with sequentially added historically relevant glycosylation sites. *J. Proteome Res.* **14**, 3957–3969 (2015).

143. Y. Do Kwon, M. Pancera, P. Acharya, I. S. Georgiev, E. T. Crooks, J. Gorman, M.

G. Joyce, M. Guttman, X. Ma, S. Narpala, C. Soto, D. S. Terry, Y. Yang, T. Zhou, G. Ahlsen, R. T. Bailer, M. Chambers, G.-Y. Chuang, N. A. Doria-Rose, A. Druz, M. A. Hallen, A. Harned, T. Kirys, M. K. Louder, S. O'Dell, G. Ofek, K. Osawa, M. Prabhakaran, M. Sastry, G. B. E. Stewart-Jones, J. Stuckey, P. V Thomas, T. Tittley, C. Williams, B. Zhang, H. Zhao, Z. Zhou, B. R. Donald, L. K. Lee, S. Zolla-Pazner, U. Baxa, A. Schön, E. Freire, L. Shapiro, K. K. Lee, J. Arthos, J. B. Munro, S. C. Blanchard, W. Mothes, J. M. Binley, A. B. McDermott, J. R. Mascola, P. D. Kwong, Crystal structure, conformational fixation and entry-related interactions of mature ligand-free HIV-1 Env. *Nat. Struct. Mol. Biol.* **22**, 522–31 (2015).

144. K. Xu, Y.-P. Chan, B. Bradel-Tretheway, Z. Akyol-Ataman, Y. Zhu, S. Dutta, L. Yan, Y. Feng, L.-F. Wang, G. Skiniotis, B. Lee, Z. H. Zhou, C. C. Broder, H. C. Aguilar, D. B. Nikolov, Crystal structure of the pre-fusion Nipah virus fusion glycoprotein reveals a novel hexamer-of-trimers assembly. *PLoS Pathog.* **11**, e1005322 (2015).

145. M. Crispin, A. B. Ward, I. A. Wilson, Structure and immune recognition of the HIV glycan shield. *Annu. Rev. Biophys.* **47** (2018), doi:10.1146/annurev-biophys-060414-034156.

146. S. Hallenberger, V. Bosch, H. Angliker, E. Shaw, H.-D. Klenk, W. Garten, Inhibition of furin-mediated cleavage activation of HIV-1 glycoprotein gpl60. *Nature*. **360**, 358–361 (1992).

147. X. Ma, M. Lu, J. Gorman, D. S. Terry, X. Hong, Z. Zhou, H. Zhao, R. B. Altman, J. Arthos, S. C. Blanchard, P. D. Kwong, J. B. Munro, W. Mothes, HIV-1 Env trimer opens through an asymmetric intermediate in which individual protomers adopt distinct conformations. *eLife*. **7** (2018), doi:10.7554/eLife.34271.

148. A. B. Ward, I. A. Wilson, The HIV-1 envelope glycoprotein structure: nailing down a moving target. *Immunol. Rev.* **275**, 21–32 (2017).

149. R. Wyatt, P. D. Kwong, E. Desjardins, R. W. Sweet, J. Robinson, W. A. Hendrickson, J. G. Sodroski, The antigenic structure of the HIV gp120 envelope glycoprotein. *Nature*. **393**, 705–711 (1998).

150. X. Wei, J. M. Decker, S. Wang, H. Hui, J. C. Kappes, X. Wu, J. F. Salazar-Gonzalez, M. G. Salazar, J. M. Kilby, M. S. Saag, N. L. Komarova, M. A. Nowak, B. H. Hahn, P. D. Kwong, G. M. Shaw, Antibody neutralization and escape by HIV-1. *Nature*. **422**, 307–312 (2003).

151. L. K. Pritchard, D. I. R. Spencer, L. Royle, C. Bonomelli, G. E. Seabright, A.-J. Behrens, D. W. Kulp, S. Menis, S. A. Krumm, D. C. Dunlop, D. J. Crispin, T. A. Bowden, C. N. Scanlan, A. B. Ward, W. R. Schief, K. J. Doores, M. Crispin, Glycan clustering stabilizes the mannose patch of HIV-1 and preserves vulnerability to broadly neutralizing antibodies. *Nat. Commun.* **6**, 7479 (2015).

152. A.-J. Behrens, S. Vasiljevic, L. Pritchard, D. Harvey, R. Andev, S. Krumm, W. Struwe, A. Cupo, A. Kumar, N. Zitzmann, G. Seabright, H. Kramer, D. R. Spencer, L. Royle, J. Lee, P. Klasse, D. Burton, I. Wilson, A. Ward, R. Sanders, J. Moore, K. Doores, M. Crispin, Composition and antigenic effects of individual glycan sites of a trimeric HIV-1 envelope glycoprotein. *Cell Rep.* **14**, 2695–2706 (2016).

153. L. Cao, J. K. Diedrich, D. W. Kulp, M. Pauthner, L. He, S.-K. R. Park, D. Sok, C. Y.

Su, C. M. Delahunty, S. Menis, R. Andrabi, J. Guenaga, E. Georgeson, M. Kubitz, Y. Adachi, D. R. Burton, W. R. Schief, J. R. Yates III, J. C. Paulson, Global site-specific N-glycosylation analysis of HIV envelope glycoprotein. *Nat. Commun.* **8**, 14954 (2017).

154. A.-J. Behrens, D. J. Harvey, E. Milne, A. Cupo, A. Kumar, N. Zitzmann, W. B. Struwe, J. P. Moore, M. Crispin, Molecular architecture of the cleavage-dependent mannose patch on a soluble HIV-1 envelope glycoprotein trimer. *J. Virol.* **91**, e01894-16 (2017).

155. L. Pritchard, S. Vasiljevic, G. Ozorowski, G. Seabright, A. Cupo, R. Ringe, H. Kim, R. Sanders, K. Doores, D. Burton, I. Wilson, A. Ward, J. Moore, M. Crispin, Structural constraints determine the glycosylation of HIV-1 envelope trimers. *Cell Rep.* **11**, 1604–1613 (2015).

156. A.-J. Behrens, M. Crispin, Structural principles controlling HIV envelope glycosylation. *Curr. Opin. Struct. Biol.* **44**, 125–133 (2017).

157. M. Crispin, K. J. Doores, Targeting host-derived glycans on enveloped viruses for antibody-based vaccine design. *Curr. Opin. Virol.* **11**, 63–69 (2015).

158. D. R. Burton, L. Hangartner, Broadly neutralizing antibodies to HIV and their role in vaccine design. *Annu. Rev. Immunol.* **34**, 635–659 (2016).

159. K. J. Doores, The HIV glycan shield as a target for broadly neutralizing antibodies. *FEBS J.* **282**, 4679–4691 (2015).

160. R. Pejchal, K. J. Doores, L. M. Walker, R. Khayat, P.-S. Huang, S.-K. Wang, R. L. Stanfield, J.-P. Julien, A. Ramos, M. Crispin, R. Depetris, U. Katpally, A. Marozsan, A. Cupo, S. Maloveste, Y. Liu, R. McBride, Y. Ito, R. W. Sanders, C. Ogohara, J. C. Paulson, T. Feizi, C. N. Scanlan, C.-H. Wong, J. P. Moore, W. C. Olson, A. B. Ward, P. Poignard, W. R. Schief, D. R. Burton, I. A. Wilson, A potent and broad neutralizing antibody recognizes and penetrates the HIV glycan shield. *Science*. **334**, 1097–1103 (2011).

161. L. M. Walker, M. Huber, K. J. Doores, E. Falkowska, R. Pejchal, J.-P. Julien, S.-K. Wang, A. Ramos, P.-Y. Chan-Hui, M. Moyle, J. L. Mitcham, P. W. Hammond, O. A. Olsen, P. Phung, S. Fling, C.-H. Wong, S. Phogat, T. Wrin, M. D. Simek, P. G. Principal Investigators, W. C. Koff, I. A. Wilson, D. R. Burton, P. Poignard, Broad neutralization coverage of HIV by multiple highly potent antibodies. *Nature*. **477**, 466–470 (2011).

162. C. K. Wibmer, P. L. Moore, L. Morris, HIV broadly neutralizing antibody targets. *Curr. Opin. HIV AIDS*. **10**, 135–143 (2015).

163. T. Zhou, A. Zheng, U. Baxa, G.-Y. Chuang, I. S. Georgiev, R. Kong, S. O'Dell, S. Shahzad-ul-Hussan, C.-H. Shen, Y. Tsybovsky, R. T. Bailer, S. K. Gift, M. K. Louder, K. McKee, R. Rawi, C. H. Stevenson, G. B. E. Stewart-Jones, J. D. Taft, E. Waltari, Y. Yang, B. Zhang, S. S. Shivatare, V. S. Shivatare, C.-C. D. Lee, C.-Y. Wu, J. C. Mullikin, C. A. Bewley, D. R. Burton, V. R. Polonis, L. Shapiro, C.-H. Wong, J. R. Mascola, P. D. Kwong, X. Wu, B. Benjamin, R. Blakesley, G. Bouffard, S. Brooks, H. Coleman, M. Dekhtyar, M. Gregory, X. Guan, J. Gupta, J. Han, A. Hargrove, S. Ho, R. Legaspi, Q. Maduro, C. Masiello, B. Maskeri, J. McDowell, C. Montemayor, J. Mullikin, M. Park, N. Riebow, K. Schandler, B. Schmidt, C. Sison,

M. Stantripop, J. Thomas, P. Thomas, M. Vemulapalli, A. Young, A neutralizing antibody recognizing primarily N-linked glycan targets the silent face of the HIV envelope. *Immunity*. **48**, 500-513.e6 (2018).

164. G.-Y. Chuang, J. Zhou, P. Acharya, R. Rawi, C.-H. Shen, Z. Sheng, B. Zhang, T. Zhou, R. T. Bailer, V. P. Dandey, N. A. Doria-Rose, M. K. Louder, K. McKee, J. R. Mascola, L. Shapiro, P. D. Kwong, Structural survey of broadly neutralizing antibodies targeting the HIV-1 Env trimer delineates epitope categories and characteristics of recognition. *Structure*. **27**, 196-206.e6 (2019).

165. D. R. Burton, What are the most powerful immunogen design vaccine strategies? Reverse vaccinology 2.0 shows great promise. *Cold Spring Harb. Perspect. Biol.* **9** (2017), doi:10.1101/cshperspect.a030262.

166. P. D. Kwong, J. R. Mascola, HIV-1 vaccines based on antibody identification, B cell ontogeny, and epitope structure. *Immunity*. **48**, 855–871 (2018).

167. R. W. Sanders, J. P. Moore, Native-like Env trimers as a platform for HIV-1 vaccine design. *Immunol. Rev.* **275**, 161–182 (2017).

168. G. E. Seabright, K. J. Doores, D. R. Burton, M. Crispin, Protein and glycan mimicry in HIV vaccine design. *J. Mol. Biol.* (2019), doi:10.1016/j.jmb.2019.04.016.

169. M. F. Boni, Vaccination and antigenic drift in influenza. *Vaccine*. **26 Suppl 3**, C8-14 (2008).

170. S. Bhatt, E. C. Holmes, O. G. Pybus, The genomic rate of molecular adaptation of the human Influenza A virus. *Mol. Biol. Evol.* **28**, 2443–2451 (2011).

171. N. C. Wu, I. A. Wilson, A perspective on the structural and functional constraints for immune evasion: insights from influenza virus. *J. Mol. Biol.* **429**, 2694–2709 (2017).

172. J. J. Skehel, D. J. Stevens, R. S. Daniels, A. R. Douglas, M. Knossow, I. A. Wilson, D. C. Wiley, A carbohydrate side chain on hemagglutinins of Hong Kong influenza viruses inhibits recognition by a monoclonal antibody. *Proc. Natl. Acad. Sci. U. S. A.* **81**, 1779–83 (1984).

173. M. Igarashi, K. Ito, H. Kida, A. Takada, Genetically destined potentials for N-linked glycosylation of influenza virus hemagglutinin. *Virology*. **376**, 323–329 (2008).

174. S. Sun, Q. Wang, F. Zhao, W. Chen, Z. Li, Glycosylation site alteration in the evolution of influenza A (H1N1) viruses. *PLoS One*. **6**, e22844 (2011).

175. B. P. Blackburne, A. J. Hay, R. A. Goldstein, Changing selective pressure during antigenic changes in human influenza H3. *PLoS Pathog.* **4**, e1000058 (2008).

176. J. L. Cherry, D. J. Lipman, A. Nikolskaya, Y. I. Wolf, Evolutionary dynamics of N-glycosylation sites of influenza virus hemagglutinin. *PLoS Curr.* **1**, RRN1001 (2009).

177. M. D. Tate, E. R. Job, Y.-M. Deng, V. Gunalan, S. Maurer-Stroh, P. C. Reading, Playing hide and seek: how glycosylation of the influenza virus hemagglutinin can modulate the immune response to infection. *Viruses*. **6**, 1294–316 (2014).

178. S. R. Das, P. Puigbò, S. E. Hensley, D. E. Hurt, J. R. Bennink, J. W. Yewdell, Glycosylation focuses sequence variation in the influenza A virus H1 hemagglutinin globular domain. *PLoS Pathog.* **6**, e1001211 (2010).

179. R. A. Medina, S. Stertz, B. Manicassamy, P. Zimmermann, X. Sun, R. A. Albrecht,

H. Uusi-Kerttula, O. Zagordi, R. B. Belshe, S. E. Frey, T. M. Tumpey, A. García-Sastre, A. García-Sastre, Glycosylations in the globular head of the hemagglutinin protein modulate the virulence and antigenic properties of the H1N1 influenza viruses. *Sci. Transl. Med.* **5**, 187ra70 (2013).

180. J. Lu, J. Raghwani, R. Pryce, T. A. Bowden, J. Thézé, S. Huang, Y. Song, L. Zou, L. Liang, R. Bai, Y. Jing, P. Zhou, M. Kang, L. Yi, J. Wu, O. G. Pybus, C. Ke, Molecular evolution, diversity, and adaptation of Influenza A(H7N9) viruses in China. *Emerg. Infect. Dis.* **24**, 1795–1805 (2018).

181. C. P. Thompson, J. Lourenço, A. A. Walters, U. Obolski, M. Edmans, D. S. Palmer, K. Kooblall, G. W. Carnell, D. O'Connor, T. A. Bowden, O. G. Pybus, A. J. Pollard, N. J. Temperton, T. Lambe, S. C. Gilbert, S. Gupta, A naturally protective epitope of limited variability as an influenza vaccine target. *Nat. Commun.* **9**, 3859 (2018).

182. S. R. Das, S. E. Hensley, A. David, L. Schmidt, J. S. Gibbs, P. Puigbò, W. L. Ince, J. R. Bennink, J. W. Yewdell, Fitness costs limit influenza A virus hemagglutinin glycosylation as an immune evasion strategy. *Proc. Natl. Acad. Sci. U. S. A.* **108**, E1417-22 (2011).

183. I. Kosik, W. L. Ince, L. E. Gentles, A. J. Oler, M. Kosikova, M. Angel, J. G. Magadán, H. Xie, C. B. Brooke, J. W. Yewdell, Influenza A virus hemagglutinin glycosylation compensates for antibody escape fitness costs. *PLoS Pathog.* **14**, e1006796 (2018).

184. S. Zhang, R. W. Sherwood, Y. Yang, T. Fish, W. Chen, J. A. McCardle, R. M. Jones, V. Yusibov, E. R. May, J. K. C. Rose, T. W. Thannhauser, Comparative characterization of the glycosylation profiles of an influenza hemagglutinin produced in plant and insect hosts. *Proteomics*. **12**, 1269–88 (2012).

185. S. Y. Mir-Shekari, D. A. Ashford, D. J. Harvey, R. A. Dwek, I. T. Schulze, The glycosylation of the influenza A virus hemagglutinin by mammalian cells. A site-specific study. *J. Biol. Chem.* **272**, 4027–36 (1997).

186. A. C. Walls, X. Xiong, Y.-J. Park, M. A. Tortorici, J. Snijder, J. Quispe, E. Cameroni, R. Gopal, M. Dai, A. Lanzavecchia, M. Zambon, F. A. Rey, D. Corti, D. Veesler, Unexpected receptor functional mimicry elucidates activation of coronavirus fusion. *Cell*. **176**, 1026-1-39.e5 (2019).

187. J. Jardine, J.-P. Julien, S. Menis, T. Ota, O. Kalyuzhniy, A. McGuire, D. Sok, P.-S. Huang, S. MacPherson, M. Jones, T. Nieusma, J. Mathison, D. Baker, A. B. Ward, D. R. Burton, L. Stamatatos, D. Nemazee, I. A. Wilson, W. R. Schief, Rational HIV immunogen design to target specific germline B cell receptors. *Science*. **340**, 711–716 (2013).

188. C.-J. Wei, J. C. Boyington, K. Dai, K. V. Houser, M. B. Pearce, W.-P. Kong, Z. -y. Yang, T. M. Tumpey, G. J. Nabel, Cross-neutralization of 1918 and 2009 Influenza viruses: role of glycans in viral evolution and vaccine design. *Sci. Transl. Med.* **2**, 24ra21 (2010).

189. R. Xu, D. C. Ekiert, J. C. Krause, R. Hai, J. E. Crowe, I. A. Wilson, Structural basis of preexisting immunity to the 2009 H1N1 pandemic influenza virus. *Science*. **328**, 357–360 (2010).

190. L. Wang, W. Shi, J. D. Chappell, M. G. Joyce, Y. Zhang, M. Kanekiyo, M. M. Becker, N. van Doremalen, R. Fischer, N. Wang, K. S. Corbett, M. Choe, R. D. Mason, J. G.

Van Galen, T. Zhou, K. O. Saunders, K. M. Tatti, L. M. Haynes, P. D. Kwong, K. Modjarrad, W.-P. Kong, J. S. McLellan, M. R. Denison, V. J. Munster, J. R. Mascola, B. S. Graham, Importance of neutralizing monoclonal antibodies targeting multiple antigenic sites on MERS-CoV Spike to avoid neutralization escape. *J. Virol.* **92** (2018), doi:10.1128/JVI.02002-17.

191. L. Wang, W. Shi, M. G. Joyce, K. Modjarrad, Y. Zhang, K. Leung, C. R. Lees, T. Zhou, H. M. Yassine, M. Kanekiyo, Z. Yang, X. Chen, M. M. Becker, M. Freeman, L. Vogel, J. C. Johnson, G. Olinger, J. P. Todd, U. Bagci, J. Solomon, D. J. Mollura, L. Hensley, P. Jahrling, M. R. Denison, S. S. Rao, K. Subbarao, P. D. Kwong, J. R. Mascola, W.-P. Kong, B. S. Graham, Evaluation of candidate vaccine approaches for MERS-CoV. *Nat. Commun.* **6**, 7712 (2015).

192. J. Pallesen, N. Wang, K. S. Corbett, D. Wrapp, R. N. Kirchdoerfer, H. L. Turner, C. A. Cottrell, M. M. Becker, L. Wang, W. Shi, W.-P. Kong, E. L. Andres, A. N. Kettenbach, M. R. Denison, J. D. Chappell, B. S. Graham, A. B. Ward, J. S. McLellan, Immunogenicity and structures of a rationally designed prefusion MERS-CoV spike antigen. *Proc. Natl. Acad. Sci. U. S. A.* **114**, E7348–E7357 (2017).

193. M. R. Hilleman, Strategies and mechanisms for host and pathogen survival in acute and persistent viral infections. *Proc. Natl. Acad. Sci.* **101**, 14560–14566 (2004).

194. L. Du, W. Tai, Y. Yang, G. Zhao, Q. Zhu, S. Sun, C. Liu, X. Tao, C.-T. K. Tseng, S. Perlman, S. Jiang, Y. Zhou, F. Li, Introduction of neutralizing immunogenicity index to the rational design of MERS coronavirus subunit vaccines. *Nat. Commun.* **7**, 13473 (2016).

195. S. R. Radoshitzky, Y. Bào, M. J. Buchmeier, R. N. Charrel, A. N. Clawson, C. S. Clegg, J. L. DeRisi, S. Emonet, J.-P. Gonzalez, J. H. Kuhn, I. S. Lukashevich, C. J. Peters, V. Romanowski, M. S. Salvato, M. D. Stenglein, J. C. de la Torre, Past, present, and future of arenavirus taxonomy. *Arch. Virol.* **160**, 1851–1874 (2015).

196. M.-L. Parsy, K. Harlos, J. T. Huiskonen, T. A. Bowden, Crystal structure of Venezuelan Hemorrhagic Fever Virus fusion glycoprotein reveals a class 1 postfusion architecture with extensive glycosylation. *J. Virol.* **87**, 13070–13075 (2013).

197. A. Zeltina, S. A. Krumm, M. Sahin, W. B. Struwe, K. Harlos, J. H. Nunberg, M. Crispin, D. D. Pinschewer, K. J. Doores, T. A. Bowden, Convergent immunological solutions to Argentine hemorrhagic fever virus neutralization. *Proc. Natl. Acad. Sci.* **114**, 7031–7036 (2017).

198. T. A. Bowden, M. Crispin, S. C. Graham, D. J. Harvey, J. M. Grimes, E. Y. Jones, D. I. Stuart, Unusual molecular architecture of the Machupo virus attachment glycoprotein. *J. Virol.* **83**, 8259–8265 (2009).

199. M. Acciani, J. T. Alston, G. Zhao, H. Reynolds, A. M. Ali, B. Xu, M. A. Brindley, *J. Virol.*, in press, doi:10.1128/JVI.00574-17.

200. S. Li, Z. Sun, R. Pryce, M.-L. Parsy, S. K. Fehling, K. Schlie, C. A. Siebert, W. Garten, T. A. Bowden, T. Strecker, J. T. Huiskonen, Acidic pH-induced conformations and LAMP1 binding of the Lassa virus glycoprotein spike. *PLoS Pathog.* **12**, e1005418 (2016).

201. J. E. Lee, E. O. Saphire, *Ebolavirus* glycoprotein structure and mechanism of entry. *Future Virol.* **4**, 621–635 (2009).

202. M.-A. de La Vega, G. Wong, G. P. Kobinger, X. Qiu, The multiple roles of sGP in Ebola pathogenesis. *Viral Immunol.* **28**, 3–9 (2015).

203. J. R. Francica, A. Varela-Rohena, A. Medvec, G. Plesa, J. L. Riley, P. Bates, Steric shielding of surface epitopes and impaired immune recognition induced by the Ebola virus glycoprotein. *PLoS Pathog.* **6**, e1001098 (2010).

204. T. A. Bowden, A. R. Aricescu, R. J. C. Gilbert, J. M. Grimes, E. Y. Jones, D. I. Stuart, Structural basis of Nipah and Hendra virus attachment to their cell-surface receptor ephrin-B2. *Nat. Struct. Mol. Biol.* **15**, 567–572 (2008).

205. R. N. Kirchdoerfer, C. A. Cottrell, N. Wang, J. Pallesen, H. M. Yassine, H. L. Turner, K. S. Corbett, B. S. Graham, J. S. McLellan, A. B. Ward, Pre-fusion structure of a human coronavirus spike protein. *Nature*. **531**, 118–121 (2016).

206. H. C. Aguilar, K. A. Matreyek, C. M. Filone, S. T. Hashimi, E. L. Levroney, O. A. Negrete, A. Bertolotti-Ciarlet, D. Y. Choi, I. McHardy, J. A. Fulcher, S. V. Su, M. C. Wolf, L. Kohatsu, L. G. Baum, B. Lee, N-Glycans on Nipah virus fusion protein protect against neutralization but reduce membrane fusion and viral entry. *J. Virol.* **80**, 4878–4889 (2006).

207. S. B. Biering, A. Huang, A. T. Vu, L. R. Robinson, B. Bradel-Tretheway, E. Choi, B. Lee, H. C. Aguilar, N-Glycans on the Nipah virus attachment glycoprotein modulate fusion and viral entry as they protect against antibody neutralization. *J. Virol.* **86**, 11991–12002 (2012).

208. A.-R. Goncalves, M.-L. Moraz, A. Pasquato, A. Helenius, P.-Y. Lozach, S. Kunz, Role of DC-SIGN in Lassa virus entry into human dendritic cells. *J. Virol.* **87**, 11504–15 (2013).

209. B. Tassaneetrithep, T. H. Burgess, A. Granelli-Piperno, C. Trumpfheller, J. Finke, W. Sun, M. A. Eller, K. Pattanapanyasat, S. Sarasombath, D. L. Birx, R. M. Steinman, S. Schlesinger, M. A. Marovich, DC-SIGN (CD209) mediates dengue virus infection of human dendritic cells. *J. Exp. Med.* **197**, 823–829 (2003).

210. T. B. H. Geijtenbeek, Y. van Kooyk, DC-SIGN: a novel HIV receptor on DCs that mediates HIV-1 transmission. *Curr. Top. Microbiol. Immunol.* **276**, 31–54 (2003).

211. A. D. Regan, G. R. Whittaker, Utilization of DC-SIGN for entry of feline coronaviruses into host cells. *J. Virol.* **82**, 11992–6 (2008).

212. A. Marzi, T. Gramberg, G. Simmons, P. Moller, A. J. Rennekamp, M. Krumbiegel, M. Geier, J. Eisemann, N. Turza, B. Saunier, A. Steinkasserer, S. Becker, P. Bates, H. Hofmann, S. Pohlmann, DC-SIGN and DC-SIGNR interact with the glycoprotein of Marburg virus and the S protein of Severe Acute Respiratory Syndrome coronavirus. *J. Virol.* **78**, 12090–12095 (2004).

213. W. B. Klimstra, E. M. Nangle, M. S. Smith, A. D. Yurochko, K. D. Ryman, DC-SIGN and L-SIGN can act as attachment receptors for alphaviruses and distinguish between mosquito cell- and mammalian cell-derived viruses. *J. Virol.* **77**, 12022–32 (2003).

214. P.-Y. Lozach, A. Kühbacher, R. Meier, R. Mancini, D. Bitto, M. Bouloy, A. Helenius, DC-SIGN as a receptor for phleboviruses. **10**, 75–88 (2011).

215. Y. Guo, H. Feinberg, E. Conroy, D. A. Mitchell, R. Alvarez, O. Blixt, M. E. Taylor,

W. I. Weis, K. Drickamer, Structural basis for distinct ligand-binding and targeting properties of the receptors DC-SIGN and DC-SIGNR. *Nat. Struct. Mol. Biol.* **11**, 591–8 (2004).

216. H. Feinberg, D. A. Mitchell, K. Drickamer, W. I. Weis, Structural basis for selective recognition of oligosaccharides by DC-SIGN and DC-SIGNR. *Science*. **294**, 2163–2166 (2001).

217. S. L. Londrigan, S. G. Turville, M. D. Tate, Y.-M. Deng, A. G. Brooks, P. C. Reading, N-Linked glycosylation facilitates sialic acid-independent attachment and entry of Influenza A viruses into cells expressing DC-SIGN or L-SIGN. *J. Virol.* **85**, 2990–3000 (2011).

218. E. G. Cormier, R. J. Durso, F. Tsamis, L. Boussemart, C. Manix, W. C. Olson, J. P. Gardner, T. Dragic, L-SIGN (CD209L) and DC-SIGN (CD209) mediate transinfection of liver cells by hepatitis C virus. *Proc. Natl. Acad. Sci.* **101**, 14067–14072 (2004).

219. S. A. Jeffers, S. M. Tusell, L. Gillim-Ross, E. M. Hemmila, J. E. Achenbach, G. J. Babcock, W. D. Thomas, L. B. Thackray, M. D. Young, R. J. Mason, D. M. Ambrosino, D. E. Wentworth, J. C. Demartini, K. V Holmes, K. V. Holmes, CD209L (L-SIGN) is a receptor for severe acute respiratory syndrome coronavirus. *Proc. Natl. Acad. Sci. U. S. A.* **101**, 15748–53 (2004).

220. W. Van Breedam, S. Pöhlmann, H. W. Favoreel, R. J. de Groot, H. J. Nauwynck, Bitter-sweet symphony: glycan–lectin interactions in virus biology. *FEMS Microbiol. Rev.* **38**, 598–632 (2014).

221. M. Crispin, D. J. Harvey, D. Bitto, S. Halldorsson, C. Bonomelli, M. Edgeworth, J. H. Scrivens, J. T. Huiskonen, T. A. Bowden, Uukuniemi Phlebovirus assembly and secretion leave a functional imprint on the virion glycome. *J. Virol.* **88**, 10244–51 (2014).

222. H. Hofmann, X. Li, X. Zhang, W. Liu, A. Kühl, F. Kaup, S. S. Soldan, F. González-Scarano, F. Weber, Y. He, S. Pöhlmann, Severe fever with thrombocytopenia virus glycoproteins are targeted by neutralizing antibodies and can use DC-SIGN as a receptor for pH-dependent entry into human and animal cell lines. *J. Virol.* **87**, 4384–94 (2013).

223. I. Phoenix, S. Nishiyama, N. Lokugamage, T. Hill, M. Huante, O. Slack, V. Carpio, A. Freiberg, T. Ikegami, N-Glycans on the Rift Valley Fever Virus envelope glycoproteins Gn and Gc redundantly support viral infection via DC-SIGN. *Viruses*. **8**, 149 (2016).

224. S. Halldorsson, S. Li, M. Li, K. Harlos, T. A. Bowden, J. T. Huiskonen, Shielding and activation of a viral membrane fusion protein. *Nat. Commun.* **9**, 349 (2018).

225. P. Léger, M. Tetard, B. Youness, N. Cordes, R. N. Rouxel, M. Flamand, P.-Y. Lozach, Differential use of the C-type lectins L-SIGN and DC-SIGN for Phlebovirus endocytosis. *Traffic*. **17**, 639–656 (2016).

226. S. Halldorsson, A.-J. Behrens, K. Harlos, J. T. Huiskonen, R. M. Elliott, M. Crispin, B. Brennan, T. A. Bowden, Structure of a phleboviral envelope glycoprotein reveals a consolidated model of membrane fusion. *Proc. Natl. Acad. Sci. U. S. A.* **113**, 7154–9 (2016).

227. J. L. Miller, B. J. M. DeWet, L. Martinez-Pomares, C. M. Radcliffe, R. A. Dwek, P. M. Rudd, S. Gordon, The mannose receptor mediates Dengue virus infection of macrophages. *PLoS Pathog.* **4**, e17 (2008).

228. E. Pokidysheva, Y. Zhang, A. J. Battisti, C. M. Bator-Kelly, P. R. Chipman, C. Xiao, G. G. Gregorio, W. A. Hendrickson, R. J. Kuhn, M. G. Rossmann, Cryo-EM reconstruction of Dengue virus in complex with the carbohydrate recognition domain of DC-SIGN. *Cell*. **124**, 485–493 (2006).

229. E. Navarro-Sanchez, R. Altmeyer, A. Amara, O. Schwartz, F. Fieschi, J.-L. Virelizier, F. Arenzana-Seisdedos, P. Desprès, Dendritic-cell-specific ICAM3-grabbing non-integrin is essential for the productive infection of human dendritic cells by mosquito-cell-derived dengue viruses. *EMBO Rep.* **4**, 723–728 (2003).

230. Y. Modis, S. Ogata, D. Clements, S. C. Harrison, Structure of the dengue virus envelope protein after membrane fusion. *Nature*. **427**, 313–319 (2004).

231. P.-Y. Lozach, L. Burleigh, I. Staropoli, E. Navarro-Sanchez, J. Harriague, J.-L. Virelizier, F. A. Rey, P. Desprès, F. Arenzana-Seisdedos, A. Amara, Dendritic cell-specific intercellular adhesion molecule 3-grabbing non-integrin (DC-SIGN)-mediated enhancement of dengue virus infection is independent of DC-SIGN internalization signals. *J. Biol. Chem.* **280**, 23698–708 (2005).

232. G. Cheng, J. Cox, P. Wang, M. N. Krishnan, J. Dai, F. Qian, J. F. Anderson, E. Fikrig, A C-Type lectin collaborates with a CD45 phosphatase homolog to facilitate West Nile virus infection of mosquitoes. *Cell*. **142**, 714–725 (2010).

233. Y. Liu, F. Zhang, J. Liu, X. Xiao, S. Zhang, C. Qin, Y. Xiang, P. Wang, G. Cheng, Transmission-blocking antibodies against mosquito C-type lectins for Dengue prevention. *PLoS Pathog.* **10**, e1003931 (2014).

234. S. Baize, J. Kaplon, C. Faure, D. Pannetier, M.-C. Georges-Courbot, V. Deubel, Lassa virus infection of human dendritic cells and macrophages is productive but fails to activate cells. *J. Immunol*. **172**, 2861–9 (2004).

235. T. B. . Geijtenbeek, D. S. Kwon, R. Torensma, S. J. van Vliet, G. C. . van Duijnhoven, J. Middel, I. L. M. H. . Cornelissen, H. S. L. . Nottet, V. N. KewalRamani, D. R. Littman, C. G. Figdor, Y. van Kooyk, DC-SIGN, a dendritic cell–specific HIV-1-binding protein that enhances trans-infection of T cells. *Cell*. **100**, 587–597 (2000).

236. Z.-Y. Yang, Y. Huang, L. Ganesh, K. Leung, W.-P. Kong, O. Schwartz, K. Subbarao, G. J. Nabel, pH-dependent entry of severe acute respiratory syndrome coronavirus is mediated by the spike glycoprotein and enhanced by dendritic cell transfer through DC-SIGN. *J. Virol.* **78**, 5642–50 (2004).

237. A. Engering, T. B. H. Geijtenbeek, S. J. van Vliet, M. Wijers, E. van Liempt, N. Demaurex, A. Lanzavecchia, J. Fransen, C. G. Figdor, V. Piguet, Y. van Kooyk, The dendritic cell-specific adhesion receptor DC-SIGN internalizes antigen for presentation to T cells. *J. Immunol.* **168**, 2118–26 (2002).

238. L. de Witte, A. Nabatov, M. Pion, D. Fluitsma, M. A. W. P. de Jong, T. de Gruijl, V. Piguet, Y. van Kooyk, T. B. H. Geijtenbeek, Langerin is a natural barrier to HIV-1 transmission by Langerhans cells. *Nat. Med.* **13**, 367–371 (2007).

239. S. Sukegawa, E. Miyagi, F. Bouamr, H. Farkašová, K. Strebel, Mannose receptor 1 restricts HIV particle release from infected macrophages. *Cell Rep.* **22**, 786–795

(2018).

240. Y. Xiang, K. Karaveg, K. W. Moremen, Substrate recognition and catalysis by GH47 α-mannosidases involved in Asn-linked glycan maturation in the mammalian secretory pathway. *Proc. Natl. Acad. Sci. U. S. A.* **113**, E7890–E7899 (2016).

241. K. K.-S. Ng, A. R. Kolatkar, S. Park-Snyder, H. Feinberg, D. A. Clark, K. Drickamer, W. I. Weis, Orientation of bound ligands in mannose-binding proteins. Implications for multivalent ligand recognition. *J. Biol. Chem.* **277**, 16088–95 (2002).

242. J. H. Lee, N. de Val, D. Lyumkis, A. B. Ward, Model building and refinement of a natively glycosylated HIV-1 Env protein by high-resolution cryoelectron microscopy. *Structure*. **23**, 1943–51 (2015).

243. D. A. Calarese, C. N. Scanlan, M. B. Zwick, S. Deechongkit, Y. Mimura, R. Kunert, P. Zhu, M. R. Wormald, R. L. Stanfield, K. H. Roux, J. W. Kelly, P. M. Rudd, R. A. Dwek, H. Katinger, D. R. Burton, I. A. Wilson, Antibody domain exchange is an immunological solution to carbohydrate cluster recognition. *Science*. **300**, 2065–71 (2003).

244. C. D. Murin, J.-P. Julien, D. Sok, R. L. Stanfield, R. Khayat, A. Cupo, J. P. Moore, D. R. Burton, I. A. Wilson, A. B. Ward, Structure of 2G12 Fab2 in complex with soluble and fully glycosylated HIV-1 Env by negative-stain single-particle electron microscopy. *J. Virol.* **88**, 10177–88 (2014).

245. W. Weis, J. H. Brown, S. Cusack, J. C. Paulson, J. J. Skehel, D. C. Wiley, Structure of the influenza virus haemagglutinin complexed with its receptor, sialic acid. *Nature*. **333**, 426–431 (1988).

246. I. A. Wilson, J. J. Skehel, D. C. Wiley, Structure of the haemagglutinin membrane glycoprotein of influenza virus at 3 Å resolution. *Nature*. **289**, 366–373 (1981).

247. L. Chen, F. Li, Structural analysis of the evolutionary origins of influenza virus hemagglutinin and other viral lectins. *J. Virol.* **87**, 4118–20 (2013).

248. L. G. Baum, J. C. Paulson, Sialyloligosaccharides of the respiratory epithelium in the selection of human influenza virus receptor specificity. *Acta Histochem. Suppl.* **40**, 35–8 (1990).

249. J. J. Skehel, D. C. Wiley, Receptor binding and membrane fusion in virus entry: the influenza hemagglutinin. *Annu. Rev. Biochem.* **69**, 531–569 (2000).

250. S. Yamada, Y. Suzuki, T. Suzuki, M. Q. Le, C. A. Nidom, Y. Sakai-Tagawa, Y. Muramoto, M. Ito, M. Kiso, T. Horimoto, K. Shinya, T. Sawada, M. Kiso, T. Usui, T. Murata, Y. Lin, A. Hay, L. F. Haire, D. J. Stevens, R. J. Russell, S. J. Gamblin, J. J. Skehel, Y. Kawaoka, Haemagglutinin mutations responsible for the binding of H5N1 influenza A viruses to human-type receptors. *Nature*. **444**, 378–382 (2006).

251. M. Imai, Y. Kawaoka, The role of receptor binding specificity in interspecies transmission of influenza viruses. *Curr. Opin. Virol.* **2**, 160–167 (2012).

252. J. M. Nicholls, R. W. Y. Chan, R. J. Russell, G. M. Air, J. S. M. Peiris, Evolving complexities of influenza virus and its receptors. *Trends Microbiol.* **16**, 149–157 (2008).

253. P. Isa, C. F. Arias, S. López, Role of sialic acids in rotavirus infection. *Glycoconj. J.* **23**, 27–37 (2006).

254. J. E. Heggelund, A. Varrot, A. Imberty, U. Krengel, Histo-blood group antigens as mediators of infections. *Curr. Opin. Struct. Biol.* **44**, 190–200 (2017).

255. G. V. Gee, A. S. Dugan, N. Tsomaia, D. F. Mierke, W. J. Atwood, The role of sialic acid in human polyomavirus infections. *Glycoconj. J.* **23**, 19–26 (2006).

256. W. Li, R. J. G. Hulswit, I. Widjaja, V. S. Raj, R. McBride, W. Peng, W. Widagdo, M. A. Tortorici, B. van Dieren, Y. Lang, J. W. M. van Lent, J. C. Paulson, C. A. M. de Haan, R. J. de Groot, F. J. M. van Kuppeveld, B. L. Haagmans, B.-J. Bosch, Identification of sialic acid-binding function for the Middle East respiratory syndrome coronavirus spike glycoprotein. *Proc. Natl. Acad. Sci.* **114**, E8508–E8517 (2017).

257. R. J. de Groot, Structure, function and evolution of the hemagglutinin-esterase proteins of corona- and toroviruses. *Glycoconj. J.* **23**, 59–72 (2006).

258. S. Olofsson, T. Bergström, Glycoconjugate glycans as viral receptors. *Ann. Med.* **37**, 154–172 (2005).

259. N. Izquierdo-Useros, M. Lorizate, P. J. McLaren, A. Telenti, H.-G. Kräusslich, J. Martinez-Picado, HIV-1 capture and transmission by dendritic cells: The role of viral glycolipids and the cellular receptor siglec-1. *PLoS Pathog.* **10**, e1004146 (2014).

260. T. Yoshida-Moriguchi, K. P. Campbell, Matriglycan: a novel polysaccharide that links dystroglycan to the basement membrane. *Glycobiology*. **25**, 702–713 (2015).

261. T. Yoshida-Moriguchi, T. Willer, M. E. Anderson, D. Venzke, T. Whyte, F. Muntoni, H. Lee, S. F. Nelson, L. Yu, K. P. Campbell, SGK196 is a glycosylation-specific O-mannose kinase required for dystroglycan function. *Science*. **341**, 896–899 (2013).

262. L. T. Jae, M. Raaben, A. S. Herbert, A. I. Kuehne, A. S. Wirchnianski, T. K. Soh, S. H. Stubbs, H. Janssen, M. Damme, P. Saftig, S. P. Whelan, J. M. Dye, T. R. Brummelkamp, Lassa virus entry requires a trigger-induced receptor switch. *Science*. **344**, 1506–1510 (2014).

263. W. Cao, M. D. Henry, P. Borrow, H. Yamada, J. H. Elder, E. V Ravkov, S. T. Nichol, R. W. Compans, K. P. Campbell, M. B. Oldstone, Identification of α-dystroglycan as a receptor for lymphocytic choriomeningitis virus and Lassa fever virus. *Science*. **282**, 2079–81 (1998).

264. G. Pasqual, J. M. Rojek, M. Masin, J.-Y. Chatton, S. Kunz, Old World arenaviruses enter the host cell via the multivesicular body and depend on the endosomal sorting complex required for transport. *PLoS Pathog.* **7**, e1002232 (2011).

265. M. Patel, M. Yanagishita, G. Roderiquez, D. C. Bou-Habib, T. Oravecz, V. C. Hascall, M. A. Norcross, Cell-surface heparan sulfate proteoglycan mediates HIV-1 infection of T-cell lines. *AIDS Res. Hum. Retroviruses*. **9**, 167–174 (1993).

266. C. D. O'Donnell, D. Shukla, The importance of heparan sulfate in herpesvirus infection. *Virol. Sin.* **23**, 383–393 (2008).

267. P. Hilgard, R. Stockert, Heparan sulfate proteoglycans initiate dengue virus infection of hepatocytes. *Hepatology*. **32**, 1069–1077 (2000).

268. D. Shukla, P. G. Spear, Herpesviruses and heparan sulfate: an intimate relationship in aid of viral entry. *J. Clin. Invest.* **108**, 503–10 (2001).

269. N. Peerboom, S. Block, N. Altgärde, O. Wahlsten, S. Möller, M. Schnabelrauch, E. Trybala, T. Bergström, M. Bally, Binding kinetics and lateral mobility of HSV-1 on end-grafted sulfated glycosaminoglycans. *Biophys. J.* **113**, 1223–1234 (2017).

270. N. Altgärde, C. Eriksson, N. Peerboom, T. Phan-Xuan, S. Moeller, M. Schnabelrauch, S. Svedhem, E. Trybala, T. Bergström, M. Bally, Mucin-like region of Herpes Simplex Virus type 1 attachment protein glycoprotein C (gC) modulates the virus-glycosaminoglycan interaction. *J. Biol. Chem.* **290**, 21473–21485 (2015).

271. R. S. Green, E. L. Stone, M. Tenno, E. Lehtonen, M. G. Farquhar, J. D. Marth, Mammalian N-glycan branching protects against innate immune self-recognition and inflammation in autoimmune disease pathogenesis. *Immunity*. **27**, 308–320 (2007).

272. C. Auriti, G. Prencipe, M. Moriondo, I. Bersani, C. Bertaina, V. Mondì, R. Inglese, Mannose-binding lectin: biologic characteristics and role in the susceptibility to infections and ischemia-reperfusion related injury in critically ill neonates. *J. Immunol. Res.* **2017**, 7045630 (2017).

273. M. Kuhlman, K. Joiner, R. A. Ezekowitz, The human mannose-binding protein functions as an opsonin. *J. Exp. Med.* **169**, 1733–45 (1989).

274. A. Miller, A. Phillips, J. Gor, R. Wallis, S. J. Perkins, Near-planar solution structures of mannose-binding lectin oligomers provide insight on activation of lectin pathway of complement. *J. Biol. Chem.* **287**, 3930–45 (2012).

275. M. Matsushita, The lectin pathway of the complement system. *Microbiol. Immunol.* **40**, 887–893 (1996).

276. R. Wallis, Interactions between mannose-binding lectin and MASPs during complement activation by the lectin pathway. *Immunobiology*. **212**, 289–99 (2007).

277. C.-B. Chen, R. Wallis, Two mechanisms for mannose-binding protein modulation of the activity of its associated serine proteases. *J. Biol. Chem.* **279**, 26058–26065 (2004).

278. M. Matsushita, T. Fujita, Ficolins and the lectin complement pathway. *Immunol. Rev.* **180**, 78–85 (2001).

279. A. Fuchs, T.-Y. Lin, D. W. Beasley, C. M. Stover, W. J. Schwaeble, T. C. Pierson, M. S. Diamond, Direct complement restriction of Flavivirus infection requires glycan recognition by mannose-binding lectin. *Cell Host Microbe*. **8**, 186–195 (2010).

280. G. T. Spear, M. R. Zariffard, J. Xin, M. Saifuddin, Inhibition of DC-SIGN-mediated trans infection of T cells by mannose-binding lectin. *Immunology*. **110**, 80–5 (2003).

281. X. Ji, G. G. Olinger, S. Aris, Y. Chen, H. Gewurz, G. T. Spear, Mannose-binding lectin binds to Ebola and Marburg envelope glycoproteins, resulting in blocking of virus interaction with DC-SIGN and complement-mediated virus neutralization. *J. Gen. Virol.* **86**, 2535–2542 (2005).

282. E. M. Anders, C. A. Hartley, P. C. Reading, R. A. B. Ezekowitz, Complement-dependent neutralization of influenza virus by a serum mannose-binding lectin. *J. Gen. Virol.* **75**, 615–622 (1994).

283. Y. Zhou, K. Lu, S. Pfefferle, S. Bertram, I. Glowacka, C. Drosten, S. Pohlmann, G. Simmons, A single asparagine-linked glycosylation site of the severe acute respiratory syndrome Coronavirus spike glycoprotein facilitates inhibition by

mannose-binding lectin through multiple mechanisms. *J. Virol.* **84**, 8753–8764 (2010).

284. A. M. Pastva, J. R. Wright, K. L. Williams, Immunomodulatory roles of surfactant proteins A and D: implications in lung disease. *Proc. Am. Thorac. Soc.* **4**, 252–7 (2007).

285. K. L. Hartshorn, M. R. White, V. Shepherd, K. Reid, J. C. Jensenius, E. C. Crouch, Mechanisms of anti-influenza activity of surfactant proteins A and D: comparison with serum collectins. *Am. J. Physiol.* **273**, L1156-66 (1997).

286. E. Crouch, K. Hartshorn, T. Horlacher, B. McDonald, K. Smith, T. Cafarella, B. Seaton, P. H. Seeberger, J. Head, Recognition of mannosylated ligands and Influenza A virus by human surfactant protein D: contributions of an extended site and residue 343. *Biochemistry*. **48**, 3335–3345 (2009).

287. M. L. B. Hillaire, M. van Eijk, S. E. van Trierum, D. van Riel, X. Saelens, R. A. Romijn, W. Hemrika, R. A. M. Fouchier, T. Kuiken, A. D. M. E. Osterhaus, H. P. Haagsman, G. F. Rimmelzwaan, Assessment of the antiviral properties of recombinant porcine SP-D against various Influenza A viruses in vitro. *PLoS One*. **6**, e25005 (2011).

288. C. A. Benne, B. Benaissa-Trouw, J. A. G. Van Strijp, C. A. Kraaijeveld, J. F. F. Van Iwaarden, Surfactant protein A, but not surfactant protein D, is an opsonin for influenza A virus phagocytosis by rat alveolar macrophages. *Eur. J. Immunol.* **27**, 886–890 (1997).

289. D. J. Vigerust, K. B. Ulett, K. L. Boyd, J. Madsen, S. Hawgood, J. A. McCullers, N-linked glycosylation attenuates H3N2 influenza viruses. *J. Virol.* **81**, 8593–600 (2007).

290. C. J. Funk, J. Wang, Y. Ito, E. A. Travanty, D. R. Voelker, K. V Holmes, R. J. Mason, Infection of human alveolar macrophages by human coronavirus strain 229E. *J. Gen. Virol.* **93**, 494–503 (2012).

291. A. M. LeVine, J. Elliott, J. A. Whitsett, A. Srikiatkhachorn, E. Crouch, N. DeSilva, T. Korfhagen, Surfactant protein-D enhances phagocytosis and pulmonary clearance of respiratory syncytial virus. *Am. J. Respir. Cell Mol. Biol.* **31**, 193–199 (2004).

292. E. L. Levroney, H. C. Aguilar, J. A. Fulcher, L. Kohatsu, K. E. Pace, M. Pang, K. B. Gurney, L. G. Baum, B. Lee, Novel innate immune functions for galectin-1: galectin-1 inhibits cell fusion by Nipah virus envelope glycoproteins and augments dendritic cell secretion of proinflammatory cytokines. *J. Immunol.* **175**, 413–20 (2005).

293. O. B. Garner, H. C. Aguilar, J. A. Fulcher, E. L. Levroney, R. Harrison, L. Wright, L. R. Robinson, V. Aspericueta, M. Panico, S. M. Haslam, H. R. Morris, A. Dell, B. Lee, L. G. Baum, Endothelial galectin-1 binds to specific glycans on Nipah virus fusion protein and inhibits maturation, mobility, and function to block syncytia formation. *PLoS Pathog.* **6**, e1000993 (2010).

294. O. B. Garner, T. Yun, O. Pernet, H. C. Aguilar, A. Park, T. A. Bowden, A. N. Freiberg, B. Lee, L. G. Baum, Timing of galectin-1 exposure differentially modulates Nipah virus entry and syncytium formation in endothelial cells. *J. Virol.* **89**, 2520–2529 (2015).

295. M.-L. Yang, Y.-H. Chen, S.-W. Wang, Y.-J. Huang, C.-H. Leu, N.-C. Yeh, C.-Y.

Chu, C.-C. Lin, G.-S. Shieh, Y.-L. Chen, J.-R. Wang, C.-H. Wang, C.-L. Wu, A.-L. Shiau, Galectin-1 binds to influenza virus and ameliorates influenza virus pathogenesis. *J. Virol.* **85**, 10010–20 (2011).

296. M. Ouellet, S. Mercier, I. Pelletier, S. Bounou, J. Roy, J. Hirabayashi, S. Sato, M. J. Tremblay, Galectin-1 acts as a soluble host factor that promotes HIV-1 infectivity through stabilization of virus attachment to host cells. *J. Immunol.* **174**, 4120–6 (2005).

297. C. St-Pierre, H. Manya, M. Ouellet, G. F. Clark, T. Endo, M. J. Tremblay, S. Sato, Host-soluble galectin-1 promotes HIV-1 replication through a direct interaction with glycans of viral gp120 and host CD4. *J. Virol.* **85**, 11742–11751 (2011).

298. C. N. Scanlan, R. Pantophlet, M. R. Wormald, E. O. Saphire, R. Stanfield, I. A. Wilson, H. Katinger, R. A. Dwek, P. M. Rudd, D. R. Burton, The broadly neutralizing anti-human immunodeficiency virus type 1 antibody 2G12 recognizes a cluster of α1→2 mannose residues on the outer face of gp120. *J. Virol.* **76**, 7306–7321 (2002).

299. C. Blattner, J. H. Lee, K. Sliepen, R. Derking, E. Falkowska, A. T. de la Peña, A. Cupo, J.-P. Julien, M. van Gils, P. S. Lee, W. Peng, J. C. Paulson, P. Poignard, D. R. Burton, J. P. Moore, R. W. Sanders, I. A. Wilson, A. B. Ward, Structural delineation of a quaternary, cleavage-dependent epitope at the gp41-gp120 interface on intact HIV-1 Env trimers. *Immunity*. **40**, 669–680 (2014).

300. E. Falkowska, K. M. Le, A. Ramos, K. J. Doores, J. H. Lee, C. Blattner, A. Ramirez, R. Derking, M. J. van Gils, C.-H. Liang, R. Mcbride, B. von Bredow, S. S. Shivatare, C.-Y. Wu, P.-Y. Chan-Hui, Y. Liu, T. Feizi, M. B. Zwick, W. C. Koff, M. S. Seaman, K. Swiderek, J. P. Moore, D. Evans, J. C. Paulson, C.-H. Wong, A. B. Ward, I. A. Wilson, R. W. Sanders, P. Poignard, D. R. Burton, Broadly neutralizing HIV antibodies define a glycan-dependent epitope on the prefusion conformation of gp41 on cleaved envelope trimers. *Immunity*. **40**, 657–68 (2014).

301. J. Huang, B. H. Kang, M. Pancera, J. H. Lee, T. Tong, Y. Feng, H. Imamichi, I. S. Georgiev, G.-Y. Chuang, A. Druz, N. A. Doria-Rose, L. Laub, K. Sliepen, M. J. van Gils, A. T. de la Peña, R. Derking, P.-J. Klasse, S. A. Migueles, R. T. Bailer, M. Alam, P. Pugach, B. F. Haynes, R. T. Wyatt, R. W. Sanders, J. M. Binley, A. B. Ward, J. R. Mascola, P. D. Kwong, M. Connors, Broad and potent HIV-1 neutralization by a human antibody that binds the gp41–gp120 interface. *Nature*. **515**, 138–142 (2014).

302. M. Pancera, S. Shahzad-ul-Hussan, N. A. Doria-Rose, J. S. McLellan, R. T. Bailer, K. Dai, S. Loesgen, M. K. Louder, R. P. Staupe, Y. Yang, B. Zhang, R. Parks, J. Eudailey, K. E. Lloyd, J. Blinn, S. M. Alam, B. F. Haynes, M. N. Amin, L.-X. Wang, D. R. Burton, W. C. Koff, G. J. Nabel, J. R. Mascola, C. A. Bewley, P. D. Kwong, Structural basis for diverse N-glycan recognition by HIV-1–neutralizing V1–V2–directed antibody PG16. *Nat. Struct. Mol. Biol.* **20**, 804–813 (2013).

303. Y. Watanabe, S. Vasiljevic, J. D. Allen, G. E. Seabright, H. M. E. Duyvesteyn, K. J. Doores, M. Crispin, W. B. Struwe, Signature of antibody domain exchange by native mass spectrometry and collision-induced unfolding. *Anal. Chem.* **90**, 7325–7331 (2018).

304. A. Rouvinski, P. Guardado-Calvo, G. Barba-Spaeth, S. Duquerroy, M.-C. Vaney, C. M. Kikuti, M. E. Navarro Sanchez, W. Dejnirattisai, W. Wongwiwat, A. Haouz, C. Girard-Blanc, S. Petres, W. E. Shepard, P. Desprès, F. Arenzana-Seisdedos, P.

Dussart, J. Mongkolsapaya, G. R. Screaton, F. A. Rey, Recognition determinants of broadly neutralizing human antibodies against dengue viruses. *Nature*. **520**, 109–113 (2015).

305. W. Dejnirattisai, W. Wongwiwat, S. Supasa, X. Zhang, X. Dai, A. Rouvinski, A. Jumnainsong, C. Edwards, N. T. H. Quyen, T. Duangchinda, J. M. Grimes, W.-Y. Tsai, C.-Y. Lai, W.-K. Wang, P. Malasit, J. Farrar, C. P. Simmons, Z. H. Zhou, F. A. Rey, J. Mongkolsapaya, G. R. Screaton, A new class of highly potent, broadly neutralizing antibodies isolated from viremic patients infected with dengue virus. *Nat. Immunol.* **16**, 170–177 (2015).

306. A. Rouvinski, W. Dejnirattisai, P. Guardado-Calvo, M.-C. Vaney, A. Sharma, S. Duquerroy, P. Supasa, W. Wongwiwat, A. Haouz, G. Barba-Spaeth, J. Mongkolsapaya, F. A. Rey, G. R. Screaton, Covalently linked dengue virus envelope glycoprotein dimers reduce exposure of the immunodominant fusion loop epitope. *Nat. Commun.* **8**, 15411 (2017).

307. W. Dejnirattisai, P. Supasa, W. Wongwiwat, A. Rouvinski, G. Barba-Spaeth, T. Duangchinda, A. Sakuntabhai, V.-M. Cao-Lormeau, P. Malasit, F. A. Rey, J. Mongkolsapaya, G. R. Screaton, Dengue virus sero-cross-reactivity drives antibody-dependent enhancement of infection with zika virus. *Nat. Immunol.* **17**, 1102–8 (2016).

308. T. Tokatlian, B. J. Read, C. A. Jones, D. W. Kulp, S. Menis, J. Y. H. Chang, J. M. Steichen, S. Kumari, J. D. Allen, E. L. Dane, A. Liguori, M. Sangesland, D. Lingwood, M. Crispin, W. R. Schief, D. J. Irvine, Innate immune recognition of glycans targets HIV nanoparticle immunogens to germinal centers. *Science*. **363**, 649–654 (2019).

309. J. E. Hudak, C. R. Bertozzi, Glycotherapy: new advances inspire a reemergence of glycans in medicine. *Chem. Biol.* **21**, 16–37 (2014).

310. A. Imberty, Y. M. Chabre, R. Roy, Glycomimetics and glycodendrimers as high affinity microbial anti-adhesins. *Chem. - A Eur. J.* **14**, 7490–7499 (2008).

311. M. von Itzstein, W.-Y. Wu, G. B. Kok, M. S. Pegg, J. C. Dyason, B. Jin, T. Van Phan, M. L. Smythe, H. F. White, S. W. Oliver, P. M. Colman, J. N. Varghese, D. M. Ryan, J. M. Woods, R. C. Bethell, V. J. Hotham, J. M. Cameron, C. R. Penn, Rational design of potent sialidase-based inhibitors of influenza virus replication. *Nature*. **363**, 418–423 (1993).

312. N. Asano, Glycosidase inhibitors: update and perspectives on practical use. *Glycobiology*. **13**, 93R – 104 (2003).

313. R. Copeland, A. Balasubramaniam, V. Tiwari, F. Zhang, A. Bridges, R. J. Linhardt, D. Shukla, J. Liu, Using a 3-O-sulfated heparin octasaccharide to inhibit the entry of herpes simplex virus type 1. *Biochemistry*. **47**, 5774–5783 (2008).

314. K. Schlie, A. Maisa, F. Lennartz, U. Stroher, W. Garten, T. Strecker, Characterization of Lassa Virus Glycoprotein Oligomerization and Influence of Cholesterol on Virus Replication. *J. Virol.* **84**, 983–992 (2010).

315. Y. Yuan, D. Cao, Y. Zhang, J. Ma, J. Qi, Q. Wang, G. Lu, Y. Wu, J. Yan, Y. Shi, X. Zhang, G. F. Gao, Cryo-EM structures of MERS-CoV and SARS-CoV spike glycoproteins reveal the dynamic receptor binding domains. *Nat. Commun.* **8**, 15092

(2017).

316. D. Wrapp, N. Wang, K. S. Corbett, J. A. Goldsmith, C.-L. Hsieh, O. Abiona, B. S. Graham, J. S. McLellan, Cryo-EM structure of the 2019-nCoV spike in the prefusion conformation. *Science* (2020), doi:10.1126/science.abb2507.

317. R. Andrabi, J. Pallesen, J. D. Allen, G. Song, J. Zhang, N. de Val, G. Gegg, K. Porter, C.-Y. Su, M. Pauthner, A. Newman, H. Bouton-Verville, F. Garces, I. A. Wilson, M. Crispin, B. H. Hahn, B. F. Haynes, L. Verkoczy, A. B. Ward, D. R. Burton, The chimpanzee SIV envelope trimer: structure and deployment as an HIV vaccine template. *Cell Rep.* **27**, 2426-2441.e6 (2019).

318. D. C. Ekiert, A. K. Kashyap, J. Steel, A. Rubrum, G. Bhabha, R. Khayat, J. H. Lee, M. A. Dillon, R. E. O'Neil, A. M. Faynboym, M. Horowitz, L. Horowitz, A. B. Ward, P. Palese, R. Webby, R. A. Lerner, R. R. Bhatt, I. A. Wilson, Cross-neutralization of influenza A viruses mediated by a single antibody loop. *Nature*. **489**, 526–32 (2012).

319. M. Alejandra Tortorici, A. C. Walls, Y. Lang, C. Wang, Z. Li, D. Koerhuis, G. J. Boons, B. J. Bosch, F. A. Rey, R. J. de Groot, D. Veesler, Structural basis for human coronavirus attachment to sialic acid receptors. *Nat. Struct. Mol. Biol.* **26**, 481–489 (2019).

320. Z. Li, A. C. A. Tomlinson, A. H. M. Wong, D. Zhou, M. Desforges, P. J. Talbot, S. Benlekbir, J. L. Rubinstein, J. M. Rini, The human coronavirus HCoV-229E S-protein structure and receptor binding. *eLife*. **8** (2019), doi:10.7554/eLife.51230.

321. E. Krissinel, K. Henrick, Inference of macromolecular assemblies from crystalline state. *J. Mol. Biol.* **372**, 774–797 (2007).

322. O. Ogbu, E. Ajuluchukwu, C. J. Uneke, Lassa fever in West African sub-region: an overview. *J. Vector Borne Dis.* **44**, 1–11 (2007).

323. V. N. Raabe, G. Kann, B. S. Ribner, A. Morales, J. B. Varkey, A. K. Mehta, G. M. Lyon, S. Vanairsdale, K. Faber, S. Becker, M. Eickmann, T. Strecker, S. Brown, K. Patel, P. De Leuw, G. Schuettfort, C. Stephan, H. Rabenau, J. D. Klena, P. E. Rollin, A. McElroy, U. Ströher, S. Nichol, C. S. Kraft, T. Wolf, S. Bell, C. Maloney, P. Cosper, N. Feistritzer, J. Lewin, B. Gartland, I. Horowitz, D. Pugh, C. Ritenour, J. Lewis, D. Hatcher, L. Scott-Harris, L. Ometer, K. Hardy, J. Broughton, R. Jackson, S. Thomas, T. Ash, C. Barnes, J. Breedlove, B. Bridgman, L. Darragh, T. Daye, D. Hillis, C. Johnson, J.-A. Johnson, D. LaFond, C. Lyons, J. Mamora, A. McCord, S. McDaniel, H. Morgan, J. Morgan, A. Sanchez, M. Simon, J. Slabach, K. Tirado, S. Watkins, T. Wilson, K. Logan, J. Buchanan, E. Burd, J. Cardella, B. Eaves, C. Evans, C. Hill, D. Igwe, K. Jenkins, M. Lindsey, J. Magee, S. McCarthy, R. Powers, J. Ritchie, J. Pack, S. Rogers, P. Olinger, K. Rengarajan, S. Thomaston, E. Meyer, E. Beck, P. Desroches, C. Hall, C. Walker, E. Baker, B. Hackman, J. Broughton, R. Jackson, J. Lewis, R. Brown-Haithco, F. Richardson, A. Krasilovsky, C. K. Jordan, S. Matthews, M. H. Lineberger, P. G. Gomes, G. McGee, P. Jones, L. Scott-Harris, J. Cain, R. Davis, T. Johnson, T. Pickett, A. Shaw, T. Truesdale, A. Isakov, S. Shartar, W. Miles, A. Jamison, J. Arevalo, G. Stallings, J. Christenbury, V. Dollard, M. De Gennaro, H. Korschun, T. Ziegler, D. P. Griffith, N. Dave, Favipiravir and Ribavirin Treatment of Epidemiologically Linked Cases of Lassa Fever. *Clin. Infect. Dis.* **65**, 855–859 (2017).

324. S. Baize, P. Marianneau, P. Loth, S. Reynard, A. Journeaux, M. Chevallier, N. Tordo,

V. Deubel, H. Contamin, Early and Strong Immune Responses Are Associated with Control of Viral Replication and Recovery in Lassa Virus-Infected Cynomolgus Monkeys. *J. Virol.* **83**, 5890–5903 (2009).

325. S. P. Fisher-Hoch, L. Hutwagner, B. Brown, J. B. McCormick, Effective vaccine for lassa fever. *J. Virol.* **74**, 6777–83 (2000).

326. I. S. Lukashevich, R. Carrion, M. S. Salvato, K. Mansfield, K. Brasky, J. Zapata, C. Cairo, M. Goicochea, G. E. Hoosien, A. Ticer, J. Bryant, H. Davis, R. Hammamieh, M. Mayda, M. Jett, J. Patterson, Safety, immunogenicity, and efficacy of the ML29 reassortant vaccine for Lassa fever in small non-human primates. *Vaccine*. **26**, 5246–54 (2008).

327. K. M. Johnson, J. B. McCormick, P. A. Webb, E. S. Smith, L. H. Elliott, I. J. King, Clinical Virology of Lassa Fever in Hospitalized Patients. *J. Infect. Dis.* **155**, 456–464 (1987).

328. P. B. Jahrling, R. A. Hesse, G. A. Eddy, K. M. Johnson, R. T. Callis, E. L. Stephen, Lassa Virus Infection of Rhesus Monkeys: Pathogenesis and Treatment with Ribavirin. *J. Infect. Dis.* **141**, 580–589 (1980).

329. M. Crispin, A. Zeltina, N. Zitzmann, T. A. Bowden, Native functionality and therapeutic targeting of arenaviral glycoproteins. *Curr. Opin. Virol.* **18**, 70–75 (2016).

330. A. Zeltina, T. A. Bowden, Human antibody pieces together the puzzle of the trimeric Lassa virus surface antigen. *Nat. Struct. Mol. Biol.* **24**, 559–560 (2017).

331. O. Lenz, J. ter Meulen, H.-D. Klenk, N. G. Seidah, W. Garten, The Lassa virus glycoprotein precursor GP-C is proteolytically processed by subtilase SKI-1/S1P. *Proc. Natl. Acad. Sci.* **98**, 12701–12705 (2001).

332. A. Shimon, O. Shani, R. Diskin, Structural Basis for Receptor Selectivity by the Whitewater Arroyo Mammarenavirus. *J. Mol. Biol.* **429**, 2825–2839 (2017).

333. K. M. Hastie, S. Igonet, B. M. Sullivan, P. Legrand, M. A. Zandonatti, J. E. Robinson, R. F. Garry, F. A. Rey, M. B. Oldstone, E. O. Saphire, Crystal structure of the prefusion surface glycoprotein of the prototypic arenavirus LCMV. *Nat. Struct. Mol. Biol.* **23**, 513–521 (2016).

334. S. Igonet, M.-C. Vaney, C. Vonrhein, G. Bricogne, E. A. Stura, H. Hengartner, B. Eschli, F. A. Rey, F. A. Rey, X-ray structure of the arenavirus glycoprotein GP2 in its postfusion hairpin conformation. *Proc. Natl. Acad. Sci.* **108**, 19967–19972 (2011).

335. J. York, J. H. Nunberg, Myristoylation of the Arenavirus Envelope Glycoprotein Stable Signal Peptide Is Critical for Membrane Fusion but Dispensable for Virion Morphogenesis. *J. Virol.* **90**, 8341–8350 (2016).

336. J. York, J. H. Nunberg, Role of the Stable Signal Peptide of Junin Arenavirus Envelope Glycoprotein in pH-Dependent Membrane Fusion. *J. Virol.* **80**, 7775–7780 (2006).

337. R. Eichler, O. Lenz, T. Strecker, M. Eickmann, H.-D. Klenk, W. Garten, Identification of Lassa virus glycoprotein signal peptide as a trans-acting maturation factor. *EMBO Rep.* **4**, 1084–8 (2003).

338. J. Oppliger, G. Torriani, A. Herrador, S. Kunz, Lassa Virus Cell Entry via Dystroglycan Involves an Unusual Pathway of Macropinocytosis. *J. Virol.* **90**, 6412–

6429 (2016).

339. H. Cohen-Dvashi, H. Israeli, O. Shani, A. Katz, R. Diskin, Role of LAMP1 binding and pH sensing by the spike complex of Lassa virus. *J. Virol.* **90**, 10329–10338 (2016).

340. R. Eichler, O. Lenz, W. Garten, T. Strecker, The role of single N-glycans in proteolytic processing and cell surface transport of the Lassa virus glycoprotein GP-C. *Virol. J.* **3**, 41 (2006).

341. K. Schlie, A. Maisa, F. Freiberg, A. Groseth, T. Strecker, W. Garten, Viral protein determinants of Lassa virus entry and release from polarized epithelial cells. *J. Virol.* **84**, 3178–88 (2010).

342. O. Lenz, J. ter Meulen, H. Feldmann, H. D. Klenk, W. Garten, Identification of a novel consensus sequence at the cleavage site of the Lassa virus glycoprotein. *J. Virol.* **74**, 11418–21 (2000).

343. M. M. Illick, L. M. Branco, J. N. Fair, K. A. Illick, A. Matschiner, R. Schoepp, R. F. Garry, M. C. Guttieri, Uncoupling GP1 and GP2 expression in the Lassa virus glycoprotein complex: implications for GP1 ectodomain shedding. *Virol. J.* **5**, 161 (2008).

344. C. Galan-Navarro, M. Rincon-Restrepo, G. Zimmer, E. Ollmann Saphire, J. A. Hubbell, S. Hirosue, M. A. Swartz, S. Kunz, Oxidation-sensitive polymersomes as vaccine nanocarriers enhance humoral responses against Lassa virus envelope glycoprotein. *Virology*. **512**, 161–171 (2017).

345. P. M. Rudd, R. A. Dwek, Glycosylation: Heterogeneity and the 3D Structure of Proteins. *Crit. Rev. Biochem. Mol. Biol.* **32**, 1–100 (1997).

346. R. Qian, C. Chen, K. J. Colley, Location and mechanism of alpha 2,6-sialyltransferase dimer formation. Role of cysteine residues in enzyme dimerization, localization, activity, and processing. *J. Biol. Chem.* **276**, 28641–9 (2001).

347. L. O. Tremblay, A. Herscovics, Cloning and expression of a specific human 1,2-mannosidase that trims Man9GlcNAc2 to Man8GlcNAc2 isomer B during N-glycan biosynthesis. *Glycobiology*. **9**, 1073–1078 (1999).

348. K. P. Coss, S. Vasiljevic, L. K. Pritchard, S. A. Krumm, M. Glaze, S. Madzorera, P. L. Moore, M. Crispin, K. J. Doores, HIV-1 Glycan Density Drives the Persistence of the Mannose Patch within an Infected Individual. *J. Virol.* **90**, 11132–11144 (2016).

349. J. E. Robinson, K. M. Hastie, R. W. Cross, R. E. Yenni, D. H. Elliott, J. A. Rouelle, C. B. Kannadka, A. A. Smira, C. E. Garry, B. T. Bradley, H. Yu, J. G. Shaffer, M. L. Boisen, J. N. Hartnett, M. A. Zandonatti, M. M. Rowland, M. L. Heinrich, L. Martínez-Sobrido, B. Cheng, J. C. de la Torre, K. G. Andersen, A. Goba, M. Momoh, M. Fullah, M. Gbakie, L. Kanneh, V. J. Koroma, R. Fonnie, S. C. Jalloh, B. Kargbo, M. A. Vandi, M. Gbetuwa, O. Ikponmwosa, D. A. Asogun, P. O. Okokhere, O. A. Follarin, J. S. Schieffelin, K. R. Pitts, J. B. Geisbert, P. C. Kulakoski, R. B. Wilson, C. T. Happi, P. C. Sabeti, S. M. Gevao, S. H. Khan, D. S. Grant, T. W. Geisbert, E. O. Saphire, L. M. Branco, R. F. Garry, Most neutralizing human monoclonal antibodies target novel epitopes requiring both Lassa virus glycoprotein subunits. *Nat. Commun.* **7**, 11544 (2016).

350. K. G. Andersen, B. J. Shapiro, C. B. Matranga, R. Sealfon, A. E. Lin, L. M. Moses,

O. A. Folarin, A. Goba, I. Odia, P. E. Ehiane, M. Momoh, E. M. England, S. Winnicki, L. M. Branco, S. K. Gire, E. Phelan, R. Tariyal, R. Tewhey, O. Omoniwa, M. Fullah, R. Fonnie, M. Fonnie, L. Kanneh, S. Jalloh, M. Gbakie, S. Saffa, K. Karbo, A. D. Gladden, J. Qu, M. Stremlau, M. Nekoui, H. K. Finucane, S. Tabrizi, J. J. Vitti, B. Birren, M. Fitzgerald, C. McCowan, A. Ireland, A. M. Berlin, J. Bochicchio, B. Tazon-Vega, N. J. Lennon, E. M. Ryan, Z. Bjornson, D. A. Milner, A. K. Lukens, N. Broodie, M. Rowland, M. Heinrich, M. Akdag, J. S. Schieffelin, D. Levy, H. Akpan, D. G. Bausch, K. Rubins, J. B. McCormick, E. S. Lander, S. Günther, L. Hensley, S. Okogbenin, S. F. Schaffner, P. O. Okokhere, S. H. Khan, D. S. Grant, G. O. Akpede, D. A. Asogun, A. Gnirke, J. Z. Levin, C. T. Happi, R. F. Garry, P. C. Sabeti, P. C. Sabeti, Clinical Sequencing Uncovers Origins and Evolution of Lassa Virus. *Cell*. **162**, 738–750 (2015).

351. L. T. Jae, M. Raaben, M. Riemersma, E. van Beusekom, V. A. Blomen, A. Velds, R. M. Kerkhoven, J. E. Carette, H. Topaloglu, P. Meinecke, M. W. Wessels, D. J. Lefeber, S. P. Whelan, H. van Bokhoven, T. R. Brummelkamp, Deciphering the Glycosylome of Dystroglycanopathies Using Haploid Screens for Lassa Virus Entry. *Science*. **340**, 479–483 (2013).

352. R. B. Brouillette, E. K. Phillips, N. Ayithan, W. Maury, Differences in Glycoprotein Complex Receptor Binding Site Accessibility Prompt Poor Cross-Reactivity of Neutralizing Antibodies between Closely Related Arenaviruses. *J. Virol.* **91** (2017), doi:10.1128/JVI.01454-16.

353. S. Mahmutovic, L. Clark, S. C. Levis, A. M. Briggiler, D. A. Enria, S. C. Harrison, J. Abraham, Molecular Basis for Antibody-Mediated Neutralization of New World Hemorrhagic Fever Mammarenaviruses. *Cell Host Microbe*. **18**, 705–13 (2015).

354. A. M. Waterhouse, J. B. Procter, D. M. A. Martin, M. Clamp, G. J. Barton, Jalview Version 2--a multiple sequence alignment editor and analysis workbench. *Bioinformatics*. **25**, 1189–1191 (2009).

355. A. Antanasijevic, G. Ueda, P. J. Brouwer, J. Copps, D. Huang, J. Allen, C. Cottrell, A. Yasmeen, L. Sewall, I. Bontjer, T. Ketas, H. Turner, Z. Berndsen, P. J. Klasse, M. Crispin, D. Nemazee, J. Moore, R. Sanders, N. King, D. Baker, A. Ward, *bioRxiv*, in press, doi:10.1101/2020.01.31.929273.

356. J. Marcandalli, B. Fiala, S. Ols, M. Perotti, W. de van der Schueren, J. Snijder, E. Hodge, M. Benhaim, R. Ravichandran, L. Carter, W. Sheffler, L. Brunner, M. Lawrenz, P. Dubois, A. Lanzavecchia, F. Sallusto, K. K. Lee, D. Veesler, C. E. Correnti, L. J. Stewart, D. Baker, K. Loré, L. Perez, N. P. King, Induction of Potent Neutralizing Antibody Responses by a Designed Protein Nanoparticle Vaccine for Respiratory Syncytial Virus. *Cell*. **176**, 1420-1431.e17 (2019).

357. P. J. M. Brouwer, A. Antanasijevic, Z. Berndsen, A. Yasmeen, B. Fiala, T. P. L. Bijl, I. Bontjer, J. B. Bale, W. Sheffler, J. D. Allen, A. Schorcht, J. A. Burger, M. Camacho, D. Ellis, C. A. Cottrell, A. J. Behrens, M. Catalano, I. del Moral-Sánchez, T. J. Ketas, C. LaBranche, M. J. van Gils, K. Sliepen, L. J. Stewart, M. Crispin, D. C. Montefiori, D. Baker, J. P. Moore, P. J. Klasse, A. B. Ward, N. P. King, R. W. Sanders, Enhancing and shaping the immunogenicity of native-like HIV-1 envelope trimers with a two-component protein nanoparticle. *Nat. Commun.* **10**, 1–17 (2019).

358. P. Gagneux, M. Aebi, A. Varki, *Evolution of Glycan Diversity* (Cold Spring Harbor

Laboratory Press, 2015).

359. G. HUAI, P. QI, H. YANG, Y. WANG, H. Yang, H. Yang, Y. Wang, Y. Wang, Characteristics of α-Gal epitope, anti-Gal antibody, α1,3 galactosyltransferase and its clinical exploitation (Review). *Int. J. Mol. Med.* **37**, 11–20 (2016).

360. A. K. Dey, A. Cupo, G. Ozorowski, V. K. Sharma, A. Behrens, E. P. Go, T. J. Ketas, A. Yasmeen, P. J. Klasse, E. Sayeed, H. Desaire, M. Crispin, I. A. Wilson, R. W. Sanders, T. Hassell, A. B. Ward, J. P. Moore, cGMP production and analysis of BG505 SOSIP.664, an extensively glycosylated, trimeric HIV-1 envelope glycoprotein vaccine candidate. *Biotechnol. Bioeng.* **115**, 885–899 (2018).

361. D. Reusch, M. L. Tejada, Fc glycans of therapeutic antibodies as critical quality attributes. *Glycobiology*. **25**, 1325–1334 (2015).

362. J. Cui, F. Li, Z. L. Shi, Origin and evolution of pathogenic coronaviruses. *Nat. Rev. Microbiol.* **17** (2019), pp. 181–192.

363. J. S. M. Peiris, Y. Guan, K. Y. Yuen, Severe acute respiratory syndrome. *Nat. Med.* **10**, S88–S97 (2004).

364. A. M. Zaki, S. van Boheemen, T. M. Bestebroer, A. D. M. E. Osterhaus, R. A. M. Fouchier, Isolation of a novel coronavirus from a man with pneumonia in Saudi Arabia. *N. Engl. J. Med.* **367**, 1814–1820 (2012).

365. C. Huang, Y. Wang, X. Li, L. Ren, J. Zhao, Y. Hu, L. Zhang, G. Fan, J. Xu, X. Gu, Clinical features of patients infected with 2019 novel coronavirus in Wuhan , China. *Lancet*. **6736**, 1–10 (2020).

366. E. I. Azhar, S. A. El-Kafrawy, S. A. Farraj, A. M. Hassan, M. S. Al-Saeed, A. M. Hashem, T. A. Madani, Evidence for camel-to-human transmission of MERS coronavirus. *N. Engl. J. Med.* **370**, 2499–2505 (2014).

367. W. Li, Z. Shi, M. Yu, W. Ren, C. Smith, J. H. Epstein, H. Wang, G. Crameri, Z. Hu, H. Zhang, J. Zhang, J. McEachern, H. Field, P. Daszak, B. T. Eaton, S. Zhang, L.-F. Wang, Bats are natural reservoirs of SARS-like coronaviruses. *Science*. **310**, 676–679 (2005).

368. Y. Zhou, S. Jiang, L. Du, Prospects for a MERS-CoV spike vaccine. *Expert Rev. Vaccines*. **17**, 677–686 (2018).

369. J. Xu, W. Jia, P. Wang, S. Zhang, X. Shi, X. Wang, L. Zhang, Antibodies and vaccines against Middle East respiratory syndrome coronavirus. *Emerg. Microb. Infect.* **8** (2019), pp. 841–856.

370. M. A. Tortorici, D. Veesler, in *Adv. Virus Res.* (2019), vol. 105, pp. 93–116.

371. V. S. Raj, H. Mou, S. L. Smits, D. H. W. Dekkers, M. A. Müller, R. Dijkman, D. Muth, J. A. A. Demmers, A. Zaki, R. A. M. Fouchier, V. Thiel, C. Drosten, P. J. M. Rottier, A. D. M. E. Osterhaus, B. J. Bosch, B. L. Haagmans, Dipeptidyl peptidase 4 is a functional receptor for the emerging human coronavirus-EMC. *Nature*. **495**, 251–254 (2013).

372. W. Li, M. J. Moore, N. Vasilieva, J. Sui, S. K. Wong, M. A. Berne, M. Somasundaran, J. L. Sullivan, K. Luzuriaga, T. C. Greenough, H. Choe, M. Farzan, Angiotensin-converting enzyme 2 is a functional receptor for the SARS coronavirus. *Nature*. **426**, 450–454 (2003).

373. P. Zhou, X.-L. Yang, X.-G. Wang, B. Hu, L. Zhang, W. Zhang, H.-R. Si, Y. Zhu, B. Li, C.-L. Huang, H.-D. Chen, J. Chen, Y. Luo, H. Guo, R.-D. Jiang, M.-Q. Liu, Y. Chen, X.-R. Shen, X. Wang, X.-S. Zheng, K. Zhao, Q.-J. Chen, F. Deng, L.-L. Liu, B. Yan, F.-X. Zhan, Y.-Y. Wang, G.-F. Xiao, Z.-L. Shi, A pneumonia outbreak associated with a new coronavirus of probable bat origin. *Nature*, 1–4 (2020).

374. T. J. Yang, Y. C. Chang, T. P. Ko, P. Draczkowski, Y. C. Chien, Y. C. Chang, K. P. Wu, K. H. Khoo, H. W. Chang, S. Te Danny Hsu, Cryo-EM analysis of a feline coronavirus spike protein reveals a unique structure and camouflaging glycans. *Proc. Natl. Acad. Sci. U. S. A.* **117**, 1438–1446 (2020).

375. G. B. E. Stewart-Jones, C. Soto, T. Lemmin, G.-Y. Chuang, A. Druz, R. Kong, P. V Thomas, K. Wagh, T. Zhou, A.-J. Behrens, T. Bylund, C. W. Choi, J. R. Davison, I. S. Georgiev, M. G. Joyce, Y. Do Kwon, M. Pancera, J. Taft, Y. Yang, B. Zhang, S. S. Shivatare, V. S. Shivatare, C.-C. D. Lee, C.-Y. Wu, C. A. Bewley, D. R. Burton, W. C. Koff, M. Connors, M. Crispin, U. Baxa, B. T. Korber, C.-H. Wong, J. R. Mascola, P. D. Kwong, Trimeric HIV-1-Env structures define glycan shields from Clades A, B, and G. *Cell*. **165**, 813–26 (2016).

376. M. Crispin, A. B. Ward, I. A. Wilson, Structure and immune recognition of the HIV glycan shield. *Annu. Rev. Biophys.* **47**, 499–523 (2018).

377. Y. Watanabe, T. A. Bowden, I. A. Wilson, M. Crispin, Exploitation of glycosylation in enveloped virus pathobiology. *Biochim. Biophys. Acta*. **1863**, 1480–1497 (2019).

378. W. H. Yu, P. Zhao, M. Draghi, C. Arevalo, C. B. Karsten, T. J. Suscovich, B. Gunn, H. Streeck, A. L. Brass, M. Tiemeyer, M. Seaman, J. R. Mascola, L. Wells, D. A. Lauffenburger, G. Alter, Exploiting glycan topography for computational design of Env glycoprotein antigenicity. *PLoS Comput. Biol.* **14**, e1006093 (2018).

379. T. Zhou, N. A. Doria-Rose, C. Cheng, G. B. E. Stewart-Jones, G.-Y. Chuang, M. Chambers, A. Druz, H. Geng, K. McKee, Y. Do Kwon, S. O'Dell, M. Sastry, S. D. Schmidt, K. Xu, L. Chen, R. E. Chen, M. K. Louder, M. Pancera, T. G. Wanninger, B. Zhang, A. Zheng, S. K. Farney, K. E. Foulds, I. S. Georgiev, M. G. Joyce, T. Lemmin, S. Narpala, R. Rawi, C. Soto, J.-P. Todd, C.-H. Shen, Y. Tsybovsky, Y. Yang, P. Zhao, B. F. Haynes, L. Stamatatos, M. Tiemeyer, L. Wells, D. G. Scorpio, L. Shapiro, A. B. McDermott, J. R. Mascola, P. D. Kwong, Quantification of the impact of the HIV-1-glycan shield on antibody elicitation. *Cell Rep.* **19**, 719–732 (2017).

380. E. P. Go, H. Ding, S. Zhang, R. P. Ringe, N. Nicely, D. Hua, R. T. Steinbock, M. Golabek, J. Alin, S. M. Alam, A. Cupo, B. F. Haynes, J. C. Kappes, J. P. Moore, J. G. Sodroski, H. Desaire, Glycosylation benchmark profile for HIV-1 envelope glycoprotein production based on eleven env trimers. *J. Virol.* **91**, e02428-16 (2017).

381. E. P. Go, A. Herschhorn, C. Gu, L. Castillo-Menendez, S. Zhang, Y. Mao, H. Chen, H. Ding, J. K. Wakefield, D. Hua, H.-X. Liao, J. C. Kappes, J. Sodroski, H. Desaire, Comparative analysis of the glycosylation profiles of membrane-anchored HIV-1 envelope glycoprotein trimers and soluble gp140. *J. Virol.* **89**, 8245–8257 (2015).

382. A. A. Hargett, Q. Wei, B. Knoppova, S. Hall, Z.-Q. Huang, A. Prakash, T. J. Green, Z. Moldoveanu, M. Raska, J. Novak, M. B. Renfrow, Defining HIV-1 envelope N-glycan microdomains through site-specific heterogeneity profiles. *J. Virol.* **93**, e01177-18 (2018).

383. M. L. Ng, S. H. Tan, E. E. See, E. E. Ooi, A. E. Ling, Proliferative growth of SARS coronavirus in Vero E6 cells. *J. Gen. Virol.* **84**, 3291–3303 (2003).

384. Z. T. Berndsen, S. Chakraborty, X. Wang, C. A. Cotrell, J. L. Torres, J. K. Diedrich, C. A. López, J. R. Yates, M. J. Van-Gils, J. C. Paulson, S. Gnanakaran, A. B. Ward, Visualization of the HIV-1 Env glycan shield across scales. *bioRxiv*, 839217 (2019).

385. R. N. Kirchdoerfer, N. Wang, J. Pallesen, D. Wrapp, H. L. Turner, C. A. Cottrell, K. S. Corbett, B. S. Graham, J. S. McLellan, A. B. Ward, Stabilized coronavirus spikes are resistant to conformational changes induced by receptor recognition or proteolysis. *Sci. Rep.* **8**, 15701 (2018).

386. T. Lemmin, C. Soto, J. Stuckey, P. D. Kwong, Microsecond dynamics and network analysis of the HIV-1 SOSIP Env trimer reveal collective behavior and conserved microdomains of the glycan shield. *Structure*. **25**, 1631-1639.e2 (2017).

387. S. Chakraborty, Z. T. Berndsen, N. W. Hengartner, B. T. Korber, A. B. Ward, S. Gnanakaran, A network-based approach for quantifying the resilience and vulnerability of HIV-1 native glycan shield. *bioRxiv*, 846071 (2019).

388. M. O. Altman, M. Angel, I. Košík, N. S. Trovão, S. J. Zost, J. S. Gibbs, L. Casalino, R. E. Amaro, S. E. Hensley, M. I. Nelson, J. W. Yewdell, Human influenza a virus hemagglutinin glycan evolution follows a temporal pattern to a glycan limit. *mBio*. **10**, e00204-19 (2019).

389. G. Bajic, M. J. Maron, Y. Adachi, T. Onodera, K. R. McCarthy, C. E. McGee, G. D. Sempowski, Y. Takahashi, G. Kelsoe, M. Kuraoka, A. G. Schmidt, Influenza antigen engineering focuses immune responses to a subdominant but broadly protective viral epitope. *Cell Host Microbe*. **25**, 827-835.e6 (2019).

390. C. Y. Wu, C. W. Lina, T. I. Tsaia, C. C. D. Leea, H. Y. Chuanga, J. Bin Chena, M. H. Tsaia, B. R. Chena, P. W. Loa, C. P. Liua, V. S. Shivatarea, C. H. Wonga, Influenza A surface glycosylation and vaccine design. *Proc. Natl. Acad. Sci. U. S. A.* **114**, 280–285 (2017).

391. H. Bisht, A. Roberts, L. Vogel, A. Bukreyev, P. L. Collins, B. R. Murphy, K. Subbarao, B. Moss, Severe acute respiratory syndrome coronavirus spike protein expressed by attenuated vaccinia virus protectively immunizes mice. *Proc. Natl. Acad. Sci. U. S. A.* **101**, 6641–6646 (2004).

392. U. J. Buchholz, A. Bukreyev, L. Yang, E. W. Lamirande, B. R. Murphy, K. Subbarao, P. L. Collins, Contributions of the structural proteins of severe respiratory syndrome coronavirus to protective immunity. *Proc. Natl. Acad. Sci. U. S. A.* **101**, 9804–9809 (2004).

393. Z. Y. Yang, W. P. Kong, Y. Huang, A. Roberts, B. R. Murphy, K. Subbarao, G. J. Nabel, A DNA vaccine induces SARS coronavirus neutralization and protective immunity in mice. *Nature*. **428**, 561–564 (2004).

394. C. Y. Yong, H. K. Ong, S. K. Yeap, K. L. Ho, W. S. Tan, Recent advances in the vaccine development against Middle East Respiratory Syndrome-coronavirus. *Front. Microbiol.* **10**, 1781 (2019).

395. J. M. Cuevas, R. Geller, R. Garijo, J. López-Aldeguer, R. Sanjuán, Extremely high mutation rate of HIV-1 in vivo. *PLoS Biol.* **13**, e1002251 (2015).

396. H. Subbaraman, M. Schanz, A. Trkola, Broadly neutralizing antibodies: What is needed to move from a rare event in HIV-1 infection to vaccine efficacy? *Retrovirology*. **15** (2018), , doi:10.1186/s12977-018-0433-2.

397. X. Yang, Y. Yu, J. Xu, H. Shu, J. Xia, H. Liu, Y. Wu, L. Zhang, Z. Yu, M. Fang, T. Yu, Y. Wang, S. Pan, X. Zou, S. Yuan, Y. Shang, Clinical course and outcomes of critically ill patients with SARS-CoV-2 pneumonia in Wuhan, China: a single-centered, retrospective, observational study. *Lancet Respir. Med.* (2020), doi:10.1016/S2213-2600(20)30079-5.

398. M. Letko, A. Marzi, V. Munster, Functional assessment of cell entry and receptor usage for SARS-CoV-2 and other lineage B betacoronaviruses. *Nat. Microbiol.*, 1–8 (2020).

399. A. C. Walls, Y.-J. Park, M. A. Tortorici, A. Wall, A. T. McGuire, D. Veesler, Structure, Function, and Antigenicity of the SARS-CoV-2 Spike Glycoprotein. *Cell* (2020), doi:10.1016/j.cell.2020.02.058.

400. F.Krammer, F.Amanat, SARS-CoV-2 vaccines: status report. *Immunity*, 1–7 (2020).

401. Y. Watanabe, Z. T. Berndsen, J. Raghwani, G. E. Seabright, J. D. Allen, J. S. McLellan, I. A. Wilson, T. A. Bowden, A. B. Ward, M. Crispin, *bioRxiv*, in press, doi:10.1101/2020.02.20.957472.

402. M. Dalziel, M. Crispin, C. N. Scanlan, N. Zitzmann, R. A. Dwek, Emerging principles for the therapeutic exploitation of glycosylation. *Science*. **343** (2014), , doi:10.1126/science.1235681.

403. C. N. Scanlan, J. Offer, N. Zitzmann, R. A. Dwek, Exploiting the defensive sugars of HIV-1 for drug and vaccine design. *Nature*. **446**, 1038–1045 (2007).

404. P. Venkatagopalan, S. M. Daskalova, L. A. Lopez, K. A. Dolezal, B. G. Hogue, Coronavirus envelope (E) protein remains at the site of assembly. *Virology*. **478**, 75–85 (2015).

405. A. A. Hargett, M. B. Renfrow, Glycosylation of viral surface proteins probed by mass spectrometry. *Curr. Opin. Virol.* **36** (2019), pp. 56–66.

406. M. Bianchi, H. L. Turner, B. Nogal, C. A. Cottrell, D. Oyen, M. Pauthner, R. Bastidas, R. Nedellec, L. E. McCoy, I. A. Wilson, D. R. Burton, A. B. Ward, L. Hangartner, Electron-Microscopy-Based Epitope Mapping Defines Specificities of Polyclonal Antibodies Elicited during HIV-1 BG505 Envelope Trimer Immunization. *Immunity*. **49**, 288-300.e8 (2018).

407. D. Sok, K. J. Doores, B. Briney, K. M. Le, K. L. Saye-Francisco, A. Ramos, D. W. Kulp, J. P. Julien, S. Menis, L. Wickramasinghe, M. S. Seaman, W. R. Schief, I. A. Wilson, P. Poignard, D. R. Burton, Promiscuous glycan site recognition by antibodies to the high-mannose patch of gp120 broadens neutralization of HIV. *Sci. Transl. Med.* **6**, 236ra63 (2014).

408. D. Pinto, Y.-J. Park, M. Beltramello, A. C. Walls, M. A. Tortorici, S. Bianchi, S. Jaconi, K. Culap, F. Zatta, A. De Marco, A. Peter, B. Guarino, R. Spreafico, E. Cameroni, J. B. Case, R. E. Chen, C. Havenar-Daughton, G. Snell, A. Telenti, H. W. Virgin, A. Lanzavecchia, M. S. Diamond, K. Fink, D. Veesler, D. Corti, *bioRxiv*, in press, doi:10.1101/2020.04.07.023903.

409. A. Trkola, M. Purtscher, T. Muster, C. Ballaun, A. Buchacher, N. Sullivan, K. Srinivasan, J. Sodroski, J. P. Moore, H. Katinger, Human monoclonal antibody 2G12 defines a distinctive neutralization epitope on the gp120 glycoprotein of human immunodeficiency virus type 1. *J. Virol.* **70**, 1100–1108 (1996).

410. A. Buchacher, R. Predl, K. Strutzenberger, W. Steinfellner, A. Trkola, M. Purtscher, G. Gruber, C. Tauer, F. Steindl, A. Jungbauer, H. Katinger, Generation of Human Monoclonal Antibodies against HIV-1 Proteins; Electrofusion and Epstein-Barr Virus Transformation for Peripheral Blood Lymphocyte Immortalization. *AIDS Res. Hum. Retroviruses*. **10**, 359–369 (1994).

411. L. M. Walker, S. K. Phogat, P.-Y. Chan-Hui, D. Wagner, P. Phung, J. L. Goss, T. Wrin, M. D. Simek, S. Fling, J. L. Mitcham, J. K. Lehrman, F. H. Priddy, O. A. Olsen, S. M. Frey, P. W. Hammond, S. Kaminsky, T. Zamb, M. Moyle, W. C. Koff, P. Poignard, D. R. Burton, D. R. Burton, Broad and Potent Neutralizing Antibodies from an African Donor Reveal a New HIV-1 Vaccine Target. *Science*. **326**, 285–289 (2009).

412. X. Wu, Z. Y. Yang, Y. Li, C. M. Hogerkorp, W. R. Schief, M. S. Seaman, T. Zhou, S. D. Schmidt, L. Wu, L. Xu, N. S. Longo, K. McKee, S. O'Dell, M. K. Louder, D. L. Wycuff, Y. Feng, M. Nason, N. Doria-Rose, M. Connors, P. D. Kwong, M. Roederer, R. T. Wyatt, G. J. Nabel, J. R. Mascola, Rational design of envelope identifies broadly neutralizing human monoclonal antibodies to HIV-1. *Science*. **329**, 856–861 (2010).

413. D. Sok, M. J. V. Gils, M. Pauthner, J. P. Julien, K. L. Saye-Francisco, J. Hsueh, B. Briney, J. H. Lee, K. M. Le, P. S. Lee, Y. Hua, M. S. Seaman, J. P. Moore, A. B. Ward, I. A. Wilson, R. W. Sanders, D. R. Burton, Recombinant HIV envelope trimer selects for quaternary-dependent antibodies targeting the trimer apex. *Proc. Natl. Acad. Sci. U. S. A.* **111**, 17624–17629 (2014).

414. H. Mouquet, L. Scharf, Z. Euler, Y. Liu, C. Eden, J. F. Scheid, A. Halper-Stromberg, P. N. P. Gnanapragasam, D. I. R. Spencer, M. S. Seaman, H. Schuitemaker, T. Feizi, M. C. Nussenzweig, P. J. Bjorkman, Complex-type N-glycan recognition by potent broadly neutralizing HIV antibodies. *Proc. Natl. Acad. Sci. U. S. A.* **109**, E3268–E3277 (2012).

415. D. Sok, D. R. Burton, Recent progress in broadly neutralizing antibodies to HIV. *Nat. Immunol.* **19** (2018), pp. 1179–1188.

416. D. R. Burton, R. Ahmed, D. H. Barouch, S. T. Butera, S. Crotty, A. Godzik, D. E. Kaufmann, M. J. McElrath, M. C. Nussenzweig, B. Pulendran, C. N. Scanlan, W. R. Schief, G. Silvestri, H. Streeck, B. D. Walker, L. M. Walker, A. B. Ward, I. A. Wilson, R. Wyatt, A blueprint for HIV vaccine discovery. *Cell Host Microbe*. **12** (2012), pp. 396–407.

417. D. Pinto, Y. Park, M. Beltramello, A. C. Walls, M. A. Tortorici, S. Bianchi, S. Jaconi, K. Culap, F. Zatta, A. De Marco, A. Peter, B. Guarino, R. Spreafico, E. Cameroni, J. B. Case, R. E. Chen, C. Havenar-daughton, G. Snell, A. Telenti, H. W. Virgin, A. Lanzavecchia, M. S. Diamond, K. Fink, D. Veesler, D. Corti, Cross-neutralization of SARS-CoV-2 by a human monoclonal SARS-CoV antibody. *Nature*, 1–10 (2020).

418. Y. Abe, E. Takashita, K. Sugawara, Y. Matsuzaki, Y. Muraki, S. Hongo, Effect of the addition of oligosaccharides on the biological activities and antigenicity of

influenza A/H3N2 virus hemagglutinin. *J. Virol.* **78**, 9605–11 (2004).

419. K. L. Hartshorn, K. Sastry, M. R. White, E. M. Anders, M. Super, R. A. Ezekowitz, A. I. Tauber, Human mannose-binding protein functions as an opsonin for influenza A viruses. *J. Clin. Invest.* **91**, 1414–1420 (1993).

420. T. Kase, Y. Suzuki, T. Kawai, T. Sakamoto, K. Ohtani, S. Eda, A. Maeda, Y. Okuno, T. Kurimura, N. Wakamiya, Human mannan-binding lectin inhibits the infection of influenza a virus without complement. *Immunology*. **97**, 385–392 (1999).

421. W. C. Chang, M. R. White, P. Moyo, S. McClear, S. Thiel, K. L. Hartshorn, K. Takahashi, Lack of the pattern recognition molecule mannose-binding lectin increases susceptibility to influenza A virus infection. *BMC Immunol.* **11**, 64 (2010).

422. F. Garces, D. Sok, L. Kong, R. McBride, H. J. Kim, K. F. Saye-Francisco, J. P. Julien, Y. Hua, A. Cupo, J. P. Moore, J. C. Paulson, A. B. Ward, D. R. Burton, I. A. Wilson, Structural evolution of glycan recognition by a family of potent HIV antibodies. *Cell*. **159**, 69–79 (2014).

423. G. E. Seabright, C. A. Cottrell, M. J. van Gils, A. D'addabbo, D. J. Harvey, A. J. Behrens, J. D. Allen, Y. Watanabe, N. Scaringi, T. M. Polveroni, A. Maker, S. Vasiljevic, N. de Val, R. W. Sanders, A. B. Ward, M. Crispin, Networks of HIV-1 Envelope Glycans Maintain Antibody Epitopes in the Face of Glycan Additions and Deletions. *Structure* (2020), doi:10.1016/j.str.2020.04.022.

424. Y. Watanabe, Z. T. Berndsen, J. Raghwani, G. E. Seabright, J. D. Allen, O. G. Pybus, J. S. McLellan, I. A. Wilson, T. A. Bowden, A. B. Ward, M. Crispin, Vulnerabilities in coronavirus glycan shields despite extensive glycosylation. *Nat. Commun.* **11**, 2688 (2020).

425. N. C. Wu, S. J. Zost, A. J. Thompson, D. Oyen, C. M. Nycholat, R. McBride, J. C. Paulson, S. E. Hensley, I. A. Wilson, A structural explanation for the low effectiveness of the seasonal influenza H3N2 vaccine. *PLoS Pathog.* **13**, e1006682 (2017).

426. S. Jo, T. Kim, V. G. Iyer, W. Im, CHARMM-GUI: A web-based graphical user interface for CHARMM. *J. Comput. Chem.* **29**, 1859–1865 (2008).

427. R. Song, D. A. Oren, D. Franco, M. S. Seaman, D. D. Ho, Strategic addition of an N-linked glycan to a monoclonal antibody improves its HIV-1-neutralizing activity. *Nat. Biotechnol.* **31**, 1047–1052 (2013).

428. Y. Watanabe, J. D. Allen, D. Wrapp, J. S. McLellan, M. Crispin, Site-specific glycan analysis of the SARS-CoV-2 spike. *Science* (2020), doi:10.1126/science.abb9983.

429. L. Kong, J. H. Lee, K. J. Doores, C. D. Murin, J.-P. Julien, R. McBride, Y. Liu, A. Marozsan, A. Cupo, P.-J. Klasse, S. Hoffenberg, M. Caulfield, C. R. King, Y. Hua, K. M. Le, R. Khayat, M. C. Deller, T. Clayton, H. Tien, T. Feizi, R. W. Sanders, J. C. Paulson, J. P. Moore, R. L. Stanfield, D. R. Burton, A. B. Ward, I. A. Wilson, Supersite of immune vulnerability on the glycosylated face of HIV-1 envelope glycoprotein gp120. *Nat. Struct. Mol. Biol.* **20**, 796–803 (2013).

430. N. E. Webb, D. C. Montefiori, B. Lee, Dose-response curve slope helps predict therapeutic potency and breadth of HIV broadly neutralizing antibodies. *Nat. Commun.* **6** (2015), doi:10.1038/ncomms9443.

431. A. S. Powlesland, T. Fisch, M. E. Taylor, D. F. Smith, B. Tissot, A. Dell, S. Pöhlmann, K. Drickamer, A novel mechanism for LSECtin binding to Ebola virus surface glycoprotein through truncated glycans. *J. Biol. Chem.* **283**, 593–602 (2008).

432. P. Acharya, W. Williams, R. Henderson, K. Janowska, K. Manne, R. Parks, M. Deyton, J. Sprenz, V. Stalls, M. Kopp, K. Mansouri, R. J. Edwards, R. R. Meyerhoff, T. Oguin, G. Sempowski, K. Saunders, B. F. Haynes, *bioRxiv*, in press, doi:10.1101/2020.06.30.178897.

433. G. Simmons, J. D. Reeves, C. C. Grogan, L. H. Vandenberghe, F. Baribaud, J. C. Whitbeck, E. Burke, M. J. Buchmeier, E. J. Soilleux, J. L. Riley, R. W. Doms, P. Bates, S. Pöhlmann, DC-SIGN and DC-SIGNR bind Ebola glycoproteins and enhance infection of macrophages and endothelial cells. *Virology*. **305**, 115–123 (2003).

434. C. P. Mason, A. W. Tarr, Human lectins and their roles in viral infections. *Molecules*. **20** (2015), pp. 2229–2271.

435. A. J. Thompson, L. Cao, Y. Ma, X. Wang, J. K. Diedrich, C. Kikuchi, S. Willis, C. Worth, R. McBride, J. R. Yates, J. C. Paulson, Human Influenza Virus Hemagglutinins Contain Conserved Oligomannose N-Linked Glycans Allowing Potent Neutralization by Lectins. *Cell Host Microbe*. **27**, 725-735.e5 (2020).

436. C. Armbruster, G. M. Stiegler, B. A. Vcelar, W. Jäger, N. L. Michael, N. Vetter, H. W. D. Katinger, A phase I trial with two human monoclonal antibodies (hMAb 2F5, 2G12) against HIV-1. *AIDS*. **16**, 227–233 (2002).

437. L. Xu, A. Pegu, E. Rao, N. Doria-Rose, J. Beninga, K. McKee, D. M. Lord, R. R. Wei, G. Deng, M. Louder, S. D. Schmidt, Z. Mankoff, L. Wu, M. Asokan, C. Beil, C. Lange, W. D. Leuschner, J. Kruip, R. Sendak, Y. Do Kwon, T. Zhou, X. Chen, R. T. Bailer, K. Wang, M. Choe, L. J. Tartaglia, D. H. Barouch, S. O'Dell, J. P. Todd, D. R. Burton, M. Roederer, M. Connors, R. A. Koup, P. D. Kwong, Z. Y. Yang, J. R. Mascola, G. J. Nabel, Trispecific broadly neutralizing HIV antibodies mediate potent SHIV protection in macaques. *Science*. **358**, 85–90 (2017).

438. D. M. Ecker, S. D. Jones, H. L. Levine, The therapeutic monoclonal antibody market. *MAbs*. **7**, 9–14 (2015).

439. P. J. Carter, G. A. Lazar, Next generation antibody drugs: pursuit of the "high-hanging fruit." *Nat. Rev. Drug Discov.* **17**, 197–223 (2018).

440. A. L. Nelson, E. Dhimolea, J. M. Reichert, Development trends for human monoclonal antibody therapeutics. *Nat. Rev. Drug Discov.* **9**, 767–774 (2010).

441. M. X. Sliwkowski, I. Mellman, Antibody therapeutics in cancer. *Science*. **341**, 1192–8 (2013).

442. P. A. Blundell, N. P. L. Le, J. Allen, Y. Watanabe, R. J. Pleass, Engineering the fragment crystallizable (Fc) region of human IgG1 multimers and monomers to fine-tune interactions with sialic acid-dependent receptors. *J. Biol. Chem.* **292**, 12994–13007 (2017).

443. N. P. L. Le, T. A. Bowden, W. B. Struwe, M. Crispin, Immune recruitment or suppression by glycan engineering of endogenous and therapeutic antibodies. *Biochim. Biophys. Acta*. **1860**, 1655–1668 (2016).

444. T. Li, D. J. DiLillo, S. Bournazos, J. P. Giddens, J. V Ravetch, L.-X. Wang, Modulating IgG effector function by Fc glycan engineering. *Proc. Natl. Acad. Sci. U. S. A.* **114**, 3485–3490 (2017).

445. R. Jefferis, Posttranslational Modifications and the Immunogenicity of Biotherapeutics. *J. Immunol. Res.* **2016**, 5358272 (2016).

446. U. Brinkmann, R. E. Kontermann, The making of bispecific antibodies. *MAbs*. **9**, 182–212 (2017).

447. P. Chames, D. Baty, Bispecific antibodies for cancer therapy: the light at the end of the tunnel? *MAbs*. **1**, 539–47 (2009).

448. G. Fan, Z. Wang, M. Hao, J. Li, Bispecific antibodies and their applications. *J. Hematol. Oncol.* **8**, 130 (2015).

449. R. W. Sanders, M. Venturi, L. Schiffner, R. Kalyanaraman, H. Katinger, K. O. Lloyd, P. D. Kwong, J. P. Moore, The mannose-dependent epitope for neutralizing antibody 2G12 on human immunodeficiency virus type 1 glycoprotein gp120. *J. Virol.* **76**, 7293–305 (2002).

450. K. J. Doores, Z. Fulton, M. Huber, I. A. Wilson, D. R. Burton, Antibody 2G12 recognizes di-mannose equivalently in domain- and nondomain-exchanged forms but only binds the HIV-1 glycan shield if domain exchanged. *J. Virol.* **84**, 10690–9 (2010).

451. D. C. Dunlop, C. Bonomelli, F. Mansab, S. Vasiljevic, K. J. Doores, M. R. Wormald, A. S. Palma, T. Feizi, D. J. Harvey, R. A. Dwek, M. Crispin, C. N. Scanlan, Polysaccharide mimicry of the epitope of the broadly neutralizing anti-HIV antibody, 2G12, induces enhanced antibody responses to self oligomannose glycans. *Glycobiology*. **20**, 812–823 (2010).

452. M. Huber, K. M. Le, K. J. Doores, Z. Fulton, R. L. Stanfield, I. A. Wilson, D. R. Burton, Very Few Substitutions in a Germ Line Antibody Are Required To Initiate Significant Domain Exchange. *J. Virol.* **84**, 10700–10707 (2010).

453. A. Ehkirch, V. D'Atri, F. Rouviere, O. Hernandez-Alba, A. Goyon, O. Colas, M. Sarrut, A. Beck, D. Guillarme, S. Heinisch, S. Cianferani, An Online Four-Dimensional HIC×SEC-IM×MS Methodology for Proof-of-Concept Characterization of Antibody Drug Conjugates. *Anal. Chem.* **90**, 1578–1586 (2018).

454. C. N. Ferguson, A. C. Gucinski-Ruth, Evaluation of Ion Mobility-Mass Spectrometry for Comparative Analysis of Monoclonal Antibodies. *J. Am. Soc. Mass Spectrom.* **27**, 822–833 (2016).

455. L. Schachner, G. Han, M. Dillon, J. Zhou, L. McCarty, D. Ellerman, Y. Yin, C. Spiess, J. R. Lill, P. J. Carter, W. Sandoval, Characterization of Chain Pairing Variants of Bispecific IgG Expressed in a Single Host Cell by High-Resolution Native and Denaturing Mass Spectrometry. *Anal. Chem.* **88**, 12122–12127 (2016).

456. G. Terral, A. Beck, S. Cianférani, Insights from native mass spectrometry and ion mobility-mass spectrometry for antibody and antibody-based product characterization. *J. Chromatogr. B.* **1032**, 79–90 (2016).

457. K. J. Pacholarz, S. J. Peters, R. A. Garlish, A. J. Henry, R. J. Taylor, D. P. Humphreys, P. E. Barran, Molecular Insights into the Thermal Stability of mAbs with Variable-

Temperature Ion-Mobility Mass Spectrometry. *ChemBioChem*. **17**, 46–51 (2016).

458. M. J. Edgeworth, J. J. Phillips, D. C. Lowe, A. D. Kippen, D. R. Higazi, J. H. Scrivens, Global and Local Conformation of Human IgG Antibody Variants Rationalizes Loss of Thermodynamic Stability. *Angew. Chemie Int. Ed.* **54**, 15156–15159 (2015).

459. K. J. Pacholarz, M. Porrini, R. A. Garlish, R. J. Burnley, R. J. Taylor, A. J. Henry, P. E. Barran, Dynamics of Intact Immunoglobulin G Explored by Drift-Tube Ion-Mobility Mass Spectrometry and Molecular Modeling. *Angew. Chemie Int. Ed.* **53**, 7765–7769 (2014).

460. R. Gahoual, A.-K. Heidenreich, G. W. Somsen, P. Bulau, D. Reusch, M. Wuhrer, M. Haberger, Detailed Characterization of Monoclonal Antibody Receptor Interaction Using Affinity Liquid Chromatography Hyphenated to Native Mass Spectrometry. *Anal. Chem.* **89**, 5404–5412 (2017).

461. K. Pisupati, Y. Tian, S. Okbazghi, A. Benet, R. Ackermann, M. Ford, S. Saveliev, C. M. Hosfield, M. Urh, E. Carlson, C. Becker, T. J. Tolbert, S. P. Schwendeman, B. T. Ruotolo, A. Schwendeman, A Multidimensional Analytical Comparison of Remicade and the Biosimilar Remsima. *Anal. Chem.* **89**, 4838–4846 (2017).

462. J. T. S. Hopper, N. J. Oldham, Collision induced unfolding of protein ions in the gas phase studied by ion mobility-mass spectrometry: The effect of ligand binding on conformational stability. *J. Am. Soc. Mass Spectrom.* **20**, 1851–1858 (2009).

463. Y. Huang, N. D. Salinas, E. Chen, N. H. Tolia, M. L. Gross, Native Mass Spectrometry, Ion mobility, and Collision-Induced Unfolding Categorize Malaria Antigen/Antibody Binding. *J. Am. Soc. Mass Spectrom.* (2017), doi:10.1007/s13361-017-1782-0.

464. N. D. Wagner, D. E. Clemmer, D. H. Russell, ESI-IM-MS and Collision-Induced Unfolding That Provide Insight into the Linkage-Dependent Interfacial Interactions of Covalently Linked Diubiquitin. *Anal. Chem.* **89**, 10094–10103 (2017).

465. Y. Tian, L. Han, A. C. Buckner, B. T. Ruotolo, Collision Induced Unfolding of Intact Antibodies: Rapid Characterization of Disulfide Bonding Patterns, Glycosylation, and Structures. *Anal. Chem.* **87**, 11509–11515 (2015).

466. J. Marcoux, T. Champion, O. Colas, E. Wagner-Rousset, N. Corvaïa, A. Van Dorsselaer, A. Beck, S. Cianférani, Native mass spectrometry and ion mobility characterization of trastuzumab emtansine, a lysine-linked antibody drug conjugate. *Protein Sci.* **24**, 1210–1223 (2015).

467. S. M. Dixit, D. A. Polasky, B. T. Ruotolo, Collision induced unfolding of isolated proteins in the gas phase: past, present, and future. *Curr. Opin. Chem. Biol.* **42**, 93–100 (2018).

468. W. B. Struwe, A. Stuckmann, A.-J. Behrens, K. Pagel, M. Crispin, Global N-Glycan Site Occupancy of HIV-1 gp120 by Metabolic Engineering and High-Resolution Intact Mass Spectrometry. *ACS Chem. Biol.* **12**, 357–361 (2017).

469. T. M. Allison, E. Reading, I. Liko, A. J. Baldwin, A. Laganowsky, C. V. Robinson, Quantifying the stabilizing effects of protein–ligand interactions in the gas phase. *Nat. Commun.* **6**, 8551 (2015).

470. J. D. Eschweiler, J. N. Rabuck-Gibbons, Y. Tian, B. T. Ruotolo, CIUSuite: A Quantitative Analysis Package for Collision Induced Unfolding Measurements of Gas-Phase Protein Ions. *Anal. Chem.* **87**, 11516–11522 (2015).

471. D. J. Harvey, M. Crispin, C. Bonomelli, J. H. Scrivens, Ion Mobility Mass Spectrometry for Ion Recovery and Clean-Up of MS and MS/MS Spectra Obtained from Low Abundance Viral Samples. *J. Am. Soc. Mass Spectrom.* **26**, 1754–67 (2015).

472. R. M. Ionescu, J. Vlasak, C. Price, M. Kirchmeier, Contribution of Variable Domains to the Stability of Humanized IgG1 Monoclonal Antibodies. *J. Pharm. Sci.* **97**, 1414–1426 (2008).

473. T. Ito, K. Tsumoto, Effects of subclass change on the structural stability of chimeric, humanized, and human antibodies under thermal stress. *Protein Sci.* **22**, 1542–51 (2013).

474. M. L. Brader, T. Estey, S. Bai, R. W. Alston, K. K. Lucas, S. Lantz, P. Landsman, K. M. Maloney, Examination of Thermal Unfolding and Aggregation Profiles of a Series of Developable Therapeutic Monoclonal Antibodies. *Mol. Pharm.* **12**, 1005–1017 (2015).

475. H. Stö, B. Adamczyk, J. Hayes, P. M. Rudd, Automated, High-Throughput IgG-Antibody Glycoprofiling Platform, doi:10.1021/ac402068r.

476. G. R. Guile, P. M. Rudd, D. R. Wing, S. B. Prime, R. A. Dwek, A Rapid High-Resolution High-Performance Liquid Chromatographic Method for Separating Glycan Mixtures and Analyzing Oligosaccharide Profiles. *Anal. Biochem.* **240**, 210–226 (1996).

477. P. Akesson, L. Moritz, M. Truedsson, B. Christensson, U. von Pawel-Rammingen, IdeS, a highly specific immunoglobulin G (IgG)-cleaving enzyme from Streptococcus pyogenes, is inhibited by specific IgG antibodies generated during infection. *Infect. Immun.* **74**, 497–503 (2006).

478. E. O. Saphire, P. W. Parren, R. Pantophlet, M. B. Zwick, G. M. Morris, P. M. Rudd, R. A. Dwek, R. L. Stanfield, D. R. Burton, I. A. Wilson, Crystal structure of a neutralizing human IGG against HIV-1: a template for vaccine design. *Science*. **293**, 1155–9 (2001).

479. M. B. Zwick, P. W. H. I. Parren, E. O. Saphire, S. Church, M. Wang, J. K. Scott, P. E. Dawson, I. A. Wilson, D. R. Burton, Molecular features of the broadly neutralizing immunoglobulin G1 b12 required for recognition of human immunodeficiency virus type 1 gp120. *J. Virol.* **77**, 5863–76 (2003).

480. S. S. Hasan, C. Sun, A. S. Kim, Y. Watanabe, C. L. Chen, T. Klose, G. Buda, M. Crispin, M. S. Diamond, W. B. Klimstra, M. G. Rossmann, Cryo-EM Structures of Eastern Equine Encephalitis Virus Reveal Mechanisms of Virus Disassembly and Antibody Neutralization. *Cell Rep.* **25**, 3136-3147.e5 (2018).

481. S. B. Halstead, Dengue virus–mosquito interactions. *Annu. Rev. Entomol.* **53**, 273–291 (2008).

482. B. R. Murphy, S. S. Whitehead, Immune response to Dengue virus and prospects for a vaccine. *Annu. Rev. Immunol.* **29**, 587–619 (2011).

483. R. J. Kuhn, W. Zhang, M. G. Rossmann, S. V Pletnev, J. Corver, E. Lenches, C. T. Jones, S. Mukhopadhyay, P. R. Chipman, E. G. Strauss, T. S. Baker, J. H. Strauss, Structure of dengue virus: implications for flavivirus organization, maturation, and fusion. *Cell*. **108**, 717–25 (2002).

484. C. L. Murray, C. T. Jones, C. M. Rice, Architects of assembly: roles of Flaviviridae non-structural proteins in virion morphogenesis. *Nat. Rev. Microbiol.* **6**, 699–708 (2008).

485. D. L. Carbaugh, R. S. Baric, H. M. Lazear, *J. Virol.*, in press, doi:10.1128/JVI.00113-19.

486. N. K. Routhu, S. D. Lehoux, E. A. Rouse, M. R. M. Bidokhti, L. B. Giron, A. Anzurez, S. P. Reid, M. Abdel-Mohsen, R. D. Cummings, S. N. Byrareddy, Glycosylation of zika virus is important in host–virus interaction and pathogenic potential. *Int. J. Mol. Sci.* **20** (2019), doi:10.3390/ijms20205206.

487. D. L. Akey, W. C. Brown, S. Dutta, J. Konwerski, J. Jose, T. J. Jurkiw, J. DelProposto, C. M. Ogata, G. Skiniotis, R. J. Kuhn, J. L. Smith, Flavivirus NS1 structures reveal surfaces for associations with membranes and the immune system. *Science*. **343**, 881–5 (2014).

488. M. A. Edeling, M. S. Diamond, D. H. Fremont, Structural basis of Flavivirus NS1 assembly and antibody recognition. *Proc. Natl. Acad. Sci. U. S. A.* **111**, 4285–90 (2014).

489. R. Matsuda, Y. Hayashi, T. Suzuki, Y. Saito, Information theory of miniaturization advantages of column liquid chromatography for quantitative analysis. *Fresenius. J. Anal. Chem.* **347**, 225–229 (1993).

490. Y. Lei, H. Yu, Y. Dong, J. Yang, W. Ye, Y. Wang, W. Chen, Z. Jia, Z. Xu, Z. Li, F. Zhang, Characterization of N-glycan structures on the surface of mature dengue 2 virus derived from insect cells. *PLoS One*. **10** (2015), doi:10.1371/journal.pone.0132122.

491. S. W. Metz, A. Thomas, L. White, M. Stoops, M. Corten, H. Hannemann, A. M. De Silva, Dengue virus-like particles mimic the antigenic properties of the infectious dengue virus envelope. *Virol. J.* **15** (2018), doi:10.1186/s12985-018-0970-2.

492. I.-M. Yu, W. Zhang, H. A. Holdaway, L. Li, V. A. Kostyuchenko, P. R. Chipman, R. J. Kuhn, M. G. Rossmann, J. Chen, Structure of the immature dengue virus at low pH primes proteolytic maturation. *Science*. **319**, 1834–7 (2008).

493. I.-M. Yu, H. A. Holdaway, P. R. Chipman, R. J. Kuhn, M. G. Rossmann, J. Chen, Association of the pr peptides with dengue virus at acidic pH blocks membrane fusion. *J. Virol.* **83**, 12101–7 (2009).

494. X. Zhang, P. Ge, X. Yu, J. M. Brannan, G. Bi, Q. Zhang, S. Schein, Z. H. Zhou, Cryo-EM structure of the mature dengue virus at 3.5-Å resolution. *Nat. Struct. Mol. Biol.* **20**, 105–10 (2013).

495. G. Barba-Spaeth, W. Dejnirattisai, A. Rouvinski, M. C. Vaney, I. Medits, A. Sharma, E. Simon-Lorière, A. Sakuntabhai, V. M. Cao-Lormeau, A. Haouz, P. England, K. Stiasny, J. Mongkolsapaya, F. X. Heinz, G. R. Screaton, F. A. Rey, Structural basis of potent Zika-dengue virus antibody cross-neutralization. *Nature*. **536**, 48–53 (2016).

496. W. C. Brown, D. L. Akey, J. R. Konwerski, J. T. Tarrasch, G. Skiniotis, R. J. Kuhn, J. L. Smith, Extended surface for membrane association in Zika virus NS1 structure. *Nat. Struct. Mol. Biol.* **23**, 865–7 (2016).